ABSTRACT

Title of Dissertation: ENGINEERING BIOMATERIALS TO PROMOTE SYSTEMIC, ANTIGEN-SPECIFIC TOLERANCE

Lisa H. Tostanoski, Doctor of Philosophy, 2017

Dissertation directed by: Christopher M. Jewell
Associate Professor
Fischell Department of Bioengineering

In autoimmune diseases, such as multiple sclerosis (MS) and type 1 diabetes, the immune system incorrectly identifies and attacks "self" molecules. Existing therapies have provided important benefits, but are limited by off-target effects, reduced efficacy as disease progresses, and lack of cure potential, necessitating frequent, life-long dosing. An exciting strategy being explored is the design of vaccine-like therapies that selectively reprogram immune responses to self-molecules. This approach could, for example, control the attack of myelin – the protective coating around neurons – that occurs during MS, without leaving patients immunocompromised. However, the realization of this idea has proven difficult; once injected, conventional approaches do not provide control over the combinations, concentrations, and kinetics of signals that reach key tissues that orchestrate immune responses, such as lymph nodes (LNs). Biomaterials have emerged as a promising

strategy to confront this challenge, offering features including co-delivery of cargos and controlled release kinetics. The research in this dissertation harnesses biomaterials to develop novel strategies to promote effective, yet selective control of autoimmunity, termed antigen-specific tolerance. In the first aim, direct injection was used to deposit degradable microparticles in LNs, enabling local controlled release of combinations of myelin peptide and Rapamycin, a drug shown to promote regulatory immune function. This work demonstrates the potency of intra-LN delivery in mouse models of MS, as a single dose of co-loaded microparticles permanently reversed disease-induced paralysis in a myelin-specific manner. The results also support this approach as a platform to study the link between local LN signaling and resultant responses in non-treated tissues and sites of disease during autoimmunity. In the second aim, myelin peptide and GpG, a regulatory ligand of an inflammatory pathway overactive in mouse models and patients with autoimmunity, were self-assembled. This approach generated microcapsules that mimic attractive features of conventional biomaterials, but eliminate synthetic carrier components that can complicate rational design and, due to intrinsic inflammatory properties, might exacerbate autoimmunity. These materials promoted tolerance in mouse cells, mouse models of MS, and samples from human MS patients. Together, these strategies could offer novel, modular approaches to combat autoimmune diseases and inform design criteria for future therapies.

ENGINEERING BIOMATERIALS TO PROMOTE SYSTEMIC, ANTIGEN-SPECIFIC IMMUNE TOLERANCE

by

Lisa H. Tostanoski

Dissertation submitted to the Faculty of the Graduate School of the
University of Maryland, College Park, in partial fulfillment
of the requirements for the degree of
Doctor of Philosophy
2017

Advisory Committee:
Professor Christopher Jewell, Chair
Professor Jonathan Bromberg
Professor Steven Jay
Professor Peter Kofinas
Professor David Mosser, Dean's Representative

Acknowledgements

First, thank you to Chris, for the countless opportunities you have afforded me over the years. I am incredibly grateful for your continued support and to call you my mentor. Thank you to the members of the Jewell Lab – past and present – for the advice, help, support, and for keeping science fun, even at odd hours of the day and night. Special thanks to Yu-Chieh, Josh, Krystina, Emily, Xiangbin, and Peipei for all of your time and assistance with experiments, to Boyan for always bringing great energy and resolve to our projects, and to Jim for, in your words, enduring the journey with me from the start. To the staff and students in the Department of Laboratory Animal Research, especially to Kim and Mary, thank you for all of your assistance with training and monitoring mice. Thank you to the Bromberg and Royal labs, for your continued generosity with your time and expertise through our collaborative projects. Last, but not least, thank you to my family and friends that have encouraged and supported me throughout this journey, especially my parents and my sister, Sarah.

Table of Contents

List of Tables

List of Figures

List of Abbreviations

Antigen Presenting Cell	APC
Central Nervous System	CNS
Dendritic Cell	DC
Experimental Autoimmune Encephalomyelitis	EAE
High Endothelial Venule	HEV
Immune Polyelectrolyte Multilayer	iPEM
Lipopolysaccharide	LPS
Lymph Node	LN
Major Histocompatibility Complex	MHC
Microparticle	MP
Myelin Oligodendrocyte Glycoprotein	MOG
Multiple Sclerosis	MS
Nanoparticle	NP
Ovalbumin	OVA
Poly(lactic-co-glycolic acid)	PLGA
Polyelectrolyte Multilayer	PEM
Rapamycin	Rapa
Regulatory T cell	T_{REG}
Poly(inosinic:cytidilic acid)	PolyIC
Toll-Like Receptor	TLR
Toll-Like Receptor Agonist	TLRa

Chapter 1. Introduction

Autoimmune disorders are characterized by a malfunction of the immune system: the incorrect attack of "self" molecules, such as myelin – the protective insulation around neurons – in multiple sclerosis (MS). Current clinical interventions have provided significant benefits for patients in controlling the symptoms of MS, debilitating neurodegeneration that leads to a loss of motor function. However, these treatments employ broad immunosuppression, rather than targeting only myelin-specific cells. This lack of specificity results in off-target effects that leave patients immunocompromised and, because these approaches are not curative, require patients to receive frequent, life-long treatments (e.g., weekly infusions, daily injections). Further, despite intervention, disease often still progresses, highlighting insufficient efficacy as another challenge associated with current clinical strategies. These limitations have sparked intense interest in the field in developing vaccine-like therapies that could reprogram how the immune system responds to myelin, while leaving healthy, protective immune function intact.

One exciting new route towards a more selective therapy aims to bias myelin-specific immune cells towards populations that promote tolerance (e.g., regulatory T cells, T_{REGS}), rather than the inflammatory subsets that cause disease. This polarization of immune cell phenotype and function is intimately linked to the combinations and doses of cues present during maturation and proliferation. Thus, strategies that could augment control over the delivery of multiple immune cues *in vivo* – with respect to both space and time – could provide new approaches to enhance restraint of disease.

Further, these approaches could also generate new tools to study the link between immune signal localization and the potential to drive systemic, but specific effects. Towards this goal, new studies are exploring the use of biomaterials, which can offer properties including tunable cargo loading, co-delivery, and controlled release, to enhance the delivery of candidate therapies.

My dissertation work has brought together strategies from materials science, engineering, and immunology to design novel biomaterials-based approaches to study and combat autoimmunity. The engineering techniques include synthesis of degradable microparticles through double-emulsion and programmable self-assembly of polyelectrolyte multilayers through layer-by-layer deposition. Materials science tools were employed to characterize the physiochemical properties of these biomaterials, including laser diffraction particle analysis, zeta potential measurement, ellipsometry, and spectrophotometry. These strategies were paired with primary cell isolation and culture, animal handling and injections, transgenic mouse breeding, mouse models of autoimmunity, flow cytometry, ELISA, and immunofluorescent staining to explore the potential for materials to polarize immune cell function towards tolerance *in vitro* and *in vivo*. Finally, metabolic assays and multiplex cytokine analyses (Luminex) were employed to reveal how engineered materials interact *ex vivo* with cell samples collected from human MS patients to restrain disease-associated inflammation. These tools, techniques, and perspectives were synthesized to investigate two main aims:

1. Direct delivery of degradable biomaterials, and encapsulated immune signals, to lymph nodes (LNs) as i) a novel therapeutic strategy to drive systemic, yet antigen-specific tolerance and ii) a modular platform technology to study the link between local LN signaling and elicited responses in non-treated immune tissues and at sites of autoimmune disease (e.g., spinal cord).

2. The design of carrier-free capsules that mimic attractive features of biomaterials, but eliminate synthetic components, to promote tolerance through down-regulation of an inflammatory pathway recently shown to be overactive in both mouse models and human autoimmune disease.

We begin by first discussing a key immune cell population, antigen presenting cells (APCs), in the context of tolerance, along with recent materials and engineering strategies being used to target these cells to promote regulatory functions (**Chapter 2**). **Chapters 3 and 4** present work linked to Aim 1, above. In **Chapter 3**, we describe a strategy to directly introduce biomaterials to LNs, the tissues that coordinate immune function. In **Chapter 4**, this platform is used to deliver degradable microparticles, encapsulating immune signals, to LNs to probe how the combinations of signals present in LNs impacts the development of tolerance in a mouse model of MS. The next two chapters link to Aim 2, above, in which tunable self-assembly of immune cues is explored to generate microcapsules that mimic attractive features of conventional biomaterials, such as the polymer microparticles

employed in Aim 1. In contrast, however, these immune polyelectrolyte multilayer (iPEM) microcapsules are composed entirely of immune signals, eliminating all carrier or synthetic components that could complicate both rational design and systematic study of the relative contributions of different immune cues to drive tolerance. We begin by discussing approaches that exploit unique features of self-assembly well-suited for a range of immunological applications, not just the induction of tolerance, but spanning diagnostics, fundamental studies, and the design of new vaccines and immunotherapies for infectious disease, cancer, and autoimmunity (**Chapter 5**). In **Chapter 6**, we focus on the iPEM approach, demonstrating the potential to harness self-assembly to promote tolerance in primary mouse cells, mouse models of MS, and samples from human MS patients. **Chapter 7** details ongoing work and future research directions for Aim 1 and Aim 2. In **Chapter 8**, my contributions are summarized, followed by appendices listing my publications thus far, intellectual property filings on which I am listed as an inventor, and references.

Chapter 2. Engineering Tolerance Using Biomaterials to Target and Control Antigen Presenting Cells[1]

2.1. Introduction

Autoimmune diseases are conditions in which the immune system mistakenly attacks host molecules, cells, and tissues. These conditions impact both children and adults, with some of the most common diseases including multiple sclerosis (MS), type 1 diabetes, lupus, and rheumatoid arthritis. Generally speaking, autoimmunity occurs when immune tolerance – the mechanisms the body uses to regulate healthy immune function – fails. The control systems governing these processes are incredibly complex, involving integration of signals from cytokines, chemokines, soluble factors, stromal components, and cells, both at sites of disease and within the spleen and lymph nodes (LNs) – organs that direct immune function. Normally, antigen presenting cells (APCs), such as dendritic cells (DCs) and macrophages, survey peripheral blood and tissue and migrate to LNs and spleen after encountering bacteria, viruses, or other foreign pathogens. Once in these sites, pathogens are processed by APCs and the resulting antigen fragments are displayed on the cell surfaces in protein assemblies termed major histocompatibility complexes (MHC) [1]. Display of antigen in MHC, along with the appropriate "warning" or co-stimulatory signal, leads to activation of resident T and B cells that exhibit specificity for the same antigen being presented on the APCs [2, 3].

[1] Adapted from: L. H. Tostanoski, E. A. Gosselin, and C. M. Jewell, "Engineering tolerance using biomaterials to target and control antigen presenting cells." *Discovery Medicine* 2016, 21, 403-410.

Because of the critical role DCs and other APCs play in generating adaptive immune response, APCs are important targets for both traditional prophylactic vaccines and for therapeutic vaccines aimed at cancer or autoimmunity [4]. In particular, many studies demonstrate the role of DCs in promoting tolerance through direct production of immunosuppressive cytokines, or by polarizing T cells and other populations that typically drive disease away from inflammatory phenotypes. For example, modulation of DC signaling can promote expansion of regulatory T cells (T_{REGS}) or other suppressive populations, as well as induce cell deletion and non-responsiveness ("anergy") [5-8]. In the past decade, there has thus been an explosion of experimental therapies aimed at exploiting these capabilities for more potent and selective autoimmune therapies. Systemic delivery of rapamycin or other immunosuppressants has been used to alter DC phenotype in the context of transplantation, type 1 diabetes, lupus, and MS. [9-12]. However, these approaches are hindered by the systemic manner in which regulatory cues are delivered, echoing a nearly universal challenge facing pre-clinical and approved autoimmune therapies: broad suppression that leaves patients immunocompromised. Further, our understanding of the complex network of lymphatics that facilitate the migration of APCs, T cells and B cells – for example, between LNs and peripheral sites of disease – is still developing, suggesting new opportunities to study and target these pathways to promote tolerance [13-15]. For example, two landmark papers in 2015 revealed new lymphatics that connect the central nervous system (CNS) – the site of autoimmune attack during MS – with deep cervical lymph nodes [13, 14]. Together all of these ideas underscore the potential for designing new tolerogenic therapies that provide more specific delivery to APCs and

the tissues in which they reside, capabilities that biomaterials are uniquely-suited to provide. In this review, we discuss properties of biomaterials that can be exploited for targeting and controlling APCs, and highlight recent examples of how these materials are being used to promote tolerance in autoimmunity and transplantation. These strategies are grouped into three categories: i) passive or active targeting of particulate carriers to APCs, ii) biomaterial-mediated control over antigen localization and processing, and iii) targeted delivery of encapsulated or adsorbed immunomodulatory signals (**Figure 2.1**).

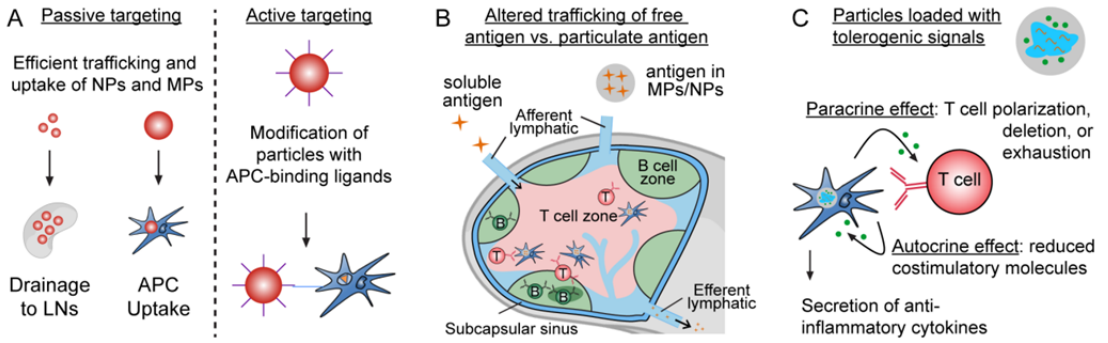

Figure 2.1 Strategies to exploit biomaterials in promoting immune tolerance.
A) Biomaterials exhibit general features that can be exploited for passive and active targeting to achieve tolerance. B) Induction of tolerogenic function using biomaterials to alter trafficking and processing of self-antigens by APCs. C) Harnessing biomaterials to generated tolerance by targeting regulatory immune cues to APCs.

2.2. Biomaterials offer general features that are useful for engineering immune response

From one perspective, biomaterials might be thought of as a broad collection of materials – synthetic polymers, lipids, imaging agents, proteins, nucleic acids – that become biomaterials when applied to biological questions or applications. These materials are commonly formulated into nanoparticles (NPs) or microparticles (MPs), organized into self-assembling structures such as nanostructured protein complexes or

liposomes, or used to fabricate biocompatible scaffolds and devices. Many of the attractive features of biomaterials are particularly useful in drug delivery, vaccination, and immunotherapy [4, 16-18]. For example, lipid and polymer particles can be formulated with multiple cargos to achieve co-delivery, modified with ligands for improved targeting, designed with programmable stabilities for controlled drug release, and used to protect biologic cargo from enzymatic degradation or pH gradients. These features, along with the ability to tune physicochemical properties such as particle size, also provide many opportunities to passively or actively target APCs.

2.2.1. Passive strategies for targeting APCs

The size of NP or MP vaccine and immunotherapy carriers, such as those formed from polymers or lipids, has two major implications for interactions with APCs [4, 19]. First, APCs have evolved to efficiently phagocytose particles over nanometer and micrometer size ranges. Thus, since most biomaterial vaccines carriers exhibit sizes from tens of nanometers to several microns, this characteristic provides an immediate advantage for recognition, internalization, and processing of antigens or other immune signals in the particles. Second, sub-100 nm NPs are able to drain to LNs following peripheral injection much more efficiently than MPs [20]. To elicit potent adaptive responses, MPs are more reliant on trafficking by APCs from the injection site, illustrating the direct impact size has on the route and efficiency with which biomaterial carriers reach LNs. A number of studies have also revealed the importance of other physicochemical features such as shape and charge in immune

cell interactions, so these aspects will likely create new levers which can be pulled to further encourage non-specific recognition and uptake of NPs and MPs by APCs [21-23].

2.2.2. Active strategies for targeting APCs

Active targeting strategies for biomaterials have been studied by exploiting APC surface markers, as well as targeting APCs at the tissue level for improved LN delivery. Several reports, for example, have improved DC targeting using polymeric or lipid NPs displaying monoclonal antibodies specific for DEC-205, a characteristic transmembrane protein on DCs [24, 25]. At the tissue level, one exciting recent approach involved co-opting a natural albumin shuttling network involved in trafficking proteins and other factors to LNs [26]. In this approach, lipids were designed with an albumin binding domain, peptide antigens, and inflammatory toll-like receptor agonists (TLRa) as adjuvants. TLRas bind receptors on APCs that have evolved to alert the immune system upon encounter of molecular patterns or danger signals are common in pathogens. Immunizing mice with the lipid conjugates produced striking antigen-specific immunity in several mouse models of cancer. Another approach focused on LNs is engineering of the LN microenvironment with MPs. In this work, immune signals were localized and retained in LNs through direct injection of degradable MPs that are too large for rapid drainage from LNs [27]. This strategy can be used to rapidly generate large populations of antigen-specific T cells with direct control over the signals introduced to APCs and other resident cells. Several recent studies illustrate an interesting feature of polymeric biomaterials: many

of these polymers can activate inflammatory immune pathways even in the absence of antigens or other adjuvants [4, 28, 29]. With improved understanding, this is a feature that can be harnessed for both prophylactic and therapeutic applications. In tolerance specifically, the possibility of intrinsic immunogenicity that could exacerbate disease creates new motivation to develop materials that provide features of biomaterials (e.g., tunable size, co-delivery, targeting) without the risk of inherent inflammatory carrier properties. Some studies have worked to mask this intrinsic activity of a widely-used polymer, poly(lactide-co-galactide) [30], and several new technology platforms based on self-assembly of proteins or nucleic acids might also be useful to exploit for tolerance [31-33].

All of the features presented thus far are of general relevance for vaccination and immunotherapy. Below we discuss specific examples in which biomaterials have been used to influence APCs in the generation and control of tolerance. These are divided into two strategies: i) use of biomaterials to change how self-antigens are trafficked or processed, and ii) use of biomaterials to deliver regulatory cues to APCs. Biomaterials are also being used in other interesting ways to induce tolerance – for example, directly altering T cell phenotype – that are summarized in recent reviews [4, 34-36].

2.3. Biomaterials can be used to alter the trafficking and processing of self-antigens

Our understanding of the pathology of many autoimmune diseases has increased remarkably in the past several decades, allowing identification of some key self-antigens in MS and type 1 diabetes, and emerging candidates for other diseases such as lupus and rheumatoid arthritis [37, 38]. In the subsections below, we discuss two strategies to promote tolerance by altering the trafficking or processing of these self-antigens.

2.3.1. Altered trafficking of self-antigen to exploit debris clearance pathways

MS is the most prevalent autoimmune disease and one of the most studied. Unsurprisingly then, several biomaterial strategies aim to generate myelin-specific tolerance to stop the attack of myelin – the molecule attacked in the CNS during MS – without the non-specific immunosuppression of existing therapies. Building on earlier work using splenocytes modified to display self-peptides, Shea, Miller, and colleagues have developed a strategy for tolerance involving covalent modification of polymeric MPs with myelin peptides [39, 40]. In these reports, both prophylactic and therapeutic treatment with myelin proteolipid protein (PLP) generated efficacious tolerance during a mouse model of relapsing remitting MS, relapsing remitting experimental autoimmune encephalomyelitis (RR-EAE). A cardinal finding of this work reveals that conjugation of PLP to the MPs leads to trafficking of peptide to cells in the marginal zone of the spleen that are positive for the Macrophage Receptor with Collagenous Structure (MARCO), a scavenger receptor involved in debris

clearance. Although the exact mechanism is still being investigated, a working hypothesis suggests upregulation of MARCO and localization to $MARCO^+$ cells improves antigen presentation, which, in the absence of other co-stimulation, might promote regulatory responses. Along these lines, functional reduction in RR-EAE severity was accompanied by increased T_{REGS}, reduced pathogenic T cell infiltration into the CNS, and anergy. This general approach has also recently been employed to improve graft survival in a pre-clinical mouse transplant model [41].

Along with MARCO, the body uses many additional pathways to clear apoptotic cells and other debris. Interestingly, antigens displayed in these milieus can nucleate antigen-specific tolerance. One of the hypotheses underlying this outcome is the possibility that the presence of antigen in the absence of other inflammatory signals or a non-activating environment drives deletion of T cells or promotes anergy [42]. The Hubbell lab has exploited this idea by conjugating antigens to erythrocytes, a cell population with a large number of apoptotic events and recycling on a daily basis. [43, 44]. These studies reveal that compared with free antigen, antigen bound to glycophorin A on erythrocytes was present in a much higher frequency of DCs, macrophages, and other APCs in the spleen and liver. This uptake, along with the absence of co-stimulation, was shown to promote T_{REGS} and to drive antigen-specific deletion of $CD4^+$ and $CD8^+$ T cells through increased PD-1 signaling, a natural negative regulator of immunity. Functionally, erythrocyte binding of candidate antigen associated with disease in diabetes prevented onset of hyperglycemia in a mouse model of type 1 diabetes. Another approach along this same theme is driven

by the intriguing idea that even particles that do not include self-antigen might help promote tolerance by exploiting apoptotic clearance mechanisms to trigger deletion or anergy. In this report, infusion of MPs formed from either degradable or non-degradable polymers induced tolerance in mouse models of myocardial infarction, EAE, colitis, peritonitis, and lethal flavivirus encephalitis [45]. This surprising result required the particles to exhibit a negative charge. Although the mechanism needs further study, negatively-charged MPs seem to be internalized by $MARCO^{+}$ inflammatory monocytes, leading to apoptosis of these cells instead of trafficking to sites of inflammation and autoimmune attack. Together these strategies underscore the link between trafficking of self-antigens or other particulates with the inter-connected regulatory pathways that cooperate to promote tolerance.

2.3.2. Disruption of interactions between APCs and T cells

In addition to altered antigen trafficking, several recent studies have exploited biomaterials to promote tolerance by blocking interactions between APCs and T cells that are required for pro-immune adaptive immunity. The Berkland lab used a hyaluronic acid backbone to graft this polymer with myelin epitopes and peptides that bind the B7 (CD80/CD86) protein on APCs [46]. This is an important pathway during APC/T cell interactions, thus mice receiving a three-injection regimen of these polymers to block B7 signaling exhibited attenuated disease during RR-EAE. Other strategies have focused on blocking pro-inflammatory T cell activation by directly targeting T cells. In one approach, NPs were functionalized with MHC complexes displaying peptide epitopes attacked during type 1 diabetes [36]. These studies

reversed autoimmunity in mouse models of type 1 diabetes, functioning through a proposed mechanism in which low, sustained stimulation of antigen-experienced $CD8^+$ T cells is generated by the NPs. This presentation without co-stimulation drives a small population of memory-like, regulatory $CD8^+$ T cells that control disease in an antigen-specific manner.

2.4. Targeting regulatory cures to APCs via biomaterials can be used to activate tolerogenic processes

The strategies discussed in the previous section relied on manipulating how antigens are received by the immune system to activate regulatory processes. An exciting parallel set of approaches is based on changing the response to self-antigens using biomaterials to control the delivery of regulatory signals either with self-antigen, or as monotherapies that alter response to self-antigens presented in LNs [4, 34]. Some of these have targeted T cells with suppressive drugs to reduce inflammation, limit self-reactive effector T cells (e.g., T_H17, T_H1), and drive regulatory populations such as T_{REGS}. Maldonado *et al.*, for example, recently reported a robust approach to induce tolerance using MPs loaded with self-antigens and rapamycin, a drug that promotes regulatory functions in both T cells and DCs [47]. In this report, particles loaded with antigen created only a modest effect, whereas co-loading with rapamycin drove efficient tolerance in several mouse models, including RR-EAE and hemophilia A. Importantly, tolerance was antigen-specific. This approach, coupled with those in the previous section involving only antigen highlight important open questions: What is the role of self-antigen delivery in promoting tolerance? Why does addition of

suppressive drugs drive synergistic effects when drug alone has significantly reduced impact? Answers to these questions will help inform clinical translation by revealing the combinations of signals that should be delivered, what tissues (e.g., LNs, disease sites) should be targeted, and the regimens or kinetics over which delivery should occur.

2.4.1. Biomaterial-mediated delivery of drugs that suppress pro-immune APC functions

Because of the importance of DCs and other APCs in tolerance, biomaterials have recently been combined with a number of different drugs and suppressive immune signals to specifically target APCs. Rapamycin, as mentioned above, is a common immunosuppressant that can polarize the phenotypes of APCs to secrete regulatory cytokines, promote T_{REGS}, and reduce activation [9]. In one of the earlier reports in the field, the Little lab used MPs to solubilize and deliver rapamycin to primary DCs, leading to reduced ability of these cells to activate T cells *in vitro* [48]. Micelles have also been used to encapsulate rapamycin and analogs of this drug to reduce maturation and activation of DCs in draining LNs after injection [49]. These effects improved tail allograft survival in a mouse transplant model. Dexamethasone, another immunosuppressant, has also been used toward similar goals in EAE by encapsulation with myelin peptides in acetalated dextran MPs [50].

2.4.2. Biomaterial-mediated delivery of drugs that enhance APC regulatory pathways

The reports just described focus on suppressing stimulatory immune functions in APCs, but immunosuppressants and other signals can also enhance regulatory pathways, or in some cases modulate both routes to enhance tolerance. Mycophenolic acid, for example, is a classic immunosuppressant. The Goldstein and Fahmy labs have used NPs loaded with this drug to prolong survival of skin allografts in mice [51]. One of the interesting features of this approach is the finding that efficacy could be achieved at concentrations 1000-fold lower than those required using soluble MPA. Mechanistic studies revealed MPA NPs upregulated the natural regulatory functions of PD-L1 signaling on DCs. In a subsequent study, injectable nanogels were designed by complexing MPA in cyclodextrin complexes [52]. These assemblies were then loaded into degradable NPs and crosslinked to form a gel that sustains the release of MPA. After either prophylactic or therapeutic treatments, gels reduced inflammatory cytokines and increased survival during murine systemic lupus erythematosus (SLE) – a common pre-clinical lupus model. Another recent approach combined two different particle sizes to target self-antigens to DCs in smaller, phagocytosable MPs while delivering signals that promote a tolerogenic milieu in larger, non-internalizable MPs [53]. The smaller MPs were loaded with vitamin D3 and diabetes antigens and mixed prior to injection with larger MPs encapsulating transforming growth factor beta 1 (TGF-β1) and granulocyte-macrophage colony-stimulating factor (GM-CSF). In this report treatment prevented the onset of type-1 diabetes in 40% of mice. Interestingly, DCs and other APCs from treated mice also

exhibited increased Gr-1, an upstream indicator of cells with the potential to differentiate into tolerogenic APCs subsets.

Several other approaches have used small molecule drugs and ligands to enhance specific regulatory pathways. The Quintana lab has worked extensively with the aryl hydrocarbon receptor, a transcription factor present on DCs and other APCs that promotes T_{REGS} upon engagement. These investigators adsorbed a ligand for this receptor to gold NPs and used these particles, particles loaded with myelin peptide, or particles loaded with both signals to treat cells and mice. NP formulations containing both the ligand and myelin peptides induced tolerogenic DCs in culture, as well as in mice with EAE, and increased T_{REG} frequencies. These effects reduced disease severity, but required the presence of myelin in the NPs, suggesting an antigen-specific characteristic to the tolerance.

Another exciting new approach is based on controlling the metabolic activity of DCs to alter the interactions of these cells with T cells. In this report, Gammon *et al.* developed NPs loaded with a metabolic modulator of glutamate metabolism, N-Phenyl-7-(hydroxyimino)cyclopropa[b]chromen-1a-carboxamide (PHCCC) [54]. DCs release glutamate during inflammation, and this molecule is processed and metabolized by the metabotropic glutamate receptor family. The specific receptors that metabolize glutamate help control the balance between inflammatory and regulatory DC function. In primary cell culture, NPs loaded with PHCCC were 36-fold less toxic then soluble PHCCC and dramatically reduced DC activation. During

co-culture, these effects polarized T cells toward T_{REGS} while reducing inflammatory cytokines and phenotypes. Subsequent studies in EAE demonstrated that sustained release of PHCCC from NPs delayed disease onset and severity at doses and intervals where soluble drug had no effect. Together, these studies suggest a new strategy to promote tolerance by altering APC/T cell interactions through programming of metabolic function. The excitement of this idea is underscored by recent discoveries that reveal new connections between metabolism and immune response [55] [56].

2.5. Conclusions

The examples discussed here illustrate the exciting potential of biomaterials to generate immune tolerance that is more specific and more potent. Thus far, most of the work in this area has been pre-clinical, so multi-disciplinary teams should support continued advancement of these technologies toward the clinic. Similarly, communication between the engineering and immunology disciplines is critical to ensure clinically-relevant problems are being attacked, and that the appropriate technologies are being deployed. The coming years are also sure to bring excitement in emerging areas where tolerance and biomaterials can be used. Some of these include regenerative medicine – for example in diabetes and transplantation, in immunometabolism where new links are being discovered between lymphocyte phenotype and function [55], and in organ-specific autoimmune-disease as new connections are made between sites of self-attack and the local microenvironment of LNs and the spleen.

Section 2.2.2 introduced an approach to target APCs by delivering biomaterials directly to key sites of interaction between APCs and naïve lymphocytes, the lymph nodes. **Chapter 3** describes this technique, linked to Aim 1, detailing i) methods to synthesize, characterize, and prepare polymer microparticles for administration, ii) steps to prepare mice for intra-lymph node injections, and iii) procedures to inject, evaluate the success of intra-lymph node delivery, and expected results.

Chapter 3. Intra-lymph Node Injection of Biodegradable Polymer Particles[2]

3.1. Introduction

The lymph nodes (LNs) are the command centers of the immune system. At this immunological site, antigen presenting cells prime naïve lymphocytes against specific foreign antigens to activate cellular and humoral immune responses. LNs have thus become an attractive target for delivery of vaccines and immunotherapies. Unfortunately, most vaccine strategies result in inefficient, transient delivery of antigen and adjuvants to the lymphoid tissue.[57] Approaches that improve the targeting and retention of vaccine components in LNs could therefore have a significant impact on the potency and efficiency of new vaccines.

One strategy for circumventing the challenge of LN targeting that has demonstrated great interest in new clinical trials is direct, intra-LN (*i.LN.*) injection.[58-60] These trials employed ultrasound guidance to deliver vaccines to LNs as a simple outpatient procedure. Compared to traditional peripheral injection routes, this approach resulted in significant dose-sparing and improved efficacy in therapeutic contexts including allergies and cancer.[58-60] These studies employed *i.LN.* injection of soluble vaccines (i.e., biomaterial-free) which were rapidly cleared by lymphatic drainage. Therefore, multiple injections – or cycles of multiple injections – were administered to achieve these impressive therapeutic effects. Improved retention in the LN could

[2] Adapted from J. I. Andorko*, L. H. Tostanoski*, E. Solano, M. Mukhamedova, and C. M. Jewell, "Intra-lymph node injection of biodegradable polymer particles." *Journal of Visual Experiments* 2014, 83, e50984. (* designates equal contribution)

enhance the interaction between antigen and/or adjuvant and immune cells, further improving the potency of immune cell priming. This potential is supported by recent studies that show kinetics of antigen and adjuvant delivery play a critical role in determining the specific immune response generated.[27, 61, 62] Further, localizing and minimizing drug and vaccine doses could reduce or eliminate systemic effects, such as chronic inflammation.

Biomaterials have been studied extensively to enhance the potency and efficiency of vaccines.[57, 63, 64] Encapsulation in or adsorption on biomaterial carriers can physically shield cargo from degradation and overcome solubility limitations. Another notable feature of biomaterial carriers, such as polymeric micro- or nano-particles, is the ability to co-load several classes of cargo and, subsequently, release these cargos over controlled intervals. However, a significant limitation that continues to hinder biomaterial vaccines and immunotherapies *in vivo* is inefficient targeting of immune cells and limited trafficking to lymph nodes. For example, peripheral injection of biomaterial vaccines through conventional routes (e.g., intradermal, intramuscular) typically exhibit poor LN targeting, with up to 99% of the injected material remaining at the site of injection.[60, 65] More recently, the size of biomaterial vaccine carriers has been tuned to improve preferential trafficking or drainage of these vaccines to LNs through interstitial flow.[63, 65] These advances have led to enhanced cellular and humoral immune responses, underscoring the importance of targeting and engineering the LN environment for new vaccines.

This paper presents a vaccination protocol that combines lipid-stabilized polymer particles and *i.LN.* delivery to generate controlled release vaccine depots.[27, 66] Building on recent studies employing surgical techniques for *i.LN.* in mice,[61, 62, 67, 68] we developed a quick, non-surgical strategy for injecting biomaterial vaccines in small animals.[27] Combining *i.LN.* delivery with biomaterial vaccine carriers potently enhanced CD8 T cell response within 7 days after a single injection of controlled release vaccine depots.[27] A strong humoral response (i.e., antibody titers) was also generated; and both enhancements were linked to increased retention of vaccine components in lymph nodes that was mediated by controlled release from the biomaterial carriers. Interestingly, the size of vaccine particles altered the fate of these materials once in the LNs: nanoscale particles showed heightened direct uptake by cells, while larger microparticles remained in the extracellular LN environment and released cargo (e.g., adjuvant) that was taken up by LN-resident antigen presenting cells.[27] These data suggest two pathways that could be exploited for new vaccines by controlling the size of biomaterials injected *i.LN.*

In this article biodegradable lipid-stabilized polymer particles (micro- and nano-scale) are synthesized using a modified double emulsion strategy.[27, 66] Particle properties are characterized by laser diffraction and microscopy. These particles are then injected directly into the inguinal LNs identified non-surgically using a common, non-toxic tracer dye.[69] Post-injection analysis of LNs by histology or flow cytometry can be used to verify the distribution of particles within the LN environment, as well as to monitor cellular uptake and retention of particles over

time. For protocols detailing histological processing and flow cytometry, readers are referred to recent *JoVE* articles and journal reports.[70-77] Typical results demonstrate local LN targeting of these depots that could be exploited to achieve potent, efficient immune responses or to tailor immunity for target pathogens.

3.2. Materials and Methods

3.2.1. Study approval

All animal studies in this protocol were completed in compliance with federal, state, and local guidelines, and using protocols reviewed and approved by the University of Maryland's institutional animal care and use committee (IACUC).

3.2.2. Synthesis of lipid-stabilized micro- and nanoparticles

In a 7mL glass vial, combine a 60:20:20 molar ratio of DOPC, DSPE-PEG, and DOTAP lipids, dry under a gentle stream of nitrogen, and store at -80 °C until use. For each batch of particles, dissolve 80 mg of PLGA in 5mL of dichloromethane and add to a vial containing dried lipids. Cap the vial and vortex for 30 seconds to prepare the organic phase. To synthesize microparticles, sonicate the organic phase containing the polymer, lipid, and any other water-insoluble cargos (e.g., hydrophobic small molecule drug) on ice at 12 W using a sonicator. Create the water-in-oil emulsion using a pipette to add 500 μL of water, or water containing water-soluble cargo (e.g., peptide, protein), to the organic phase. Continue sonicating for 30 seconds at 12 W on ice, gently rocking the vial up and down and side to side around the sonicator tip to ensure complete emulsification. Create a water-in-oil-in-water emulsion by pouring

the water-in-oil emulsion into 40 mL of water in a 150 mL beaker. Homogenize for 3 minutes at 16,000 rpm using a digital homogenizer. Add a magnetic stir bar, transfer the beaker to a stir plate, and allow the complete emulsion to stir overnight to remove the excess solvent.

To synthesize nanoparticles instead, prepare the phases, as above, and sonicate the organic phase and inner aqueous phase on ice at 14 W for 30 seconds to prepare the water-in-oil emulsion. Next, pour the emulsion into 40 mL of water and sonicate at 16 W on ice for 5 minutes to generate the final water-in-oil-in-water emulsion and stir overnight to evaporate excess solvent, as above.

After overnight stirring, wash and collect the micro- or nanoparticles. Pour the emulsion through a 40 μm nylon mesh cell strainer affixed to a 50 mL conical tube. Centrifuge the particles for 5 minutes at 5,000 x *g* or 24,000 x *g* for microparticles or nanoparticles, respectively. Decant the supernatant and wash the particles by re-suspending in 1mL of water, then transfer the entire volume to a 1.5 mL microcentrifuge tube. Centrifuge for 5 minutes at 5,000 x *g* or 24,000 x *g* for micro- or nanoparticles, respectively. Wash the particles two more times by decanting the supernatant and re-suspending in 1 mL of fresh water, centrifuging in between, as above. After washing, suspend particles in 1 mL of water or PBS for immediate use, or lyophilize for extended storage.

3.2.3. Microparticle characterization

To measure particle yield, transfer a known volume (e.g., 100 μL) of the final particles suspension to a pre-weighed vial. Dry the vial under a gentle stream of air or lyophilize. Weigh the vial containing the dried particles and calculate the particle weight by subtracting the original weight of the empty vial. Determine total particle yield for the batch by dividing the dry particle mass in the vial by the fraction of total volume removed for the aliquot. To determine percent yield, divide the total particle mass by the maximum theoretical input mass and multiply by 100%. To measure particle size by laser diffraction, dilute the particle suspension into a blanked fraction cell to appropriate signal strength, indicated by the software interface, and record size using the relevant refractive index (e.g., 1.60 for PLGA).

3.2.4. Preparation of mice for i.LN. injection

Prepare a tracer dye working solution by dissolving Evans blue at 0.1% weight per volume in water. Sterilize the dye solution into a glass vial using a 0.2 μm syringe filter. One day prior to injection, anesthetize the mouse using isoflurane according to an IACUC-approved animal protocol. To evaluate the depth of anesthesia, perform a toe pinch reflect test and monitor breathing rate. Shave the fur at the base of the tail and the hindquarters while the mouse is anesthetized. Remove the fur from the ventral size of the animal, as well as laterally around the dorsal side just above the joint of the hind limb. For each dye injection, use a micropipette to transfer 10 μL of dye solution into a microcentrifuge tube, and aspirate the entire 10 μL into a 31 gauge needle

attached to a 1 mL syringe. Inject 10 μL of dye solution subcutaneously on each side of the tail base where the hair was clipped, reloading in between injections. Complete the hair removal by applying a mild depilatory cream with cotton swabs. Ensure to coat the area between the hind thigh and abdomen. Allow the depilatory cream to incubate on the skin for three minutes. After incubation, wet a gloved hand with warm water and gently rub the depilatory cream into the skin. Immediately remove the depilatory cream with a wet gloved hand and repeat until excess depilatory is removed, making sure to keep hand wet to avoid irritation. Remove any residual depilatory from the mouse by wetting a soft cloth or paper towel with warm water and, in a single motion, wiping lower portion of mouse. Avoid a rubbing motion to prevent abrasion or skin damage to the mouse. Allow the mouse to recover under a heat lamp and return to holding.

3.2.5. i.LN. injection of particles

On the following day, anesthetize the mouse using isoflurane according to an IACUC-approved animal protocol. Examine the mouse to confirm drainage of the tracer dye into each inguinal lymph node. The lymph node should be visible as a dark spot near the hind thigh and abdomen. To prepare the particle solution injections, resuspend the particles in distilled water at the desired injection concentration. For each injection, use a micropipette to transfer 10 μL of the particle solution into a microcentrifuge tube and aspirate the entire 10 μL into a 31 gauge insulin needle attached to a 1 mL syringe. After visualizing the LN, tighten the skin around the LN using the thumb, index finger, and middle finger to pull the skin taught and allow for

controlled placement of the injection volume. Approach the LN with the needle at a 90° angle to the skin and penetrate the skin to a depth of 1 mm. Slowly inject the entire volume, while observing the LN through the skin to confirm injection by visible LN enlargement. Allow the mouse to recover under a heat lamp and return to holding or conduct additional testing.

3.3. Representative Results

Expected results for the protocols presented in this manuscript can be divided into three categories: particle synthesis, animal preparation and particle injection.

Figure 3.1 depicts the synthesis and characterization of biodegradable polymer particles, stabilized by amphiphilic lipids. Results of the emulsion/solvent evaporation synthesis protocol (**Figure 3.1A**) can be qualitatively assessed by visual inspection of the final emulsions generated; particle batches should be homogenous, stable emulsions with an opaque appearance. Complications include emulsions that cream or flocculate, often due to improper storage of lipid stabilizers. To avoid this instability, lipids should be stored at -80 °C in a dehydrated state or in a sealed vial purged with nitrogen. Quantitative assessment of particle synthesis can be performed using laser diffraction or dynamic light scattering to analyze size distribution (**Figure 3.1B**). Expected results include tightly-distributed, monomodal particles, indicating a uniform population of particles. The synthesis parameters described in this manuscript generate number averaged distributions centered at approximately 100 nm or 3 μm for nanoparticles and microparticles, respectively. Further qualitative

assessment of particle synthesis can be achieved through modification of the above protocol to incorporate multiple classes of fluorescent cargo. In **Figure 3.1C**, microscopy images of microparticles loaded with a fluorescent peptide (FITC, green), a lipophilic dye (DiD, red), and an overlay image (yellow) confirm creation of particles within the desired size range and encapsulation of peptide within the volume of the particle.

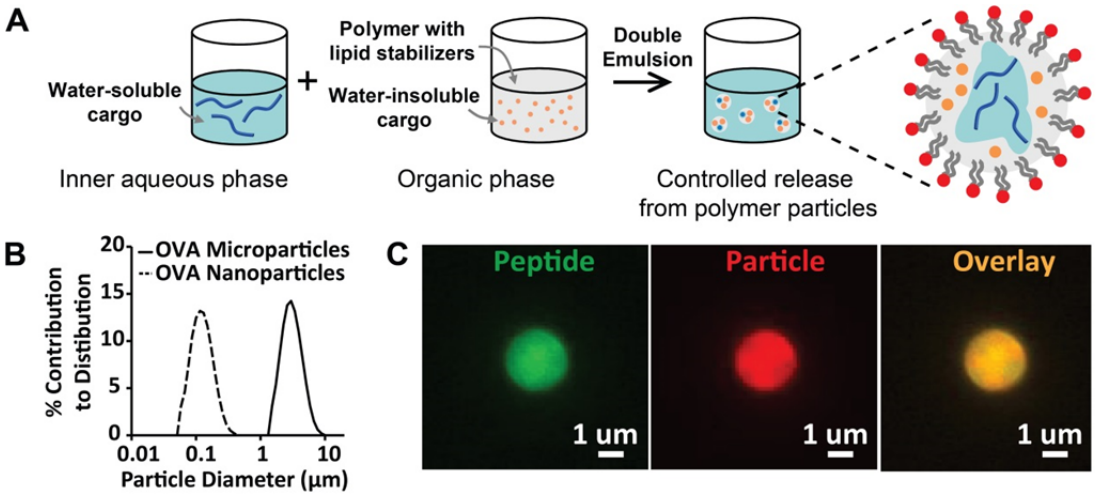

Figure 3.1 Synthesis and Characterization of Lipid Stabilized Particles.
A) Schematic diagram describing the synthesis of lipid-stabilized particles prepared by emulsion/solvent evaporation. B) Size distributions of microparticles (solid line, diameter = 2.8 µm) and nanoparticles (dashed line, diameter = 113 nm). C) Fluorescent microscopy images of particles loaded with fluorescently-labeled peptide and a fluorescent particle dye. Labels: peptide (green) and particle (red).

The first two panels of **Figure 3.2** summarize the expected results of animal preparation for the *i.LN.* injection strategy described in this paper. The methodology involves marking inguinal LNs by peripheral injection of a non-toxic tracer to identify the location for subsequent *i.LN.* injection of particles (**Figure 3.2A**).[27] As noted, drainage of the tracer dye following subcutaneous injection at the tail base will enable visualization of the inguinal LNs (**Figure 3.2B**).[27] Injection of approved depilatory creams can pose hazards to the mice. Thus, care should be taken to

thoroughly remove all cream applied, paying particular attention to paws, and the ventral side of the mice. Depilatory should be removed using a wet, soft cloth or wet paper towel in a single, smooth motion. Avoid rubbing to remove cream, as this can lead to abrasions on the exposed skin of the mice.

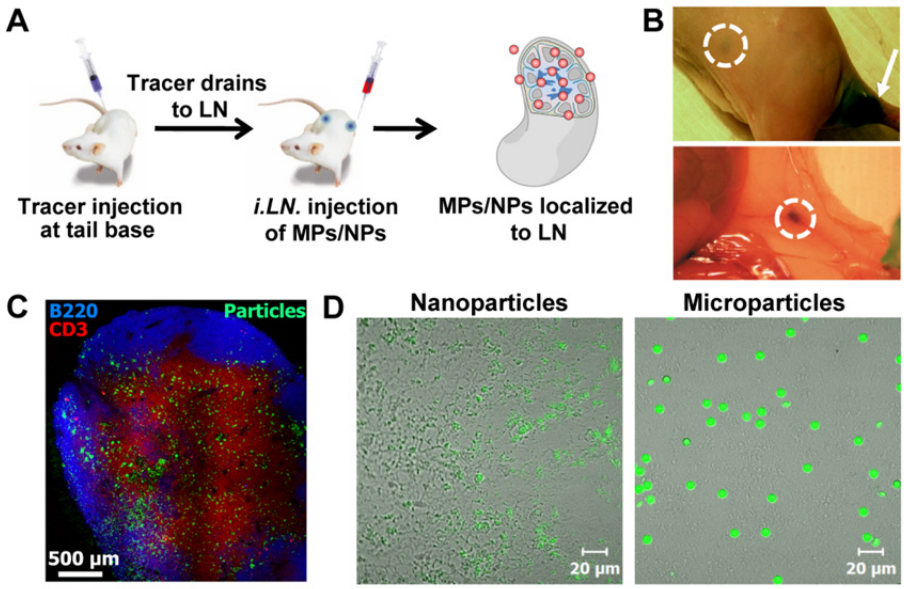

Figure 3.2 Injection and Distribution of Biodegradable Particles within LN.
A) Methodology for *i.LN.* injection. B) Visualization of LNs in a mouse through skin (upper image) and following necropsy (lower image).Adapted from [27] C) Histological staining of a LN confirming deposition and distribution of fluorescently-labeled polymer microparticles (particles, green; T-cells, red; B-cells, blue). C) Fluorescently-labeled nanoparticles (50 nm, left image) and microparticles (6 µM, right image) in LNs 24 hours after injection.

Confirmation of local of delivery to the inguinal LN can be evaluated through observational or histology. The LN volume can be monitored visually during injection as an indicator of successful injection. Expected results include efficient cargo distribution throughout the LN structure, without significant leakage to adjacent tissues or cells. Further, as injected fluid displaces/dilutes the tracer in the LN, dye concentration/coloring should become less intense after injection. Observation of the tissue should reveal an intact, but enlarged LN due to fluid injection. Potential

challenges include injecting too rapidly or missing the LN, both of which can cause elution of the volume into surrounding subcutaneous tissue. These undesirable outcomes can be confirmed by necropsy or histology, where the particle suspension will be observed spreading to cells and tissue remote from nodes targeted for injection. In contrast, an expected result would be the identification of an enlarged inguinal LN due to containment of particles within the LN structure. Histological processing of excised LNs can definitively confirm delivery of cargo to the lymphoid tissue, as shown in **Figure 3.2C** and **3.2D**. Note that the particles in **Figure 3.2** incorporate fluorescent cargo to allow for visualization of cargo during injection, as well as during histological processing and fluorescent microscopy.

3.4. Discussion

The technique described in this protocol allows controlled delivery of vaccines to LNs and to LN-resident antigen presenting cells. Biomaterial encapsulated cargo can be localized within the LN, enabling manipulation of the doses of one or more types of cargo delivered to the LN microenvironment. The localization and controlled release from polymer particles has been shown to generate a potent cellular and humoral immune response at significantly lower doses than conventional approaches. Further, through the manipulation of biomaterial carrier size, the primary mode of cellular processing can be modulated between direct uptake of nanoparticles or extracellular cargo release from larger microparticles.[27] These results establish the feasibility of *i.LN.* biomaterial delivery as a platform for therapeutic vaccine delivery.

The synthesis of PLGA particles by emulsion/solvent evaporation has been widely employed in drug delivery applications.[78, 79] Thus potential challenges associated with this technique relate mostly to successful identification and deposition of vaccines in the LN target site. Although the use of tracer dye facilitates the visualization of the targeted inguinal LNs, the target size and depth beneath the skin are small. Thus, the authors recommend allotting time and mice for practicing the preparation and injections of mice. During animal preparation (i.e., shaving and application of depilatory), care should be taken not to cut the mice on the ventral side of the animal where the angle of the leg with the abdomen makes the skin more prone to injury from clippers. Additionally, all depilatory should be removed with warm water to prevent animals from ingesting the cream during normal grooming behavior. To practice LN injections, a higher tracer dye concentration can be administered and practice animals can be euthanized, and then injected multiple times. Following injection mice can be necropsied and the size of LNs from injected animals can be compared with an uninjected control LN. One limitation of this technique is the physical limit of the injection volume that can be loaded into the LN structure. Our protocol suggests an injection volume of 10 μL in mice, though other studies have reported larger injection volumes at least as high as 20 μL.[68] However, direct delivery of vaccines to *i.LN.* permits dramatic dose-sparing so the function of these vaccines should generally not be limited by volume constraints.

As noted, changing the physical property of the particles (i.e., size) is an effective mechanism to alter the pathway or outcomes induced by biomaterials and

encapsulated cargos in LN tissue. The emulsion/solvent evaporation protocol can easily be modified to alter physical or chemical properties such as surface charge or functionality, and the rate of biodegradation/cargo release.[23,24] For example, the release kinetics can be tuned through alternative polymer compositions, and surface function can be altered using modified lipid compositions or poly(vinyl alcohol). The cargo loaded in particles can be easily manipulated to contain different antigens or adjuvants for target pathogens. The advantage of this approach is achieved through the combination of *i.LN.* delivery with local, controlled release of cargo from biomaterials. This synergy establishes a platform that can be exploited to efficiently generate adaptive immune responses using minute doses and with reduced non-specific/systemic side effects.

Chapter 4 describes Aim 1 of this dissertation, applying the technique described above to a new area: combatting autoimmune disease, specifically a mouse model of multiple sclerosis. As the direct injection approach enables control over the combinations, doses, and kinetics of signals present in LNs, we explored *i.LN.* delivery as a platform to examine the link between local LN signaling and the development of systemic, but myelin-specific tolerance.

Chapter 4. Reprogramming the local lymph node microenvironment promotes tolerance that is systemic and antigen specific[3]

4.1. Introduction

Multiple sclerosis (MS) is an autoimmune disease that occurs when self-reactive $CD4^+$ T cells enter the central nervous system (CNS), recognize myelin self-antigen, secrete inflammatory cytokines, and recruit additional infiltrating myelin-specific T cells and antibodies [80, 81]. These effects drive demyelination of neurons, destruction of oligodendrocytes, and loss of motor function that have traditionally been treated using non-specific, systemic immunosuppression [82]. The need for more effective and selective therapeutic options has sparked intense interest in vaccine-like strategies that promote myelin-specific tolerance [37, 83]. For example, several recent reports have studied administration of myelin, cytokines, or immunomodulatory drugs to bias T cell differentiation away from inflammatory subsets (e.g., T_H1, T_H17) and towards regulatory T cells (T_{REGS}) without broad suppression [34, 37, 84, 85]. Recently, nanoparticles (NPs) have been explored as carriers of self-antigens or tolerogenic signals [36, 39, 40, 43, 46, 47, 52, 54, 86] because biomaterials can enhance delivery and targeting of cell types (e.g., dendritic cells, DCs) that play an important role in controlling tolerance [4, 6, 34]. Findings from several studies indicate NP-mediated co-delivery of self-antigen and regulatory cues drives a synergistic effect in restraining mouse models of MS [47, 86]. However,

[3] Adapted from L. H. Tostanoski, Y. C. Chiu, J. M. Gammon, T. Simon, J. I. Andorko, J. S. Bromberg, and C. M. Jewell, "Reprogramming the local lymph node microenvironment promotes systemic antigen-specific tolerance." *Cell Reports* 2016, 16, 2940-2952.

other reports, such as those of Miller, Shea, and colleagues, demonstrate that NPs loaded with or displaying self-antigen alone can promote tolerance [39, 40, 87]. Thus, the unique role of each component in controlling self-reactivity is unclear. Whereas these past approaches used systemic or peripheral injection routes, here we used direct LN delivery as a tool to isolate the impact of self-antigen and regulatory cues on the local function of injected LNs, the resultant effects on non-treated tissues, and, ultimately, the progression of disease.

This approach is motivated by the fact that T cell polarization occurs in the spleen and lymph nodes (LNs), tissues that coordinate adaptive immunity [1], but that are anatomically distinct from the site of attack in MS and other tissue-specific autoimmune diseases. Thus, LNs play a critical role in defining the inflammatory or regulatory functions of T cells that eventually migrate to sites of disease. This relationship is further evidenced by the clinical success of natalizumab, a monoclonal antibody that non-specifically blocks lymphocyte migration across the blood-brain barrier [88], underscoring the link between pathogenic cells armed in the periphery and infiltration into the CNS to drive disease. In addition, a network of lymphatic vessels was recently discovered in the brains of mice and shown to communicate directly with peripheral LNs [13, 14]. This landmark finding suggests new routes by which myelin self-antigen might exit the CNS for processing in draining LNs, where the local microenvironment controls the response to incoming antigens. However, direct study of the link between local LN signaling and systemic tolerance has

previously been hindered by poor control over how therapeutic cues are trafficked to and processed in LNs following injection via conventional routes.

We recently reported that direct, intra-LN (*i.LN.*) delivery of degradable polymer depots can be used to retain encapsulated adjuvants in LNs and drive potent expansion of antigen-specific effector T cells against model antigens [27, 89]. We hypothesized this platform could be exploited to study how spatially-localized self-antigen and tolerogenic immune cues in LNs impact the progression of autoimmune disease. Since many vaccines and immunotherapies must ultimately reach LNs or spleen for efficacy, this knowledge could inform new therapies, irrespective of injection route, while also indicating the clinical potential of controlling local LN function with polymer depots. Using two immune cues widely-studied in recent tolerogenic vaccines – a peptide fragment of myelin oligodendrocyte glycoprotein (MOG) and rapamycin (Rapa) – we show that a single *i.LN.* dose of particles administered at the peak of disease reverses disease-induced paralysis. In our studies, efficacy is dependent on localization of depots to LNs, requires encapsulation of myelin self-antigen, and is enhanced when Rapa is co-incorporated in depots along with MOG. Underlying the functional effects is a local reorganization in cell composition of the injected LNs that results in systemic restraint of inflammation and polarization of $CD4^+$ T cells toward T_{REGS}. These changes are also accompanied by formation of tolerogenic structural subdomains in both treated LNs and non-treated CNS-draining LNs, as well as a decrease in the frequency of T cells infiltrating CNS tissue.

4.2. Materials and Methods

4.2.1. Materials and Reagents

Myelin oligodendrocyte glycoprotein (MOG_{35-55}, MOG) and ovalbumin ($OVA_{323-339}$, OVA) peptides, with or without a fluorescein isothiocyanate (FITC) tag conjugated to the N-terminus, were synthesized by GenScript at ≥ 98% purity. Poly(lactide-co-galactide) (PLGA) and poly(vinyl alcohol) (PVA) were purchased from Sigma. Rapamycin (Rapa) was purchased from LC Laboratories. Antibodies for flow cytometry, including CD16/CD32, V450 CD4 (clone RM4-5), PE-Cy7 CD25 (clone PC61), Alexa Fluor 488 Foxp3 (clone MF23), PE-Cy7 CD3 (clone 145-2C11), FITC CD4 (clone RM4-5), PE CD8 (clone 53-6.7), PE F4/80 (clone T45-2342) and allophycocyanin-Cy7 CD11c (clone HL3), were purchased from BD Biosciences.

4.2.2. Particle synthesis

Double emulsion/solvent evaporation was used to generate degradable PLGA microparticles (MPs) as previously reported [27, 89]. Briefly, an inner aqueous phase was prepared as either 500 μL of water or 1 mg of peptide (i.e., MOG or OVA) dissolved in 500 μL of water. The inner aqueous phase was sonicated with an organic phase comprised of 80 mg of PLGA dissolved in 5 mL of dichloromethane for 30 seconds at 12 W to form a water/oil emulsion. In MP formulations containing Rapa, polymer solution was added to a vial containing 2 mg of dried drug before sonication to incorporate Rapa into the organic phase. For all formulations, the primary emulsion was homogenized with 40 mL of 2% PVA for 3 minutes at 16,000 RPM to form final, stabilized double emulsions. Particles were stirred for 16 hours to allow for solvent

evaporation. After 16 hours, MPs were poured through a 40 μm cell strainer to remove any aggregates and collected by centrifugation (5 minutes, 5000 *g*, 4°C). The supernatants were decanted and MPs were washed three times with 1 mL of water, collecting by centrifugation between each wash, and resuspended in water.

4.2.3. Particle characterization

Particle size was measured using an LA-950 laser diffraction size analyzer (Horiba). A known aliquot of MPs was dried under air and the dry mass was used calculate total particle yield and normalized to the polymer input (i.e., percent yield). The loading of peptide was quantified via Micro BCA™ Protein Assay Kit (Thermo Scientific Pierce) as previously described [90]. The loading of Rapa was measured via UV/Vis spectrophotometry after dissolution of a known mass of dried particles in dimethyl sulfoxide. For all cargos, standard curves of known concentrations were used to calculate loading, reported as the mass of cargo per mass of particles and normalized to the input to synthesis (i.e., encapsulation efficiency). For studies involving immunofluorescent analysis of intra-nodal MP deposition, fluorescently tagged MOG peptide (FITC-MOG) was incorporated into the inner aqueous phase and 10 μL of a fluorescent dye (Vybrant® DiI Cell-Labeling Solution, Molecular Probes) was added to the organic phase of MP synthesis to enable visualization of particles and encapsulated cargo in tissue sections.

4.2.4. EAE Induction and monitoring

Experimental autoimmune encephalomyelitis (EAE) was induced in 10-11 week old female C57BL/6J mice (The Jackson Laboratory) according to the manufacturer's instructions (Hooke Laboratories). Briefly, on day 0, mice were administered two subcutaneous injections of an emulsion of Complete Freund's Adjuvant and a peptide fragment of MOG (MOG_{35-55}). Two and 24 hours later, mice were administered pertussis toxin via intra-peritoneal injections. Beginning seven days after induction, mice were monitored daily for weight fluctuation and symptoms of paralysis, which were assigned a clinical score to reflect disease severity (0 – no symptoms, 1 – limp tail, 2 – hind limb weakness, 3 – hind limb paralysis, 4 – full hind limb and partial front limb paralysis, and 5 – moribund). Incidence of disease was defined as the first day a mouse exhibited a clinical score >0 and was reported as the percentage of mice in each group with detectable symptoms of disease over time. Mean maximum score of each group was calculated by averaging the maximum score reached throughout the duration of the experiment of each mouse.

4.2.5. Immunizations

Doses of MP formulations were administered via non-surgical, direct intra-lymph node injection as we previously described [27, 89]. Briefly, one day prior to injection, mice were administered a bilateral injection of tracer dye (Evans blue, Alfa Aesar) subcutaneously at the tail base and their fur was removed with a mild depilatory cream. On the day of treatment, each mouse received a single dose of indicated MP formulations, dissolved in the appropriate final injection volume (2 x 10μL).

Immunizations were administered as bilateral injections to the inguinal LNs, with each LN receiving half of the total dose. Irrespective of formulation, each mouse was treated with 2 mg of MPs (i.e., 1 mg per LN), containing the indicated cargos at the levels shown in **Table 4.1**. In control studies, matched masses of MPs were administered via bilateral intra-muscular (*i.m.*) injections in the caudal thigh, with injection volumes adjusted to 2 x 25 μL.

4.2.6. Tissue processing

At indicated time points, injected inguinal LNs, spleen and, in some cases, non-treated axillary and brachial LNs were excised and processed by manual dissociation through a 40 μm cell strainer. Cells were collected by centrifugation (5 min, 800 *g*, 4°C). Spleen samples were resuspended in Ack lysing buffer (Invitrogen) to remove red blood cells, and then washed with PBS. LN cells were washed with PBS without lysis. Cells were counted using an automated cell counter (NanoEnTek) or counting beads according to the manufacturer's instructions (BD Biosciences) and either plated for *ex vivo* restimulation assays or analyzed immediately by flow cytometry.

4.2.7. Ex vivo restimulation assays

To characterize cellular response after encounter of disease-relevant (i.e., MOG) or irrelevant (i.e., OVA) antigen, a uniform number of cells (1 x 10^6) was plated from each tissue sample in duplicate. One well was restimulated in culture with MOG (25 μg/mL) and the second well received a matched dose of OVA peptide. After 48 hours of incubation, culture supernatants were collected for analysis by ELISA.

4.2.8. ELISA

All ELISA assays were performed according to the manufacturer's instructions for IL-17 (R&D Systems), GM-CSF (R&D Systems), and IFN-γ (BD Biosciences) detection. Supernatants were collected from cell culture samples and analyzed at 1-20x dilutions.

4.2.9. Flow cytometry experiments

Immediately after tissue excision and processing, cells were washed with 200 μL 1% BSA in 1xPBS, resuspended in Fc block (anti-CD16/CD32) and incubated for 10 minutes at room temperature to inhibit non-specific binding. Cells were then incubated with indicated antibodies against cell surface markers, including CD3, CD4, CD8, F4/80, CD11c, and CD25. Cells were washed to remove unbound antibody, then either stained for viability (DAPI, Invitrogen) and analyzed immediately, or fixed and permeabilized to enable staining for intracellular markers (i.e., transcription factors). After fixation and permeabilization (Foxp3/Transcription Factor Staining Buffer Set, eBioscience), cells were stained for expression of Foxp3, then washed and analyzed. All analysis was performed on a FACS Canto II (BD Biosciences) and data analysis was conducted using Flowjo v. 10 (Treestar).

4.2.10. Immunofluorescent analysis

At indicated time points, treated inguinal LNs, non-treated cervical LNs, or spinal cords were excised and immediately submerged in OCT compound (Tissue-Tek) and frozen. Cryosections were cut at 6 μm using a Microm HM 550 cryostat (Thermo

Fisher Scientific Inc.). Sections were fixed with cold acetone for 5 minutes, then washed with PBS and blocked with 5% donkey serum (Sigma) and 5% goat serum (Sigma) in PBS for 30 minutes. Following a PBS wash, samples were stained for 1 hour with primary antibodies against indicated markers, including T cells (CD3e, Rb pAb, Abcam), B cells (B220, clone RA3-6B2, eBioscience), DCs (CD11c, Ham pAb, BD Pharmingen), high endothelial venules (HEVs) (PNAd, clone MECA-79, BD pharmingen), stroma (ER-TR7, clone sc-73355, Santa Cruz Biotechnology) and Foxp3 (Rb pAb, Abcam). Sections were washed once with PBS, and fluorescently-conjugated secondary Ab was applied for 45 minutes. Slides were washed 3 times in PBS for 5 minutes, fixed with 4% paraformaldehyde (Electron Microscopy Sciences) and treated with 1% glycerol in PBS before mounting with Prolong Diamond Antifade Mountant (LifeSciences) – in some cases containing DAPI – and imaged using a confocal microscope.

For quantitative analyses, tissues were collected five days after *i.LN.* injection (i.e., day 15) of either empty MPs or MOG/Rapa MPs (n=4 mice; 8 injected inguinal LNs, at least 16 cervical LNs, 4 spinal cords). Quantitative analysis was performed on images of treated inguinal LNs, cervical LNs, and spinal cords using Volocity image analysis software (PerkinElmer). For LN analyses, the percentage of $CD11c^+$ area was defined as the fraction of tissue area staining positive for CD11c among cortical ridge area, defined as area positive for ER-TR7. The threshold for positive area for both signals was defined using appropriate iso-type control-stained sections. The number of $Foxp3^+$ cells among the cortical ridge was similarly quantified using an

iso-type control to define positive cells. In spinal cord analyses, the percent $CD3^+$ area was defined as the fraction of area staining positive for CD3 among total spinal cord area imaged. Similarly, an iso-type control was used to set the threshold for positive area. All quantitative analysis was performed on at least 20 images of LN or spinal cord per MP formulation and statistical analyses were performed using two-tailed student's *t* tests.

4.2.11. In vivo study design

On the day of induction, mice were screened to identify animals with the most consistent starting body weights to be included in the study. Mice were then induced with EAE, as described above, and randomized into treatment groups. In studies involving late-stage therapy, the clinical scores of mice were assessed and mice were randomized into two groups with equivalent mean scores just before treatment. Mice were removed from studies according to humane endpoints, including loss of $\geq 25\%$ of initial (day 0) body weight, presentation with a clinical score of 4 for two consecutive days, or presentation with a clinical score of 4.5 or 5 on a single day. In mechanistic studies designed to investigate the kinetics of disease or tolerance, mice were induced with EAE, randomized into groups, and identically-treated groups of mice were euthanized at indicated time points for analysis. Data collection and analyses were not blinded and no outliers were excluded.

4.2.12. Statistics

Student's *t* tests were used in comparisons of two groups and ANOVA was used to compare three or more groups, with post-test corrections for multiple comparisons as indicated in figure captions. Log-rank tests were used in analyses of disease incidence or persistence. All tests were two-sided analyses and were performed using GraphPad Prism software. Error bars in all panels represent mean ± SEM and p values ≤ 0.05 were considered significant.

4.2.13. Study approval

All animal studies were carried out under the supervision of the University of Maryland IACUC in compliance with local, state, and federal guidelines.

4.3. Results

4.3.1. i.LN. injection of depots co-loaded with MOG and Rapa confers synergistic restraint of autoimmunity

Our previous studies using inflammatory signals for pro-immune vaccination revealed that particles with diameters of several microns or more maximized retention in LNs following *i.LN.* injection [27]. Thus, a double-emulsion process was used to prepare degradable poly(lactide-co-glycolide) microparticle (MP) depots in this size range, encapsulating various combinations of MOG and Rapa. MP formulations were then introduced into the inguinal LNs of mice [27, 89] utilizing a common model of MS, experimental autoimmune encephalomyelitis (EAE). We used this approach to study the local impact of each component on treated nodes, corresponding changes in

non-injected LNs, spleen, and CNS, as well as how these effects alter the nature and specificity of systemic tolerance during CNS autoimmunity (**Figure 4.1A**).

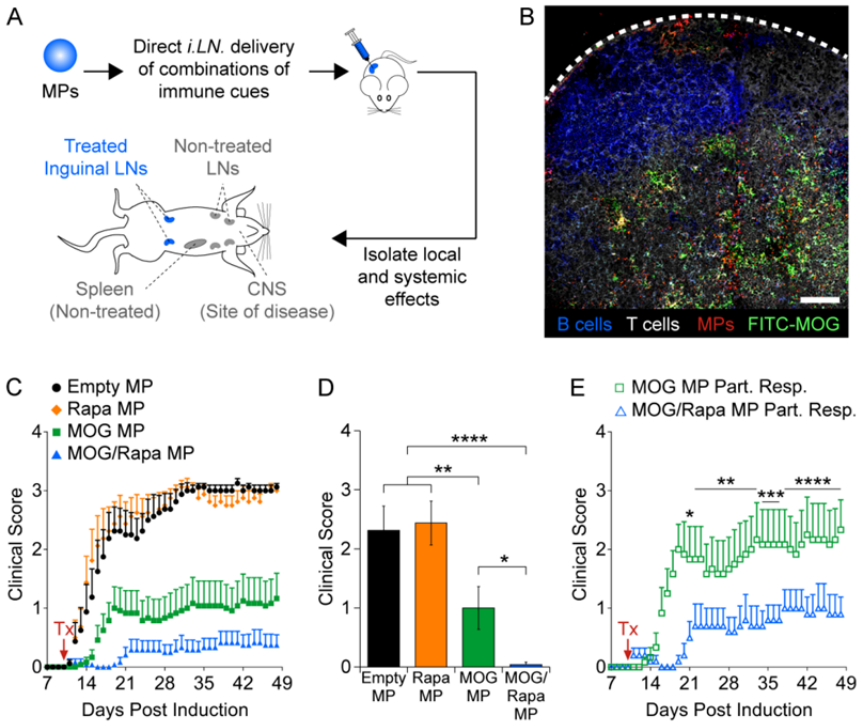

Figure 4.1. Intra-nodal injection of MPs to promote tolerance.
(A) Direct control over LN signaling via i.LN. injection of MPs encapsulating immune cues. (B) Immunofluorescent image of inguinal LN excised 30 min after i.LN. injection with fluorescent MPs (red) encapsulating fluorescent MOG peptide (green) and Rapa. B cells (B220, blue), T cells (CD3e, white), Scale bar: 100 µm. (C) Mean clinical score of mice induced with EAE and treated i.LN. on day 10 (Tx, red arrow) with empty MPs (n = 8), MOG MPs (n = 12), Rapa MPs (n = 8) or MOG/Rapa MPs (n = 12). Statistics are shown in panels (D) and (E) for clarity. (D) Mean clinical scores at day 19. (E) Mean clinical scores of mice in (C) that developed symptoms ("Part. Resp.") after MOG MP or MOG/Rapa MP treatment. Statistical analysis in (D) was performed using one-way ANOVA with a Tukey post-test and in (E) using multiple t tests, one at each time point, with a Holm-Sidak post-test correction for multiple comparisons. Data in all panels represent mean ± SEM (*, $p \leq 0.05$; **, $p \leq 0.01$; ***, $p \leq 0.001$; ****, $p \leq 0.0001$). See also **Table 4.1** and **Figure 4.2, 4.3**.

Immunofluorescent analysis was first used to confirm *i.LN.* injection localized MPs in LNs. Fluorescently-labeled MPs and cargo were detected dispersed throughout the LN paracortex, without disrupting the classic arrangement of B and T cell zones (**Figure 4.1B**). Myelin self-antigen and Rapa are two of the most intensely studied molecules in tolerance therapies, having been explored independently in models of

MS, and also recently shown to exert synergistic effects when administered systemically [47]. Thus, we next designed experiments to decipher the roles of MOG and Rapa in the development and maintenance of tolerance following *i.LN.* injection. Mice were induced with EAE, then 10 days later – to mimic an early therapeutic intervention – immunized intra-LN with MPs encapsulating MOG, Rapa, or both (**Table 4.1**). A control group of empty MPs (i.e., polymer and stabilizer only) exhibited no significant effect on the severity of clinical scores compared with induced, untreated mice (**Figure 4.2**). Similarly, MPs encapsulating Rapa alone had no impact on EAE measured by clinical score (**Figure 4.1C-D**), incidence of disease (**Figure 4.3**), and weight loss – an indirect indicator of disease (**Figure 4.3**). In contrast, both MOG MPs and MOG/Rapa MPs markedly and permanently reduced the onset and severity of clinical EAE scores (**Figure 4.1C, 4.3**) and weight loss (**Figure 4.3**), with co-loaded MPs conferring a synergistic therapeutic effect in attenuating disease severity. In particular, at time points corresponding to the development of EAE symptoms in MOG MP-treated mice, MOG/Rapa MP-treated mice remained almost completely asymptomatic (**Figures 4.1D, 4.3**). Although MOG/Rapa MPs generally delayed disease onset relative to MOG MPs, there was only a modest difference in the final incidence of disease between the two groups, 33.3% versus 50%, respectively (**Figure 4.3**). The MOG/Rapa MP-treatment exhibited a trend of less severe disease, with a 2.70 point reduction in final mean score relative to empty MP-treated mice, compared with a 1.90 point reduction in MOG MP-treated mice. However, most pronounced was the result that among mice that did develop disease, termed partial responders, MOG/Rapa MPs (final clinical

score of 0.90 ± 0.29) significantly decreased the severity of paralysis compared with MOG MPs (final clinical score of 2.33 ± 0.51; **Figure 4.1E**).

Table 4.1 Physical properties of microparticles (MPs) used in studies.
Percent yield of MPs was calculated using the dry mass of a known aliquot of final MP solution, and particle size was recorded via laser diffraction. Loading of MOG peptide and rapamycin were measured by microBCA and UV/Vis spectrophotometry, respectively, after particle dissolution and are reported per mass of particles and as encapsulation efficiencies. All measurements were pooled from five to six repeat particle synthesis and characterization experiments and represent mean ± SEM.

	Polymer Core		MOG Loading		Rapa Loading	
	% Yield	Diameter (μm)	μg MOG/ mg peptide	Encapsulation Efficiency	μg Rapa/mg peptide	Encapsulation Efficiency
Empty	63.3 ± 3.9 %	3.1 ± 0.4	N/A	N/A	N/A	N/A
MOG	58.5 ± 6.2 %	4.1 ± 0.9	8.5 ± 0.8	41.1 ± 7.1 %	N/A	N/A
Rapa	70.8 ± 3.1 %	3.3 ± 0.6	N/A	N/A	15.3 ± 1.3	43.2 ± 3.3 %
MOG/Rapa	63.3 ± 6.5 %	3.9 ± 0.6	7.3 ± 0.6	38.0 ± 5.8 %	16.9 ± 1.7	42.1 ± 4.8 %

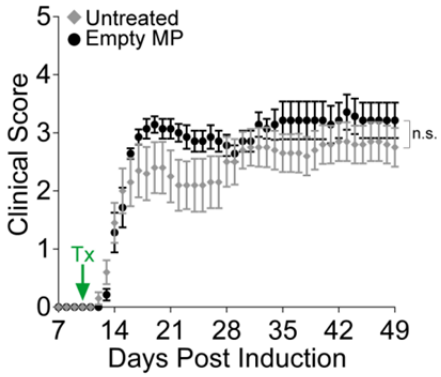

Figure 4.2 *i.LN.* injection of empty MPs does not alter typical progression of EAE,
Mean clinical score of mice induced with EAE (day 0) and either left untreated or administered a single intra-LN dose of empty MPs on day 10 (Tx, green arrow), monitored through day 49 post induction. Untreated, n = 10; Empty MPs, n = 7. Statistical analysis was performed using multiple t tests, one at each time point, with a Holm-Sidak post-test correction for multiple comparisons. Data are reported as mean ± SEM.

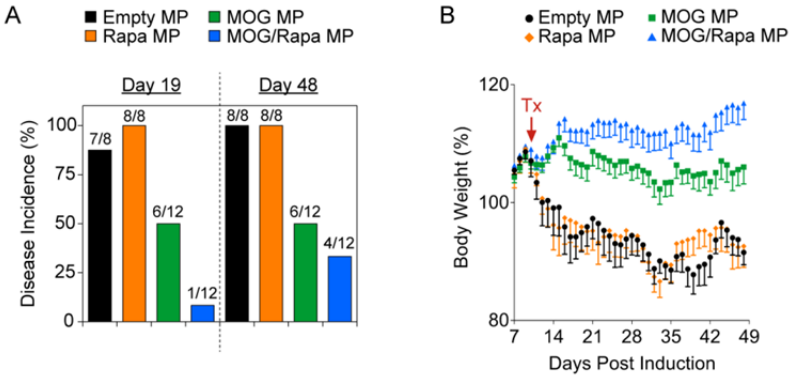

Figure 4.3 Co-delivery of self-antigen and Rapa confers synergistic restraint of EAE.
(A) Incidence of disease on day 19 (left) and day 48 (right) post EAE induction and (B) relative body weight over time in mice treated *i.LN.* on day 10 with empty MPs (n = 8), MOG MPs (n = 12), Rapa MPs (n = 8) or MOG/Rapa MPs (n = 12). Data in (B) are reported as mean ± SEM.

To assess the functional impact of *i.LN.* treatments on pathogenic cell infiltration into the CNS, spinal cords were collected five days after MP treatment (i.e., day 15 post EAE induction) and sections were analyzed for the frequency of T cells. As expected, we observed a significant infiltration of $CD3^+$ cells in empty MP-treated mice (**Figure 4.4A-B**). Consistent with clinical score data, Rapa MPs did not reduce $CD3^+$ cell infiltration, resulting in frequencies that were similar to that of sections from empty MP-treated mice. Both MOG MPs and MOG/Rapa MPs drove a significant reduction in infiltration compared with empty MP- and Rapa MP-treated mice (**Figure 4.4B**). Compared with MOG MPs, a trend of reduced infiltration was observed when co-loaded MPs were administered, though this result was not statistically significant. Thus, *i.LN.* delivery of MPs drove significant changes in the pathogenic T cell populations at a site that is anatomically distinct from the injection site, inguinal LNs, which are non-CNS draining nodes.

4.3.2. Localization of self-antigen and Rapa in LNs alters tissue composition

The decrease in T cells in the CNS motivated study of how the frequency and number of T cells changed in LNs, a key site of T cell expansion and polarization. To analyze the impact of these signals on the cellular composition of injected LNs, mice were treated on day 10, then flow cytometry was used to measure the frequency and number of T cell and antigen presenting cell (APC) populations in the treated LN (**Figure 4.4C**). MOG MPs, Rapa MPs, and MOG/Rapa MPs all drove a local decrease in the frequency of $CD4^+$ T cells compared with empty MP controls (**Figure 4.4D, 4.5**); this decrease was greatest in mice treated with MOG/Rapa MPs.

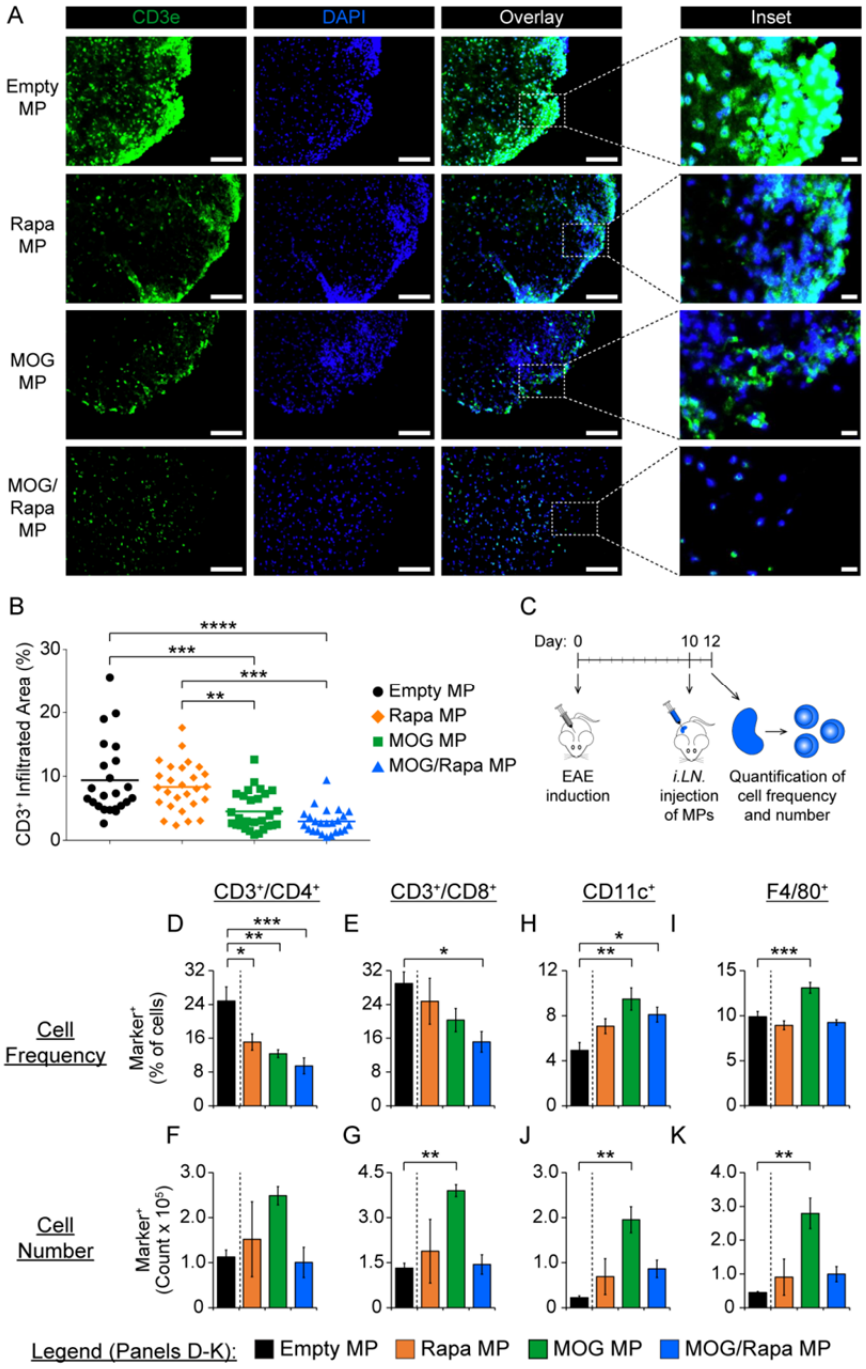

Figure 4.4 Intra-LN injection of MPs restrains inflammatory cell infiltration into the CNS and alters local cell compartments.

Mice were induced with EAE, treated *i.LN.* with the indicated MP formulations (n = 4) on day 10, then spinal cords were isolated on day 15. (A) Immunofluorescent analysis of sections of the spinal cord showing the expression of CD3 (green), DAPI (blue), and an overlay, Scale bar: 100 µm. An inset of the overlay channel is shown on the far right column, Scale bar: 10 µm. (B) Quantification of the frequency of $CD3^+$ cells in spinal cord sections shown in (A) following treatment with empty MPs (n = 23), MOG MPs (n = 28), Rapa MPs (n = 27) or MOG/Rapa MPs (n = 24). Statistical analysis in (B) was performed using one-way ANOVA with a Tukey post-test to compare the means of all groups. (C) In similar experiments, mice were induced with EAE, treated *i.LN.* with the indicated MP formulations (n = 4-6) on day 10, and then treated LNs were isolated two days later. The frequency of (D) $CD4^+$ T

cells ($CD3^+/CD4^+$), and (E) $CD8^+$ T cells ($CD3^+/CD8^+$) and the number of (F) $CD4^+$ and (G) $CD8^+$ T cells was quantified. (H) The frequency of macrophages ($F4/80^+$) and (I) dendritic cells ($CD11c^+$) and (J-K) the number of these populations in treated LNs was determined. Statistical analyses in (D-K) were performed using one-way ANOVA with a Tukey post-test to compare each group to empty MP-treated controls. Data in panels (D-K) represent mean ± SEM (*, $p \leq 0.05$; **, $p \leq 0.01$; ***, $p \leq 0.001$; ****, $p \leq 0.0001$). See also **Figure 4.5**.

MOG/Rapa MPs were also the only formulation that caused a significant decrease in the frequency of $CD8^+$ T cells in treated LNs (**Figure 4.4E, 4.5**). Despite the reduced frequencies in both T cell subsets, we observed a statistically similar number of cells in MOG/Rapa MP-treated LNs relative to empty MPs, and an increase in the number of $CD4^+$ (**Figure 4.4F**) and $CD8^+$ (**Figure 4.4G**) T cells following MOG MP treatment. This reduction in frequency, but similar or increased number of T cells, led us to hypothesize that another immune cell type (i.e., APCs) was increasing in both frequency and number to account for some or all of the remaining cell population. Relative to treatment of LNs with empty MPs, both MOG MPs and MOG/Rapa MPs significantly increased the frequency of cells expressing a classic DC marker (CD11c) (**Figure 4.4H**); Rapa MPs also increased the frequency of DCs, but not to a level that was statistically significant (**Figure 4.4H**). Similar outcomes were observed in analyzing the number of $CD11c^+$ cells (**Figure 4.4J**), as well as the number and frequency of cells expressing a classic macrophage marker (F4/80), but only MOG MPs caused a significant increase in these populations (**Figures 4.4I,K**). These results were generally consistent with the idea that T cell frequencies, but not numbers, decreased in treated nodes, while APC populations increased. Taken together, our findings in **Figures 4.1-4.5** confirm a critical role for self-antigen in controlling EAE – including reorganization of cellular composition in injected LNs and infiltration of T cells into the CNS – as well as a synergistic effect conferred by

inclusion of Rapa in depots. These results also suggest that therapeutic efficacy is antigen-specific and impacts both innate and adaptive responses. Thus, we selected the most potent formulation, MOG/Rapa MPs, to probe the local tissue- and cell-level changes in LNs that lead to systemic tolerance.

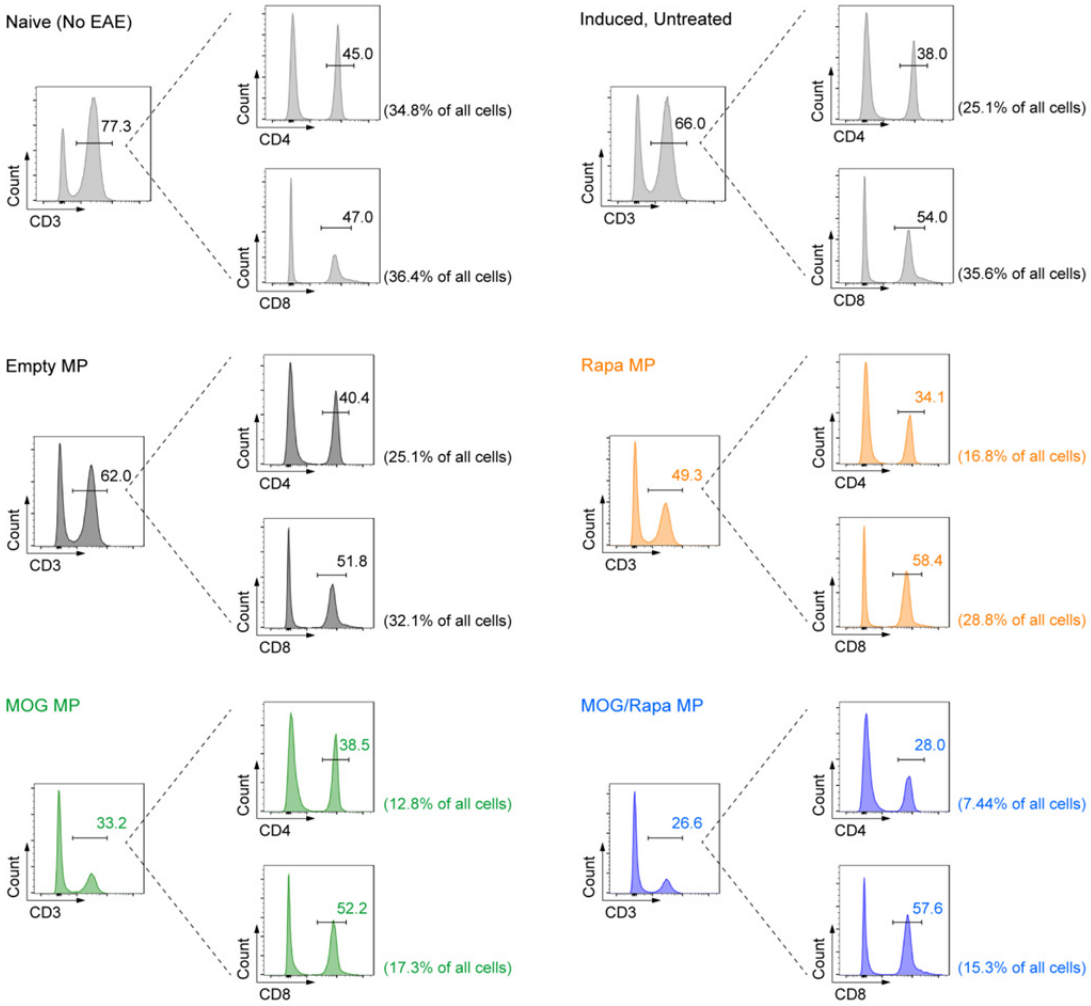

Figure 4.5 *i.LN.* delivery of MPs alters T cell frequency in treated LNs.
Mice were induced with EAE and treated on day 10 with empty MPs, MOG MPs, Rapa MPs, or MOG/Rapa MPs (n = 4-6 per group). Treated LNs were collected on day 12, processed into single cell suspensions and analyzed by flow cytometry. Representative histograms showing $CD3^+/CD4^+$ and $CD3^+/CD8^+$ T cells in injected LNs in **Figure 4.4D-K** are shown. In addition, histograms are shown for naïve mice (i.e., no EAE) and mice that were induced with EAE, but left untreated.

4.3.3. Localization of self-antigen and Rapa in LNs alters tissue organization and phenotype

To explore the local changes in the organization of treated LNs, mice were injected on day 10, then histological analysis was carried out on day 15 (**Figure 4.6A**). These experiments revealed a classic follicular organization of B cells and T cells with interspersed DCs in LNs treated with empty MPs (**Figure 4.6B**). In contrast, LNs injected with MOG/Rapa MPs exhibited increases in DCs (**Figure 4.6C**, red signal), consistent with flow cytometry results (**Figure 4.4H**). This finding motivated more quantitative study of LN structural organization following MP treatment. Thus, we prepared sections from replicate animal groups and analyzed the expression of CD11c, stromal features of LNs, and a prototypical T_{REG} marker, forkhead box P3 (Foxp3) (**Figure 4.6D**) among at least 20 sections as a function of area. Similar to preliminary tissue staining (**Figure 4.6B-C**) and flow cytometry (**Figure 4.4H**) results, calculation of the frequency of $CD11c^+$ area revealed a statistically significant increase following MOG/Rapa MP-treatment relative to empty MPs (**Figure 4.6E**). To assess whether these local changes in APCs were accompanied by altered expression or localization of T_{REGS}, we analyzed the number of $Foxp3^+$ cells per area in the cortical ridge of LNs (**Figure 4.6D**) – indicated by co-localization with a stromal marker, ER-TR7 – a structural microdomain associated with T_{REG} localization during tolerance [91]. Enumeration of Foxp3 staining revealed that relative to treatment with empty MPs, MOG/Rapa MPs drove a significant increase in the accumulation of $Foxp3^+$ cells in the cortical ridge (**Figure 4.6F**).

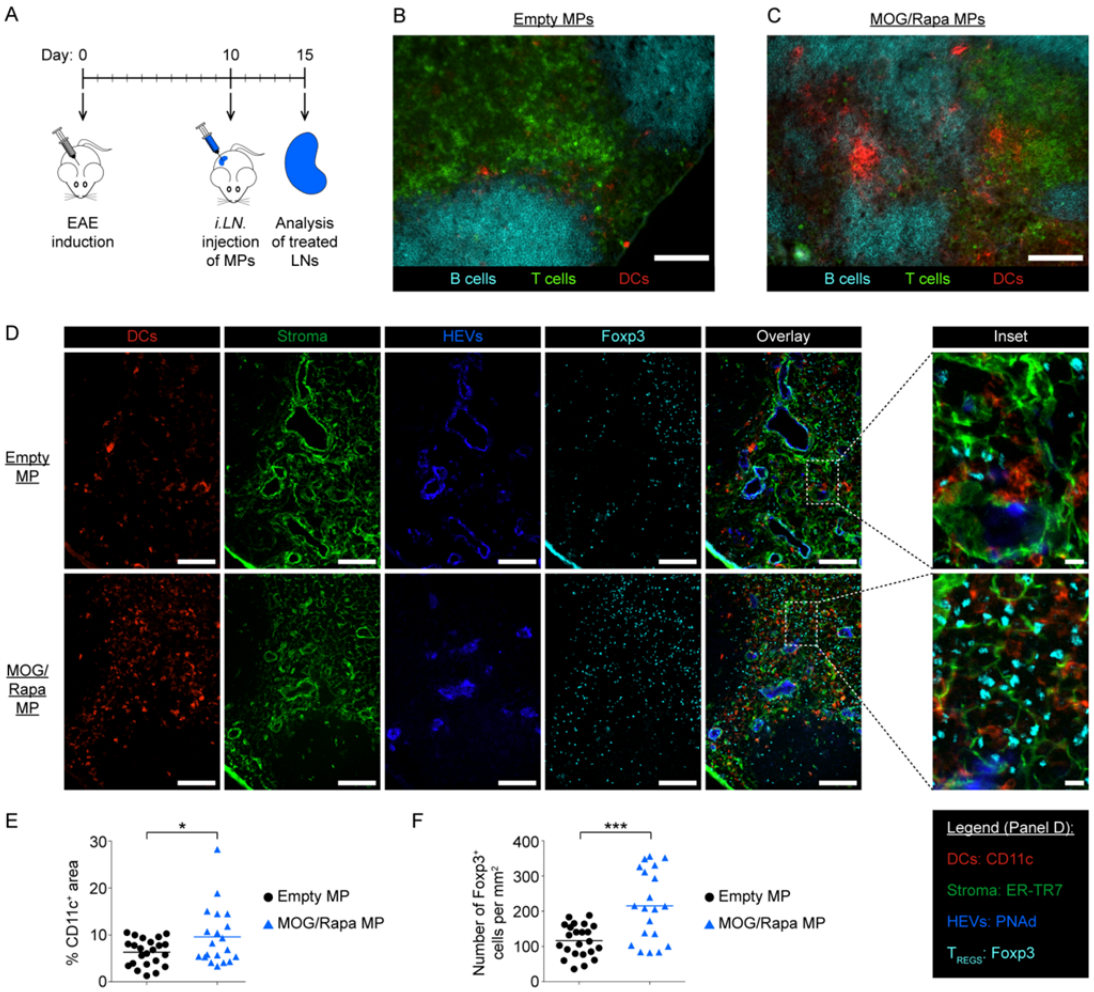

Figure 4.6 MOG/Rapa MPs elicit changes in the organization and composition of treated LNs. (A) Mice were treated i.LN. on day 10 post EAE induction, then the injected inguinal LNs were excised on day 15. Immunofluorescent analysis of LNs injected with (B) empty MPs or (C) MOG/Rapa MPs showing B cells (B220+, cyan), T cells (CD3e+, green), and dendritic cells (DCs, CD11c+, red), Scale bars: 100 µm. (D) Images of the cortical ridge of LNs, injected with empty MPs or MOG/Rapa MPs, showing DCs (CD11c+, red), reticular fibroblasts (stroma, ER-TR7+; green), high endothelial venules (HEVs, PNAd, blue), Foxp3+ cells (cyan) and an overlay, Scale bars: 100 µm. An inset of the overlay channel is shown on the far right column, Scale bar: 10 µm. Quantitative image analysis was used determine the frequency of (E) DCs and (F) Foxp3+ cells following empty MP (n = 23) or MOG/Rapa MP (n = 20) treatment in the cortical ridge of sections like the representative images shown in (D). Statistical analyses in (E) and (F) were two-tailed student's t tests.

4.3.4. Control of autoimmunity is dependent on i.LN. delivery and encapsulation of self-antigen

Our flow cytometry and immunofluorescent analyses led us to hypothesize that local delivery of MOG and Rapa drives recruitment of DCs due to the presence of MOG in animals with active EAE. In addition, the altered cellular composition of treated LNs

and increase in the presence of T_{REGS} localized in tolerogenic subdomains motivated analysis of how cells in these tissues respond to encounter of self-antigen. Thus, we next characterized the inflammatory recall responses in cells isolated from treated LNs at different time points before and after MP treatment. On day 9 (i.e., prior to MP treatment), restimulation of cells from LNs with MOG peptide induced high levels of IL-17 (**Figure 4.7A**), GM-CSF (**Figure 4.7B**), and IFN- γ (**Figure 4.7C**) secretion. In contrast, no effect was observed in response to an irrelevant peptide from ovalbumin (OVA, **Figure 4.8**), consistent with the myelin-specific inflammatory response associated with disease. This local inflammatory response in the inguinal lymph node is expected in induced MS models since inguinal LNs drain the peripheral injection sites used to induce disease. At time points after *i.LN.* injection, MOG/Rapa MPs generally reduced inflammatory cytokine secretion during restimulation relative to treatment with empty MPs (**Figure 4.7A-C**). However, these decreases were significant only on day 15 for IL-17 and GM-CSF. Interestingly, when we analyzed similar cultures prepared from splenocytes, significant reductions in IL-17 were observed at days 12 and 15 (**Figure 4.7D**), as well for GM-CSF (**Figure 4.7E**) and IFN-γ (**Figure 4.7F**) at day 12. Together, these results indicate that local introduction of MOG/Rapa MPs to LNs can control disease while reducing self-antigen-triggered inflammation in both treated and non-treated tissues.

As LN delivery of MPs drove both local and systemic effects, we sought to test the importance of localization of signals in LNs for the development tolerance. Mice were induced with EAE and treated on day 10 with MOG/Rapa MPs either *i.LN.* or

intra-muscularly (*i.m.*) to mimic a common peripheral vaccination route (**Figure 4.7G**). Compared with empty particles administered *i.LN.*, *i.m.* injection of MOG/Rapa MPs provided no significant improvement to disease progression scores (**Figure 4.7H**), severity (**Figure 4.7I**), or incidence (**Figure 4.7J**). In contrast, a matched dose of MOG/Rapa MPs administered *i.LN.* again caused a potent therapeutic impact (**Figure 4.7H-J**). Further, to test how the site of injection impacted systemic protection against inflammation, cells were collected from the spleens on day 21 and restimulated with either MOG or OVA peptide. In cells isolated from mice treated with empty MPs, restimulation with MOG drove a significant increase in the secretion of IFN-γ (**Figure 4.7K**) compared with OVA stimulation. *i.LN.* treatment with MOG/Rapa MPs, but not with *i.m.* injection, resulted in a significant reduction in IFN-γ secretion following MOG pulse (**Figure 4.7K**).

Since attenuation of EAE and inflammatory responses required local *i.LN.* delivery, we next tested whether encapsulation of signals was required for efficacy. Owing to the poor solubility of Rapa and the miniscule volumes used for *i.LN*. injection, we were unable to formulate ad-mixed (i.e., without MPs) treatments of soluble MOG and Rapa as controls. Thus, Rapa MPs were mixed with soluble MOG and administered *i.LN.* 10 days after EAE induction to assess the role of antigen co-encapsulation. We observed no significant differences between empty MP controls and soluble MOG + Rapa MPs with respect to either clinical score (**Figure 4.7L**) or relative body weight (**Figure 4.7M**). These findings indicate that both antigen

encapsulation and local, LN injection of MOG/Rapa depots play critical roles in tolerance.

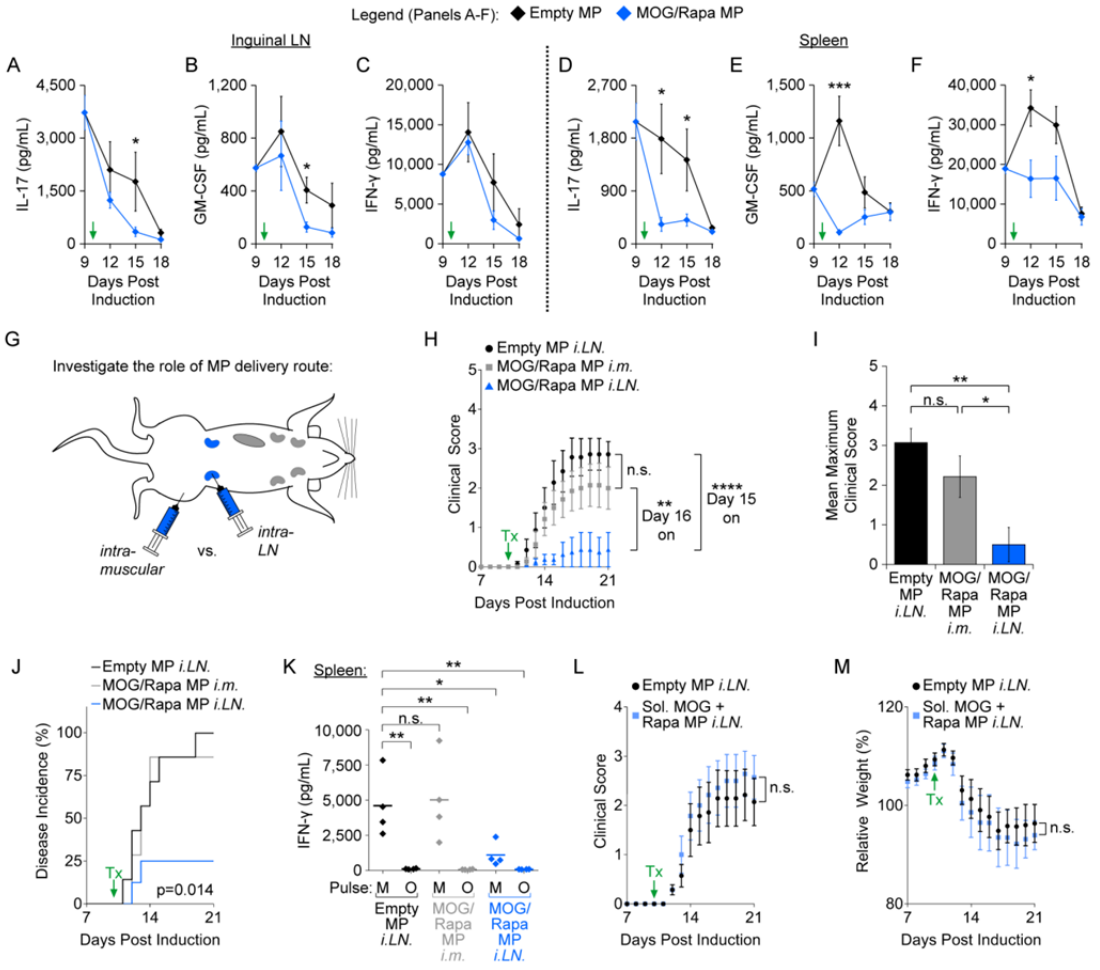

Figure 4.7 *i.LN.* delivery and antigen encapsulation restrain EAE and MOG-triggered inflammation.

Secretion of (A) IL-17, (B) GM-CSF, and (C) IFN-γ in cells from treated LNs and (D-F) spleens stimulated *ex vivo* with MOG. Identical groups (n = 3-6) were prepared for each time point and tissues were isolated before (day 9) or after (days 12, 15, and 18) *i.LN.* treatment on day 10. In (A-F), t tests were used to compare empty MP and MOG/Rapa MP treatments at each time point. (G) Benchmarking *i.LN.* injection against peripheral intra-muscular (*i.m.*) injection. (H) Mean clinical score, (I) mean maximum score, and (J) incidence of disease in mice treated on day 10 (Tx, green arrow) post EAE induction with empty MPs *i.LN.* (n = 7), MOG/Rapa MPs *i.LN.* (n = 8), or an equivalent dose of *i.m.* MOG/Rapa MPs (n = 7). Statistical analysis in (H) was performed using two-way ANOVA with a Tukey post-test, in (I) with a one-way ANOVA with a Tukey post-test, and in (J) with a log-rank test. (K) Secretion of IFN-γ after MOG or OVA restimulation of splenocytes on day 21. Statistical analysis in (K) was performed using one-way ANOVA with a Tukey post-test to compare each group to a control group of cells isolated from mice treated with empty MPs *i.LN.* and pulsed with MOG. (L) Mean clinical score and (M) relative body weight of mice induced with EAE and treated *i.LN.* on day 10 with either empty MPs (n = 7) or soluble MOG peptide mixed with Rapa MPs (n = 7). Statistical analyses in (L) and (M) were performed using multiple t tests, one at each time point, with a Holm-Sidak post-test correction for multiple comparisons. Data in all panels represent mean ± SEM (*, $p \leq 0.05$; **, $p \leq 0.01$). See also **Figure 4.8**.

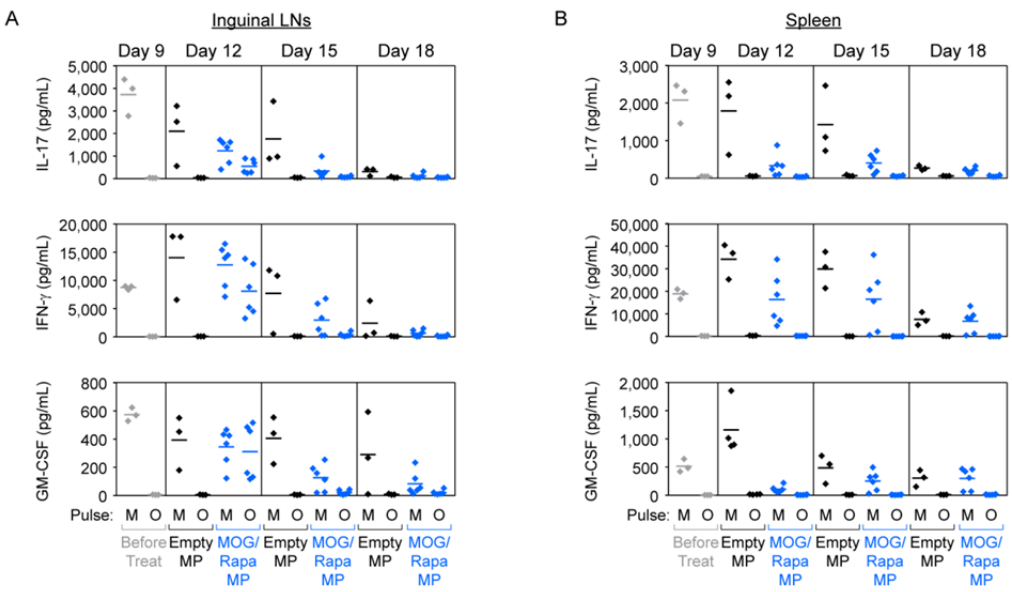

Figure 4.8 *i.LN.* delivery of MOG/Rapa MPs restrain local and systemic inflammatory cytokine secretion.
Mice were induced with EAE and either before (day 9) or after (days 12, 15, and 18) the administration of a single *i.LN.* dose of MPs on day 10, cells were isolated from the indicated tissues and restimulated with either MOG peptide (Pulse: M) or OVA peptide (Pulse: O) for 48 hours. ELISA was used to quantify the levels of IL-17 (Upper), IFN-□of MPs on day 10, cells were isolated from the indicated tissues and restimulated with either MOG peptide (Pulse: M) or OVA peptide (Pulse: O) for OG/Rapa MPs. Day 9: $n = 3$; days 12, 15, 18: empty MPs, $n = 3$; MOG/Rapa MPs, $n = 6$.

4.3.5. Restraint of autoimmunity is myelin-specific

Together, our results suggest a scenario where *i.LN.* treatment results in antigen presentation with limited inflammation. We hypothesized that this local LN reprogramming might also drive T_{REG} expansion and the development of tolerance in a myelin-dependent manner. To investigate this hypothesis, we directly studied the importance of including disease-relevant myelin antigen in the restraint of EAE-induced paralysis and underlying changes in immune cell function. Mice were treated on day 10 with empty MPs, MOG/Rapa MPs, or MPs encapsulating Rapa and an irrelevant antigen, OVA (OVA/Rapa MPs). Cells from the treated LNs and spleen were isolated, restimulated with MOG peptide, then secretion of inflammatory cytokines was analyzed. Surprisingly, both MOG/Rapa MPs and OVA/Rapa MPs

caused significant and equivalent local suppression of IFN-γ (**Figure 4.9A**), GM-CSF (**Figure 4.9B**), and IL-17 (**Figure 4.9C**) compared with empty MP-treated controls. Similar effects were observed in the spleen (**Figure 4.9D-F**), but the differences were more modest, with statistically significant effects only observed for IL-17 (**Figure 4.9F**). We also observed a trend that the lowest inflammatory cytokine levels were associated with MOG/Rapa MPs. Since inclusion of disease-relevant antigen in depots was not critical to reduce inflammatory recall response, we hypothesized MOG/Rapa depots might more effectively expand T_{REGS} that can control pathogenic populations. This hypothesis was supported by our observation above of significant reorganization of treated LNs with respect to Foxp3 localization in the cortical ridge following MOG/Rapa MP treatment (**Figure 4.6D,F**). However, when we analyzed the frequency of $CD4^+/CD25^+Foxp3^+$ among all cells, rather than in structural microdomains, we observed only a trend of increased T_{REG} frequency after treatment with either MOG/Rapa or OVA/Rapa MPs, findings that were not statistically significant (**Figure 4.9G-H Upper, 4.10**). In stark contrast, however, MOG/Rapa MPs significantly increased the frequency of T_{REGS} in non-injected tissues – pooled untreated LNs and spleen – compared with OVA/Rapa MPs and empty MPs (**Figure 4.9G-H, Middle, Lower; 4.10**).

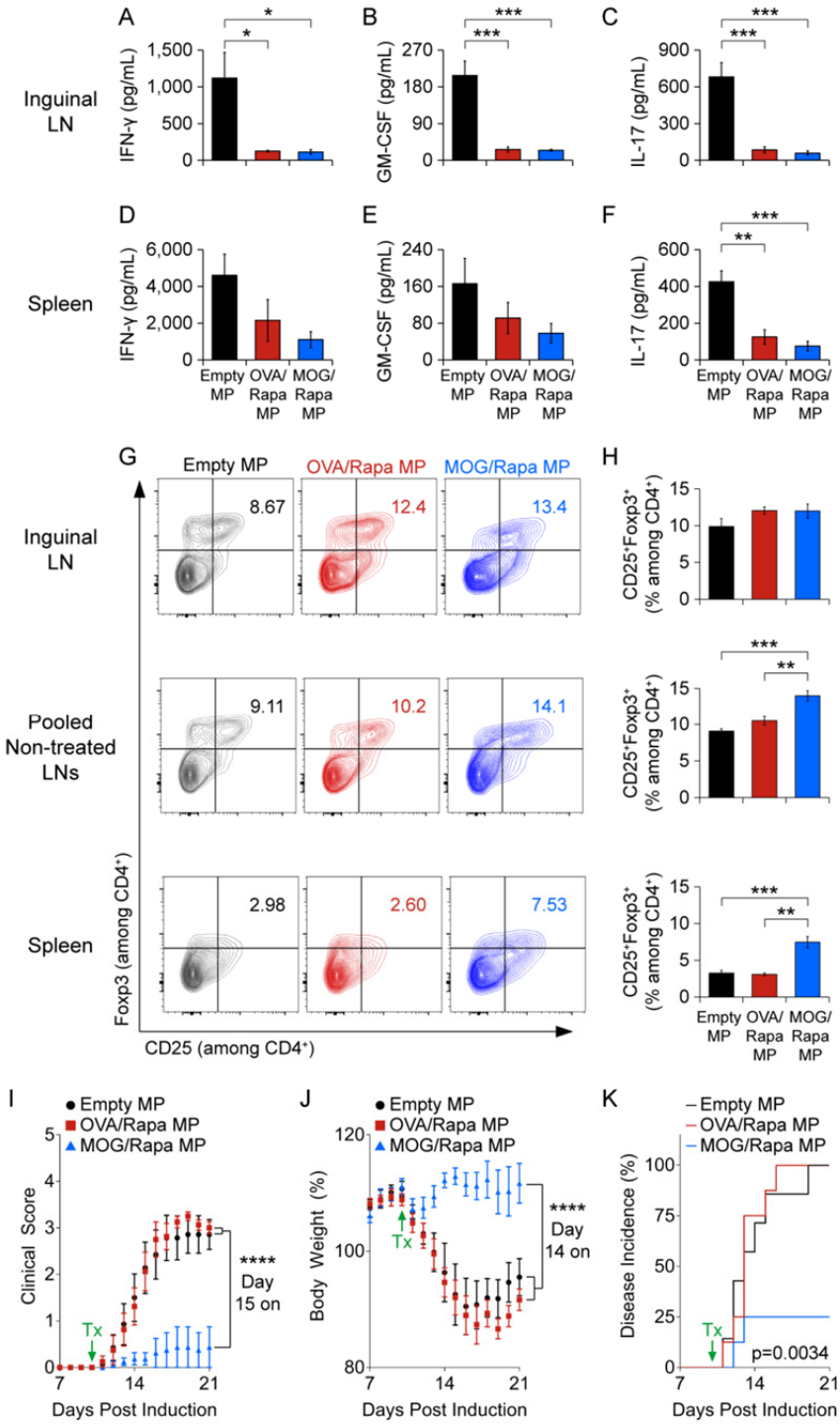

Figure 4.9 Incorporation of self-antigen is required for T_{REG} induction and attenuation of disease, but not for local suppression of inflammation.

Mice were induced with EAE and treated *i.LN.* on day 10 with empty MPs, OVA/Rapa MPs, or MOG/Rapa MPs (n = 4 for each MP formulation). On day 21, cells were isolated from treated LNs, restimulated with MOG peptide, and secretion of (A) IFN-γ, (B) GM-CSF, and (C) IL-17 was measured. (D-F) Similar analyses were performed on cells isolated from splenocytes. (G) Scatter plots and (H) mean T_{REG} ($CD25^+Foxp3^+$ among $CD4^+$) frequencies in treated inguinal LNs (*Upper*), non-treated axillary and brachial LNs (*Middle*), and spleens (*Lower*), after *i.LN.* injection on day 10 post EAE induction and analysis on day 12 (n = 4-6 for each MP formulation). (I) Mean clinical score, (J)

relative body weight, and (K) disease incidence of mice induced with EAE and treated *i.LN.* on day 10 (Tx, green arrows) with empty MPs (n = 7), OVA/Rapa MPs (n = 8), or MOG/Rapa MPs (n = 8). Statistical analyses in panels A-F, H were performed using one-way ANOVA with a Tukey post-test; all statistically significant differences are indicated. Statistical analyses in (I) and (J) were performed using two-way ANOVA with a Tukey post-test and in (K) using a log-rank test. Data in all panels represent mean ± SEM (*, $p \leq 0.05$; **, $p \leq 0.01$; ***, $p \leq 0.001$; ****, $p \leq 0.0001$). See also **Figure 4.10**.

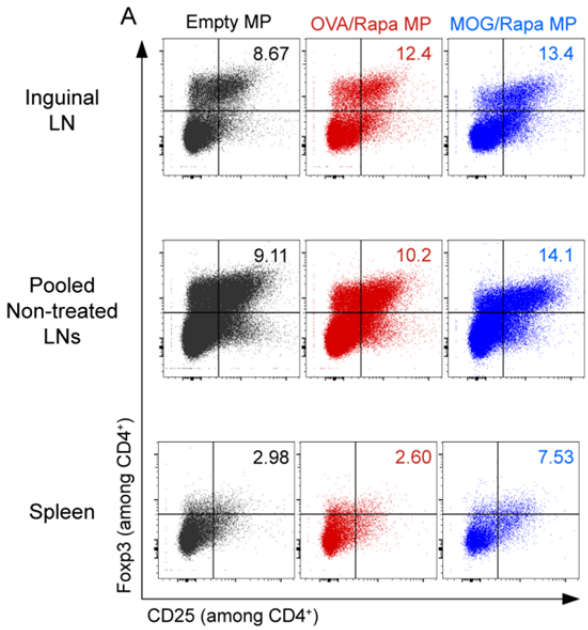

Figure 4.10 Incorporation of self-antigen is required for T_{REG} induction.
Representative dot plots, showing CD25 and Foxp3 expression among $CD4^+$ events in treated inguinal LNs (*Upper*), non-treated axillary and brachial LNs (*Middle*), and spleens (*Lower*), after *i.LN.* injection on day 10 post EAE induction and analysis on day 12 (n = 4-6 for each MP formulation).

We next tested if these changes in immune cell function and phenotype might have differential implications for disease progression. Mice were again induced with EAE, treated with MPs as above, and monitored for disease symptoms. Strikingly, mice treated with empty MPs or OVA/Rapa MPs developed paralysis that was severe and equivalent (**Figure 4.9I-K**), while MOG/Rapa MPs dramatically improved clinical scores (**Figure 4.9I**), body weight (**Figure 4.9J**), and disease incidence, (**Figure 4.9K**).

4.3.6. i.LN. injection of MOG/Rapa MPs drives the accumulation of T_{REGS} in CNS-draining LNs and reverses autoimmunity

Together, the results in **Figure 4.9** support a mechanism by which non-specific suppression occurs at the site of injection due to local Rapa introduction, but whereby treatment with MPs also incorporating myelin drives expansion of T_{REGS} that circulate systemically to other tissues and sites of disease. This hypothesis motivated the study of the frequency and localization of Foxp3 expression in a key non-treated disease-relevant tissue, cervical LNs, which drain the CNS. For these studies, mice were induced with EAE and treated with empty MPs or MOG/Rapa MPs on day 10. Five days later, the cervical LNs were excised and analyzed by immunofluorescent analysis (**Figure 4.11A**). Quantitative analysis of at least 20 sections for each MP treatment revealed statistically similar frequency of DCs in both MP treatments (**Figure 4.11B**), but a large increase in the number of $Foxp3^+$ cells in the cortical ridge of LNs (**Figure 4.11C**). These data support the hypothesis that MOG/Rapa depots delivered to non-CNS draining LNs increase T_{REG} frequencies in distant LNs that drain the sites of disease during MS.

Since locally reprogramming of LNs resulted in strong, systemic effects that generated antigen-specific control of disease, we last tested if this approach could reverse established disease. In these studies, mice were treated with a single injection of MOG/Rapa MPs or empty MPs at the peak of EAE (day 16). MOG/Rapa MPs drove a dramatic reduction in mean clinical score (**Figure 4.12A**), reversing paralysis and promoting weight gain (**Figure 4.12B**). Strikingly, while 100% of mice treated

with empty MPs exhibited sustained, severe disease, 75% of MOG/Rapa MP-treated mice experienced durable reductions in clinical score of at least two points (**Figure 4.12C-D**). Thus, a single *i.LN.* treatment with MOG/Rapa MPs restored CNS function, even when administered at the peak of disease. Together, these findings suggest that *i.LN.* injection is not only a tool to study the role of specific therapeutic components in tolerance, but also a powerful approach to generate antigen-specific control of disease, even when intervention occurs late in established disease.

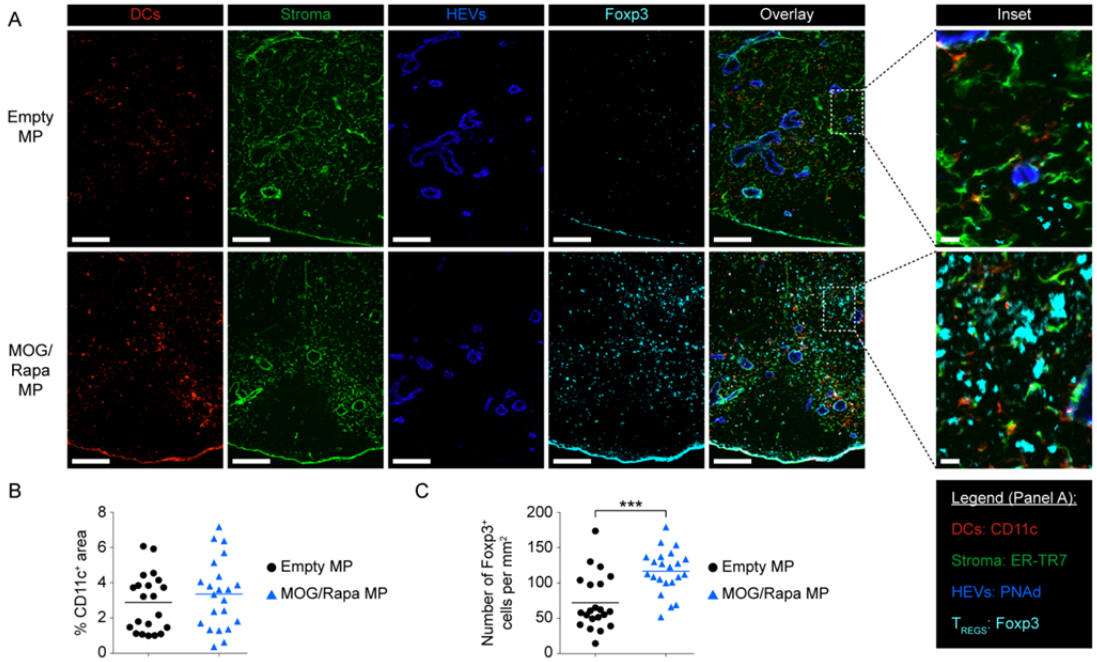

Figure 4.11 MOG/Rapa MPs promote tolerogenic reorganization and accumulation of T_{REGS} in CNS-draining LNs.
Mice were induced with EAE and treated *i.LN.* on day 10 with empty MPs or MOG/Rapa MPs (n = 4) and cervical LNs were excised for analysis five days later. (A) Immunofluorescent analysis of cervical LNs, showing DCs ($CD11c^+$, red), reticular fibroblasts (stroma, $ER\text{-}TR7^+$; green), high endothelial venules (HEVs, PNAd, blue), $Foxp3^+$ cells (cyan) and an overlay, Scale bars: 100 µm. An inset of the overlay channel is shown on the far right column, Scale bar: 10 µm. Quantitative image analysis was used determine the frequency of (B) DCs and (C) Foxp3 following empty MP (n = 21) or MOG/Rapa MP (n = 22) treatment in the cortical ridge of sections like the representative images shown in (A). Statistical analyses in (E) and (F) were two-tailed student's t tests.

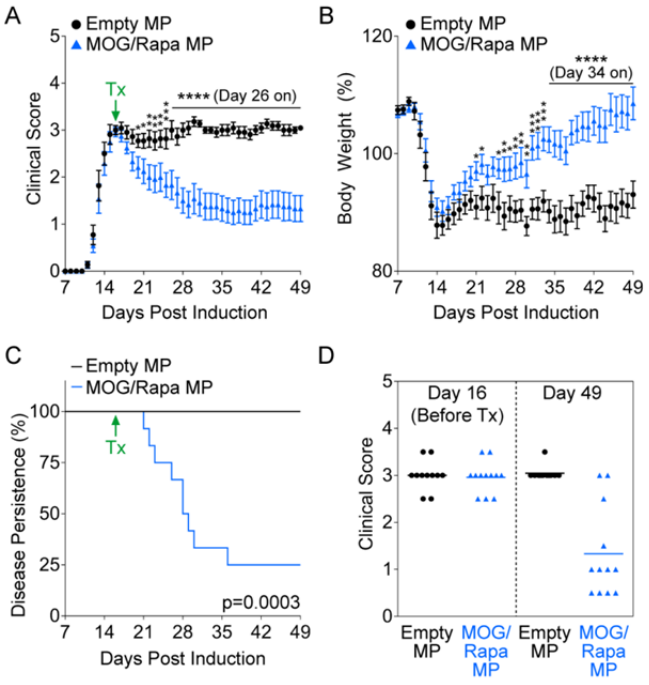

Figure 4.12 A single *i.LN.* dose of MOG/Rapa MPs reverses disease-induced paralysis.
Mice were treated at the peak of EAE (day 16; Tx, green arrow) using a single *i.LN.* dose of empty MPs ($n = 11$) or MOG/Rapa MPs ($n = 12$) and (A) mean clinical score and (B) weight were monitored. (C) Persistence of disease, with recovery from disease defined as at least a two point reduction in clinical score relative to the score just prior to treatment. (D) Score distribution of mice in (A-C) just before treatment (day 16, *Left*) and at day 49 (*Right*). Statistical analysis in (A) and (B) was performed using multiple *t* tests, one at each time point, with a Holm-Sidak post-test correction for multiple comparisons and in (C) using a log-rank test. Data in all panels represent mean ± SEM (*, $p \leq 0.05$; **, $p \leq 0.01$; ***, $p \leq 0.001$; ****, $p \leq 0.0001$).

4.4. Discussion

The need for more effective and selective treatments for MS has stimulated new clinical trials aimed at myelin-specific or personalized therapies [37]. These approaches focus on cell-based adoptive transfer strategies, for example, peripheral blood mononuclear cells coupled to myelin peptides, or patient-specific, myelin-reactive, irradiated T cells. In parallel, several preclinical reports describe soluble treatments or biomaterial-based approaches to deliver self-antigen, regulatory small molecules, or both to restrain self-reactivity [36, 39, 40, 45, 47, 54, 84-87]. While these approaches demonstrate exciting opportunities for translation toward the goal of

more effective and selective control of human disease, the approaches reflect different strategies in the immunomodulatory signals delivered. As noted, some studies demonstrate co-delivery of self-antigen and a regulatory signal confers therapeutic effects [47, 86], while other reports suggest changing the physical form of self-antigen can trigger existing debris clearance pathways to promote tolerance in the absence of explicit immunoregulatory cues [39, 40, 45]. Further, studies in animal models and human MS identify the presence of myelin self-antigen in LNs [92-94]. These results indicate that CNS antigens are present in peripheral sites of T cell polarization during disease, suggesting that delivery of tolerogenic signals alone may be sufficient to restrain myelin-specific self-attack. Thus, the role of candidate immunomodulatory signals and combinations of these signals is not well-defined, particularly in the context of the impact on the LN microenvironment.

The connections between systemic tolerance and local LN function are of particular interest to MS, since pathogenic T cells are armed in LNs prior to CNS infiltration. Past studies, for example, reveal that excision of CNS-draining LNs restricts T cell infiltration to the CNS and limits EAE in rat models [95]. In addition, recent work identifies APCs and T cells in newly-discovered lymphatics that connect the CNS with cervical LNs outside the CNS [13, 14]. These findings, along with human trials using *i.LN.* injection of free antigens for cancer or allergy therapy [96], suggest clinical opportunities based on controlling the local response to myelin in LNs during MS as a direct route to promote myelin-specific tolerance. Thus, one outcome of our work is a new possibility for locally programming LN function – through co-delivery

from depots, local controlled release, or other biomaterials-enabled features – to generate systemic and specific control of disease. In addition to assessing clinical potential, we sought to use *i.LN.* depots as a tool to study how the local inflammatory or tolerogenic state of LNs controls the magnitude and specificity of systemic tolerance. This platform provides a unique opportunity to probe the spatial and temporal dynamics of immune response to self-antigens; in contrast, approaches that employ systemic injections or repeated doses complicate these kinds of perturbations.

Our experiments reveal that reprogramming discrete LNs can generate systemic tolerance. The dependence of therapeutic efficacy on intra-LN delivery of encapsulated, disease-relevant self-antigen highlights three unique results of this platform. First, a role for controlled kinetic release from micron-scale depots retained in LNs following injection [27, 89] is supported by the observation that substitution of soluble myelin self-antigen eliminates therapeutic efficacy (**Figure 4.7**). Second, perhaps in parallel, direct deposition of MPs in LNs may drive higher frequency encounters with resident APC populations that have been shown to promote tolerance [47]. This approach might provide a means to by-pass the relatively inefficient drainage and trafficking mechanisms by which signals traditionally reach LNs and spleen following peripheral injection [4, 27, 89] and, therefore, enhance efficacy compared with *i.m.* delivery of a matched dose tested here (**Figure 4.7**). Third, the observation that both MOG MPs and MOG/Rapa co-loaded MPs attenuate disease (**Figure 4.1**) suggests a possible contribution from altered trafficking or more

efficient processing of antigen in particulate form relative to soluble antigen [39, 40, 45].

In addition to the need for encapsulation and targeted LN injection, *ex vivo* restimulation further revealed a less inflammatory milieu was established in LNs by MOG/Rapa depots (**Figure 4.7A-C, 4.9A-C**). We observed a decrease in the myelin-triggered secretion of three key cytokine drivers of inflammation during disease in mice and humans: IL-17, IFN-γ, and GM-CSF. In particular, IL-17 is a characteristic cytokine secreted by T_H17 cells, while IFN-γ is a broad pro-inflammatory signal, secreted by T_H1 subsets during autoimmunity [81]. Further, GM-CSF has been shown to be secreted by self-reactive T helper cells, triggering an inflammatory cascade that enhances pathogenic monocyte-derived cell infiltration into the CNS and subsequent tissue damage [97]. Together, these findings support a possible mechanism by which myelin is presented in LNs, but whereby the response is altered by the presence of T_{REG}-inducing signals in the case of MOG/Rapa MPs, or at least a lack of co-stimulation in the case of MOG MPs. Supporting this idea, we discovered that MOG/Rapa MPs drive distinct remodeling of the LN stroma, with $Foxp3^+$ cells accumulating in the cortical ridge of LNs in close proximity to high endothelial venules (HEVs) – routes of T cell entry into LNs [91]. Our measurements of this phenomena in treated LNs (**Figure 4.7D,F**) and non-treated, CNS-draining LNs (**Figure 4.11A,C**) suggest that local perturbation of LNs with self-antigen and Rapa promotes this tolerogenic reorganization.

After *i.LN.* injection of MOG/Rapa MPs, we also observed a significant increase in the frequency of T_{REGS} in the spleen and pooled non-treated LNs, relative to empty MPs or OVA/Rapa MPs (**Figure 4.9G-H**). This result further underscores the self-antigen-specific nature of efficacy, though new tools such as MHC-II tetramer could help directly verify the antigen-specificity of TCRs on the expanding T_{REGS} [98]. Interestingly, effects were least pronounced – and statistically insignificant – in treated LNs (**Figure 4.9G-H, Upper**). One explanation for this outcome may be that local delivery of myelin triggers resident myelin-reactive cells, but little expansion of regulatory cells occurs because Rapa inhibits proliferation. This hypothesis is supported by the discovery that while MPs encapsulating Rapa and irrelevant antigen, OVA, did not impact disease (**Figure 4.9I-K**), these particles caused local suppression of inflammatory recall response equivalent to that of MOG/Rapa MPs (**Figure 4.9A-C**) in treated nodes. There was an intermediate reduction in the spleen, an untreated site – likely due to non-specific, systemic effects of Rapa. Supporting this hypothesis, recent literature demonstrates that systemic treatments with modulatory or suppressive drugs can cause differential impacts on inflammatory responses in different tissues – findings that also illustrate the utility of having a tool to directly probe how signals in one tissue impact the course, efficiency, and durability of tolerance [99]. One further rationale for co-delivery of tolerogenic signals (e.g., Rapa) with self-antigen is to mitigate the risk of exacerbating disease with a therapy containing disease-relevant antigen during active autoimmunity [47].

Our findings reveal antigen-specific tolerance can be generated with striking efficacy by locally reprogramming LNs, results demonstrating the unique potential of this strategy to study and combat autoimmunity. Some of the important follow-on studies include the need to further assess the trafficking of T cells from treated LNs to the cervical LNs and CNS, and importantly, to confirm remyelination – a critical criterion for human MS therapy. The functional selectivity of tolerance should also be assessed by confirming intact pro-immune responses to exogenous antigens after recovery. Lastly, mouse models do not fully recapitulate the myelin reactivity and epitope spreading present in human disease. The modular nature of the engineering approach reported here allows facile incorporation of multiple peptide epitopes and could support future studies in other models or in humans to assess these dynamics. Thus, this work demonstrates unique potential to study, control, and reverse established autoimmune disease in a selective fashion by modulating local LN function.

These follow-on studies, and the link to both ongoing and planned future research directions for Aim 1 of this dissertation, are discussed in further detail in **Chapter 7**. One potential challenge associated with the current approach is the use of a polymer microparticle to deliver immune signals. While, importantly, we have included empty MP controls in studies to isolate the role of encapsulated cargos, strategies that eliminate synthetic or carrier components could simplify materials design and reduce potential risk associated with the intrinsic inflammatory properties of many common biomaterial carriers, including PLGA. One approach that could contribute towards this goal is the use of self-assembly to generate biomaterial assemblies. In **Chapter 5**,

we review reports in the literature that employ self-assembly techniques to i) generate new diagnostic tools, ii) study fundamental aspects of immune responses, and iii) design new therapeutic strategies to combat infectious disease, cancer, or autoimmune diseases. This chapter links to Aim 2 and will set the framework for **Chapter 6**, in which we self-assemble carrier-free immune polyelectrolyte multilayer "iPEM" capsules toward the goal of promoting immune tolerance.

Chapter 5. Engineering self-assembled materials to study and direct immune function[4]

5.1. Introduction

Vaccines are a transformative technology, enabling activation of the immune system to recognize and destroy specific pathogens, and supporting near eradication of diseases such as polio and small pox [100-102]. Even so, the potential of engineering immune function is far richer than vaccines alone. The immune system is an exquisitely complex control system that is not just a means of activating responses to combat pathogens. Rather, a dynamic balance exists between pro-immune/inflammatory processes, regulatory/suppressive functions, and homeostatic (i.e., resting) activity levels (**Figure 5.1**). In vaccination, a common goal is to induce specific and long-lasting adaptive responses against foreign pathogens for future protection against infection (i.e., immunological memory), while during cancer immunotherapy, one objective is to generate fast-acting killer T cells that destroy existing tumors [101, 103, 104]. Yet to combat autoimmune disease, where the immune system malfunctions and attacks healthy tissue, a therapy may seek to turn off or suppress particular aspects of inflammatory responses [81, 105]. Thus, there is great interest in better understanding the interplay between activated, resting, and regulatory immune functions. Harnessing this knowledge could help overcome the divergent hurdles that continue to persist in infectious disease, cancer, and autoimmunity. For example, HIV undergoes rapid mutation to evade immune

[4] Adapted from L. H. Tostanoski, and C. M. Jewell, "Engineering self-assembled materials to study and direct immune function." *Advanced Drug Delivery Reviews* 2017 (In press).

recognition and clearance [106], cancer cells secrete suppressive signals to actively subdue anti-tumor immunity [103, 107], while during autoimmune diseases, such as multiple sclerosis and diabetes, defects in immune checkpoints lead to inflammation and destruction of self-cells or tissues [81, 108]. These nuances highlight the idea that overcoming existing and emerging challenges to public health requires not just generation of immune function, but control over the specific characteristics of immune response. This idea is termed immunomodulation.

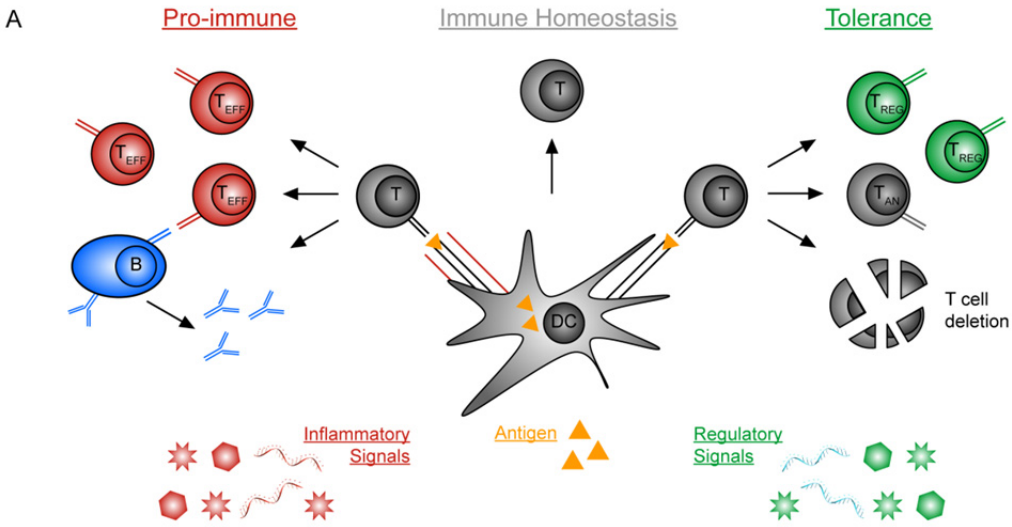

Figure 5.1 The immune system operates under a dynamic mix of maintenance processes, pro-immune functions, and tolerogenic functions.
The balance between these functions is dictated by how antigen-presenting cells, such as dendritic cells (DCs), encounter antigens and integrate inflammatory or regulatory signals present in the local microenvironment. For example, during infection or inflammatory disease, DCs detect antigen in the presence of inflammatory or danger signals, which drives the expansion of effector T cells (T_{EFF}) and triggers antibody responses. In contrast, during tolerance, detection of antigen in the presence of a regulatory environment can lead to the expansion of regulatory T cells (T_{REGS}), the induction of anergic T cells (T_{AN}), or the deletion of T cells. Typically, following a perturbation that skews immune function – such as an infection, or the administration of a vaccine – the immune system returns to a resting or homeostatic state.

The immune system naturally governs function by integrating the relative concentrations and kinetics of antigens – peptide fragments from pathogens that determine the target of an immune response – along with immune cues that range from nucleic acids, to signaling proteins called cytokines, to small molecule ligands

and drugs [109-111]. Multi-disciplinary strategies that bring together immunology, translational perspective, and engineering technologies will be vital in continuing to decode and better direct these interactions. In particular, materials that allow precise control over how signals are encountered – the density or valency, for example – can reveal new knowledge of how immune cells detect and engage pathogens or a vaccine. Similarly, systems with molecular-scale control over the presentation of multiple signals offer the opportunity to exploit and direct function through co-delivery. As these demands for greater spatial and temporal control increase, so does the complexity of candidate vaccines and immunotherapies. Yet across fundamental research, pre-clinical development, and translation to humans, the need for vaccines and immunotherapies that are well defined and can be characterized remains constant; this latter point is an increasing challenge both from manufacturing and regulatory perspectives [101, 112-114].

An emerging technology that can enable the rational, tunable, well-defined nature discussed above is self-assembly. In this review, we discuss the unique features of self-assembly as a means to study immune function, to enhance immunosensing and diagnostics, and to improve vaccine and immunotherapy delivery technologies. We begin with brief background on the immune system and the characteristics of self-assembled materials, then describe key examples from recent literature highlighting how the unique advantages of self-assembly are and can be exploited to probe and control immune function. Throughout the review, we emphasize new ways in which self-assembly might be applied to current clinical challenges, as well as some of the

hurdles self-assembly might help tackle from the viewpoint of manufacturing and the regulatory process.

5.2. Background

5.2.1. The immune system initiates, balances, and suppresses immune function

The professional antigen presenting cells (APCs) of our immune system actively survey tissues throughout the body to verify the identity of healthy "self" molecules, cells, and tissues. These processes prevent incorrect attacks by sampling and display of self-antigens in the absence of stimulatory immune cues. A series of regulatory mechanisms also help maintain this "tolerance," some of which occur during development, while others are ongoing throughout life. Simultaneously, these same APCs sense cues from the surrounding environment, such as inflammatory cytokines [111], and the presence of danger signals common on invading pathogens [115]. APCs, such as dendritic cells (DCs), integrate these signals to control their own cytokine secretion and the expression level of surface proteins that lead to maturation and activation. This information is relayed through: i) recruitment of cells of the innate immune system that secrete chemical signals (i.e., chemokines, cytokines), and ii) interaction with cells of the adaptive immune system in tissues that coordinate immunity, such as lymph nodes (LNs). Innate immune functions, such as engulfment of bacteria and triggering of inflammatory immune cell recruitment can occur in minutes or hours, but is less specific and does not provide immunological memory. In contrast, adaptive responses against pathogens (e.g., viruses, bacteria) develop over days, weeks, or months, drive molecularly-specific destruction and neutralization of pathogens, and can lead to immune memory that lasts for decades or longer.

Lymphocytes, T cells and B cells, are the major players in exerting the functional effects of adaptive immunity. These cells express surface receptors that bind a target or "cognate" antigen, a peptide moiety for which a particular cell has developed specificity against. Upon recognition of cognate antigen presented in a major histocompatibility protein complex (MHC) by an APC, lymphocytes bind; this antigen display is called "signal 1" (**Figure 5.1**). In the case of intra-cellular antigens, such as those displayed by cells infected by a virus, presentation occurs via the MHC-I pathway, driving the expansion of $CD8^+$ cytotoxic T cells that can directly kill target cells. In contrast, extra-cellular antigens that are engulfed – fragments of bacteria, for example – are presented via the MHC-II pathway to expand $CD4^+$ helper T cells. Importantly, simultaneously, lymphocytes receive cues that guide proliferation and differentiate to enable particular T or B cell functions. For instance, costimulatory markers expressed at different levels on the surface of APCs can engage receptors on lymphocytes during cell-cell interactions, an example of "signal 2", while the combinations of cytokines present in the local cell environment is now considered "signal 3" [111]. Together, these signals bias lymphocyte development toward specific functions. $CD4^+$ T cells with the same cognate antigen may differentiate towards either pro-inflammatory or tolerogenic phenotypes (**Figure 5.1**). Helper T cells can further interact with B cells, and by working with other APCs, drive B cells to mature and secrete high affinity antibodies that can neutralize extracellular toxins or tag extracellular pathogens for destruction. B and T cell activation share some features, but differences exist that ultimately determine how strongly the antibodies that B cells secrete will bind a pathogen, and the features that

these molecules will exhibit, for example, dimerization or transport through mucosal membranes.

Selectively exploiting active, resting, and suppressive immune mechanisms is a critical goal for new vaccines and immunotherapies [116]. The potential to promote cell-mediated (i.e., $CD8^+$ T cell-driven) immunity continues to be particularly advantageous in viral disease and cancer. In these cases, viral antigens or antigens over-expressed on tumor cells are targeted by killer T cells, in some cases, those that arise naturally, and in others, via T cells that are engineered and infused into cancer patients [117, 118]. In contrast, the potential to control the phenotype of $CD4^+$ T cells may be a vital capability to promote tolerance during autoimmune disease. In multiple sclerosis, T_H1 and T_H17 cells that specifically recognize components of myelin – the matrix that insulates and protect neurons – drive inflammation and disease through attack against myelin [4, 119, 120]. The capacity to instead expand these myelin-recognizing cells toward regulatory T cells (e.g., T_{REGS}) could enable myelin-specific control of disease, without the broad immunosuppressive effects associated with current clinical therapies. Similarly, regulating metabolic function away from states of extreme activation or suppression, and toward moderated, homeostatic levels, might help address diseases that cause systemic, chronic inflammation or that result in loss of immune tolerance [121, 122]. Thus, eliciting better control over the interactions between immune cells and, ultimately, immune function is a core theme in the field [123-125]. Here, we focus on self-assembled materials, which offer a unique opportunity to contribute to this vision.

5.2.2. Self-assembled materials offer high levels of molecular precision control

Biomaterials have emerged as promising technologies to enhance the spatial and temporal control over immune signal display and delivery [109, 110, 117, 126]. Broadly, biomaterials offer attractive properties, such as delivery of multiple classes of cargo, cell and tissue targeting, protection of payloads from enzymatic degradation, increased circulation time, and defined delivery kinetics [109, 110, 127, 128]. However, there are significant challenges that continue to limit these materials for clinical use, for example, inefficient loading of immunological cargos into carriers, heterogeneous size distribution, and lack of control over the physical arrangement of molecules. Further, the low frequency of success of biomaterials in the clinic over the past decades reveals a need for critical assessment of translational biomaterials research in stringent models, and for ensuring clinically-relevant questions or pathways are targeted. The complexity of many materials approaches also adds hurdles for technologies aimed at human use, as the difficulty in manufacturing, characterizing, and approving these systems can be much greater relative to drug or antibody therapies. This disparity is in part due to the historical experience that manufacturers and regulators have with drugs and antibodies. Lastly, the need for better definition and control is particularly important for applications targeting the immune system, where the signaling pathways control a dynamic equilibrium.

Within the realm of biomaterials, self-assembled materials represent a unique opportunity to generate well-controlled structures from a diverse array of molecular building blocks, including peptides, nucleic acids, lipids, and synthetic polymers

(**Figure 5.2**, center) [129, 130]. Here, we define self-assembly as spontaneous interactions of these molecules, driven by conversion to more entropically-favored states. These processes can occur over nano-, micro-, and macro-scales via non-covalent forces, such as electrostatic or hydrophobic interactions and, owing to the spontaneous nature, self-assembled materials can often be generated with low energy input and at temperature and pH values in the physiological range. These characteristics are, generally, compatible with inherently less stable biological building blocks.

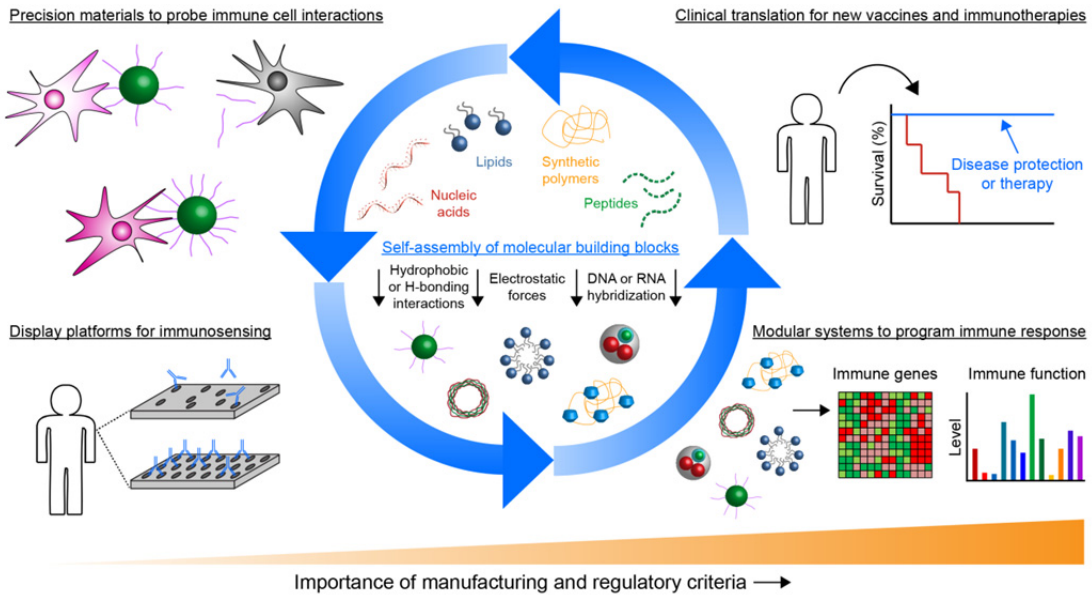

Figure 5.2 Self-assembly exhibits unique features that can be harnessed to program the assembly of a diverse array of macromolecules.
The non-covalent interactions that regulate self-assembly, including hydrophobic interactions, hydrogen bonding, electrostatic interactions, and DNA or RNA hybridization, have been exploited to design materials with programmable physiochemical characteristics (inside of circle). The interactions between these materials and cells and tissues of the immune system have been interrogated to generate design rules that could inform the development of new vaccines or immunotherapies (top left). In parallel, self-assembled materials have been employed to develop new platform technologies for immune sensing and diagnostic applications (bottom left). Finally, the potential for self-assembled biomaterials to program the magnitude and nature of immune responses (bottom right), as well as efficacy in models of infectious disease, cancer, autoimmunity, and transplant, have been studied to explore the clinical potential of emerging self-assembly technologies (top right). These endeavors create a feedback loop that inform one another. Lastly, the feasibility and requirements for manufacturing need to be considered early in the design and development process (bottom).

There are several types of self-assembled materials in the immune engineering field being used to modify the surface of two- or three-dimensional surfaces (e.g., spherical particles, complex micro- or nano-scale topographies), or to directly generate structured particulate materials. Three emerging classes of these materials can be described by the non-covalent interactions that drive self-assembly (**Figure 5.2**, center). First, hydrophobic or amphiphilic molecules often assemble through hydrophobic interactions into micelles, liposomes, or elongated, fibril-like structures. For example, lipids are inherently amphiphilic, making these molecules well-suited for hydrophobic interaction-based assembly, while peptides can be designed to incorporate motifs that fold into secondary structures (e.g., alpha helices, beta sheets) to provide hierarchical organization. Second, electrostatic interactions can drive association of peptides with charged residues, nucleic acids, synthetic polymers, or other charged molecules. This driving force can be harnessed to condense or complex building blocks into nanoparticles or microparticles, as well as to drive programmable layer-by-layer assembly into polyelectrolyte multilayers. Finally, nucleic acids can be designed with base complementarity to promote folding or assembly into predictable, well-defined structures. Broadly speaking, these types of self-assembled materials have been tapped for applications ranging from optics, to energy, to drug delivery, and, recently, in immunology, vaccines, and immunotherapy [129-132].

Below we describe recent literature demonstrating the transformative potential self-assembly offers for engineering immune function. As depicted in **Figure 5.2**, we focus on four areas harnessing self-assembly i) as a tool to interrogate fundamental

aspects of immune responses, ii) for immune sensing and diagnostics, iii) to generate design guidelines for new vaccines and immunotherapy delivery strategies, and iv) in applications aimed at clinical translation that span infectious disease, cancer, and autoimmunity. We also integrate into the discussion the increasing importance of considering the manufacturing and regulatory requirements for new vaccines and immunotherapies even in the pre-clinical and design stages (**Figure 5.2**, bottom). While this review centers on self-assembly, new innovations in materials science, immunology, and engineering are also poised more generally to enable new capabilities in the immune engineering field. As evidence, simply examine the diverse body of exciting work that comprises this special issue.

5.3. Self-assembled materials create new tools to probe fundamental immune interactions

A new aspect of immunology to which self-assembly is being applied is deciphering fundamental characteristics of immune response. This understanding provides new basic knowledge to inform the design of better vaccines, immunotherapies, and carriers for these technologies. An important example is the use of virus-like particles (VLPs). VLPs are recombinant proteins designed to self-assemble into particulate structures after expression in cell culture systems (e.g., yeast, bacteria, plant cells) that have been engineered to produce the sequences of interest. These particles mimic native viruses, but cannot replicate and, therefore, pose lower safety risks compared with live or attenuated vaccines [133-136]. VLPs are currently used in clinically-approved vaccines to protect humans against human papillomavirus (HPV) [137-141]

and hepatitis B virus (HBV) [133, 142]. These clinical uses highlight a key advantage of VLPs, the presentation of sets of antigens in the same physical conformations that is found on native pathogens to maximize immunogenicity [135]. This is in contrast to many other approaches in which the conformation of antigens is either poorly controlled, or may result in a consistent arrangement of antigens, but one that differs in spacing, geometry, and shape from that of the native pathogen. This disparity between synthetic platforms and target pathogens can result in poor immunogenicity and efficacy. Despite the advantages of VLPs, a limitation of existing VLPs in the clinic is that the combinations of antigens delivered are not well-defined or well-controlled. Instead, fragments of pathogens are isolated, expressed in recombinant systems (e.g., bacterial cells), then screened for immunogenic potential [143]. While this approach has identified both approved vaccines and promising candidates, the potential to program the combinations of antigens displayed without sacrificing immunogenicity could generate strong responses with greater selectivity.

The efficiency of VLPs is also motivating work to harness specific structural moieties for rationally-designed synthetic systems that are well defined in both formulation and in the specific antigens against which responses are generated. For example, in the context of HIV, synthetic nanoparticles have been used as a tool to interrogate the role of antigen conformation and valency [144]. This study was motivated by recent reports revealing a portion of an HIV envelope glycoprotein that coats the viral capsid – a trimer composed of three monomers – is critical for recognition of HIV by the immune system. He and colleagues hypothesized that using nanoparticles could

enable surface display of the trimer at high density (**Figure 5.3A**) [144]. This report compared the binding affinity of the nanoparticle-displayed trimer to that of a free (i.e., nanoparticle-free) monomer using two well-characterized antibodies. Tests with an antibody that recognizes the monomer, either in monomer or trimer form, revealed low affinity binding to the monomer (**Figure 5.3B**, top left) and higher affinity binding to nanoparticle-displayed trimer (**Figure 5.3B**, top right), as indicated by a dramatic decrease in the dissociation constant (K_D). Next, an antibody previously shown to bind to the native trimer was tested. As expected, free monomer did not bind the trimer-specific antibody (**Figure 5.3B**, bottom left), while the nanoparticle assembly drove high affinity binding (**Figure 5.3B**, bottom right). These results confirmed that nanoparticle display did not interfere with the physical conformation of the trimer, but rather enabled rapid recognition and binding by the antibody through high density presentation of the trimers. This case demonstrates a concrete advantage of the self-assembly-enabled approach: the potential to mimic viral surface presentation of specific antigens to investigate the role of physical arrangement in engaging interactions with biological molecules, like antibodies.

While the research above focused on understanding the display of antigens with higher order structure, self-assembled particles are also being used to understand VLP assembly. For example, the link between amino acid sequence and the integrity and mechanical properties of VLPs have been investigated [145]. In this study, the authors introduced amino acid point mutations into monomers of the minute virus of mice, a virus with a well-characterized structure. Several of the mutations partially or

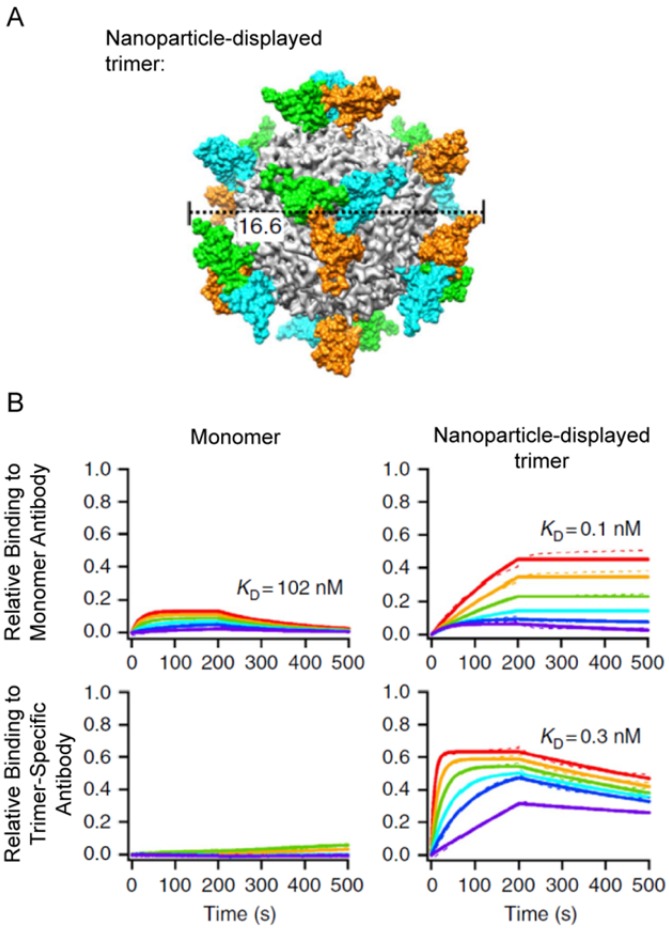

Figure 5.3 Conserved conformational display of an HIV antigen on a nanoparticle surface promotes high affinity binding to antibodies.
A) Structural model of a self-assembled nanoparticle, 16.6nm in diameter, displaying a trimeric HIV antigen on the surface. The ferritin core is indicated in gray, while the three monomers that make up each trimer, derived from the V1V2 region of a glycoprotein (gp120) are indicated in green, cyan, and orange. B) The binding affinity of the free monomer (ZM109 V1V2, left) was compared with that of the nanoparticles displaying the trimer (ZM109 V1V2Ext-FR, right) shown in (A). Binding to an antibody that can detect V1V2 in either monomer or trimer form (PG9) and to an antibody that that detects V1V2 only when expressed in the correct trimeric format (PGDM1400) was assessed. The dissociation constant (K_D) of each binding assay is reported, with the exception of monomer binding to PGDM1400 (bottom left), as this antibody, expectedly, did not exhibit binding affinity for V1V2 in monomer form. Adapted from [144] with permission.

completely inhibited the spontaneous assembly of VLPs. This result underscores the vital role of native, non-covalent interactions between side-chains of amino acids in monomers to drive self-assembly. Further, in formulations that maintained the potential to assemble spontaneously into VLPs, atomic force microscopy studies generally revealed an increase in stiffness when sequences were mutated. Stiffness

and other physiochemical properties have been shown to impact T cell activation and proliferation [146, 147]. Thus, future studies to elucidate the role of VLP properties in influencing immunomodulatory function, as well as comparisons between VLPs and other synthetic carriers (e.g., polymer emulsions, micelles, polymer-nucleic acid complexes) could inform the design of materials with specific mechanical properties to tune responses for translational applications.

5.4. New immunosensing and diagnostic applications and enabled by the well-controlled physical arrangement of self-assembled cues

Broadly speaking, immunosensing requires the detection of rare antigens, antibodies, or immune cells among complex, heterogeneous biological samples (e.g., patient blood or serum) to diagnose patients or inform therapeutic interventions. Thus, there is interest in developing strategies that enhance the specificity and sensitivity of detection and screening platforms. This knowledge is important for vaccine and immunotherapy delivery as specific design features may be advantageous depending on the specific cargos to be delivered. One way in which self-assembly is being harnessed along these lines is functionalizing surfaces with reproducible, defined physical arrangements of molecular species. Some of these approaches have involved immobilization of antibodies that specifically recognize key proteins, enzymes, or nucleic acid sequences that are known biomarkers of disease. For example, antibody against an enzyme upregulated in prostate cancer, prostate-specific antigen (PSA), has been used to design an electrochemical sensor [148]. Antibodies consist of two components: a constant region that is conserved across all antibodies (Fc), and a

variable “Fab” region that gives antibodies exquisite specificity to bind to a particular molecule. Thus, the sensor construction involved self-assembly of a linker molecule, β-cyclodextrin, onto a surface, followed by chemical conjugation of the Fc-binding domain to this linker. This approach resulted in well-ordered localization of the antibody on the surface, but left the domain that binds selectively to PSA available for interaction with samples. These sensors provided a high specificity and sensitivity for the detection of the rare PSA antigen in human serum. This was accomplished without fluorescent labeling to amplify the signal that is common in current approaches for detecting this biomarker.

In another study, self-assembly was used to localize antibodies against known antigens of influenza in a particular orientation on surfaces [149]. In this study, Le Brun and colleagues designed a system in which an engineered protein – Protein G, a cell wall-associated protein derived from *Streptococcus* – is self-assembled onto a gold surface through adsorption mediated by thiol functional groups. Importantly, this engineered Protein G preferentially binds to the Fc region of antibodies with an affinity two orders of magnitude higher than that of binding to Fab regions, facilitating capture of antibody on the surface via the Fc region [149]. This feature allows the variable regions – which bind specifically, in this case, to a nucleoprotein of influenza – to orient away from the surface and remain free to bind antigen. One advantage of the design is maximizing the number of available influenza-specific binding sites (i.e., two per antibody). Because assembly is mediated by the conserved Fc region, antibodies with specificities for alternative influenza antigens, or antigens

of other pathogens, can also be easily exchanged in this platform without changing the basic architecture of the system.

While these approaches demonstrate some of the advantages of surface immobilization for detection, many platforms – both those driven by self-assembly and those governed by different types of interactions, such as chemical conjugation – have limitations. For example, linking molecules to a surface can alter physical conformation and, as a result, the capacity to bind to an antigen or molecule of interest. In addition, increasing the density of detection molecules (e.g., antibodies) on a surface may offer more binding sites, but these high packing densities can also result in steric hindrance to binding. Thus, some studies have explored self-assembly that integrates linker structures to provide high density arrangements of molecules with predictable orientation and spacing on surfaces [150, 151]. In one report, a self-assembling coiled-coil peptide structure was used to display a glycopeptide found on the surface of a potent biological toxin at a controlled, high density [150]. This strategy led to higher avidity with the detection antibody, enhancing the sensitivity of the assay compared with direct display (i.e., without self-assembly).

Nucleic acids provide a unique platform to design well-controlled structures that could be used to link detection probes to surfaces, because their inherent controlled sequence length and composition can be exploited to drive spontaneous, hierarchical assembly. One recent illustration of this idea involved engineering single stranded DNA sequences to spontaneously assemble into a DNA tetrahedron structure probe

(TSP). This probe was linked on three sides to a glass substrate, while the unbound free side of the tetrahedron was used to display probes for different classes of target molecules, including nucleic acids, protein, and small molecules [151]. The authors tested the role of this design by comparing the sensitivity of a purified, DNA-targeting structure (TSP monomer) with three controls, i) the probe in free form (i.e., tetrahedron-free ssDNA), ii) the unpurified product of self-assembly (unpurified TSP), and iii) a purified structure unrelated to the target structure (TSP polymer) **(Figure 5.4A)**. Equivalent doses of the DNA probe were conjugated to glass substrates in the test and control formats just described, then a complementary structure labeled with a fluorophore was incubated with each group, followed by a wash step to remove unbound fluorescent probe. A dramatic signal enhancement using the TSP monomer formulation was observed qualitatively through fluorescence microscopy (**Figure 5.4B**) and quantitatively by fluorescence intensity (**Figure 5.4C**). The TSP monomer exhibited 14-fold increase in signal intensity compared with that of free ssDNA, as well as enhanced signal levels compared with the unpurified or unrelated control structures, described above. These findings support the authors' hypothesis that oriented conjugation and self-assembly were responsible for the regular spacing of molecules on the substrate. The authors also demonstrated the potential to immobilize multiple classes of molecules, supporting the flexibility of this diagnostic tool. In future studies, the modular nature of such platforms could be exploited to control the distance between ligands by, for example, increasing or decreasing the length of the DNA tetrahedron chains and, by extension, the footprint of the self-assembled structure. In contrast, approaches that use alternative strategies,

such as direct conjugation of molecules to a surface, may generate precise control over total ligand bound, but might not offer the same level of control over the spacing or physical arrangement of those ligands. The application of self-assembly to enable the surface-bound display, as well as to control the spacing and valency of antigens could also extend to the design of new strategies to deliver immune cues *in vivo*, as discussed further in **Section 5.5.2**.

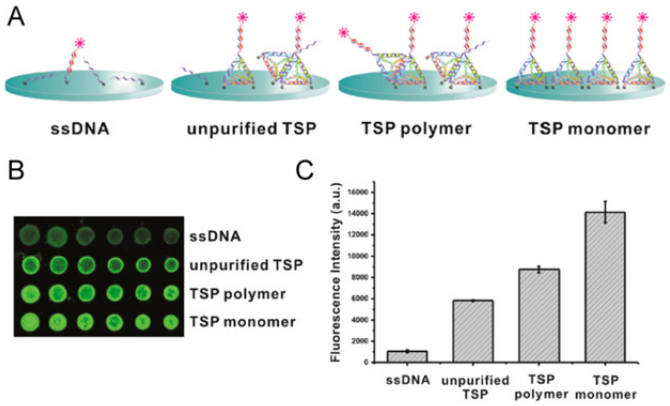

Figure 5.4 Engineered self-assembled DNA structures enhance the sensitivity of an immunosensing platform.
A) Schematic depiction of physical arrangements of the tetrahedron structure probe (TSP monomer), compared with three controls: i) the single stranded DNA (ssDNA) probe in free form, ii) the unpurified, heterogeneous TSP product, and iii) a polymeric TSP product. In each case, a complementary DNA sequence, linked to a fluorescent reporter, depicted in pink, has been added to show expected degree and orientation of binding. To test the sensitivity of these probe conformations, a uniform quantity of the capture probe, in the four formulations depicted in (A), was deposited on glass substrates. An equivalent mass of the detection probe was added to each well and after an incubation period, excess unbound probe was washed away. The level of fluorescent signal detected could be visualized qualitatively through fluorescent microscopy (B) as well as determined quantitatively (C). Adapted from [151] with permissions.

5.5. Self-assembled systems can create design guidelines for new vaccines and immunotherapy strategies

5.5.1. Physiochemical properties of self-assembled materials help determine the magnitude and nature of immune response

Self-assembled nano- and micro-scale materials are being used as platforms to explore the relationship between the physical and chemical characteristics of

materials and the magnitude and nature of responses elicited. For example, the role of particle size and shape has been studied, comparing spherical formulations to higher aspect ratio conformations, such as rods or filaments [152-154]. One intriguing theme in this area has been to develop materials that mimic the size and shape of pathogens, such as nanoscale spherical particles that represent viruses, or anisotropic shapes that represent bacteria. The goal is to investigate whether these properties impact immunogenicity and the interactions with immune cells [152-154]. For example, the Scott lab has demonstrated that the size and shape of particles impacts the association of materials with target APC populations, such as DCs, following intra-venous injection in mice [154]. The materials in these studies were self-assembled via hydrophobic interactions using the same co-polymer, poly(ethylene glycol)-bl-poly(propylene sulfide), which enabled the study of different particle geometries with a fixed composition and conserved surface chemistry. Their findings revealed enhanced uptake of spherical particles 113.7nm in diameter by DCs compared with smaller nanoparticles, 22.5nm in diameter; the latter were instead found to associate highly with macrophages in the liver. In contrast, fibrous structures formed from the same polymer, termed filomicelles, remained associated with phagocytic cell populations in the blood over time, suggesting an increased circulation time and decreased uptake by phagocytic cells. Together, these results indicate the shape and size of self-assembled particles can alter the biodistribution and retention of nanomaterials. These features and guidelines could be harnessed for translational applications to target particular subsets of cells.

In addition to size and shape, surface properties of self-assembled carriers have been investigated. One recent finding used a platform to generate nanofibrils from peptide monomers that self-assemble through the formation of beta-sheets. These fibrils were used to display defined concentrations and combinations of peptide antigens on the surfaces and to investigate the role of fibril properties in promoting pro-inflammatory responses [155]. Fibrils with a negative zeta potential, a measure of surface charge, were found to exhibit significantly reduced or even undetectable T cell and B cell (i.e., antibody) responses. In contrast, fibril formulations containing equivalent doses of a common model peptide antigen derived from chicken ovalbumin (OVA), SIINFEKL, but with a positive charge, drove potent expansion of antigen-specific T and B cell responses. This finding could be used to inform design criteria – for self-assembled materials, as well as for biomaterials-based approaches more generally. For example, in translational applications where strong pro-inflammatory responses are desired (e.g., infectious disease, cancer immunotherapy), design of nanomaterials with positive surface charge may help further tune the potency and effectiveness of immune response.

An important example of pro-inflammatory signals garnering interest in the clinic is adjuvants, agents designed to amplify the magnitude of immune responses. Current clinical adjuvants include potassium aluminum sulfate (alum), aluminum hydroxide, and mycophenolic acid (MPL) [133, 134, 136]. However, the mechanism of action of these adjuvants is not fully-understood and they offer limited control over the nature of responses elicited [114, 156], motivating exploration of signals that still drive

enhanced immunogenicity, but with more definition and molecular specificity. As discussed in **Section 5.2.1**, APCs have evolved to detect molecular signatures of pathogens. Pattern recognition receptors, such as toll like receptors (TLRs), detect molecules and structures that are not present in mammalian cells (i.e., "self"), but are common among bacteria and viruses. Agonistic ligands for these receptors – such as lipoprotein components of bacterial cell walls, or distinctive nucleic acid structures frequent in viruses – have emerged as promising stimulatory immune cues to enhance the immunogenicity of candidate vaccines [109, 115, 157-159]. TLR agonists (TLRas) are well-suited for this function, as they trigger defined molecular pathways to upregulate the expression of activation markers on APCs (signal 2) and drive inflammatory cytokine secretion (signal 3), both of which can promote expansion of pro-inflammatory T cells and trigger potent antibody responses.

Generally, nucleic acids are intriguing molecular building blocks owing to the ability to design predictable structures of DNA or RNA. Fortuitously, a number of nucleic acid classes also activate TLRs. Thus, in the self-assembly field, molecular TLR agonists are of great interest. Some of these studies are investigating how the shape of carriers used to deliver TLR ligands [153], or the tunable surface display of TLR ligands [160-162], impacts the degree of DC activation and the cytokine secretion profiles. As discussed in **Section 5.4**, DNA sequences can be finely tuned to form defined structures, enabling control over the organization and spacing of tertiary features. For example, dendrimers have been assembled to control the loading of a TLR9 ligand, CpG, in nano-assemblies that trigger secretion of an inflammatory

cytokine, TNF-α [163]. In another example, CpG was integrated with a helical DNA assembly to form different shapes, including triangle, square, and polygon assemblies. In these structures, increasing the number of sides in the carrier enabled increased loading of CpG per assembly. This control over CpG assembly and, as a result, dose, directly correlated to the level of inflammation measured during incubation with a macrophage cell line [164]. These strategies are just two examples of biomaterials-based approaches to deliver CpG or other TLRs, but they demonstrate the potential of predictable, well-controlled self-assembly of nucleic acids for designer immunogenic materials.

In another example of modulating immunogenic nucleic acid delivery, Lynn *et al.* controlled the conformation of a TLRa by tuning the display of a small molecule agonist of TLRs 7 and 8 (TLR-7/8a) on a N-(2-hydroxypropyl)methacrylamide (HPMA) polymer scaffold (**Figure 5.5A**) [162]. As the mass of TLR-7/8a per mass of polymer was increased, spontaneous self-assembly of conjugates of TLR-7/8a and polymer was observed. Interestingly, when equivalent doses of TLR-7/8a were administered in either a low density formulation that existed primarily as small, individual polymer coils (PC-7/8a, **Figure 5.5B**) or in a high density formulation that assembled into polymer particles (PP-7/8a, **Figure 5.5B**), the resulting responses differed. Delivery of TLR-7/8a in particulate form in mice drove significantly increased levels of IL-12p40, a key inflammatory cytokine involved in the expansion of pro-inflammatory T cells, compared with an equivalent dose in small polymer coil form (**Figure 5.5C**). This observation was accompanied by an increased level of

fluorescently-labeled TLR-7/8a present in draining LNs of mice treated with the particulate form (PP-7/8a), compared with a small molecule formulation (SM 7/8) or the polymer coil form (PC-7/8a) (**Figure 5.5D**). As LNs are key sites of interactions between APCs and lymphocytes, they are a crucial target for candidate vaccines and immunotherapies. Thus, many strategies focus on design of carriers that drain to these sites [20, 165] or are carried to LNs after encounter with APCs [4, 109, 120], or directly access these tissues through targeted introduction of soluble or biomaterials-based formulations [4, 27, 60]. In the above example, Lynn *et al.* used a library of candidate materials to interrogate the role of carrier properties in modulating the biodistribution of signals and magnitude of responses.

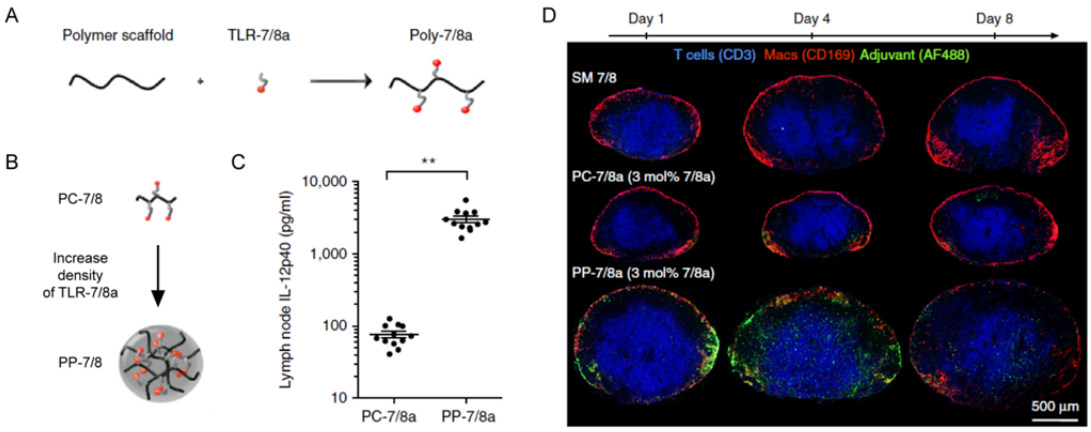

Figure 5.5 Programmable density of ligand display enables modulation of the biodistribution and stimulatory capabilities of a molecular adjuvant.
A) Schematic of linking a TLR-7/8 agonist to a polymer scaffold to generate assemblies with controlled ligand density. B) Depictions of a polymer coil displaying TLR-7/8 (PC-7/8) and the assembled polymer particle containing TLR-7/8 (PP-7/8) that was observed as ligand density was increased. C) Quantification of the level of inflammatory cytokine IL-12p40 in the draining lymph node following injection of either PC-7/8 or PP-7/8 shown in (B). D) Immunofluorescent staining of draining lymph nodes following injections of small molecule TLR-7/8a (SM 7/8), PC-7/8a, or PP-7/8a. Images show T cells (CD3, blue), macrophages (CD169, red) and signal from the TLR-7/8a (AlexaFluor 488, green) at the indicated timepoints. Adapted from [162] with permissions.

5.5.2. Self-assembly facilitates programmable densities of defined combinations of antigens

The previous section demonstrates some of the advantages of self-assembly for adjuvant delivery and parsing out the role of physicochemical features of carriers in the magnitude and nature of responses elicited. This section focuses on antigens, and the ways in which self-assembly is being exploited to link immune outcomes to antigen physical arrangement, combination, and relative dose. Discussion of VLPs (see **Section 5.3**) motivates this goal. Although VLPs replicate the high density antigen display and physical conformation of target pathogens, modifications to the amino acid sequences that comprise VLPs – to, for example, integrate a different antigen of interest into a carrier – can impair nanoparticle formation [145]. These changes may interfere with or inhibit the non-covalent interactions that typically drive uniform self-assembly. Thus, alternative strategies that can condense defined peptide antigens at high density, with well-controlled physical organization could mimic a key feature of VLPs, but enable flexible platforms for vaccine and immunotherapy delivery.

Along these lines, the Collier lab has used nanofibrils, to deliver controlled combinations, doses, and densities of antigens [31, 143, 166-170]. A beta-sheet-forming peptide sequence (e.g., Q11), can be linked to peptides or proteins of interest and, following self-assembly through hydrogen bonding interactions, these antigens are displayed on the surface of the fibril structure (**Figure 5.6A**) [31]. These fibers have been shown to drive robust antibody (i.e., B cell) responses against model

antigens derived from OVA compared with antigen in free form. Intriguingly, the expansion of OVA-specific antibodies was triggered by fibrils without the addition of an explicit adjuvant or immunostimulatory signal [166]. This property is of particular interest because despite excellent safety profiles and important successes in clinically-used vaccines, the mechanism of conventional adjuvants (e.g., aluminum salts, emulsions) are not fully understood [113, 114, 156, 159].

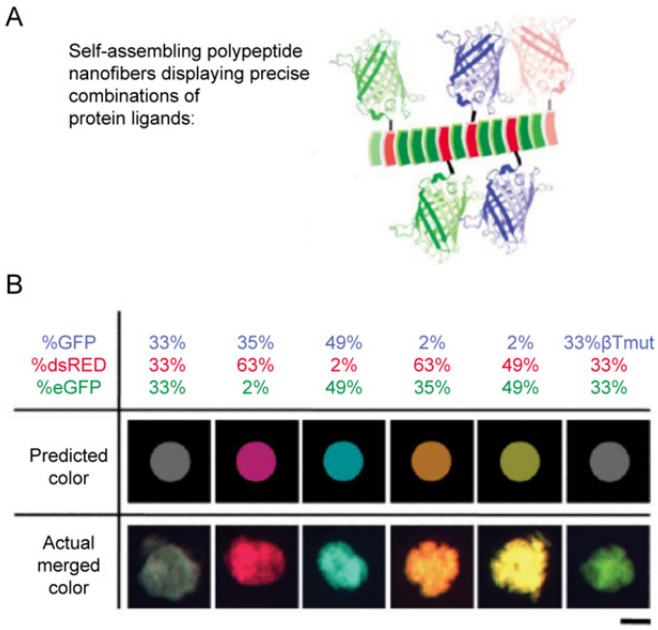

Figure 5.6 Fibrilizing peptide monomers enable co-assembly of multiple proteins with tight control over relative doses.
A) Schematic of a polypeptide nanofiber, self-assembled through a β-sheet fibrilizing peptide sequence, displaying combinations of proteins shown in red, green and blue. B) Tunable incorporation of the three proteins, GFP, dsRED, and eGFP, demonstrated by a matched predicted and actual color values of self-assembled nanofibers, assembled into microgels, at the indicated combinations of each protein ligand. The predicted color value was determined by using the protein mole ratio as an RGB pixel ratio. In one case, a mutated βtail was incorporated, disrupting the self-assembly process and resulting in microgels that, expectedly, did not match the predicted color value. Scale bar = 40μm. Adapted from [31] with permissions.

This nanofibril platform is a salient example of an approach that enables tunable incorporation of cues, as the relative doses of multiple proteins in a single batch can be precisely controlled [31]. To demonstrate this characteristic, three proteins with distinct fluorophores were incorporated into fibrils at tunable ratios that could be

individually visualized (**Figure 5.6B**). Beyond reporter proteins, new work has also explored defined antigen display properties using peptide antigens: i) a sequence from *Staphylococcus aureus* that can be recognized by B cells, but not T cells, and ii) a peptide sequence that binds to the MHC II molecules expressed on the surface of T cells of mice termed PADRE [169]. Defined combinations and concentrations of these sequences were incorporated into fibrils (**Figure 5.7A,** top) that could be visualized by transmission electron microscopy (TEM, **Figure 5.7A**, bottom). The authors demonstrate that co-delivery of both sequences in the same nanofiber drove enhanced antibody production when compared with an equivalent dose of each peptide sequence delivered as a mixture of nanofibers incorporating each peptide separately (**Figure 5.7B**). The hypothesized mechanism of action is that co-incorporation of both sequences promotes co-delivery of both peptides to a single B cell. Next, the dose of the B cell sequence was fixed and the dose of PADRE peptide introduced was titrated. After injection in mice, the number of PADRE-specific T cells was found to depend on the amount of PADRE assembled in the nanofibril (**Figure 5.7C**). The nature or phenotype of these specific T cells was further characterized by staining for transcription factors characteristic of three helper T cell types, T follicular helper (Tfh), type 1 helper (Th1), and type 2 helper (Th2) (**Figure 5.7C**). Interestingly, dose-dependent polarization was observed, with higher doses of PADRE promoting Tfh cells, which enhance the magnitude of antibody responses, over Th1/Th2 cells, which promote T cell-mediated immunity. Thus, these findings could be harnessed to program the specific phenotype of immune responses to, for

example, promote antibody production to combat extracellular bacteria (i.e., Tfh), or promote effector T cell responses (e.g., Th1, Th2) for cancer immunotherapy.

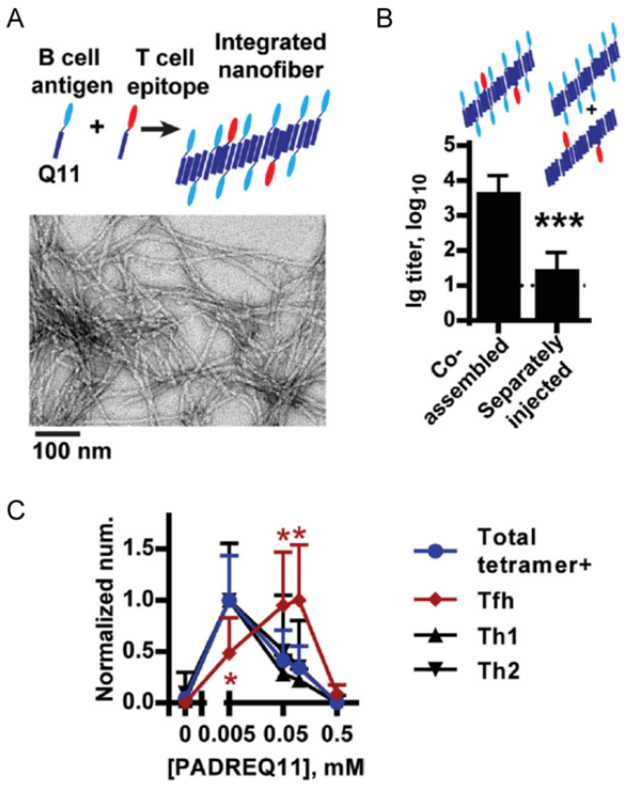

Figure 5.7 Defined nano-architectures allow for direct interrogation of the role of B and T cell epitope co-delivery and relative dosing in shaping the nature of immune response.
A) Schematic depiction of nanofibers that self-assemble through a β-sheet fibrilizing domain, Q11, co-incorporate a B cell peptide sequence and a T cell peptide were visualized under transmission electron microscopy (bottom). B) The potential for either fibers that co-deliver both epitopes, or a mixture of fibers that individually incorporate the T cell or B cell peptides, to raise B cell responses was assessed by measuring antibody titers 7 days after injection in mice. C) The response to fibers co-incorporating a fixed dose of the B cell peptide and titrated doses of the T cell peptide, PADRE, was characterized. The number of PADRE-specific T cells, and the number of PADRE-specific T cells that exhibit T follicular helper (Tfh), T helper 1 (Th1), or T helper 2 (Th2) phenotypes was quantified and reported normalized to the maximum value for each subset. Adapted from [169] with permissions.

In addition to the nanofiber approach above, other researchers have used alternative self-assembly strategies to control antigen delivery [171-176]. For example, antigens have been linked to hydrophobic peptide sequences that assemble into coiled-coil domains to condense into spherical nanoparticles [177]. Other reports focus on coiled-coiled domains that fold into nanoparticles with tunable ligand display and size

by controlling parameters such as pH and salt concentration during folding [178]. A synthetic polymer, poly(hydroxyethyl methacrylate) (pHEMA) – which contains a hydrophobic side chain that drives self-assembly – has also been used to complex and condense a protein antigen into nanoparticles with sizes that can be tuned by controlling the concentration of protein incorporated [173]. In parallel, synthetic peptide amphiphiles have been designed to generate fibers or micelle structures [179-182]. For instance, the Tirrell group has demonstrated that peptide amphiphile-based nanofibers, assembled through hydrophobic interactions, drive $CD8^+$ T cell responses against the model epitope SIINFEKL and enhance survival in a subcutaneous melanoma model expressing the same model antigen, B16-OVA [179].

Together, the strategies in this section demonstrate the potential to incorporate defined combinations of peptide antigens into self-assembled nano- or micro-scale materials. This characteristic could prove particularly advantageous in the context of pathogens and diseases which exhibit non-uniform or heterogeneous characteristics within and across patients. From this perspective, eliciting responses against multiple antigens simultaneously could enhance the protective capacity of a prophylactic vaccine, or the efficacy of an immunotherapy. Two current clinical examples include influenza – which undergoes rapid mutation and, as a result, a new formulation of the flu vaccine is required each year – and cancer, in which tumor associated antigens can vary greatly from patient to patient, within a given tumor, and over time. A final consideration is that the immunostimulatory activity of both synthetic VLPs (see **Section 5.3**) and self-assembled structures for multivalent delivery of antigens (see

Section 5.5.2) has been demonstrated without the inclusion of an explicit adjuvant in pre-clinical studies. Such intrinsic stimulatory characteristics can be a significant advantage for pro-inflammatory applications. However, the formulations explored that enable presentation of antigen without triggering strong inflammatory responses could instead be harnessed for alternative applications, such as promoting tolerance to "self" antigens during autoimmune diseases. For example, Shen and colleagues have induced tolerance during a pre-clinical model of rheumatoid arthritis by harnessing a mechanism that the severe acute respiratory syndrome (SARS) virus uses to evade immune surveillance [183]. Thus, rationally-assembled structures could inform the design of therapies for either pro-inflammatory or tolerogenic targets, described in further detail in **Section 5.6.3**.

5.5.3. Self-assembly enables co-delivery of multiple classes of immune cargos to trigger responses through selective molecular pathways

While the previous two sections focused on carrier properties and the delivery of either antigen or adjuvant alone, vaccines and immunotherapies often deliver antigens along with adjuvants or modulatory cue to direct the response to the antigen. This is a central paradigm in vaccines for infectious disease, and also a developing area in cancer immunotherapy, where tumor-associated antigens are delivered with molecular adjuvants (e.g., TLRas) or antibody therapeutics during cancer vaccination regimens. Co-delivery of antigen with one or multiple TLRas [165, 184, 185] could enhance inflammatory signaling cascades during antigen presentation, promoting the expansion of antigen-specific $CD8^+$ T cells or pro-inflammatory phenotypes of $CD4^+$

T cells (e.g., Th1). In contrast, in the context of autoimmunity, an emerging goal is delivery of "self" antigen with a regulatory immune cue to induce tolerogenic T cell phenotypes, such as regulatory T cells (T_{REGS}). In either case, the principle of co-delivery of antigens and immunomodulatory signals presents a fundamental challenge: coordinated delivery of multiple signals to target cells and tissues *in vivo*. This hurdle can be compounded by disparate physiochemical properties (e.g., molecular weight, charge) of cargos that results in differences in biodistribution and trafficking after injection. In this section, we will describe strategies that exploit unique characteristics of self-assembled materials to co-deliver immune signals.

Several approaches have emerged to co-assemble and co-deliver antigen and adjuvant using non-covalent interactions, including electrostatic or hydrophobic interactions, and other driving forces. For example, micelles and other particulate strategies have been used to deliver model antigens and either individual TLRas or defined combinations of TLRs [176, 186-188]. Interestingly, one example of this approach demonstrates that co-incorporation of antigen and adjuvant enhances the potency of the response with minimal systemic inflammation [188], an off-target side effect often associated with adjuvant delivery. These results highlight an advantage of assemblies that enable co-encapsulation, as simple mixtures do not offer control over how each signal is distributed following injection.

A general advantage of particulate-based systems for co-delivery of immune cues is the potential to target APCs, which have evolved to detect and engulf particulates.

This function offers an opportunity to tune uptake and processing of antigens using controlled architectures of self-assembled materials. As discussed in **Section 5.2.1**, extra-cellular or "exogenous" antigens are typically processed and presented through an MHC II pathway, which leads to $CD4^+$ helper T cell responses. Yet, for many applications, expanding $CD8^+$ T cells against an antigen of interest is a critical goal. Thus, strategies that direct the processing and presentation of delivered antigen toward the MHC I pathway – typically reserved for intra-cellular peptides, such as those formed during degradation of viral particles that have infected host cells – are of key interest. When APCs engulf a pathogen or particle, these materials are generally entrapped in endosomal or lysosomal compartments. This pathway triggers presentation of antigens along the MHC II pathway to communicate to cells of the adaptive immune system that extracellular, foreign peptides were detected. However, for pathogens requiring $CD8^+$ cytotoxic T cell activity to destroy infected cells, antigens must reach the cytosol of cells to enable presentation through the MHC I pathway. This process of presentation of endocytosed antigen being presented by the cytosolic MHC I pathway is termed "cross-presentation" [189]. To support this process using synthetic materials, the Swartz and Hubbell groups have reported self-assembling polymersomes that are oxidation sensitive. These assemblies can be loaded with immune signals and, on delivery to cells, promote endosomal escape and cytosolic delivery of antigen or TLR7/8 ligands [190]. In another example, pH sensitive micelles, which self-assemble through hydrophobic interactions among a polymer carrier, were used to study intracellular antigen trafficking to promote cross-presentation of the model antigen OVA [191]. Nanoparticles condensed through

hydrophobic interactions were used to entrap OVA, CpG, and a pH sensitive polymer poly(propylacrylic acid). These assemblies exhibited pH-dependent membrane disruption properties, which resulted in enhanced presentation of OVA through the MHC I pathway compared with simple mixtures of the OVA peptide and the polymer nanoparticles [192, 193]. Together, these results highlight opportunities to design self-assembled carriers that target APCs, are responsive to environmental cues, and control how immunological cargo is trafficked in intracellular components.

One driving force of non-covalent self-assembly that has emerged as an approach to organize immune cues into well-controlled assemblies is electrostatic interactions [194-196]. This strategy is particularly well-suited for immunological applications, as many immune signals of interest are inherently charged. For example, nucleic acid ligands of TLRs can serve as an immunostimulatory cargo and facilitate self-assembly through the negative charges of the phosphate backbone. In addition, peptide antigens can exhibit intrinsic charge from amino acid side chains, or peptide antigens can be linked to charged amino acid sequences to alter charge ratio. These properties have been exploited to drive spontaneous (e.g., complexation) or sequential (e.g.., layer-by-layer adsorption) of cargos. In one example, layer-by-layer assembly was used to co-assemble and co-deliver a T cell antigen and a B cell antigen for a cancer model [172]. These antigens were modified with lysine residues to confer positive charge and facilitate electrostatic association with a synthetic anionic polymer, γ-polyglutamic acid (γ-PGA). The self-assembled particles drove significant increase in antibody titers, while control formulations without the lysine

modifications exhibited significantly diminished responses. These results demonstrate the importance of the cationic modification to drive electrostatic self-assembly, and underscore the synergistic effect observed when multiple antigens were co-delivered [172], consistent with the enhanced effects upon co-delivery of T and B cell antigens on a single nanofiber, described in **Section 5.5.2** [169].

In other approaches, synthetic polymers have been exploited to co-assemble antigens and TLR agonists via electrostatic assembly. De Geest *et al.*, have reported a polyelectrolyte multilayer strategy to co-deliver antigen and TLR agonists in microcapsules [197]. In this example, OVA is precipitated in a calcium carbonate core, which is then coated in a layer-by-layer fashion with two synthetic polyelectrolytes, poly-L-arginine and dextran sulfate. In some cases, a final layer of CpG was added. These capsules drove significant expansion of transgenic T cells with receptors specific for OVA peptide, as well as secretion of a pro-inflammatory cytokine among these cells. In mice, assembled capsules drove dramatically increased inflammatory cytokine secretion among the $CD4^+$ and $CD8^+$ T cell subsets and enhanced the level of antibody production when compared with soluble OVA, a soluble mixture of OVA and CpG, or capsules that encapsulated OVA only [197]. This result supports a synergistic effect of co-delivery of antigen and adjuvant, enabled by electrostatically-driven co-assembly.

Our lab has recently reported a platform to co-assemble antigens and adjuvants into nanostructured materials constructed entirely from immune signals [32, 33, 198-201].

These immune polyelectrolyte multilayers ("iPEMs") are built using the electrostatic, layer-by-layer process hallmark of PEMs, yet are unique in that they mimic attractive features of biomaterials, but eliminate all polymer matrices or carriers. This approach simplifies composition, provides modularity and high absolute cargo loadings, and also eliminates intrinsic carrier effects. iPEMs can be assembled on gold nanoparticles [32, 200], used to form carrier-free hollow microcapsules [33, 198, 201], or coated on microneedle arrays [199]. To form capsules, a model antigen (SIINFEKL) was linked to cationic arginine residues to confer positive charge, and assembled with an inherently anionic nucleic acid-based TLR3 agonist, polyIC. Thus each cargo, antigen and adjuvant, served both as a functional immune signals and as a structural component that enabled electrostatic assembly and formation of iPEM capsules upon core removal (**Figure 5.8A**). Layer-by-layer assembly enabled control over the loading as a function of the number of bilayers deposited (**Figure 5.8B**). Compared with an equivalent vaccine composed of a mixture of antigen and adjuvant, components assembled into iPEMs dramatically enhanced the expansion of antigen-specific T cells, indicated by an increased frequency of SIIN-specific $CD8^+$ T cells after both prime and boost injections (**Figure 5.8C**). This increase correlated to prolonged survival when vaccinated mice were challenged with a melanoma expressing SIINFEKL antigen, B16-OVA (**Figure 5.8D**). The flexibility of this platform for cancer vaccination was demonstrated by using microneedle arrays as substrates to assemble iPEMs composed of CpG and a tumor antigen, Trp2 (**Figure 5.8E**). These arrays enabled co-delivery of both signals to the skin of mice (**Figure 5.8F**) and drove significant expansion of tumor-specific $CD8^+$ T cells in following

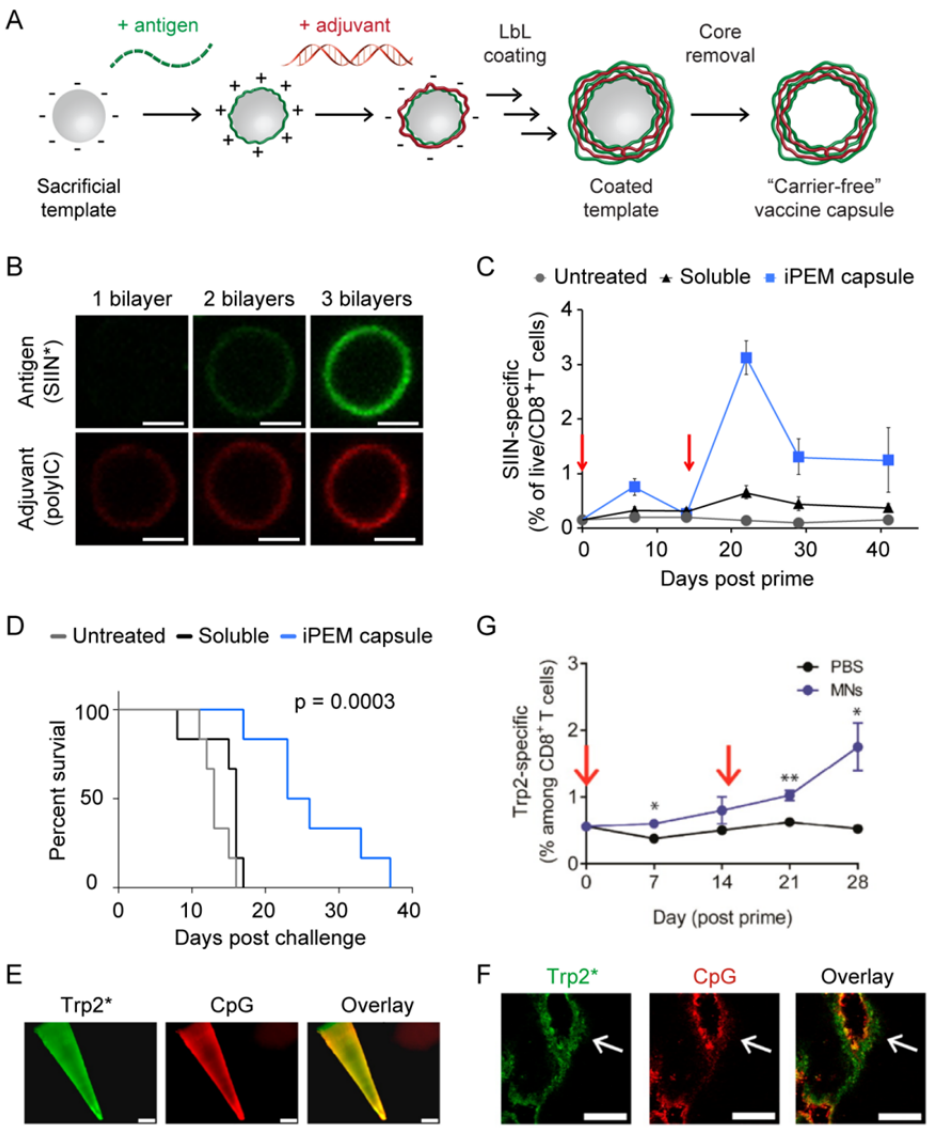

Figure 5.8 Tunable, electrostatically-driven assembly and antigens and adjuvants in carrier-free assemblies.
A) Schematic of layer-by-layer assembly of antigen and adjuvant to form carrier-free immune polyelectrolyte multilayer "iPEM" capsules. B) Tunable loading of fluorescent antigen and adjuvant into iPEMs as a function of the number of bilayers deposited on a microparticle core. C) Expansion of antigen-specific (i.e., SIIN-specific) T cells following two administration of iPEMs, compared with frequencies in untreated mice or mice given simple mixtures of antigen and adjuvant. D) Survival of mice following challenge with a model of melanoma. E) Microneedle coated with a melanoma antigen (Trp2*) and a TLR9 agonist, CpG and F) delivery of these signals to the skin of mice following microneedle application. G) Expansion of Trp2-specific T cells following two applications of Trp2/CpG coated microneedles (MNs), indicated in red arrows. Panels A-D adapted from [33] and panels E-G adapted from [199] with permissions.

application of the coated arrays (**Figure 5.8G**). Together, examples here demonstrate the potential of the iPEM platform to co-localize immune signals over multiple

length-scales and without the inclusion of synthetic polymers or carrier components. This simplicity and modulatory could support the design of well-defined vaccines formulations that facilitate characterization and, ultimately, translation of vaccines and immunotherapies.

5.6. Pre-clinical studies using self-assembled materials demonstrate exciting translational potential in infection and disease models

5.6.1. New vaccines and immunotherapies face challenges in both performance and production

Work described in **Section 5.5** is beginning to reveal design rules for how self-assembled materials interact with immune cells. This section focuses on the translational component of self-assembly, presenting recent examples that involve pre-clinical models and that target current clinical challenges. For example, a fundamental issue in the development of new vaccines and immunotherapies is balancing efficacy and safety. On one extreme, the delivery of live viruses or bacteria can trigger strong protective immune responses, but increases the risk of infecting patients. In contrast, small subunits of pathogens (e.g., short peptide monomers) confer less risk, but are also less immunogenic. This characteristic may result in suboptimal or inadequate responses, necessitating multiple doses and the addition of adjuvants to amplify responses, which complicates the composition and characterization of formulations, and can cause adverse reactions [113, 114, 156].

Traditionally, vaccines have incorporated live, but attenuated or inactivated (e.g., heat-killed) pathogens, often co-delivered with adjuvants, to balance these two factors [100, 102]. However, this approach requires the availability of pathogen in large quantities for manufacturing. Recent developments in the seasonal influenza vaccine also reflect some of these critical challenges associated with prophylactic vaccine manufacturing and distribution. Two general vaccines for influenza have been approved: the first, an injected vaccine formulation, is composed of inactivated virus; the second is a live, but attenuated virus delivered intra-nasally. A recent study to evaluate vaccine effectiveness in children ages 2-17 conducted by the Centers for Disease Control and Prevention (CDC) revealed that the nasal spray formulation exhibited reduced efficacy compared with the injected formulations of the vaccine [202]. This result led the CDC's Advisory Committee on Immunization Practices, to vote that the nasal spray formulation should not be used in the 2016-2017 season [202].

In addition, despite the reliable level of protective immunity conferred by many vaccines – including flu, there are still significant improvement opportunities for these cases. The current vaccine is primarily generated by growing the virus in chicken eggs, which inevitably takes time to generate in large scale [203], by some estimates a 20-28 week timeline to produce [204]. In contrast, cell culture-based approaches may require roughly half of this duration to produce [204] The delay with these approaches is particularly relevant to the example of the seasonal influenza vaccine, because the formulation must be changed each year to reflect the strain most

likely to spread. Thus, strategies that would allow for rapid and economical production, as well as the flexibility to incorporate antigens to one or more target strains of the virus, could be transformative. Further, incorporation of live, attenuated virus mentioned above can still pose risk of infection, motivating the exploration of synthetic approaches – perhaps that incorporate self-assembly – to recapitulate the structure of pathogens that do not have the potential to replicate.

Another challenge facing vaccines is stability. As an illustration, in one recent study, storage of alum, a clinically-approved adjuvant, for 6 months at 45 °C led to a significant decrease in immunogenicity [170]. This result exemplifies a hurdle for the field: the requirement for a cold chain of refrigeration in order to disseminate vaccines or immunotherapies worldwide. Current clinical options are typically sensitive to both extreme heat and cold; carefully controlled storage is required to maintain the stability of emulsion-based adjuvants and the viability and long-term potency of live, attenuated pathogens. This limitation is particularly relevant because some of the most critical regions to deliver vaccines are in the developing world, where access to healthcare professionals and refrigeration are extremely limited [205, 206]. Self-assembly is already being utilized in this area: one study confirmed that self-assembled nanostructures displaying a peptide epitope of *Mycobacterium tuberculosis* maintained immunogenicity even after storage for 6 months at 45 °C, compared freshly-prepared doses [170]. This is just one example where self-assembly is being weighed with a specific translational focus. In **Sections 5.6.2** and **5.6.3** we bring other translationally-geared reports to the forefront, illustrating new self-

assembly strategies for either promoting or regulating responses to vaccines and immunotherapies.

5.6.2. Self-assembled materials generate efficacious responses in pre-clinical models of infection and cancer

One recent approach to minimize risk, but maximize efficacy in a therapeutic context is the use of VLP-based vaccines to incorporate and deliver influenza antigens [133, 203, 204, 207, 208]. The potential for these VLPs to protect against viral challenge with the same strain from which the VLPs are derived (i.e., homologous strain), as well as against challenges with other strains, have been tested [208]. Importantly, the potential to protect against multiple strains could help determine whether candidate vaccine and therapies have the potential to confer broad protection; this question is particularly relevant for influenza, as the virus mutates rapidly to evade immune clearance. While VLPs exhibit have demonstrated exciting pre-clinical and clinical success, there are considerations beyond efficacy. The production of recombinant proteins (i.e., VLPs) in cell lines is associated with high cost and low yield, and requires careful purification and characterization to ensure homogeneity, reproducibility, and potency [131, 136, 209]. Thus, ongoing studies aim to enhance the efficiency, yield, and purity of the final vaccine product [175, 177, 209, 210]. In parallel, researchers have also investigated the use of short, synthetic monomers, which are simpler to produce in cell culture compared with full recombinant proteins, or could enable cell-culture-free production. These monomers could then be

harnessed to incorporate defined target antigens into nano- or micro-scale materials through self-assembly.

The nanofiber strategies to enable high valency display of model antigen described in **Section 5.5.2** have also been harnessed to elicit responses against disease-relevant antigens. For example, the platform from the Tirrell lab has been extended for immunization against group A streptococcus [182], while Rudra and colleagues demonstrate an approach to trigger antibody responses against a malaria antigen [167]. The driving force of the self-assembly in the latter approach – beta-sheet formation – has also been employed to incorporate a protein from the envelope of West Nile virus (EIII) [211]. In this work, the self-assembling peptide containing a beta-sheet-forming domain spontaneously formed an injectable hydrogel that entrapped EIII to enable sustained, subcutaneous delivery to mice. The hydrogel formulation conferred significant protection in a viral challenge model, with a final survival of 60%, compared with 20% in untreated mice or mice treated with EIII incorporated in a clinical adjuvant, alum [211].

The example just discussed represents an approach using self-assembly to generate a hydrogel that has larger dimensions on the macro scale; along these same lines, others have developed peptide fibers that self-assemble after injection to mimic the antigen "depots" often formed by conventional emulsion-based adjuvants. The goal of this approach is to generate a persistent source of antigen for prolonged immunostimulation, a partial mechanism of action of alum and other current

adjuvants used in the clinic [113]. This fiber-based approach was employed to deliver a hepatitis B antigen with CpG, which triggered enhanced humoral and cellular responses when compared with a formulation containing alum and an equivalent dose of EIII [212]. Together, these results support the potential to use self-assembled materials to generate *in vivo* depots of antigen and immunostimulatory cues that can enhance immunogenicity. This approach could also simplify depot-like vaccine formulations by incorporating well-defined peptide sequences rather than complex adjuvant systems.

Molecular adjuvants delivered in self-assembled systems are also being explored in disease contexts either with or without antigens. In the latter case, these strategies often exploit the fact that, during disease, the immune system is actively surveying and processing disease-relevant antigens. Yet, the responses to those antigens are not effective in generating responses that combat disease. For example, in cancer, lymph nodes often contain tumor associated antigens that have reached these sites either through passive drainage through the lymphatics or active transport via APCs. However, the tumor microenvironment is often highly immunosuppressive, evading detection and clearance by the immune system [4, 118, 165, 213]. Cells in tumors may alter the expression of key surface markers or secrete regulatory cytokines that suppress tumor-infiltrating immune cells. This reduction in signal 2 and signal 3 effectively reduces the level of "danger" signals, inhibiting the generation of the robust responses needed to clear tumors. Thus, the incorporation of modulatory

signals may be able to redirect or skew the types of responses generated against disease-relevant antigens.

One example of an approach to modulate responses in clinically-relevant contexts has been to incorporate molecular adjuvants into self-assembled materials. CpG has been incorporated into multiple self-assembled nanoparticle formulations, through non-covalent interactions with lipids [161], gold nanoparticles [160, 214], or synthetic polymers [215]. Broadly, these strategies aim to enhance circulation time as well as target CpG to target cell populations – APCs, like dendritic cells – through nanoparticle-mediated delivery. This approach has been shown to slow tumor growth and enhance survival in a mouse model of melanoma [214, 215]. In another example, self-assembly was harnessed to incorporate multiple TLRas, for TLR2 and TLR9, into a nanoparticle with a tumor associated antigen – MUC1, a mucin transmembrane glycoprotein. These nanoparticles were designed to self-assemble through electrostatic interactions to co-deliver these three therapeutic cargos. Treatment of mice with the nanoparticles conferred a synergistic effect on survival in an aggressive melanoma model compared with formulations that contained antigen and a single adjuvant, or antigen alone [216].

Finally, the electrostatic assembly approaches described in **Section 5.5.3** have also been exploited for pro-immune disease applications by, for example, condensing adjuvant and antigens for either cancer or viral infection [217]. De Geest *et al.* demonstrate a dramatic enhancement in mouse survival using layer-by-layer

assembled capsules to deliver antigen compared with soluble antigen in a model of melanoma. The modular nature of the PEM system was then exploited to instead incorporate an antigen for influenza A. In challenge studies, PEM-mediated delivery of antigen again exhibited an enhanced protective effect over soluble antigen, supporting a role for delivery of antigen in self-assembled particles to enhance protective immune effects [217]. One final example of electrostatic assembly for pro-inflammatory, therapeutic application involves the use of layer-by-layer assembly to co-deliver immune signals for an HIV vaccine administered via transdermal delivery. The Irvine lab has demonstrated an approach to coat microneedle arrays with a degradable cationic polymer, a poly(β-amino-ester), and layers of plasmid DNA encoding for HIV antigens and a TLR3a, polyIC, as the anions [218]. Following microneedle application, the coatings are engineered with a releasable layer to detach from the microneedle substrate and remain in the skin. The co-delivery of these signals was confirmed via immunofluorescent analysis of mouse skin following microneedle application, and the persistence of signals at the site of administration compared with intra-dermal injection at the same site (i.e., mouse ear). Release of films from microneedles drove potent antigen-specific T cell expansion and enhanced antibody titers compared with intramuscular or intradermal injection. Finally, skin penetration and delivery of immune signals was demonstrated in non-human primate skin, supporting the translational potential of this approach in moving towards human disease applications.

5.6.3. Harnessing self-assembly to regulate immune response and promote tolerance during autoimmunity or transplantation

As discussed earlier, during autoimmune disease, "self" antigens are incorrectly recognized and trigger inflammatory attacks. For example, in multiple sclerosis, peptide fragments from myelin, the matrix that lines neurons, are attacked [92-94]. Delivery of tolerogenic immune signals may be able to redirect immune response against the self-antigens by skewing T cell differentiation away from inflammatory phenotypes and toward regulatory phenotypes. However, the potential to expand therapeutic cell types, such as regulatory T cells, involved in tolerance during active autoimmunity is a significant hurdle. MS and other autoimmune diseases are characterized by excess inflammation, but the development of regulatory cells is dependent on the potential for APCs and, subsequently, lymphocytes to process, present, and recognize self-antigens in the absence of stimulatory immune cues (e.g., signal 2, 3).

Toward the goal of downregulating pro-immune signaling, the Mellor group has described electrostatic condensation of plasmid DNA to promote tolerogenic immune function [219-221]. The nucleic acid cargos are targeted to the stimulator of IFN genes (STING) pathway, which is responsible for producing cytokines that potentiate inflammation. Nucleic acids are condensed through electrostatic assembly with a common polycation, polyethyenimine (PEI) to form polyplexes designed to enhance gene delivery. To test the therapeutic potential of this approach, DNA condensed into NP form (DNPs) were tested in a well-characterized mouse model of multiple

sclerosis (MS), experimental autoimmune encephalomyelitis (EAE). In this model, mice are injected with MOG peptide emulsified in a strong pro-inflammatory signal, Complete Freund's Adjuvant (CFA), followed by administration of pertussis toxin to serve as an adjuvant and open the blood-brain-barrier. The pro-inflammatory MOG-specific cells are then able to migrate to the central nervous system (i.e., spinal cord, brain) where they recognize and attack myelin. The result of this attack is progressive paralysis that develops over a few weeks. In this study, a significant decrease in mean clinical score (i.e., reduced disease-induced paralysis) was observed after 5 treatments of DNPs compared with a vehicle control treatment regimen. This effect was observed when treatment was initiated at either the time of disease induction (**Figure 5.9A**) or at the onset of disease symptoms **(Figure 5.9B**). DNPs were shown to restrain the secretion of numerous inflammatory cytokines implicated in disease **(Figure 5.9**C). Importantly, restraint of disease was dependent on delivery of DNA cargo in NP format, as a matched soluble dose caused no effect, supporting the role of self-assembly to enhance delivery of therapeutic immune cargos *in vivo*.

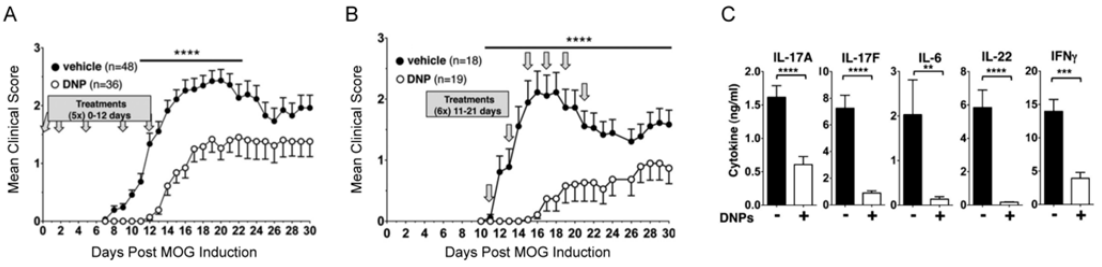

Figure 5.9 Self-assembly-enabled delivery of DNA ligands to the STING pathway limits autoimmunity and inflammation.
A) Mice were induced with a model of multiple sclerosis (EAE) on day 0 and treated at the time of induction with the regiment depicted with either a vehicle control or DNA nanoparticles (DNPs). Mean clinical score of the level of disease-induced paralysis was determined. B) Mean clinical score of mice induced with EAE as in (A), and either treated with a vehicle or DNPs around the onset of disease-induced paralysis using the regimen depicted. C) The level of inflammatory cytokines in lymph nodes of mice immunized with MOG as in and either injected with a vehicle control or DNPs five times beginning at the time of immunization as in (A). Adapted from [221] with permissions.

An intriguing recent idea is to employ biomaterials to co-deliver self-antigen with regulatory immune cues to promote the expansion of cells that are self-antigen-specific, but exert tolerogenic or regulatory functions [47, 201, 222-224] instead of inflammatory attacks. This idea is underpinned in part by a fascinating new role of TLR signaling during autoimmune disease. Recent studies have revealed excess signaling through TLRs contributes to the pathogenesis of autoimmunity in both mouse models and human patients [225-231]. Further, work by the Steinman lab has demonstrated the potential for an antagonistic ligand of TLR9, GpG, to partially restrain inflammation and reduce the severity of the symptoms of EAE in mice when administered in soluble form [85, 232]. Our lab hypothesized that co-delivery of myelin self-antigen electrostatically assembled with GpG might blunt the TLR9 signaling present during multiple sclerosis and skew T cell responses towards T_{REGS} able to control disease (**Figure 5.10A**).

We have formed polyplex-like structures composed of the GpG signal and myelin antigen (MOG) conjugated to one or two arginine residues to confer positive charge, $MOGR_1$ and $MOGR_2$, respectively, eliminating synthetic components [224]. Varying the input of each cargo to the electrostatically-driven self-assembly leads to formation of nano-scale complexes 100-200nm in diameter with tunable properties, such as loading and zeta potential (i.e., surface charge) (**Figure 5.10B**). MOG/GpG complexes were shown to down-regulate TLR9 signaling – the target ligand of the GpG cargo (**Figure 5.10C**), restrain the proliferation of antigen-specific T cells using

a co-culture system with transgenic T cells specific for the MOG peptide (**Figure 5.10D**), and to attenuate EAE.

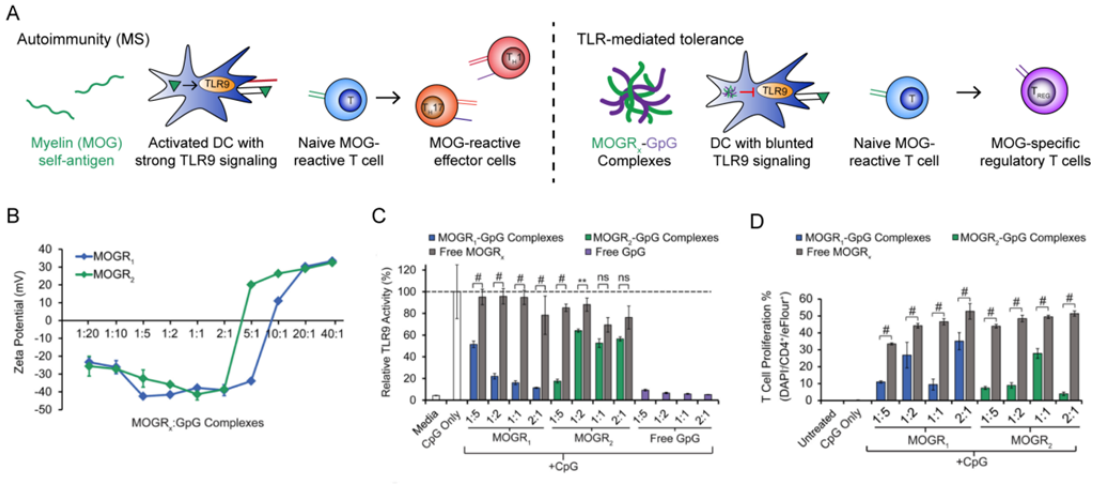

Figure 5.10 Electrostatic complexation of immune signals to restrain inflammatory signaling during autoimmunity.
A) Schematic depicting the hypothesized mechanism for MOG/GpG complexes. Typically during MS, self-antigen, MOG, is processed and presented by DCs in the presence of excess TLR9 signaling, which drives expansion of self-antigen-specific effector T cells (left). In contrast, co-administration of self MOG peptide – modified with arginine residues to confer positive charge, MOG-R_X – with an antagonistic ligand of TLR9, GpG could blunt inflammatory signaling, leading to the development of MOG-specific regulatory T cells (right). B) Nano-scale MOG/GpG complexes exhibited tunable surface charge as a function of the input ratio of MOG peptide to GpG. C) TLR9 signaling was assessed in a reporter cell line following stimulation of cells with CpG and addition of either free MOG-R_X, free GpG, or MOG-R_X/GpG complexes to investigate the potential to restrain CpG-induced signaling. D) Proliferation of MOG-specific transgenic T cells following co-culture with splenic DCs that were isolated from wild-type mice and treated with CpG and either free MOG-R_X, or MOG-R_X/GpG complexes. Adapted from [224] with permissions.

In parallel, we have adapted the iPEM platform described in **Section 5.5.3** promote tolerance by assembly of GpG and myelin self-antigens (**Figure 5.11A**). iPEM capsules formed from myelin peptide and GpG enabled tunable absolute and relative cargo loading of each component (**Figure 5.11B**). Interestingly, these MOG/GpG iPEMs promote antigen-specific T cell proliferation in the co-culture system mentioned above. However, the expanding myelin-reactive T cells were found to secrete lower levels of inflammatory cytokines (**Figure 5.11C**) and higher expression levels of markers characteristic of T_{REGS} (**Figure 5.11D**) when compared with a

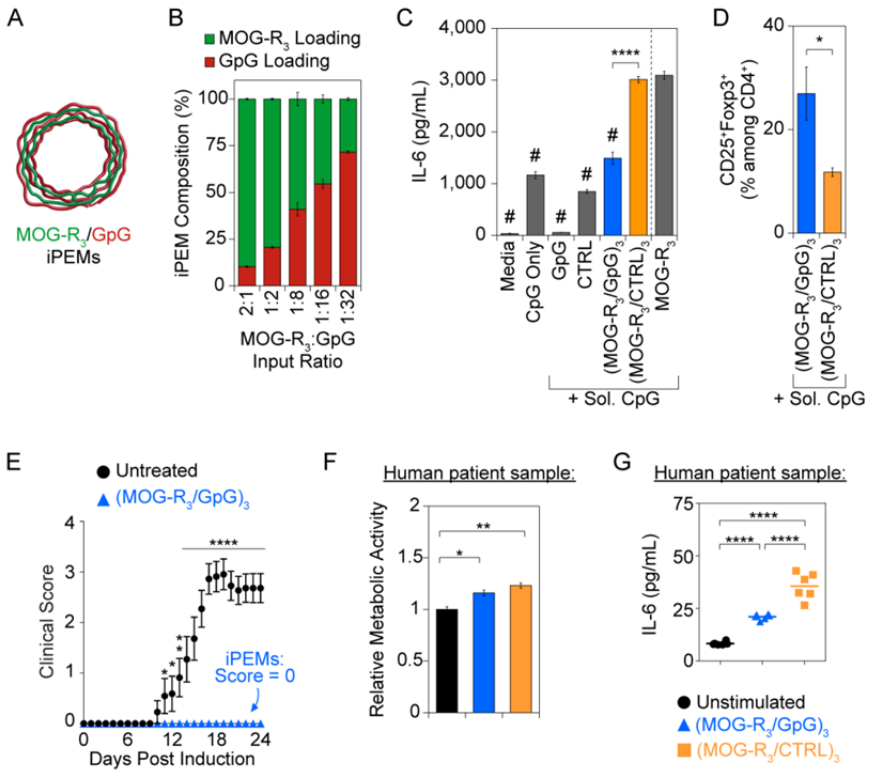

Figure 5.11 Carrier-free co-localization of self-antigen and a TLR9 regulator promotes tolerance in mouse cells, mouse models of autoimmunity, and samples from human patients.
A) Schematic of carrier-free iPEM capsules formulated from an antagonistic ligand of TLR9 (GpG) and myelin self-antigen modified with three arginine residues (MOG-R_3). B) iPEMs exhibited tunable relative loading of each cargo as a function of the cargo input to the synthesis process. C) Secretion of an inflammatory cytokine, IL-6, from co-cultures prepared by isolating wild-type splenic DCs from mice and incubating with media alone, soluble CpG alone, or CpG and either soluble GpG, a soluble control oligonucleotide that does not regulate TLR9 signaling (CTRL), iPEMs assembled from MOG-R_3 and GpG (MOG-R_3/GpG)$_3$, or from MOG-R_3 and CTRL, or free MOG-R_3. After overnight culture, MOG-specific T cells were isolated from transgenic mice, added to cultures, allowed to incubate for three days, and supernatants were analyzed by ELISA. D) A subset of co-culture samples described in (C) were analyzed for expression of markers of regulatory T cells ($CD4^+$/$CD25^+Foxp3^+$) by flow cytometry. E) Mice were induced with a model of multiple sclerosis (EAE) and either left untreated or administered two doses of (MOG-R_3/GpG)$_3$ iPEMs on days 5 and 10 post induction. The severity of disease-induced paralysis was assessed using a clinical scoring scale. F) Peripheral blood mononuclear cells from a human MS patient were incubated with media alone, (MOG-R_3/GpG)$_3$ iPEMs, or (MOG-R_3/CTRL)$_3$ iPEMs and metabolic activity was measured using an MTT assay. G) Supernatants from the cultures in (F) were analyzed for the secretion of inflammatory IL-6 using a Luminex assay. Adapted from [201] with permissions.

control formulation that incorporated myelin peptide and a nucleotide that does not regulate TLR9 signaling (CTRL) **(Figure 5.11C-D**, orange bars). This finding suggests that iPEMs might promote the expansion of myelin-specific T_{REGS} that control disease in a highly specific manner, rather than acting through broad

immunosuppressive pathways. In the EAE model, iPEMs were found to protect 100% of mice from the onset of EAE symptoms **(Figure 5.11E**). Finally, in samples from human MS patients, iPEMs provided similar benefits to those observed in primary mouse cells (**Figure 5.11C-D**); iPEMs containing MOG and either GpG or CTRL activated cells, as measured by an increase in metabolic activity (**Figure 5.11F**). However, iPEMs containing GpG restrained inflammatory cytokine secretion relative to CTRL-containing iPEMs (**Figure 5.11G**). These results in human MS patient samples highlight a unique opportunity to regulate TLR signaling to impact human immune cell function.

Another application of interest to promote immune tolerance is transplantation. Following transplant, the host immune system often recognizes the graft – the cells, tissues, or organs transferred – as foreign and mounts an attack. While care is taken to ensure that donors are close matches to recipients, patients are administered life-long regimens of potent immunosuppressive drugs to resist the graft rejection, which can leave these individuals immunocompromised [3]. Approaches to generate durable, specific transplant tolerance could, therefore, dramatically improve patient outcomes and quality of life. Many of the candidate drugs along these lines are highly hydrophobic small molecules. The use of amphiphilic carriers, such as lipids or polymers with hydrophobic residues [233], can allow for incorporation of hydrophobic moieties and, ultimately, easier incorporation into aqueous-based injectable formulations. Along these lines, hydrophobic dexamethasone [234] and tacrolimus [235] have been incorporated into self-assembled materials to promote

tolerance and control inflammation. In the latter example, a hydrogel approach was used to entrap tacrolimus in a macro-scale assembly (**Figure 5.12A**). This approach enabled controlled release of encapsulated tacrolimus, triggered by degradation of the hydrogel in the presence of enzymes (e.g., matrix metalloprotease 9, MMP-9) (**Figure 5.12B**). Local introduction of the hydrogel containing tacrolimus in close proximity to the graft in a hind limb transplant model dramatically improved survival, with 100% of the grafts surviving through 100 days post-transplant (**Figure 5.12C-D**). In contrast, administration of the same formulation on the opposite side of the

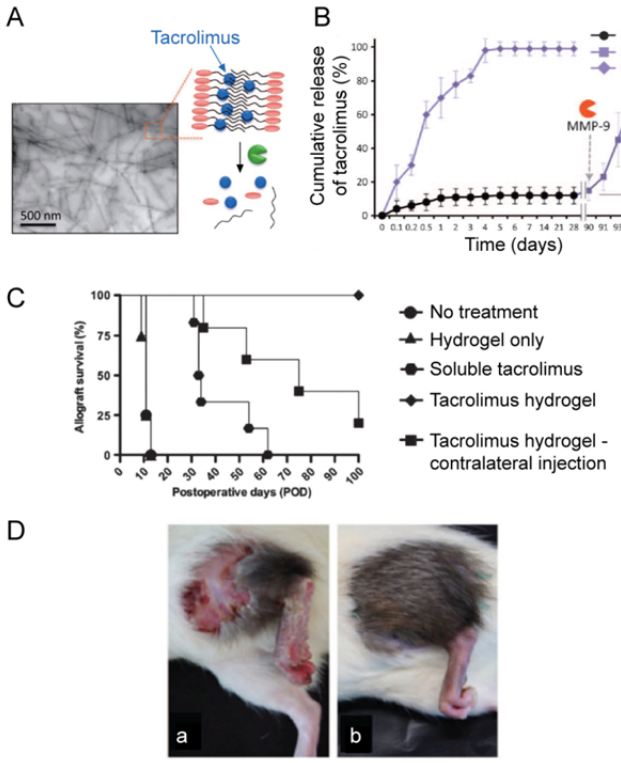

Figure 5.12 Controlled release formulation of tacrolimus to prevent graft rejection.
A) Schematic representation of encapsulation of a small molecule immunomodulator, tacrolimus, in an enzyme-degradable hydrogel. B) Release kinetics of tacrolimus from the hydrogel represented in (A) when incubated in PBS or in the presence of and enzyme (MMP9) to drive hydrogel degradation. The tacrolimus-containing hydrogel in (A) was injected subcutaneously on the same side as a hind limb transplant in a rat model. Control treatments included no treatment, hydrogel alone (vehicle control), a soluble bolus injection of tacrolimus, and the tacrolimus hydrogel injected on the opposite (i.e., contralateral) side of the hind limb transplant. Graft survival was quantified (C) and could be assessed qualitatively through images comparing transplanted hind limbs from a mouse treated with soluble tacrolimus (a) or the tacrolimus hydrogel formulation (b). Adapted from [235] with permissions.

transplant (i.e., contralateral) promoted survival over untreated mice and mice treated with a single dose of soluble tacrolimus, but did not achieve the same level of protection as local delivery in close proximity to the graft. This example underscores an opportunity to harness self-assembly for targeted, local delivery of immunomodulatory signals in key tissues.

5.7. Conclusion

The translation of nanotechnology from pre-clinical studies to human use has seen relatively little success. This limitation has sparked intense interest in the rational design of nano-systems that provide controlled composition and well-characterized mechanisms of action to trigger immune responses. Self-assembly offers a unique opportunity to generate simple, well-defined materials with precise control over parameters like shape, size, valency, charge, and both relative and absolute loading of cargos. As discussed here, this potential has been harnessed to design new immunosensing and diagnostic tools, study fundamental interactions between biomaterials and immune cells, interrogate the link between physiochemical properties and immunogenicity, and develop self-assembly-enabled therapeutics to elicit tunable immune responses. A critical need to help the field move forward is a greater focus on the use of clinically-relevant experimental systems and animal models. Further, comparison to existing clinical options and well-characterized pre-clinical nanomaterial formulations as benchmarks will also help improve the robustness and consistency of emerging technologies. Owing to the complexity of immune response, more wide spread discussion between engineers, immunologists,

and clinicians will help frame research goals and the questions being addressed. Lastly, as self-assembled technologies and, more generally, biomaterial vaccines and immunotherapies, are developed, consideration to manufacturing and regulatory issues need to be considered early on, as even very promising technologies will not have a clinical impact if they are not feasible to produce or characterize. Despite these needs, the immune engineering field is poised to make real impact in our understanding of the role materials play in biasing both innate and adaptive immune functions, and in enabling new immune technologies.

Section 5.6.3 above introduces immune polyelectrolyte multilayers "iPEMs" as a strategy that mimics advantageous properties of conventional biomaterials, but simplifies design by eliminating carrier components, such as the polymer microparticles explored in Aim 1. **Chapter 6** describes this approach, the focus of Aim 2, in detail. Myelin self-antigen is self-assembled with a regulatory nucleic acid (GpG) to generate microcapsules composed entirely of immune cues. We describe the synthesis and characterization, as well as demonstrate the potential of iPEMs to restrain inflammation and promote tolerance in three systems: primary murine immune cells, mouse models of MS, and human MS patient samples.

Chapter 6. Design of polyelectrolyte multilayers to promote immunological tolerance[5]

6.1. Introduction

Autoimmune diseases such as multiple sclerosis (MS), type 1 diabetes, and lupus occur when self-molecules are incorrectly recognized as foreign and attacked by the immune system. New studies reveal excess inflammation through toll like receptors (TLR) – a class of inflammatory pathways typically triggered by foreign pathogens – strongly contributes to the pathology of autoimmune diseases.[225-231, 236] Recent reports also demonstrate that co-administration of regulatory signals and self-molecules attacked during autoimmunity – myelin in MS, for example – can promote tolerance.[34] Biomaterial carriers have been explored to facilitate this co-delivery,[34, 47, 86] but these materials exhibit intrinsic features that can activate inflammatory pathways that could exacerbate autoimmune disease.[28, 29, 237] To address these challenges, here we designed immune polyelectrolyte multilayer (iPEM) capsules that promote tolerance by mimicking features of biomaterials, but that are self-assembled entirely from myelin and a regulatory TLR antagonist.[85, 232]

Existing therapies for autoimmune diseases are not curative and employ broad immunosuppression that often leaves patients immunocompromised.[88] These limitations have motivated the exploration of alternative approaches, including

[5] Adapted from L. H. Tostanoski, Y. C. Chiu, J. I. Andorko, M. Guo, X. Zeng, P. Zhang, W. Royal III, and C. M. Jewell, "Design of polyelectrolyte multilayers to promote immunological tolerance." *ACS Nano* 2016, 10, 9334-9345.

vaccine-like strategies that offer the potential for both efficacy and specificity by, for example, expanding regulatory T cells (T_{REGS}) specific for self-molecules attacked during MS or other autoimmune diseases. Importantly, the signaling milieu in which myelin is processed and presented by antigen presenting cells plays a major role in programming the balance between autoimmunity and tolerance.[47] Thus, strategies that allow precise control over the relative composition of self-antigen and therapeutic components could be transformative in enabling more specific treatments for autoimmune disease. Biomaterials offer attractive features to achieve this goal – including co-delivery – and have recently been studied to deliver and target tolerogenic drugs, cytokines, and self-antigen to key immune tissues (*e.g.*, lymph nodes, spleen).[39, 43, 47, 54, 86, 87] PEMs are particularly well-positioned for this application: these materials are self-assembled through a layer-by-layer process that enables juxtaposition of multiple signals with tunable, stepwise control over the absolute and relative loading of several cargos.[195, 238, 239] However, despite ubiquitous application to drug delivery and vaccination,[195, 197, 218, 240-243] PEMs have not been studied to regulate immune function or promote immunological tolerance. We recently described a layer-by-layer approach to assemble model antigens and TLR-based adjuvants into vaccines that drive strong, pro-immune T cell function.[32, 33] These nanostructures, termed iPEMs, were assembled through electrostatic interactions using model antigen and a nucleic acid-based TLR3 agonist that served as a stimulatory adjuvant. Thus iPEMs are composed entirely of immune signals (*i.e.*, antigen, TLR agonist), in contrast to traditional PEMs integrating synthetic or natural polymers.[33] We hypothesized the iPEM platform would be

advantageous for tolerance by enabling co-delivery of self-antigens and tolerogenic immune cues at high concentrations, while eliminating carrier components – such as poly(lactide-co-galactide) (PLGA) – that have recently been shown to activate inflammasomes and other pro-inflammatory pathways that could increase the severity of autoimmune disease.[28, 29, 237]

During MS, myelin-specific pathogenic $CD4^+$ T cells (*e.g.*, T_H1, T_H17) and antibodies infiltrate the central nervous system (CNS) to drive inflammation and de-myelination. Thus, to design iPEMs for tolerance, we selected a myelin peptide implicated in human MS and animal models, myelin oligodendrocyte glycoprotein (MOG).[244] Two discoveries motivated our approach to assemble this peptide with a nucleic acid-based regulatory ligand of TLR9, GpG (**Figure 6.1A**). First, new research reveals signaling through TLRs plays an important role in driving disease during MS, lupus, and type 1 diabetes;[225-231, 236] blunting this signaling during T cell expansion might reduce inflammation and expand T cell phenotypes (*e.g.*, T_{REGS}) specific for myelin, but that selectively control disease. Second, seminal work by the Steinman lab demonstrates TLR9-specific activity of GpG and that systemic administration helps promote tolerance.[85, 232] While the mechanism of GpG has not been fully elucidated, these reports support a role for competitive binding with TLR9, polarization away from inflammatory cells, and perhaps in parallel, the promotion of a protective T_H2-like response to restrain inflammatory immune cell activity.[232] In contrast, the agonistic TLR9 ligand, CpG, is under intense study as a vaccine adjuvant for infectious disease and cancer.[157] Together, these discoveries suggest co-

delivery of self-antigens with signals to modulate TLR9 or other TLR pathways could efficiently promote tolerance. Thus, we formed iPEMs by exploiting the polyanionic character of GpG – which is an oligonucleotide with a phosphorothiate backbone structurally similar to CpG, but in which cytosine residues are replaced by guanine residues – for electrostatic assembly with MOG conjugated to arginine residues as cationic anchors. We hypothesized juxtaposition of these tolerogenic signals in the nanostructure of iPEMs would mute TLR9 signaling during antigen presentation to bias differentiating T cells away from inflammatory function and, instead, promote regulatory T cells (T_{REGS}) able to control autoimmunity. *In vitro*, we show iPEMs co-deliver both cargos to dendritic cells (DCs), downregulate TLR9 signaling, restrain DC activation, and polarize antigen-specific T cells towards T_{REGS}. In mice, iPEMs reduce inflammation, expand T_{REGS}, and eliminate disease in a common mouse model of MS. Using samples from human MS patients, we discovered iPEMs bias the function of T cells toward tolerance. These results demonstrate that PEMs can be used to regulate immune function and promote tolerance.

6.2. Materials and Methods

6.2.1. Materials

MOG peptide (MOG_{35-55}, MEVGWYRSPFSRVVHLYRNGK), MOG modified with a cationic arginine amino acids (MOG-R_3, MEVGWYRSPFSRVVHLYRNGKRRR), and $OVA_{323-339}$ (ISQAVHAAHAEINEAGR) were synthesized and HPLC purified to > 98% purity by Genscript. TLR9 agonist CpG (5-T*C*C*A*T*G*A*C*G*T*T*C*C*T*G*A*C*G*T*T-3), TLR9 antagonist GpG

(5-T*G*A*C*T*G*T*G*A*A*G*G*T*T*A*G*A*G*A*T*G*A-3), and irrelevant nucleotide (CTRL, 5-T*C*C*T*G*A*G*C*T*T*G*A*A*G*T-3), were synthesized by IDT with a phosphorothioate backbone.

6.2.2. Preparation of planar substrates

Quartz slides (VWR) and silicon wafers (Silicon Inc.) were cut into 5 mm x 25 mm or 5 mm x 20 mm substrates, respectively, using a diamond-tipped saw (Micro Automation). Substrates were cleaned *via* sequential rinsing in acetone, ethanol, methanol, and water, dried under air, and charged with an oxygen plasma system (Jupiter III, March). Prepared substrates were then coated with baselayers of strong polyelectrolytes, poly(ethyleneimine) (PEI, Polysciences, Inc.) and poly(sodium 4-styrene sulfonate) (SPS, Sigma-Aldrich), as previously reported [33]. Briefly, chips were incubated in 20 mM PEI with 50mM NaCl and 5 mM HCl for 5 min, washed twice in water for 1 min, incubated in 20 mM SPS with 50mM NaCl for 5 min, and washed two more times with water. This process was repeated for a total of ten deposition cycles using a DR3 dipping robot (Riegler & Kirstein GmbH) and chips were dried under air and stored at room temperature until subsequent coating with iPEMs.

6.2.3. iPEM assembly and characterization on planar substrates

Cargo solutions were prepared by dissolving MOG-R_3 and GpG at 0.5 mg/mL in 1 X PBS. iPEMs were assembled by dipping baselayer-coated substrates in MOG-R_3 for 5 min, washing twice in PBS for 1 min, incubating in GpG for 5 min, and washing two

additional times in fresh aliquots of PBS. This process was repeated to deposit the desired number of MOG-R_3/GpG bilayers. For experiments designed to monitor film thickness, iPEMs were deposited on silicon chips and, every two bilayers, dried under air and measured using a Stokes Ellipsometer (Gaertner Scientific). At each measurement step, the thickness at five locations on at least three separate substrates was recorded and averaged. In studies designed to quantify relative cargo loading, iPEMs were assembled on quartz chips and UV-Visible spectrophotometry was used to record the absorbance values from 250 nm to 600 nm every two bilayers, as above. Measurements were recorded at three locations on at least three separate substrates and averaged. Wavelengths of 260 nm and 500 nm were used to indicate the loading of GpG and FITC tagged MOG-R_3, respectively. Following deposition of eight bilayers of FITC labeled MOG-R_3 and Cy5 labeled GpG on a quartz substrate, fluorescence microscopy (Olympus IX-83) was used to confirm co-localization of both cargos in an iPEM assembly. In these experiments, a portion of the film was removed with a needle scratch to provide contrast. Atomic Force Microscopy images were obtained in tapping mode in air using a Digital Instruments (Veeco) Multimode Atomic Force Microscope with a Nanoscope III controller and 10 micron scanner. Images were analyzed and root mean square roughness was calculated using NanoScope Analysis software (v1.50).

6.2.4. iPEM assembly and characterization on colloidal substrates

Calcium carbonate microparticle (MP) templates were precipitated, as previously described [33]. Briefly, sodium carbonate (Alfa Aesar) and calcium chloride

dihydrate (Sigma-Aldrich) were dissolved at 0.33 M in water. Equal volumes of these solutions were combined, under stirring (800 rpm), and allowed to mix for 5 min. For each batch of iPEMs, 500 μL of the MP solution was transferred to a 1.5 mL microcentrifuge tube and aliquots were centrifuged (20 seconds, 1000 x g) to collect MPs, and washed twice in water. To deposit iPEMs, MPs were then resuspended in 600 μL of MOG-R_3 cargo solution (0.5 mg/mL in water), incubated for 3 min, washed twice in water, incubated in 600 μL of GpG cargo solution (1 mg/mL in water) for 3 min, and washed two more times to complete one bilayer. As noted, between each coating and washing step, particles were collected with a short centrifugation (20 seconds, 1000 x g). In experiments to monitor iPEM growth, aliquots of MPs were collected after deposition of 1, 2, and 3 bilayers and imaged by fluorescence microscopy at a fixed exposure time. Pixel intensity was determined along line traces through the diameter of representative images using ImageJ. In separate studies, aliquots of iPEM-coated MPs were collected after deposition of each cargo layer and surface charge was measured using a Malvern Zeta Sizer Nano ZS90. To measure iPEM composition, the concentrations of cargo solutions before and after coating, as well as the concentrations of cargos in wash solutions, were quantified using spectrophotometry, comparing absorbance values to standard curves of MOG-R_3 and GpG. These values were used to calculate the mass of cargos deposited on MPs *via* indirect loading measurement. To vary the input ratio of cargos, the mass of GpG was fixed at 600 μg/batch, as above, and the input mass of MOG-R_3 was titrated from 1200 μg to 18.75 μg, at the indicated ratios. iPEM composition for each ratio tested is reported in **Table 6.1**. To remove the calcium carbonate core and form iPEM

capsules, calcium carbonate MPs were coated with three MOG-R_3/GpG bilayers, as above, and then incubated in 1 mL of 0.1 M ethylenediaminetetraacetic acid (EDTA, Sigma-Aldrich), adjusted to pH 6 with 1 M HCl and 1 M NaOH solutions, for 30 min. Capsules were then centrifuged (3 min, 1000 x g), washed with 600 μL of 1X PBS, and resuspended in 1 X PBS for imaging and cell or animal studies. In some studies, iPEM capsules were formed from MOG-R_3 and CTRL, with or without a Cy3 label, following the same protocols above, for materials characterization and *in vitro* experiments.

6.2.5. Dendritic cell uptake and activation

DCs were isolated from the spleens of naïve C57BL/6J mice (The Jackson Laboratory) using a $CD11c^+$ magnetic isolation kit, according to the manufacturer's instructions (Miltenyi Biotec). Cells were plated (1 x 10^5 cells/well) in RPMI 1640 media (Lonza), supplemented with 10% fetal bovine serum (Corning), 2 mM L-glutamine (Gibco), 55 μM β-mercaptoethanol (Sigma-Aldrich) 1 X Non-Essential Amino Acids (Fisher Scientific), 10mM HEPES (Fisher Scientific), and 1 X Pen/Strep (Gibco). For cell uptake studies, dilutions of dual-labeled iPEM capsules were incubated with cells for 4 h. Cells were then washed twice in 1% bovine serum albumin (Sigma-Aldrich) in 1 X PBS (FACS buffer), stained for viability with 4',6-diamidino-2-phenylindole (DAPI, Invitrogen), and analyzed by flow cytometry (BD FACS Canto II). For DC activation studies, cells were isolated and plated, as above and, with the exception of media only controls, activated with soluble CpG (1 μg/well). Soluble MOG-R_3 (10 μg), GpG (10 μg), and CTRL (10 μg), as well as

$(MOG\text{-}R_3/GpG)_3$ or $(MOG\text{-}R_3/CTRL)_3$ capsules (30 μg), were added to CpG-treated wells. Cultures were incubated for 16 h, and then cells were collected, washed in FACS buffer, and blocked with anti-CD16/CD32 (BD Biosciences). Cells were then stained with anti-CD40 and anti-CD86 (BD Bioscience) for 20 min at room temperature, washed two more times as above, and resuspended in DAPI for analysis by flow cytometry. All flow cytometry data analysis was conducted using FlowJo software (Tree Star).

6.2.6. TLR9 signaling assays

To assess TLR9-specific signaling, HEK-Blue mTLR9 reporter cells (InvivoGen) were plated at 5 x 10^5 cells/well in HEK-Blue Detection medium (InvivoGen). Soluble CpG (4 μg) – a TLR9 agonist – was added to cells alone or in addition to soluble GpG (10 μg), soluble CTRL (10 μg), $(MOG\text{-}R_3/GpG)_3$ iPEMs (30 μg), or $(MOG\text{-}R_3/CTRL)_3$ iPEMs (30 μg). To verify that increases in signaling were TLR9-specific, control wells were treated with a TLR3 agonist (PolyIC, 10 μg, InvivoGen) or a TLR4 agonist (lipopolysaccharide, LPS, 1 μg, InvivoGen). Cultures were then incubated for 16 h and absorbance at 650 nm was recorded per the manufacturer's instructions.

6.2.7. Transgenic T cell proliferation

To characterize MOG-specific T cell interactions, DCs from naïve C57BL/6J mice were isolated, as above, and treated with CpG (1 μg) and either soluble $MOG\text{-}R_3$ (60 μg), GpG (10 μg), or CTRL (10 μg), or iPEM formulations (10 μg). After 16 h of

culture, $CD4^+$ T cells were isolated from the spleens of transgenic 2D2 mice (C57BL/6-Tg(Tcra2D2,Tcrb2D2)1Kuch/J, The Jackson Laboratory) with a magnetic isolation kit (StemCell Technologies), according to the manufacturer's instructions. Isolated $CD4^+$ T cells were then incubated with a cell proliferation dye (eFluor 670, eBioscience), washed, and 2.5 x 10^5 labelled cells were added to DC cultures. After 72 h of co-culture, cells were collected, washed and blocked, as above. Cells were then stained with anti-CD4 (BD Biosciences) for 20 min at room temperature, washed to remove unbound antibody, and resuspended in DAPI for analysis by flow cytometry. In separate studies, $CD4^+$ T cells with receptors specific for $OVA_{323-339}$ were isolated from the spleens of transgenic OT-II mice (B6.Cg-Tg(TcraTcrb)425Cbn/J, The Jackson Laboratory), labeled with proliferation dye, and added to DC cultures, as above. In these experiments, control wells were treated with CpG (1 μg) and soluble $OVA_{323-339}$ (60 μg).

6.2.8. ELISA

Supernatants from 2D2 co-cultures were analyzed by ELISA according to manufacturer's instructions for the secretion of IFN-γ and IL-6 (BD Biosciences).

6.2.9. Transgenic T cell phenotype

To analyze the expression of markers for T_{REG} phenotype, co-cultures were prepared, as above, without fluorescent labeling of $CD4^+$ 2D2 T cells. After 72 h of co-culture, cells were collected, washed twice and blocked as above. Cells were then incubated in antibodies against CD4 (BD Biosciences) and CD25 (BD Biosciences) for 45 min

at 4 °C, protected from light. Following staining for surface markers, cells were washed, and then fixed and permeabilized using a Foxp3Transcription Factor Staining Buffer Set, according to the manufacturer's instructions (eBioscience). Cells were then stained for the expression of Foxp3 overnight at 4 ^{0}C, washed and analyzed by flow cytometry.

6.2.10. Capsule immunization

Mice were immunized with 400 μg of (MOG-R_3/GpG)$_3$ iPEMs, administered as bilateral injections (2 x 25 μL injections, containing 200 μg of iPEMs each) subcutaneously at the tail base. Capsules were administered to either naïve mice for immunohistochemical analysis of iPEM drainage to lymph nodes, or to mice induced with EAE on days 5 and 10 post induction.

6.2.11. Immunohistochemical analysis

Two days after immunization, draining inguinal lymph nodes were excised from (FITC-MOG-R_3/GpG)$_3$ iPEM-treated mice. Tissues were immersed in Optimal Cutting Temperature Medium (Tissue-Tek) and frozen. Blocks were sectioned at 6 μm thickness using a Microm HM 550 cryotstat. Sections were fixed in ice cold acetone, dried, and washed in PBS. Sections were then blocked using appropriate serum and stained with primary antibodies for CD3e and B220 for 1 h at room temperature. After two 5 min washes, fluorescently-labeled secondary antibodies were added for 45 min at room temperature. Sections were then washed, fixed with 4% paraformaldehyde, quenched with 1% glycerol, and mounted using ProLong

Diamond Antifade Mountant (Thermo Fisher Scientific). Images were collected on an Olympus IX-83 fluorescent microscope.

6.2.12. EAE induction and monitoring

EAE was induced in C57BL/6J mice with kits according to the manufacturer's instructions (Hooke Laboratories). Mice were monitored for body weight fluctuation and paralysis, which was assigned a clinical score (0 – no symptoms, 1 – limp tail, 2 – hind limb weakness, 3 – hind limb paralysis, 4 – full hind limb and partial front limb paralysis, and 5 – moribund). All animal care and experiments were carried out using protocols approved and overseen by the University of Maryland IACUC committee in compliance with local, state and federal guidelines.

6.2.13. Tissue collection and processing

Three days after dosing with iPEMs (*i.e.*, day 13 post induction), indicated tissues were collected and mechanically dissociated through 40 μm cell strainers. Spleen samples were resuspended in Ack lysing buffer (Invitrogen) to deplete red blood cells, and then washed with PBS. Single cell suspensions were split to perform three analyses. First, cell counts were recorded by flow cytometry using counting beads according to the manufacturer's instructions (BD Biosciences). Second, using these cell counts, a uniform number of cells (5×10^5) from each tissue was plated in duplicate, with one well receiving a pulse of MOG peptide (25 μg/mL) and the other an equivalent dose of $OVA_{323-339}$ peptide. Restimulated cells were cultured for 72 h, and supernatants were analyzed for IFN-γ, IL-6, and IL-17 (R & D Systems)

secretion by ELISA, as described above. Third, the remaining aliquot of the single cell suspension was analyzed immediately for the expression of phenotypic markers of T_{REGS} – CD4, CD25, and Foxp3 – as described above.

6.2.14. Human PBMC samples

Human MS patient peripheral blood mononuclear cell samples were collected in conjunction with the IRB-approved VALOMS study protocol with informed signed consent. VALOMS is an observational study that has been initiated by the VA MS Center of Excellence-East to examine factors associated with disease progression among U.S. military veterans with MS. Frozen PBMC samples selected randomly from the patient sample repository were thawed, washed and a Ficoll gradient was used to remove dead cells. Cells were then counted and plated in 96-well plates at 1.5 x 10^5, 2.0 x 10^5, or 5 x 10^4 cells/well for Patients 1, 2, and 3, respectively. Cells were left untreated or incubated with 30 μg of either $(MOG\text{-}R_3/GpG)_3$ iPEMs or $(MOG\text{-}R_3/CTRL)_3$ iPEMs. After 72 h of incubation, 20 μL of 5 mg/mL 3-(4, 5-dimethlythiazol-2-yl)-2, 5-diphenyltetrazolium bromide (MTT) was added to each well and cultures were subsequently incubated for 4 h at 37 °C. Plates were then centrifuged at 2000 rpm for 10 min. Supernatants were collected for analysis of cytokine secretion, and then 150 μL dimethyl sulfoxide was added to each well. The absorbance at 570 nm, with a reference of 630 nm, was recorded. Cell culture supernatants were analyzed by Luminex Multianalyte System for secreted human TNF-α, IL-6, IL-10, and IFN-γ according to the manufacturer's instructions.

6.3. Results

6.3.1. iPEM assembly and characterization

iPEMs were first deposited on planar substrates to characterize the assembly of GpG with MOG conjugated to tri-arginine (MOG-R_3). Fluorescence microscopy was used to visualize the co-localization of both cargos during assembly of 16 layers to form $(MOG\text{-}R_3/GpG)_8$ (**Figure 6.1B**). Both fluorescence and atomic force microscopy (**Figure 6.1B**) revealed surface topography with a root mean square roughness of 51.6 nm. Next we confirmed film thickness and cargo loading could be controlled by varying the number of deposition cycles. Ellipsometry revealed increasing iPEM thicknesses to a value of ~150 nm after 8 bilayers (**Figure 6.1C**). Similarly, spectrophotometric analysis revealed linearly increasing absorbance values at characteristic wavelengths for GpG (R^2 = 0.99) and fluorescently-labeled MOG-R_3 (R^2 = 0.98) (**Figure 6.1D, 6.2A**). These results indicate the loading of each signal can be tuned through the number of bilayers deposited.

To facilitate cell and animal studies, we assembled iPEMs on sacrificial calcium carbonate templates[245, 246] then used a chelator to dissolve the core and create support-free MOG-R_3/GpG iPEM capsules. Consistent with our results on planar substrates, fluorescence microscopy (**Figure 6.1E**, top) and quantitative analysis of pixel intensity (**Figure 6.1E**, bottom) indicated increasing GpG loading as more layers were deposited. Zeta potential measurements revealed a corresponding oscillation in surface charge, indicative of electrostatically-driven layer-by-layer assembly (**Figure 6.2B**). We next investigated whether the cargo loading of iPEMs

could be tuned, as the combinations and relative doses of immune signals play a major role in determining the magnitude and polarization of antigen-specific response.[61] We discovered the relative loading of MOG-R_3 and GpG could be directly controlled over a range of 89.7 ± 0.4% MOG-R_3 and 10.3 ± 0.4% GpG, to 28.4 ± 0.7% MOG-R_3 and 71.6 ± 0.7% GpG (**Figure 6.1F, Table 6.1**) by altering the relative mass input during adsorption. Another notable characteristic of this approach

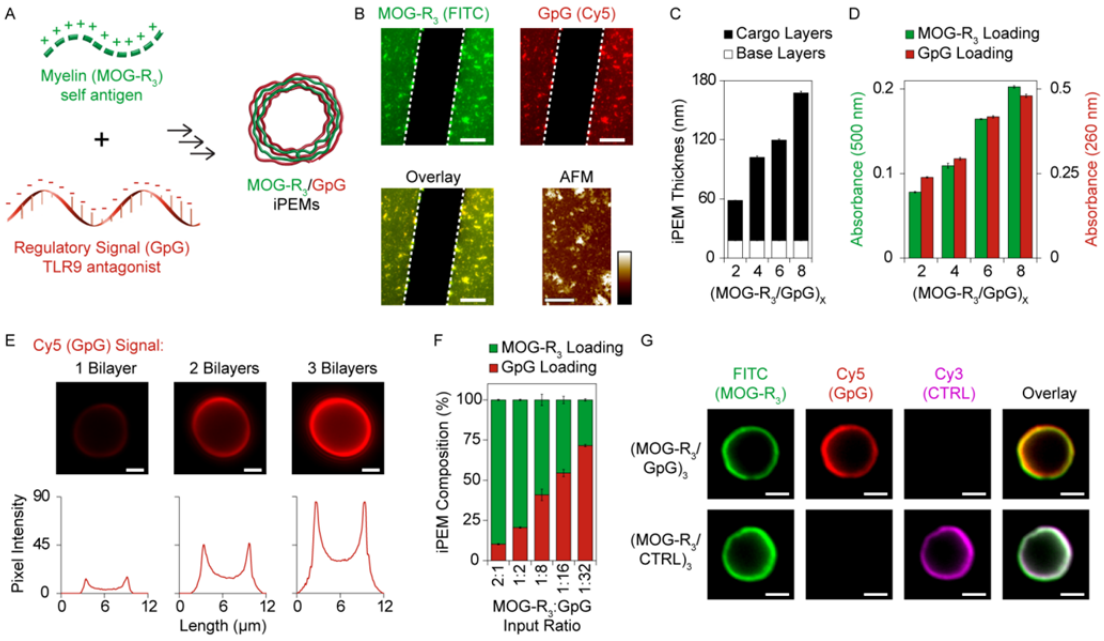

Figure 6.1 Tunable assembly and characterization of iPEMs on planar and colloidal substrates. (A) Schematic view of layer-by-layer electrostatic assembly of myelin self-antigen (MOG-R_3) and a TLR9 antagonist (GpG) to form iPEMs. (B) Representative fluorescence microscopy images of quartz substrates, following deposition of eight MOG-R_3/GpG bilayers (green, FITC-MOG-R_3; red, Cy5-GpG; scale, 20 μm). A needle was used to remove a portion of the film to provide contrast (dotted white lines). Atomic force microscopy analysis of the surface morphology of $(MOG\text{-}R_3/GpG)_8$ iPEMs (x-y scale, 3 μm; z scale, 400 μm). (C) Stepwise measurements of iPEM thickness with increasing numbers of MOG-R_3/GpG bilayers deposited on silicon substrates, quantified by ellipsometry. Data represent mean ± s.e.m. (n = 3). (D) Spectrophotometric analysis of relative loading of MOG-R_3 (500 nm) and GpG (260 nm) as a function of the number of bilayers deposited on quartz substrates. Data represent mean ± s.e.m. (n = 3). (E) Representative images (top) and quantitative pixel analysis (bottom) of relative GpG loading with subsequent iPEM deposition cycles on a calcium carbonate microparticle core (red, Cy5-GpG; scale, 2 μm). (F) Spectrophotometric quantification of tunable relative composition of iPEMs as a function of the relative input mass of MOG-R_3 and GpG into iPEM synthesis. Data represent mean ± s.e.m. (n = 4 for each input ratio). (G) Representative fluorescence microscopy images of hollow iPEM capsules composed entirely of either MOG-R_3 and GpG (top) or MOG-R_3 and a non-immunoregulatory oligonucleotide (CTRL, bottom), following removal of the calcium carbonate core by incubation in EDTA (green, FITC-MOG-R_3; red, Cy5-GpG; magenta, Cy3-CTRL; scale, 2 μm).

is that 100% of the PEM coating is comprised of MOG-R_3 and GpG; therefore, following incubation of (MOG-R_3/GpG)$_3$-coated templates in EDTA, hollow capsules comprised entirely of immune signals were formed (**Figure 6.1G**, top) with negligible loss of either cargo following core removal (**Figure 6.2C**). Control iPEM capsules – (MOG-R_3/CTRL)$_3$ – could also be assembled from MOG and an inactive control oligonucleotide (CTRL) (**Figure 6.1G**, bottom). These iPEMs exhibited myelin and oligonucleotide loading similar to that of (MOG-R_3/GpG)$_3$ iPEMs (**Figure 6.2D**). Using these sets of iPEM architectures we next tested if self-antigens and regulatory cues incorporated into iPEMs promote tolerogenic functions in DCs and T cells.

Table 6.1 Relative iPEM composition can be tuned.
The relative loading of MOG-R_3 and GpG cargos in iPEMs synthesized with the indicated input mass ratios was quantified by spectrophotometry. Data represent mean ± s.e.m. (n = 4 for each input ratio).

Input Ratio	iPEM Composition	
(MOG-R3:GpG)	MOG-R_3 (Mass %)	GpG (Mass %)
2:1	89.7 ± 0.4 %	10.3 ± 0.4 %
1:2	79.4 ± 0.4 %	20.6 ± 0.4 %
1:8	59.0 ± 3.5 %	41.0 ± 3.5 %
1:16	45.5 ± 2.3 %	54.5 ± 2.3 %
1:32	28.4 ± 0.7 %	71.6 ± 0.7 %

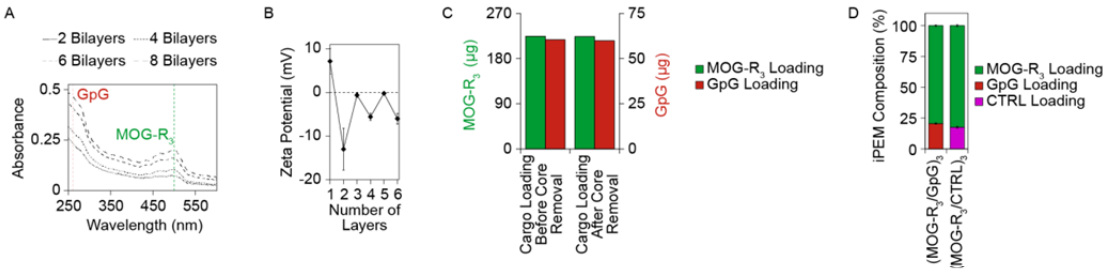

Figure 6.2 Characterization of iPEM synthesis on planar and colloidal substrates.
(A) Representative spectrophotometric scans used to quantify the relative loading of cargos in iPEMs as a function of the number of bilayers deposited on quartz substrates as in Fig. 1d. The characteristic wavelengths used to monitor the relative loading of MOG-R_3 (FITC, 500 nm) and GpG (260 nm) are indicated by the green and red dashed lines, respectively. (B) Measurement of the surface charge of calcium carbonate microparticle templates following coating with the indicated numbers of alternating MOG-R_3 and GpG layers. Data represent the mean ± s.e.m. of three independent batches of iPEMs at each stage of synthesis. (C) MOG-R_3 and GpG loading on $CaCO_3$ cores per batch, compared with the mass of cargos remaining in capsules following core removal. The mass lost in the core removal process was calculated by analyzing incubation and wash solutions *via* spectrophotometry. (D) Spectrophotometric measurement of the composition of (MOG-R_3/GpG)$_3$ or (MOG-R_3/CTRL)$_3$ iPEMs (n = 4 for each formulation).

6.3.2. iPEMs restrain TLR9 signaling and DC activation

We hypothesized iPEMs assembled from MOG and GpG might polarize T cells away from effector cells and toward T_{REGS} by reducing TLR9 signaling during differentiation of myelin-specific T cells being expanded by antigen presenting cells (*e.g.*, DCs). To investigate this idea, we first tested if iPEMs co-deliver both signals to DCs by culturing dual-labeled $(MOG\text{-}R_3/GpG)_3$ iPEMs with primary splenic DCs. In these studies, flow cytometry revealed a dose-dependent uptake of capsules without toxicity (**Figure 6.3**) and, interestingly, irrespective of iPEM dose, > 80% of cells positive for at least one component were positive for both MOG-R_3 and GpG (**Figure 6.4A,B**). In contrast, incubation of DCs with ad-mixed MOG-R_3 and GpG resulted in dramatically reduced (< 45%) co-delivery of cargos compared with matched doses in formulated as iPEMs (**Figure 6.5**). Promoting co-delivery is of particular interest for autoimmune therapy as the administration of regulatory signals (*e.g.*, GpG) in the absence of self-antigen may drive non-specific immunosuppression, while delivery of self-antigen alone creates a risk of triggering self-reactivity that exacerbates disease.[47]

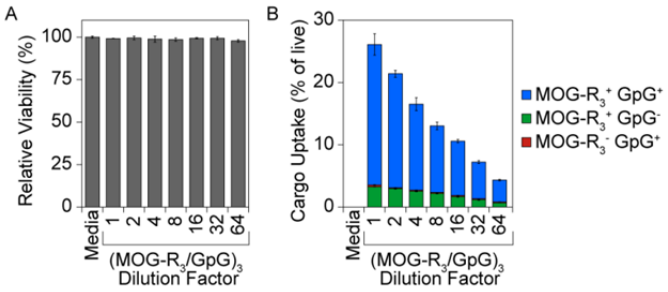

Figure 6.3 Dendritic cells exhibit dose-dependent uptake of iPEMs without associated toxicity. (A) Viability of DCs following incubation with dilutions of iPEMs, expressed relative to media only control wells. (B) Flow cytometry analysis following incubation of DCs with dilutions of dual-labeled $(MOG\text{-}R_3/GpG)_3$ iPEMs, as in a, for the frequency of cells positive for MOG-R_3 only (green, FITC-MOG-R_3), cells positive for GpG only (red, Cy5-GpG) or cells double-positive for both cargos (blue). Data in all panels represent mean ± s.e.m. (n = 3).

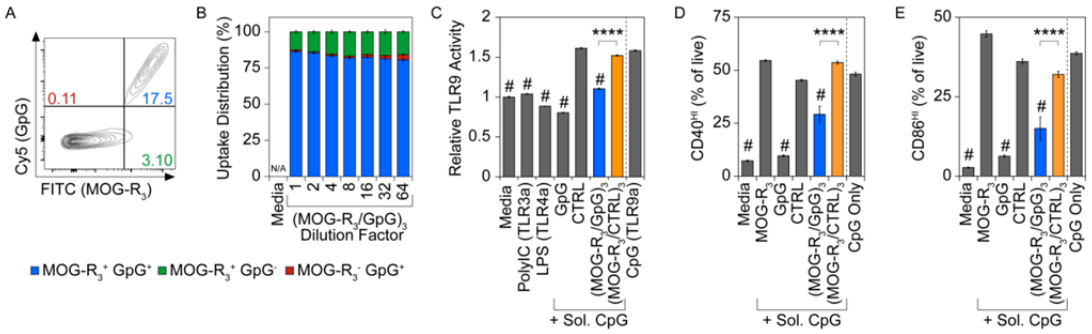

Figure 6.4 iPEMs promote co-delivery of cargos, down-regulate DC activation, and restrain TLR9 signaling.
(A) Representative scatter plot and b, quantification of uptake of dual-labeled MOG-R3/GpG iPEMs following a 4 h incubation with splenic DCs. The frequency of cells positive for MOG-R3 only (green, FITC-MOG-R3), cells positive for GpG only (red, Cy5-GpG) or cells double-positive for both cargos, among events positive for at least one signal is shown in (B). (C) Quantification of TLR9 specific signaling in reporter cells following 16 h incubation with TLR9 agonist CpG and either iPEM or soluble formulations of GpG and CTRL. Controls of PolyIC (TLR3a) and LPS (TLR4a) were included to verify pathway specificity. (D) Expression of CD40 and (E) CD86, surface markers of activation, following a 16 h incubation of splenic DCs with soluble CpG, and either indicated iPEM formulation or soluble iPEM components. Values in panels B-E indicate the mean ± s.e.m of studies conducted in triplicate. In panels C-E, data were analyzed with one-way ANOVA with a Tukey post-test to correct for multiple comparisons. For clarity, only key statistical comparisons are shown: # markers indicate a statistically significant difference (# = $P \leq 0.0001$) between the labeled group and a control – wells treated with CpG only (dashed lines). Brackets indicate statistically significant comparisons between (MOG-R3/GpG)3 and (MOG-R3/CTRL)3 iPEMs (**** = $P \leq 0.0001$).

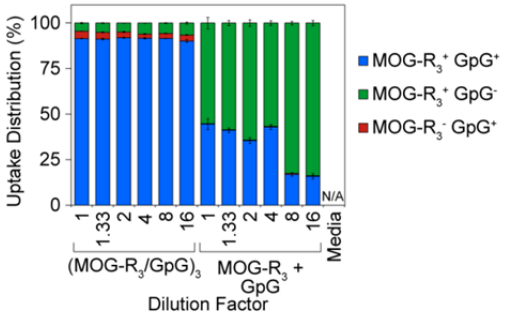

Figure 6 5 iPEMs promote co-localization of cargos in DCs versus ad-mixed treatments.
Flow cytometry analysis following incubation of DCs with dilutions of either dual-labeled (MOG-R_3/GpG)$_3$ iPEMs, or matched doses of labeled MOG-R_3 and GpG in soluble form. Frequencies were measured for cells positive for MOG-R_3 only (green, FITC-MOG-R_3), GpG only (red, Cy5-GpG), or double-positive for both cargos (blue); frequencies are normalized to cells positive for at least one signal. The highest dose (i.e., dilution factor of 1) incorporated 40µg (MOG-R_3/GpG)$_3$ iPEMs or equivalent dose of each component (~32µg MOG-R_3, ~8µg GpG) ad-mixed. Data represent mean ± s.e.m. (n = 3).

TLR9 typically senses pathogen-associated nucleic acids that are unmethylated and rich in cytosine and guanine residues (*e.g.*, CpG). Interestingly, autoimmune disease

in a common mouse model of MS is attenuated when induced in TLR9 knockout mice, and completely eliminated in mice deficient in MyD88, a downstream activator of many TLRs.[229] Further underscoring the role of TLR9 in driving autoimmunity, administration of GpG – which consists of a nucleic acid sequence similar to CpG, but with cytosine replaced by guanine – reduces self-antigen triggered T cell proliferation and helps controls disease in mice.[85, 232] Thus, we used TLR9 reporter cells to directly investigate the impact of GpG-containing iPEMs on TLR9 signaling. Treatment with CpG (TLR9 agonist), but not TLR3 or TLR4 agonists, drove high levels of TLR9 activity in reporter cells relative to untreated control wells (**Figure 6.4C**). The addition of soluble GpG or $(MOG\text{-}R_3/GpG)_3$ iPEMs to CpG-treated wells significantly reduced TLR9 signaling, while a control nucleotide, CTRL, in either soluble form or assembled into iPEMs with $MOG\text{-}R_3$ had no effect. To investigate the impact on DC function, splenic DCs were next isolated, activated with CpG, and treated with $(MOG\text{-}R_3/GpG)_3$ iPEMs, $(MOG\text{-}R_3/CTRL)_3$ iPEMs, or soluble components. Both soluble GpG and $(MOG\text{-}R_3/GpG)_3$ iPEMs downregulated expression of prototypical DC activation markers, CD40 (**Figure 6.4D, 6.6**) and CD86 (**Figure 6.4E, 6.6**). In contrast, soluble $MOG\text{-}R_3$, soluble CTRL, and $(MOG\text{-}R_3/CTRL)_3$ iPEMs did not impact CpG-induced activation. Together our results in **Figure 6.4C-E** suggest that MOG and GpG can be assembled into iPEMs without supports or carriers, and without impacting the selectivity of GpG. However, we noted that the dose of GpG in iPEMs (~6μg/well) did not reduce the level of TLR9 signaling or expression of surface markers of DC activation to the same degree as the high dose of soluble GpG (10μg/well) included in the positive control reference

sample. Thus, we conducted studies over a range of matched doses of GpG in soluble or iPEM form to enable direct comparison of potency. We discovered that soluble GpG exhibited more potent restraint of TLR9 signaling (**Figure 6.7**) and DC activation (**Figure 6.7**) compared with GpG-containing iPEMs. While future studies could test if this result may be due to an increase in the required processing time following electrostatic complexation of GpG, iPEMs improved co-delivery to cells (**Figure 6.4, 6.5**) and caused significant attenuation of inflammatory cell activity *in vitro* (**Figure 6.4C-E, 6.7**). Further iPEMs offer unique advantages—co-delivery and tunable compositions, for example—relative to soluble components or simple mixtures, and these are features of particular importance for autoimmune therapies in animal models or human patients. Thus, we next sought to investigate whether cells can properly process and present self-antigen following incorporation into iPEMs, and whether co-delivery of myelin self-antigen and GpG polarizes myelin-specific T cell responses against this antigen towards tolerance.

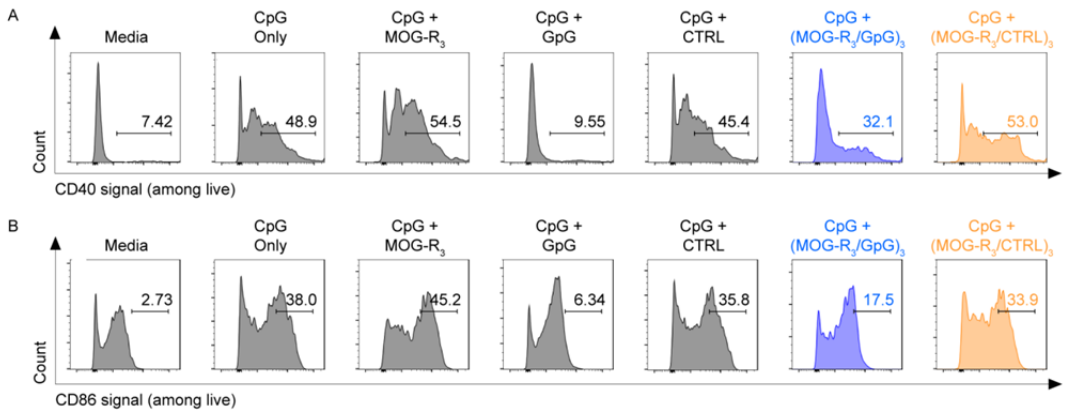

Figure 6.6 GpG-containing iPEMs restrain CpG-induced dendritic cell activation.
Representative histograms of the frequency of cells expressing high levels of (A) CD40 and (B) CD86, following incubation with CpG and indicated iPEM formulation or soluble components. Mean frequencies are shown in **Figure 6.4D,E**.

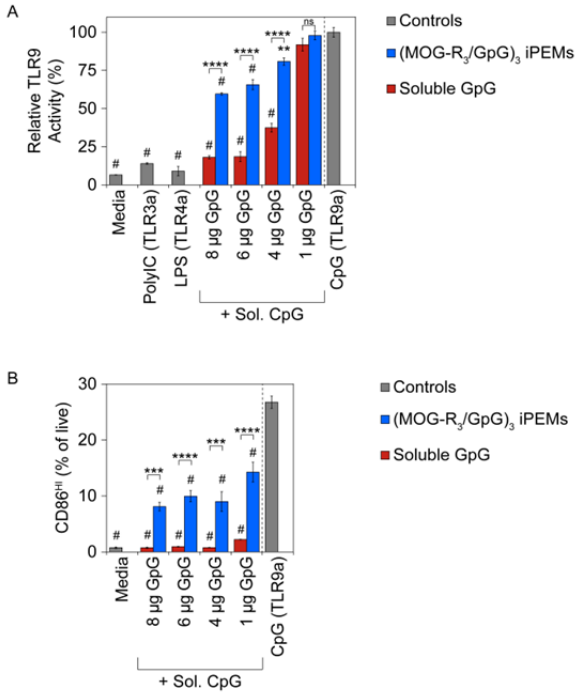

Figure 6.7 GpG-containing iPEMs restrain CpG-induced TLR9 signaling and dendritic cell activation.
(A) Quantification of TLR9 specific signaling in reporter cells following 16 h incubation with TLR9 agonist CpG and matched doses of GpG in either iPEM (blue series) or soluble form (red series). Controls of media alone and CpG only were included along with PolyIC (TLR3a) and LPS (TLR4a) to verify pathway specificity. (B) Expression of CD86, a surface marker of activation, following a 16 h incubation of splenic DCs with media only, CpG only, or CpG and either soluble or iPEM form of GpG. For clarity, only key statistical comparisons are shown: # markers indicate a statistically significant difference (** = $P \leq 0.01$; # = $P \leq 0.0001$) between the labeled group and a control – wells treated with CpG only (dashed lines). Brackets indicate statistically significant comparisons between matched doses of GpG in iPEM or soluble form (*** = $P \leq 0.001$; **** = $P \leq 0.0001$).

6.3.3. iPEMs polarize antigen-specific T cell function and phenotype in vitro

To test whether MOG-R_3 promotes myelin-specific T cell interactions in iPEM form, fluorescently-labeled $CD4^+$ MOG-reactive transgenic T cells were added to DCs isolated from wild-type mice and treated with CpG, along with either iPEMs or free components. After 72 h, flow cytometry revealed high levels of proliferation (*i.e.*, dilution of dye) in cultures treated with a positive control of CpG and cognate antigen, soluble MOG-R_3. Significant proliferation was also observed in wells treated with CpG and either (MOG-R_3/GpG) iPEMs, or (MOG-R_3/CTRL)$_3$ iPEMs, but not in

wells absent of MOG-R_3 (**Figure 6.8A,B, 6.9**). Equivalent results were observed over a range of doses (**Figure 6.10**). In contrast, during analogous studies with transgenic $CD4^+$ T cells specific for an irrelevant epitope from ovalbumin ($OVA_{323-339}$), no proliferation was detected with MOG-R_3 in soluble or iPEM form (**Figure 6.8C,D, 6.9**), indicating that iPEMs support antigen-specific T cell expansion. Strikingly, when supernatants from co-cultures were analyzed by ELISA, we discovered that despite similar levels of proliferation (**Figure 6.8A,B**), (MOG-R_3/GpG)$_3$ iPEM-treated cells secreted dramatically lower levels of inflammatory IL-6 (**Figure 6.8E**) and IFN-γ (**Figure 6.8F**) compared with wells receiving (MOG-R_3/CTRL)$_3$ iPEMs. Further, in similar co-culture studies, (MOG-R_3/GpG)$_3$ iPEMs caused a significant increase in the frequency of T_{REGS} ($CD4^+$/$CD25^+Foxp3^+$) compared with (MOG-R_3/CTRL)$_3$ treatments (**Figure 6.8G,H**). This polarization was observed in studies performed in the presence of self-antigen alone (*i.e.*, without CpG; **Figure 6.11**), and when both self-antigen and a strong TLR9 agonist were present (**Figure 6.8G,H**). Together, these differences in the processing of MOG-R_3/GpG and MOG-R_3/CTRL formulations indicate iPEM-loaded MOG-R_3 triggers antigen-specific T cell proliferation, but that inclusion of GpG in iPEMs directs these cells toward T_{REGS} and away from key inflammatory functions that drive autoimmune disease.

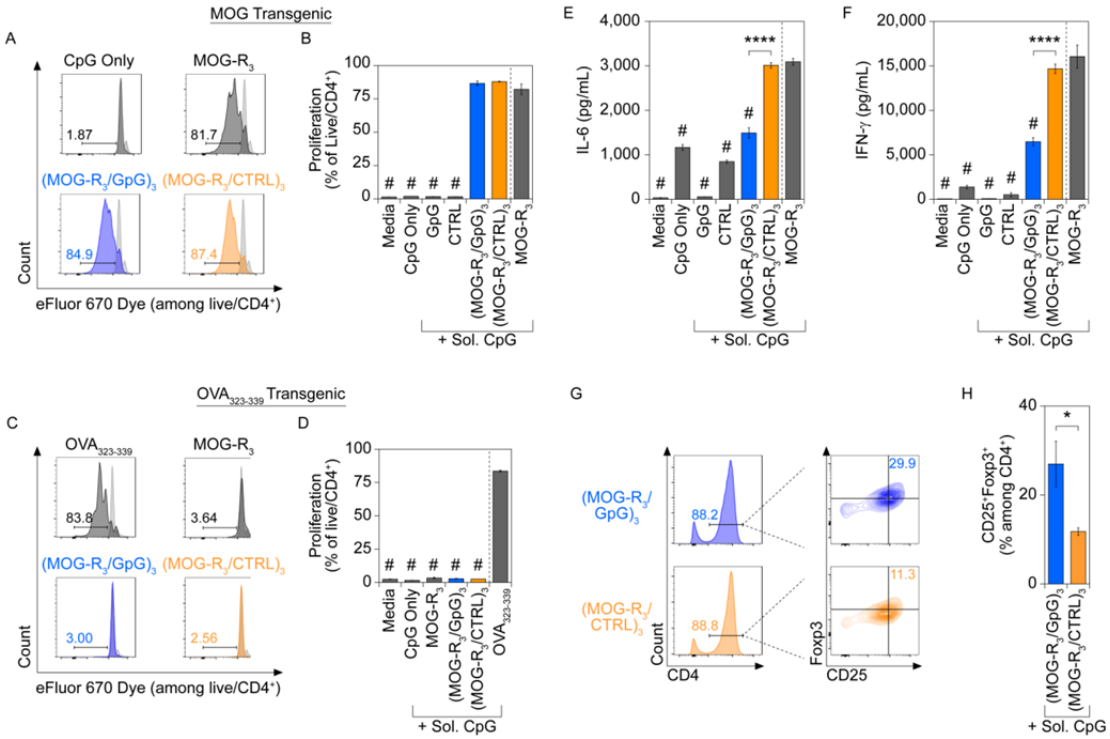

Figure 6.8 iPEMs drive antigen-specific T cell proliferation and polarize T cells towards regulatory function.

(A) Representative histograms and (B) quantification of proliferation of MOG-specific $CD4^+$ T cells. T cells were isolated from transgenic 2D2 mice, labeled with a proliferation dye (eFluor 670) and co-cultured with wild-type DCs treated with CpG and indicated soluble or iPEM formulations. After 72 h of co-culture, proliferation was assessed by flow cytometry analysis of the dilution of dye. In similar studies, wild-type DCs were incubated, as above, with CpG and indicated iPEMs or soluble components and co-cultured with $OVA_{323-339}$-specific $CD4^+$ T cells isolated from transgenic OT-II mice. Proliferation was assessed after 72 h, as illustrated by (C) representative histograms and (d) quantification of dye dilution. Control samples were incubated with $OVA_{323-339}$ to verify cognate-antigen-induced proliferation. ELISA was used to measure inflammatory (E) IL-6 and (F) IFN-γ secretion in supernatants from 2D2 co-cultures in (A-B). (G-H) In separate studies, MOG-specific $CD4^+$ T cells were co-cultured with wild type DCs, incubated with CpG and indicated iPEM forumations, and the frequency of T_{REGS}, $CD4^+/CD25^+Foxp3^+$ cells, was analyzed by flow cytometry using the gating scheme shown in (G), which was assigned using control samples treated with media alone (**Figure 6.11**). Data in all panels indicate mean ± s.e.m for studies conducted in triplicate. In panels B, D, E, F, data were analyzed with one-way ANOVA with a Tukey post-test to correct for multiple comparisons. For clarity, only key comparisons are shown: In panels B, E, F, # markers indicate the comparison (# = $P \leq 0.0001$) of each group to a strong positive control – wells treated CpG and a high dose of soluble cognate antigen, $MOG\text{-}R_3$ (60 μg, dashed lines). Comparisons between $(MOG\text{-}R_3/GpG)_3$ and $(MOG\text{-}R_3/CTRL)_3$ iPEMs are indicated by a bracket (**** $P \leq 0.0001$). In panel D, # markers indicate the comparison (# = $P \leq 0.0001$) of each group to a control of wells treated CpG and soluble OT-II cognate antigen, $OVA_{323-339}$ (dashed line). In panel H, statistics indicate the results of a two-tailed t test (* $P \leq 0.05$).

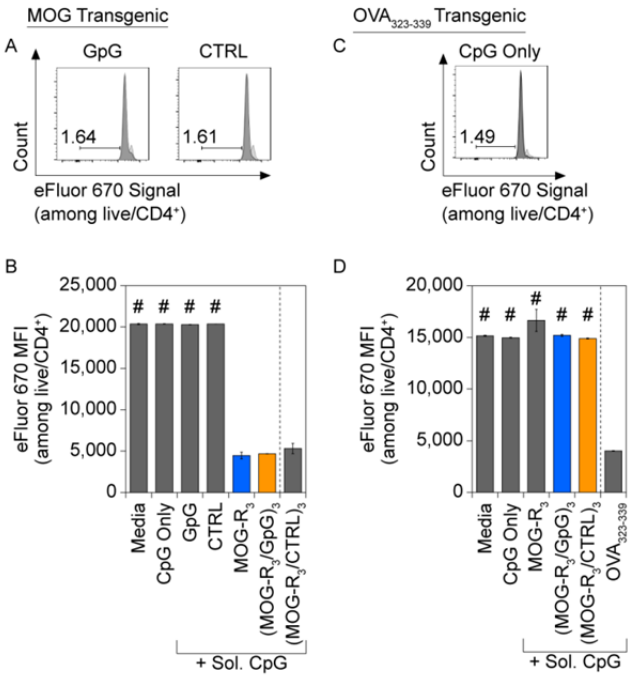

Figure 6.9 MOG-R_3-containing iPEMs drive proliferation of MOG-specific, but not OVA-specific, T cells.
(A) Representative histograms of additional control samples in 2D2 co-cultures shown in Fig. 3A,B. (B) Median fluorescence intensity (MFI) of 2D2 T cells following co-culture with DCs treated with indicated iPEM formulations or soluble components. (C) Representative histogram of an additional control samples from OT-II co-cultures, shown in Fig. 3C,D. (D) Median fluorescence intensity (MFI) of OT-II T cells following co-culture with DCs treated with indicated iPEM formulations or soluble iPEMs components, or positive control of CpG and $OVA_{323-339}$. Data in panels B, D indicate mean ± s.e.m. from studies conducted in triplicate. Data in panels B, D indicate mean ± s.e.m for studies conducted in triplicate and data were analyzed with one-way ANOVA with a Tukey post-test to correct for multiple comparisons. For clarity, only key comparisons are shown: In panel B, # markers indicate the comparison (# = $P \leq 0.0001$) of each group to a strong positive control – wells treated CpG and soluble cognate antigen, MOG-R_3 (60 µg dashed line). In panel D, # markers indicate the comparison (# = $P \leq 0.0001$) of each group to a control of wells treated CpG and soluble $OVA_{323-339}$ (dashed line).

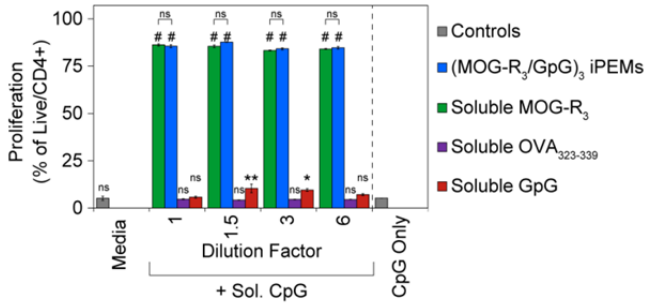

Figure 6.10 MOG-R_3-containing iPEMs and soluble MOG-R_3 drive proliferation of MOG-specific T cells.
Analysis of the percent proliferated of 2D2 T cells following co-culture with DCs treated with soluble CpG and the indicated iPEM formulations or matched doses of either soluble MOG-R_3, soluble GpG, or soluble $OVA_{323-339}$ peptide. The highest does (i.e., dilution factor of 1) incorporated 30µg (MOG-R_3/GpG)$_3$ iPEMs, an equivalent dose of each component (~24µg MOG-R_3, ~6µg GpG), or an equivalent dose of irrelevant $OVA_{323-339}$ peptide (~24µg) in free form. Data indicate mean ± s.e.m for

studies conducted in triplicate and data were analyzed with one-way ANOVA with a Tukey post-test to correct for multiple comparisons. For clarity, only key comparisons are shown: Markers indicate the comparison (* = $P \leq 0.05$; ** = $P \leq 0.01$; # = $P \leq 0.0001$, ns = not significant) of each group to a control of CpG only. Brackets indicate the comparison (ns = not significant) of iPEMs to a matched dose of soluble MOG-R_3 peptide.

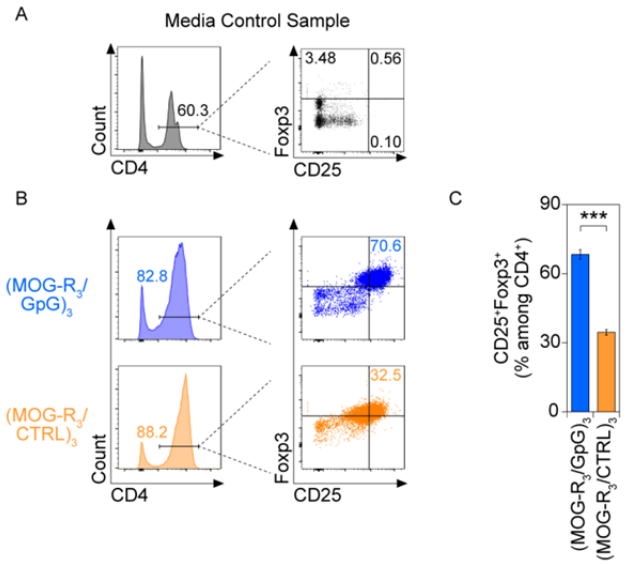

Figure 6.11 $(MOG\text{-}R_3/GpG)_3$ iPEMs promote the expansion of T_{REGS}.
(A) Representative flow cytometry plots of a media only control sample showing the gating scheme to analyze the data in Fig 3G,H. (B) Representative flow cytometry plots and (C) mean frequency of $CD4^+/CD25^+Foxp3^+$ cells in co-cultures of 2D2 T cells with wild type DCs incubated with $(MOG\text{-}R_3/GpG)_3$ iPEMs or $(MOG\text{-}R_3/CTRL)_3$ iPEMs. Data in panel C indicate mean ± s.e.m. from studies conducted in triplicate. A two-tailed t test was used to determine statistical significance (*** = $P \leq 0.001$).

6.3.4. iPEMs restrain inflammatory immune cell function and halt a model of MS in vivo

We next tested if iPEMs promote tolerance in mice. Lymph nodes and spleen are important tissues in this context, as these are the sites where differentiating T cells develop toward inflammatory or regulatory phenotypes. Recent studies, for example, reveal distinct structural microdomains form in these tissues to promote tolerance whereas other domains form to support pro-immune function, depending on the cells, structural elements, and immune signals present in each local microenvironment.[91]

The ability to co-deliver self-antigen and regulatory signals to these tissues without inflammatory components could create opportunities to promote tolerance by reprogramming the local signaling milieu and the expansion of T_{REGS} that migrate to sites of disease (*e.g.*, CNS) to control inflammation. Thus, we investigated if iPEMs deliver cargos to lymphoid tissues and effectively restrain self-antigen triggered inflammatory cytokine secretion at these sites. 48 h after subcutaneous injection, histological analysis revealed an accumulation of iPEMs in the subcapsular sinus of draining lymph nodes and distribution in the paracortex, while no signal was observed in lymph nodes from naïve mice (**Figure 6.12**).

To test if iPEMs redirect inflammatory response to myelin self-antigen, mice were induced with a common myelin-driven model of MS, experimental autoimmune encephalomyelitis (EAE).[86, 87, 247] In this model, untreated mice develop severe paralysis over the course of several weeks as the CNS is attacked by infiltrating T cells. Mice were either left untreated or treated with $(MOG\text{-}R_3/GpG)_3$ iPEMs 5 and 10 days after inducing EAE (**Figure 6.13A**). Three days after the second treatment (*i.e.*, day 13), splenocytes were isolated and pulsed with either MOG or irrelevant $OVA_{323\text{-}339}$ peptide. As expected – because myelin-specific T cells drive disease during EAE – in cells from untreated mice, MOG pulse increased the secretion of inflammatory cytokines IL-17 (**Figure 6.13B**), IFN-γ (**Figure 6.13C**), and IL-6 (**Figure 6.13D**) compared with identical cultures pulsed with OVA. In contrast, restimulating cells from iPEM-treated mice with MOG peptide did not increase inflammatory cytokines and, instead, resulted in the baseline levels of secretion

measured in cells from either group pulsed with OVA. Similar effects were also observed upon restimulation of cells isolated from axillary lymph nodes (**Figure 6.14**). These results indicate MOG-R_3/GpG capsules strongly blunt myelin-triggered inflammatory recall response.

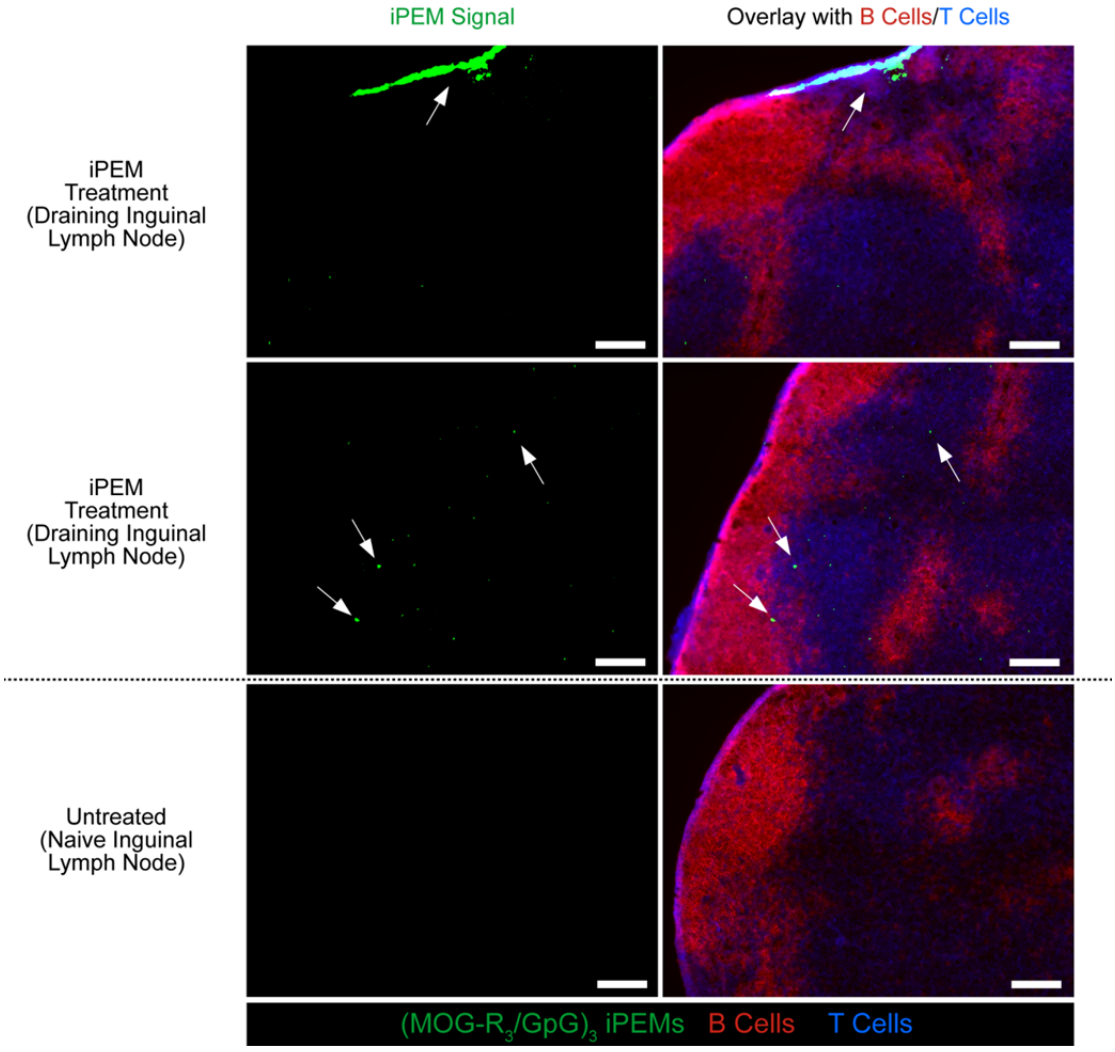

Figure 6.12 $(MOG\text{-}R_3/GpG)_3$ iPEMs accumulate in draining lymph nodes following subcutaneous injection.
Two days after subcutaneous injection of fluorescently-labeled $(MOG\text{-}R_3/GpG)_3$ capsules at the tail base, draining inguinal lymph nodes were excised. Immunohistochemical analysis was performed for the expression of B cells (B220, red), T cells (CD3e, blue) and the presence of capsules (FITC-labeled iPEMs, green). In some sections, an accumulation of iPEM signal was observed in the subcapsular sinus (top row, white arrow), while in other sections a distribution of iPEMs throughout the lymph node paracortex was detected (middle row, white arrows). Control samples were also prepared identically from naïve mice (bottom row). Scale 100 µm.

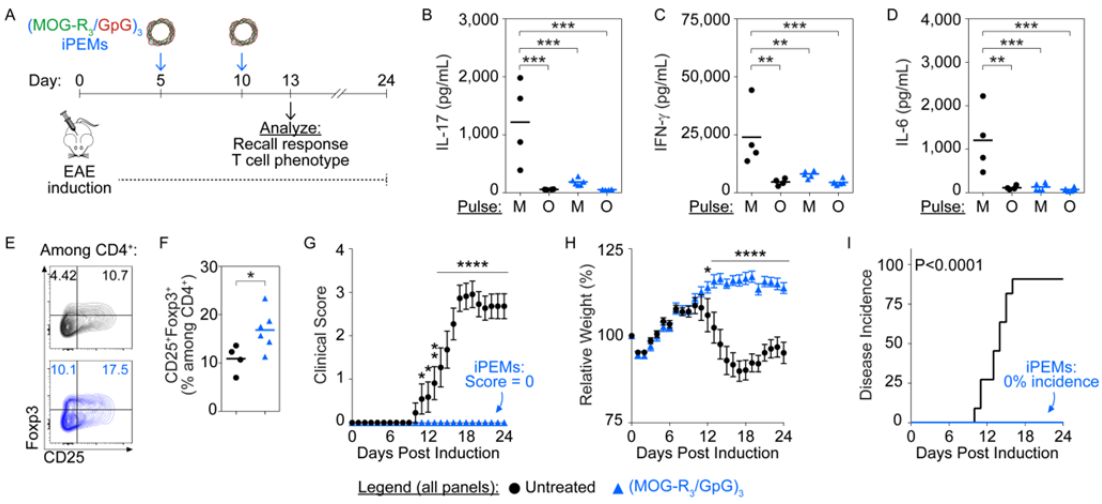

Figure 6.13 iPEMs restrain pro-inflammatory immune cell function and progression of a model of autoimmunity *in vivo*.
(A) Schematic of experiment timeline. Mice were induced with EAE and either left untreated or administered two doses of MOG-R_3/GpG iPEMs on days 5 and 10 post-induction. On day 13, splenocytes from induced, untreated mice (n = 4), or iPEM-treated mice (n = 4) as in (A) were restimulated with either MOG (Pulse: "M") or $OVA_{323-339}$ (Pulse: "O") for 48 h and ELISA was used to quantify peptide-triggered secretion of inflammatory (B) IL-17, (C) IFN-γ, and (D) IL-6. (E,F) In similar studies, splenocytes were isolated (n = 4 for both groups) on day 13 and analyzed immediately for the frequency of $CD4^+/CD25^+Foxp3^+$ cells. To assess therapeutic efficacy of iPEMs, mice were induced with EAE and either left untreated (n = 11) or administered iPEMs (n = 10) as in (A) and monitored for (G) mean clinical score, (H) disease-associated weight loss, and (I) incidence of disease. In panels B-D, data were analyzed with one-way ANOVA with a Tukey post-test. In (F), statistics indicate the results of a two-tailed t test. In (G,H), data were analyzed with multiple t tests, one at each time point, with a post-test correction for multiple comparisons. Disease incidence in (I) was analyzed with a log-rank test. (* = P ≤ 0.05; ** = P ≤ 0.01; *** = P ≤ 0.001; **** = P ≤ 0.0001).

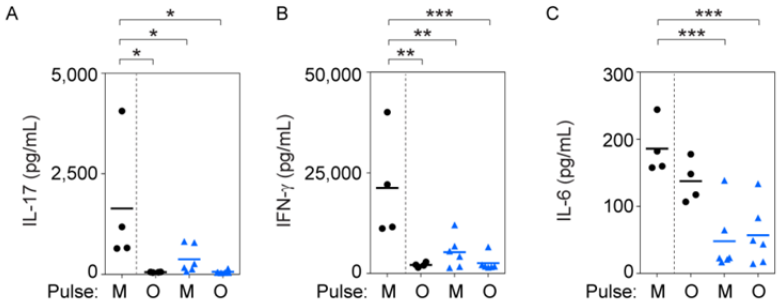

Figure 6.14 iPEMs restrain inflammatory recall response *in vivo*.
On day 13 post EAE induction, cells isolated from axillary lymph nodes from induced, untreated mice (n = 4), or mice treated with iPEMs on days 5 and 10 (n = 4) as in Fig. 4a, were restimulated with either MOG (Pulse: "M") or $OVA_{323-339}$ (Pulse: "O") peptide, cultured for 48 h, and ELISA was used to quantify peptide-triggered secretion of inflammatory (A) IL-17, (B) IFN-γ, and (C) IL-6. In all panels, statistics indicate the results of a one-way ANOVA comparing each group to a control of MOG-pulsed cells from untreated mice with a Tukey post-test. (* = P ≤ 0.05; ** = P ≤ 0.01; *** = P ≤ 0.001).

To investigate whether differences in cytokine secretion were due to polarization of T cell phenotype, cells were isolated from treatment groups analogous to those above, and stained immediately (*i.e.*, without restimulation) for T_{REG} markers. As with *in vitro* studies, iPEMs significantly increased $CD4^+/CD25^+Foxp3^+$ T_{REGS} (**Figure 6.13E,F**), and we also observed a trend of increased frequency of $CD4^+/CD25^-Foxp3^+$ cells (**Figure 6.13E**), though this latter result was not statistically significant. These findings support the hypothesis that $(MOG\text{-}R_3/GpG)_3$ iPEMs polarize T cells away from inflammatory subtypes and towards tolerogenic phenotypes. Next we assessed the functional impact of this T cell biasing by inducing mice with EAE and administering $(MOG\text{-}R_3/GpG)_3$ iPEMs on days 5 and 10. Each cohort was then monitored for clinical disease symptoms. Untreated mice developed severe paralysis (mean clinical score = 2.95 ± 0.30; **Figure 6.13G**), experienced dramatic weight loss (**Figure 6.13H**), and exhibited a high disease incidence of 87.5% (**Figure 6.13I**). In stark contrast, iPEM treatment completely eliminated EAE, with $(MOG\text{-}R_3/GpG)_3$ iPEM-treated mice remaining asymptomatic (*i.e.*, clinical score = 0, disease incidence = 0%) for the duration of the study without evidence of indirect symptoms such as weight loss (**Figure 6.13G-I**).

6.3.5. iPEMs attenuate inflammatory response in human MS patient samples

Building on our findings in mouse models of MS, we explored whether the tolerogenic effects of iPEMs would extend to human MS patient samples. Recent studies in MS patients confirm signaling in TLR9 and other TLR pathways drives inflammation and disease *via* cytokines that promote T_H1 and T_H17 polarization.[225,

227, 236] Thus, modulating signaling through this pathway could restrain self-attack in human disease. To begin investigating this possibility, we drew on an approach used in recent clinical trials: *ex vivo* restimulation of peripheral blood mononuclear cells (PBMCs) from MS patients to test for a reduction in myelin-triggered recall responses conferred by experimental therapies.[244] In our studies, we tested this impact by incubating iPEMs with PBMCs collected from three randomly selected MS patients participating in the Veterans Affairs Longitudinal MS (VALOMS) observational study (**Table 6.2**). PBMCs were cultured in media (*i.e.*, unstimulated) or with either $(MOG\text{-}R_3/GpG)_3$ or $(MOG\text{-}R_3/CTRL)_3$ iPEMs. MTT analysis revealed an increase in metabolic activity after iPEM treatment, irrespective of the sequence of the nucleic acid component (**Figure 6.15A**). This result confirms the expected myelin-triggered increase in cell function associated with myelin-reactive immune cells that develop during MS in humans. However, similar to murine co-cultures, despite equivalent levels of metabolic activity, $(MOG\text{-}R_3/GpG)_3$ iPEMs polarized cytokine profiles away from pro-inflammatory function compared with $(MOG\text{-}R_3/CTRL)_3$ iPEMs. Strikingly, in nearly every case, TNF-α (**Figure 6.15B**), IL-6 (**Figure 6.15C**), IL-10 (**Figure 6.15D**), and IFN-γ (**Figure 6.15E**) were lower when PBMCs were treated with GpG-containing iPEMs compared with CTRL-containing

Table 6.2 Patient demographic and clinical data.
Reported patient information, obtained in conjunction with the VALOMS observation study, including patient stage of disease, Extended Disability Status Score (a clinical assessment of MS symptoms in which a higher score indicates more severe disease), and history of clinical treatment. These patient data correspond to the PBMC samples analyzed in **Figure 6.15**.

Patient Number	Age (Years)	Gender	Stage of Disease	Kurtzke Extended Disability Status Scale	Treament with Disease Modifying Therapy	
					At Enrollment	At Any Time
1	58	Male	Relapsing-Remitting	2.5	No	No
2	39	Female	Relapsing-Remitting	1.5	No	Yes
3	43	Male	Secondary Progressive	6.5	Yes	Yes

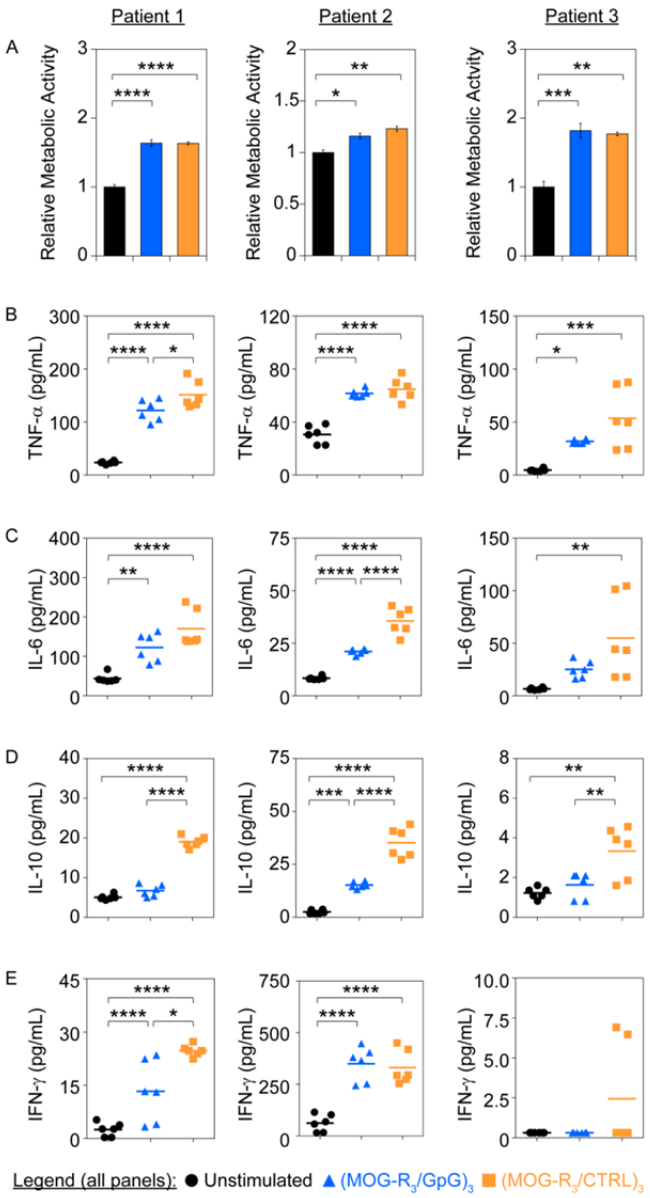

Figure 6.15 iPEMs activate human MS patient PBMCs but attenuate inflammatory cytokine secretion.
(A) Metabolic activity of PBMCs from three randomly selected MS patients following incubation with either $(MOG\text{-}R_3/GpG)_3$ or $(MOG\text{-}R_3/CTRL)_3$ iPEMs for 72 h, measured *via* MTT analysis. For each patient, the metabolic activity of cells treated with each iPEM formulation was normalized to control wells of PBMCs incubated with media only (untreated). Supernatants of cultures in a were collected and analyzed *via* a Luminex Multiplex assay for to quantify the secretion of (B) TNF-α, (C) IL-6, (D) IL-10, and (E) IFN-γ. Data in all panels represent mean ± s.e.m. ($n = 3$).

iPEMs, though the specific cytokines where these decreases were statistically significant varied across patients. For example, in Patient 1, a significant reduction of TNF-α, IFN-γ, and IL-10 was observed. Although IL-6 secretion exhibited lower

values, the differences were not significant relative to CTRL-containing iPEMs. Together, these results suggest inclusion of GpG with myelin peptide can restrain inflammatory immune function typically triggered by encounter of myelin-reactive cells from human patients. Further, while these samples were from patients with different stages of disease and treatment plans (**Table 6.2**), significant effects were observed in all three cases, highlighting the possibility of robust therapeutic effects enabled by iPEMs for future therapies.

6.4. Discussion

The ability to assemble biological cargo into PEMs without impacting function – along with direct control of cargo loading, modularity, and the ability to coat onto substrates over a range of length scales – are features that have motivated the use of PEMs in applications spanning electronics,[248] optics,[249] drug delivery,[195] and vaccines designed for traditional prophylactic applications (*i.e.*, pro-immune). In the latter, PEMs have been used to encapsulate antigen or adjuvant within PEMs shells composed of synthetic polymers, as surfaces to adsorb adjuvants or antigens, and to coat larger-scale vaccine substrates such as arrays of microneedles.[195, 197, 218, 240-243] These directions all seek to amplify immune response against infectious disease or cancer, but PEMs have never been used to regulate immune function or promote tolerance. This is an area that is particularly interesting for PEMs because one of the growing challenges in the vaccine and immunotherapy field is the increasing complexity of these formulations, and the associated difficulties in producing, characterizing, and understanding the mechanism of increasing complex

therapeutics.[250] The modular nature of PEMs could help support more rational design of tolerance-inducing therapies through self-assembly of several immune cues to form simpler, more-defined materials.

Modularity is also an important aspect for clinical translation because one of the current challenges facing development of more effective and specific autoimmune therapies is the diversity of antigens (*i.e.*, peptide epitopes) that are attacked during MS and other autoimmune diseases. For example, in MS there are a variety of myelin-based antigens that are incorrectly recognized as foreign, but these vary from patient to patient and can also expand during disease progression through a phenomenon termed epitope spreading.[37] In humans, one recent clinical trial is exploring infusion of MS patients with cells coupled with combinations of myelin peptides to generate antigen-specific tolerance.[244] In the biomaterials field, several exciting approaches are investigating the challenge of epitope spreading in pre-clinical models of autoimmunity. The Santamaria lab has prepared iron oxide nanoparticles displaying self-peptide in immune protein complexes (major histocompatibility complex, MHC) to expand regulatory cell populations with the capacity to suppress responses against a broader set of self-antigens.[36, 87] Miller and co-workers have used PLGA particles displaying self-epitopes to induce tolerance, and have discovered that tolerance generated against particles displaying one myelin antigen can also help protect against epitope spreading in mice.[39]

iPEMs offer unique features that can be exploited as tools to probe the progression of autoimmune disease and development of tolerance. In particular, iPEMs allow incorporation of one or multiple antigens and regulatory signals with control over the relative compositions by specifying the concentrations or number of layers of each component (**Figure 6.1**). Thus, while we selected a single epitope and ratio of myelin:GpG for our studies to investigate the therapeutic efficacy (*i.e.*, 1:2 MOG-R_3:GpG; **Figure 6.1F, Table 6.1**), this platform could be used to create libraries of materials that exhibit defined concentrations or combinations of epitopes and regulatory signals. This capability might be useful, for example, to investigate how such parameters impact epitope spreading. Relative to other biomaterials being studied in tolerance, iPEMs offer a composition that is simplified by elimination of supports, polymeric carriers, and stabilizers (*e.g.*, poly(vinyl alcohol)) – components that often exhibit intrinsic inflammatory functions, as noted above. iPEMs also eliminate recombinant or higher order protein structures such as MHC molecules, instead juxtaposing self-antigen with signals (*i.e.*, GpG) aimed at redirecting the response to a given self-antigen.

In our studies, we observed reduction in myelin-triggered inflammatory cytokines in mouse cells, mouse models of MS, and human patient samples (**Figures 6.8, 6.13--6.15**). These molecules – IL-6, IL-17, IFN-γ, for example – represent some of the key biomolecular drivers of inflammation during MS and other autoimmune diseases. In particular, seminal work indicates IL-6 expands T_H17 cells associated with disease in mouse models of MS and also in humans; this cytokine also inhibits development of

the T_{REGS} that can help control disease.[247] Similarly, IL-17 is a characteristic cytokine of the T_H17 subset, and IFN-γ is a broadly-acting pro-inflammatory effector cytokine produced by T cells during infection and autoimmunity. Intriguingly, while these reductions were occurring, the level of myelin-specific T cell expansion (*e.g.*, proliferation, metabolic function) was unchanged (**Figures 6.8, 6.15**). Further, we observed polarization toward T_{REGS} when measured in both co-culture and mice (**6.8, 6.11, 6.13**). Data from our studies with MS patient PBMCs exhibited similar changes in cytokine profiles, though further studies will need to include T_{REGS} measurements. Taken together, these current findings indicate MOG-R_3/GpG iPEMs activate self-antigen-specific cells, but bias the phenotype and function of these populations towards tolerance.

Our experiments with PBMCs from MS patient samples also suggest the possibility of polarizing the function of cells from patients with a variety of disease stages and severities, though samples from larger patient cohorts will be needed to confirm this possibility. The idea of disease heterogeneity is a consideration of general importance because no cures exist for MS, and existing treatments rely on non-specific suppression – either of broad immune function, or through targeting all instances of a specific cytokine or molecule.[37] Further, patient responses to treatments plans are variable. Lastly, while treatments for earlier stages of MS have progressed and provided important benefits to patients, very few options are available for patients in progressive and later stages of disease. Thus treatments that provide therapeutic

effects even during later stages of disease would greatly improve both patient outcome and quality of life.

Another important question in the autoimmune field is what types of components are required for tolerogenic therapies. In the recent biomaterials literature, for example, several reports demonstrate self-antigens must be co-delivered with regulatory signals to reprogram the responses against these antigens.[47, 86] However, other studies demonstrate changing the physical form of antigen – free peptide *versus* peptide displayed on a cell or particle – alters the trafficking of these self-antigens, leading to activation of debris clearance pathways involved in tolerance.[39, 43] And, finally, several studies demonstrate that myelin is already presented in the lymph nodes of mice and humans during MS,[95, 251] motivating the possibility that even delivery of GpG or other TLR modulators alone might support antigen-specific tolerance. These possibilities are exciting because excess TLR signaling is associated with a number of autoimmune disease and numerous target TLR ligands are arising.[225-231, 236]

In our *in vitro* studies we observed each iPEM component maintained selectivity, but GpG was less potent relative to free GpG at the assessed time. We also observed that iPEMs provide more efficient co-delivery of cargo compared with admixed formulations, thus one possibility is that the strong electrostatic interactions between iPEM components increases the time needed to process these signals in immune cells. Intracellular trafficking and processing studies could help elucidate this hypothesis, but many of the unique features of iPEMs are most relevant for the *in vivo* setting. As

already mentioned, for example, the ability to co-deliver and control the relative doses of self-peptides and regulatory signals is important in developing new, more-specific therapies for autoimmunity. The modular nature of iPEMs could enable these design features through assembly of strategically-selected combinations of disease-relevant or irrelevant antigens and inert or tolerizing signals. Future mechanistic studies will explore how the role and relative concentrations of GpG, myelin peptide, and other iPEM components (*e.g.*, irrelevant peptide antigens, CTRL) impact inflammation and T cell function using knockout models and trafficking of transgenic reporter cells. In our platform, as well as in development of other nano-material platforms, linking efficacy with treatment-associated changes in pathology is also critical, for example, by demonstrating treatment reduces infiltration of myelin-reactive T cells to the brain and promotes remyelination during reversal of disease. In some of our other recent work, we showed iPEMs built from model immune signals promote co-delivery of immunological cargos to draining lymph nodes.[33] In the current setting of tolerance, understanding how iPEMs built from regulatory signals impact the local microenvironment of lymph nodes is another fascinating question, one that will help reveal how iPEMs polarize T cell differentiation in these tissues and how specific the resulting tolerance is.

6.5. Conclusions

PEMs offer features that have sparked exploration in fields from energy to medicine. Here we use three experimental systems—mouse cells, mouse models of MS, and human MS patient samples—to demonstrate PEMs can also be exploited to promote

immunological tolerance. The potency of the results in the restraint of EAE onset and progression suggests future studies to determine whether late stage treatment with iPEMs can reverse established disease and drive remyelination in the CNS. Similarly, studies with statistically-relevant sizes of human patient sample sets will help reveal the utility and mechanisms underpinning the function of iPEMs. These future questions are catalyzed by the current work, which demonstrates the potential of PEMs to combat autoimmunity. More generally our results demonstrate that regulating TLR signaling can be used to promote tolerance, an idea that can be extended to other biomaterials to study or treat autoimmune diseases and conditions such as allergies and asthma.

Chapter 7. Conclusions and Future Work

7.1. Outlook

The two research aims described in this dissertation have revealed the potential to i) target delivery of biomaterial-encapsulated immune signals to distinct LNs to drive systemic, but specific restraint of disease and ii) harness PEM technology to modulate inflammatory TLR9 signaling and promote immunological tolerance. These current findings, however, have sparked several outstanding research questions, motivating the ongoing work and future directions described below.

7.2. Lymph node engineering

7.2.1. Understanding specificity and mechanism of restraint of disease

An important criterion for experimental therapies for MS is the potential to control self-reactivity without compromising the rest of the immune system. As described in **Chapter 4**, we have demonstrated that therapeutic effects are dependent on delivery of encapsulated myelin self-antigen to the LNs and enhanced with co-delivery of Rapa. Further, an expansion of T_{REGS} was observed following administration of MOG/Rapa MPs, but not OVA/Rapa MPs. Together, these results support a hypothesized mechanism of myelin-specific restraint of disease underscored by polarization of immune cells towards tolerogenic phenotypes and functions. However, further studies could inform our understanding of the mechanism and specificity of control of autoimmunity.

Overall, the completed studies – and proposed studies, below – could be repeated with an expanded range of MP formulations, incorporating single component MPs (i.e., MOG MPs, OVA MPs, Rapa MPs), to investigate the role of individual signals vs. synergistic effects and the contributions from either disease-relevant or irrelevant antigen. Studies could begin by more closely examining the sites of disease, the brain and spinal cord. Our current analyses reveal a decrease in the frequency of $CD3^+$ cells in the spinal cord following *i.LN.* injection of tolerogenic MPs (**Figure 4.4**). These cell types could be further characterized by flow cytometry or immunofluorescent staining to examine the frequency of $Foxp3^+$ cells or inflammatory T cell subsets (e.g., T_H1, T_H17), as well as the presence of other immune cells types (e.g., APCs, B cells). Further, the CNS-resident cells, including microglia and oligodendrocytes – the cells typically responsible for re-myelination – could be analyzed to investigate whether *i.LN.* treatment, for example, protects oligodendrocytes from typical inflammation-induced damage. Further, stains for myelination (e.g., Luxol Fast Blue) or axonal damage (e.g., Bielschowsky's Silver) could be used to determine if early- or late-stage treatment protects the myelin sheath and underlying axons from damage, or reverses disease-driven lesions, respectively. In all of these studies, analyses could also be conducted in multiple tissue sites, such as different regions of the brain and levels of the spinal cord, comparing sacral, lumbar, thoracic, and cervical effects.

Next, to test if the expanded T_{REG} population is responsible for control of autoimmunity, antibodies (e.g., anti-CD25, anti-IL-10) could be used to deplete these populations *in vivo* and reveal the impact on disease progression. As we hypothesize

that T_{REGS} are critical for amelioration of EAE, we would expect deletion or inactivation of these cell types to attenuate or eliminate therapeutic effects. In parallel, the functional capacity of T_{REGS} could be revealed through adoptive transfer studies. In these experiments, magnetic bead kits or fluorescent-activated cell sorting could be used to isolate all $CD4^+$ T cells, $CD4^+CD25^+$ cells, or other T cell subsets. These cells could then be transferred to naïve mice, followed by an EAE induction challenge to test if transferred cells protect from disease onset. Alternatively, cells could be transferred to mice induced with EAE – in either early-stage or peak disease – to test if cells can restrain or reverse disease-induced paralysis. We hypothesize that these studies could support the role of T_{REGS} to transfer tolerance and functionally restrain self-reactivity. Studies could also be coupled with either congenic or fluorescently-labeled cells to enable trafficking studies to identify whether transferred T cells or T_{REGS} travel to treated LNs, the CNS, or other sites following injection. Finally, additional flow cytometry markers (e.g., transcription factors, such as T-bet and RORγ, chemokine or cytokine receptors) could be coupled with new tools – such as MHC-II tetramer to assess the T cell receptor specificity – to further characterize the T cell population and to determine if these cells are myelin-specific.

Another indication of selective tolerance is the potential for mice that have been protected from EAE to mount responses against foreign antigens or pathogens. To begin to assess the integrity of healthy, protective immune function I have completed a pilot study using a model antigen derived from ovalbumin, SIINFEKL (SIIN). In this experiment, mice were either left completely untreated (i.e., naïve) for the

duration of the study, or induced with EAE and treated 10 days post induction *i.LN.* with MOG/Rapa MPs. On day 49 post-EAE induction, a small volume of peripheral blood was collected from both naïve and treated mice and analyzed for the frequency of $CD8^+$ T cells specific for SIIN (**Figure 7.1** Day 0). Following blood draw, induced, MOG/Rapa MP-treated mice were immunized *via* intramuscular injection with a mixture of ovalbumin protein and an adjuvant, polyIC. Excitingly, seven days post-immunization, a repeat blood draw revealed an expansion of SIIN-specific T cells in immunized, MOG/Rapa MP treated mice that were protected from EAE, but not in naïve mice (**Figure 7.1** Day 7). Importantly, however, future studies should incorporate control groups of mice that receive the vaccine alone as well as mice that are induced with EAE and administered the vaccine to compare the magnitudes of SIIN-specific responses. The regimen could also be expanded to include one or more booster immunizations to indicate recall response and development of immunological memory through monitoring $CD8^+$ SIIN-specific T cells in blood over time, as well as analyzing serum samples for the development of ovalbumin-specific antibody titers. In addition, the function and phenotypes of these cells could be explored through flow cytometry and either intracellular cytokine staining, or ELISA analysis of culture supernatants following *ex vivo* peptide restimulation, to confirm desired pro-inflammatory responses. Experiments could also be coupled with monitoring of how cells respond to encounter of myelin peptide, either *ex vivo* through peptide restimulation as above, or *in vivo* through delayed type hypersensitivity assays. These studies would confirm that cells have been tolerized against myelin, and reveal how this effect impacts the magnitude and nature of responses to other antigens. Finally,

the studies could be advanced from model antigens to include non-lethal pathogen challenges, such as a Leishmania infection challenge, to examine if mice can successfully clear infections, a critical limitation associated with current clinical interventions.

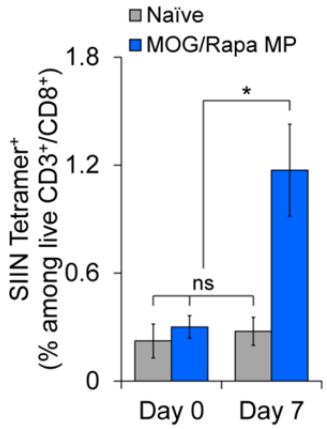

Figure 7.1 Mice tolerized with *i.LN.* MOG/Rapa MP-treatment mount T cell responses against a model antigen.
Mice were either left untreated for the duration of the study (naïve) or induced with EAE and treated with MOG/Rapa MPs *i.LN.* on day 10 post induction. On day 49 post-EAE induction, peripheral blood samples were collected from both groups and analyzed for the frequency of SIIN-specific $CD3^+/CD8^+$ T cells (Day 0). Following blood draw, MOG/Rapa MP-treated mice were immunized with ovalbumin and polyIC and, seven days later, peripheral blood analysis was repeated (* = $P \leq 0.05$, ns = not significant).

7.2.2. Explore the role of DCs and other APC populations to drive tolerance

From a more fundamental perspective, an intriguing finding in our initial studies was a large influx of $CD11c^+$ cells in MOG/Rapa MP-treated LNs (**Figure 4.4, 4.6**). Follow-up studies could further characterize these cells to explore the phenotype, activation state, and function of these APCs. Studies could analyze cells directly via flow cytometry analysis of surface expression of markers including CD11c, CD11b, PDCA-1, CD103, F4/80, and more, as well as intracellular cytokine staining to assess cell function. In parallel, functional assays could include isolation of DCs from treated mice, followed by *ex vivo* co-culture of these cells with naïve 2D2 $CD4^+$ T

cells that recognize myelin peptide. These co-cultures could be analyzed for the potential of DCs to drive antigen-specific T cell proliferation as well as the phenotype and cytokine secretion profiles of dividing T cells.

7.2.3. Exploit modular, platform-based approach to develop fundamental knowledge

As the *i.LN.* injection approach allows for control over the combinations and doses of signals present in LNs, this strategy could be used as a tool to study tolerance and inform the design of new therapies. For example, the properties of the polymer used to encapsulate signals could be varied by controlling the molecular weight or monomer ratio of PLGA, or changing the polymer altogether, to tune polymer stability and degradation kinetics and, subsequently, the timescale over which signals are present in LNs. These studies could inform understanding of the role of antigen and regulatory signal persistence, building upon our initial findings that soluble myelin peptide did not confer protective effects when delivered *i.LN.* mixed with Rapa MPs (**Figure 4.7**). The dependence of tolerance on the geography or anatomic location of signal delivery could also be further explored. For example, we have observed that *i.LN.* delivery of MPs co-loaded with MOG and Rapa exhibits synergistic therapeutic effects compared with MOG MPs, but this treatment regimen was tested by delivering a single dose of MPs split between both left and right inguinal LNs (i.e., two injections/dose). Alternative approaches could include delivering the same total dose to a single inguinal LN, delivering MOG MPs to one LN and Rapa MPs to the contralateral LN, or treating alternative LNs, such as the cervical LNs, which drain a key site of disease, the brain. Together, these studies

could enhance our understanding of how perturbation of a single tissue, or delivering signals in disparate tissues, alters elicited systemic response.

7.2.4. Test i.LN platform in other diseases

Along the lines of the **Section 7.2.3**, a final future research direction for this strategy is to tailor the biomaterials to target alternative antigens relevant for other autoimmune diseases, allergies, or transplant applications. In our lab, we are actively working on projects in models of type 1 diabetes as well as another model of MS, relapsing-remitting EAE (RR-EAE). In RR-EAE, mice exhibit waves of disease-induced paralysis, rather than a progressive disease course as in EAE. This model captures aspects of early stages of MS that the majority of human patients present with; in particular, RR-EAE incorporates a phenomenon termed epitope spreading, in which reactivity develops against more than one distinct peptide fragment of myelin over time. While in humans epitope reactivity can vary greatly across patients and for a given patient over time, in mice, the spread is relatively well-characterized. Mice are induced with a protocol similar to that used in EAE, but T cells are primed to recognize a portion of myelin proteolipoprotein (PLP), rather than MOG. These mice then develop reactivity to a different fragment of PLP, resulting in a second wave of disease and allowing researchers to study the potential for candidate therapies to control reactivity against prime and spread peptide sequences, as well as the potential to inhibit epitope spreading. I have been training a new graduate student, Emily Gosselin, who will take over and explore this aspect of the project, and she has recently shown successful application of this approach to RR-EAE through a pilot

study. Her experiment revealed that while mice treated with PBS or empty MPs exhibited expected disease course, mice treated *i.LN.* with MPs co-encapsulating PLP and Rapa at the peak of the first wave of disease were significantly protected from relapse (**Figure 7.2**). The next steps will include expanding the MPs tested to incorporate PLP alone or Rapa alone to confirm antigen specificity of therapeutic effects, as well as studies to test delivery of the spread, rather than prime, PLP epitope. Follow on experiments could also explore the mechanism of tolerance, as in **Chapter 4** and future work studies described in **Section 7.2.1-7.2.3**.

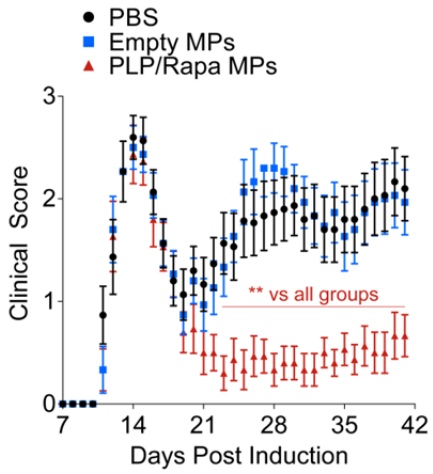

Figure 7.2 A single *i.LN.* dose of PLP/Rapa MPs protects mice from relapse in RR-EAE.
Mice were induced with RR-EAE and on day 13 post-induction randomized into groups with equal mean clinical scores. Mice were then treated *i.LN.* with either PBS, empty MPs, or MPs co-encapsulating PLP and Rapa, and clinical scores were monitored. (For all groups, N=15; ** = $P \leq 0.01$)

In parallel, our lab has partnered with the Bromberg Lab at the University of Maryland School of Medicine to test this idea in a model of islet transplantation. In this model, C57BL/6 mice are injected with streptozocin (STZ) to induce diabetes. Following onset of hyperglycemia, islets from naïve BALB/c mice are isolated and transplanted into the kidney capsule of the diabetic C57BL/6 recipients. Transplanted islets initially help to return blood glucose to normal levels but, due to the strain

mismatch, will be rejected by the recipient immune system within the first two weeks post-transfer. This rejection can be observed as a reversion to hyperglycemia in peripheral blood. To test the *i.LN.* injection platform in this model, I synthesized and characterized MPs encapsulating Ea_{52-68}, a known alloantigen, and/or Rapa (**Table 7.1**). Indicated MP formulations were then administered as a single dose *i.LN.* at the same time as the islet transfer, and blood glucose was monitored daily. Mice administered islets, but no MP treatment, exhibited a rapid return to hyperglycemia (**Figure 7.3A**), resulting in a mean graft survival time of 9.2 days (**Figure 7.3B**). In contrast, mice administered Rapa MPs *i.LN.* on the day of transplant exhibited prolonged normoglycemia and graft survival (mean survival time 23.6 days), while mice treated with co-loaded Ea_{52-68}/Rapa MPs exhibited a dramatic increase in survival, with a mean survival of 47.2 days (**Figure 7.3A-B**). Next steps in these studies will include performing nephrectomies to remove grafted islets; we hypothesize that these procedures would lead to a loss of glycemic control, revealing the critical sustained role of transplanted cells in regulating blood glucose. In addition, co-loaded Ea_{52-68}/Rapa MPs will be compared against MPs loaded with Ea_{52-68} peptide alone and, in future experiments, multiple MP formulations will be screened in experiments to study the mechanism of tolerance as in **Chapter 4** and above. Finally, we are working with the Bromberg lab and additional collaborators at the University of Maryland School of Medicine, the Pierson lab, to test the idea in more complex models of transplant, including pilot studies in non-human primates that will begin this summer. Together, the studies outlined in this section will test the robustness of *i.LN.* injection of MPs as a platform to reprogram responses to distinct

individual or combinations of peptide epitopes relevant to multiple disease models, as well as inform translational potential through testing in higher order animal models.

Table 7.1 Physiochemical characterization of microparticles for transplant model.
Percent yield of indicated MP formulations was calculated using the dry mass of a known aliquot of final MP solution and laser diffraction was used to measure particle diameter. Peptide and rapamycin loading were measured by microBCA and UV/Vis spectrophotometry, respectively, after particle dissolution and are reported per mass of particles and as encapsulation efficiencies.

	Polymer Core			Rapamycin Loading		Ea_{52-68} Loading	
	Yield (mg)	Yield (%)	Diameter (μm)	μg Rapa/ mg particle	Encapsulation Efficiency (%)	μg Ea_{52-68}/ mg particle	Encapsulation Efficiency (%)
Empty MP	52.1	65.1	4.14	N/A	N/A	N/A	N/A
Ea_{52-68} MP	49.9	62.4	5.32	N/A	N/A	3.61	36.0
Rapa MP	56.3	70.4	4.67	14.2	40.1	N/A	N/A
Ea_{52-68}/Rapa MP	56.3	70.4	4.64	18.0	50.6	3.72	41.9

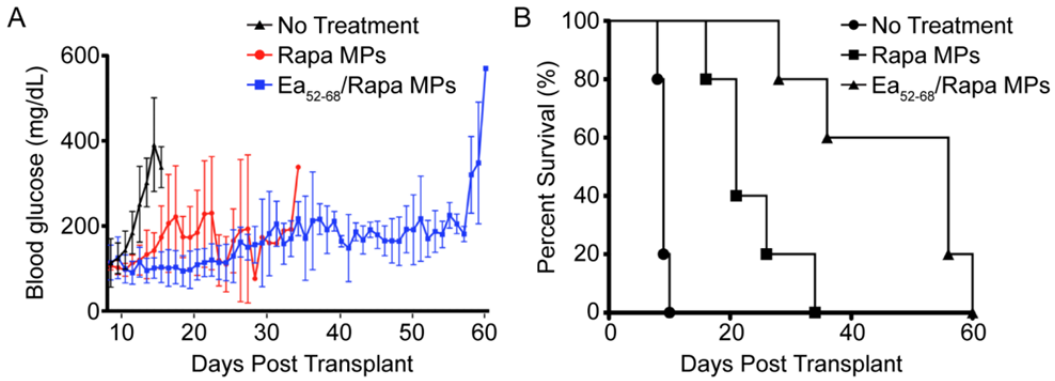

Figure 7.3 *i.LN.* delivery of alloantigen/Rapa co-loaded MPs enhances graft survival in islet transplant model.
C57BL/6 mice were injected with streptozocin (STZ) to induce hyperglycemia. Islets from naïve BALB/c mice were transferred to diabetic recipients along with either no additional treatment (n=5), or a single dose of intra-LN MPs encapsulating either Rapa alone (n=5) or Ea_{52-68} peptide and Rapa (n=5). A) Peripheral blood of recipient mice was then monitored for blood glucose level daily as an indicator of (B) graft survival.

7.3. iPEMs

7.3.1. Test potency of iPEM approach and explore the mechanism and specificity of tolerance

Similar to the *i.LN.* delivery platform, the iPEM approach described in **Chapter 6** could benefit from more detailed study of the robustness and mechanism of tolerance induced by capsules. Our current studies have tested iPEMs in an early treatment regimen, beginning five days post EAE induction. To investigate the potential to reverse established disease, I have completed a pilot study in which mice were induced with EAE and, at peak disease, randomized into groups with equal mean scores and either left untreated or administered $(MOG\text{-}R_3/GpG)_3$ iPEMs on days 15, 20, and 25. While induced, untreated mice exhibited sustained disease-induced paralysis, mice administered iPEMs significantly decreased in mean clinical score, corresponding to a functional reversal of paralysis (**Figure 7.4A**) and disease-induced weight loss (**Figure 7.4B**). These preliminary results suggest that iPEMs redirect existing self-reactivity, but the mechanism of this reversal has yet to be explored. For example, studies could examine whether iPEMs alter the number and types of cells – and phenotypes of these cell subsets – infiltrating the brain and spinal cord. Additional readouts could analyze oligodendrocytes and myelination to explore if iPEMs protect cells from damage due to inflammation and drive re-myelination, a critical criterion for new therapies to treat late-stage disease in human patients as described in **Section 7.2.1**.

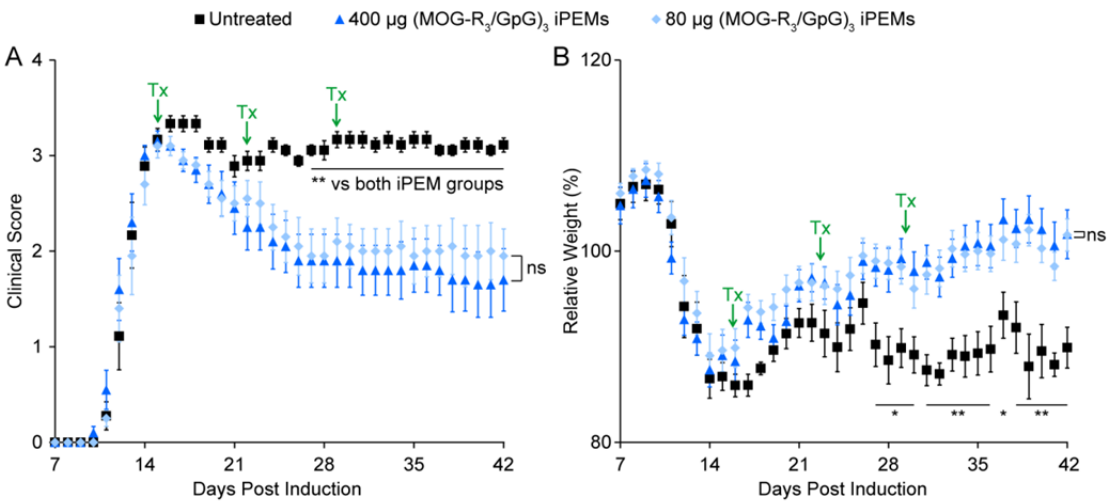

Figure 7.4 iPEMS reverse established disease-induced paralysis
Mice were induced with EAE and monitored until day 15, then randomized into groups with equal mean scores. Mice were then either left untreated or administered $(MOG\text{-}R_3/GpG)_3$ iPEM capsules *via* subcutaneous injection on days 15, 20, and 25, and monitored for clinical score and relative weight change. (Untreated, N = 11; $(MOG\text{-}R_3/GpG)_3$ iPEMs, N=12). * = $P \leq 0.05$; ** = $P \leq 0.01$; ns = no significant difference.

In parallel to the studies above, future experiments could further explore the processes that underpin restraint or reversal of disease following iPEM administration. First, the role of each component, myelin peptide and GpG, could be studied by testing iPEMs with different ratios of each cargo, as in **Figure 6.1**. This flexibility in assembly could allow for different dose screening regimens, such as fixing the total dose of iPEMs, but titrating the relative dose of myelin and GpG, or fixing the dose of one component while varying the dose of the other cargo. These studies could help to optimize the combinations and doses of signals critical to restraint of disease, as well as reveal the relative contribution of each signal. Toward this goal, the pilot late-stage treatment experiment included an initial test of different total doses of iPEMs at a fixed cargo ratio (i.e., dilutions of iPEM capsules), and we observed significant therapeutic effects with a 5X dilution of iPEM dose compared with previous studies (**Figure 7.4A-B**).

This finding could be expanded to include more doses, the screening regimens above, as well as to iPEM formulations with either relevant (i.e., myelin peptide, GpG) or inactive cargos (i.e., control antigen, control oligonucleotide). We have demonstrated synthesis of capsules with MOG-R_3 and either GpG or CTRL, as well as the potential to isolate the effects of GpG to restrain TLR9 signaling in reporter cells and both DC activation and inflammatory cytokine secretion in primary immune cells (**Figure 6.4, 6.6**). However, these two formulations have not been compared directly *in vivo* and, further, studies should also incorporate iPEMs synthesized from a control peptide to demonstrate myelin-specificity of therapeutic effects.

Initial attempts to generate stable capsules from alternative antigens have been challenging, motivating experiments to study how iPEMs assemble and are processed by cells, including how the arginine modification impacts these properties. For immediate study of an epitope that is not involved in the pathology of EAE (i.e., disease irrelevant), I have synthesized capsules assembled from a diabetes peptide epitope (GADp17) appended with nine arginine residues (GADp17-R_9) and GpG (**Figure 7.5**). Longer term, however, the identification of a peptide antigen with similar properties (e.g., molecular weight, charge, hydrophobicity) to MOG and modified with the same peptide sequence (R_3) could enable more direct isolation and comparison of the link between antigen identity and potential to control disease.

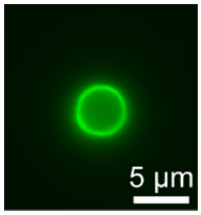

Figure 7.5 Synthesis of iPEM capsules from control (i.e., non-myelin) antigen
iPEMs were synthesized by depositing three bilayers of fluorescently-labeled GADp17-R_9 and GpG on $CaCO_3$ MP templates. Coated MPs were incubated in 0.1M EDTA to dissolve the core and remaining hollow capsules were imaged by fluorescence microscopy.

In parallel, the studies above could be coupled with many of the immunological techniques described in **Chapters 4, 6, and 7** to study the phenotypes, functions, and localization of immune cells *in vivo* that accompany the observed halt or reversal of disease. Of particular relevance for the iPEM platform could be to analyze TLR9 signaling *in vivo* through RT-PCR to investigate whether GpG restrains TLR9 and downstream signaling pathways during disease, including studying the tissues in which these effects are observed (e.g., draining vs. non-draining LNs). These findings could be supported by repeating studies using TLR9 knockout or other transgenic mouse strains to demonstrate that effects are dependent on TLR9 signaling. As our hypothesized mechanism is that MOG/GpG iPEMs enable presentation of myelin antigen in the presence of reduced inflammatory signaling based on current *in vitro* and *in vivo* results, together these experiments could support that these effects are occurring through the expected TLR9 pathway to impact the phenotype, activation state, and cytokine secretion profiles of DCs and other APCs *in vivo*.

7.3.2. Explore how iPEMs interact with PBMCs from human MS patients

As introduced in **Chapter 6**, we have worked with collaborators in Dr. Walter Royal's lab at the Baltimore VA to test how iPEMs interact with samples isolated

from human MS patients enrolled in an observational study (VALOMS). Our pilot results suggest that inclusion of GpG in iPEMs, compared with CTRL, does not impact metabolic activity of cells, but downregulates inflammatory cytokine secretion in these cultures (**Figure 6.15**). These studies could be expanded to include statistically-relevant patient populations. Further, a large amount of de-identified patient data was recorded at each visit accompanying the blood draw, including age, gender, stage and severity of disease, treatment regimen, MRI scans, and more. Coupling this data with results from repeat studies to test how iPEMs bias immune function and phenotype in cell samples could enable links to further understand the role of TLR signaling in human MS, including differences in observations across different stages of disease or other patient stratification categories.

7.3.3. Incorporating tunable degradation features into iPEMs

In parallel, the iPEM platform could be enhanced by incorporating a mechanism for programmable release of cargo and degradation of multilayers. One approach toward this goal that we are actively studying is the incorporation of polymers as a cargo component. I helped to design and start this project, and have been mentoring an undergraduate researcher, Boyan Xia, for the past four years as she has developed increasing independence to lead experiments in materials design, synthesis, characterization, and optimization. Boyan has combined a poly(beta-amino ester), Poly1, with GpG to synthesize iPEMs; this polymer is cationic, facilitating incorporation into multilayers through electrostatic interactions, and incorporates ester bonds in the backbone, enabling hydrolytic degradation (**Figure 7.6A**). More

broadly, this class of polymers, PBAEs, has been widely-studied for nucleic acid delivery, as their charge facilitates electrostatic condensation or assembly, and they are minimally toxic to cells as they degrade. The potential to control kinetics of regulatory signal (i.e., GpG) delivery is of particular interest for MS and corresponding mouse models because previous studies have demonstrated elevated TLR signaling in different stages of disease [229], and required repeat administration of soluble GpG to partially attenuate disease [232]. Thus, we hypothesized that sustained release of GpG following administration might prolong or enhance therapeutic effects.

To test this idea, we began by synthesizing iPEMs on planar substrates to characterize film growth and stability in well-controlled conditions. We have observed layer-dependent incorporation of GpG into iPEM structures on two different scales: every two bilayers through eight total dipping cycles (**Figure 7.6B**) and every eight bilayers through fifty-six dipping cycles (**Figure 7.6C**), measured *via* UV/Vis spectrophotometry. The latter result was generated using an automated protocol to deposit PEMs using a dipping robot, facilitating deposition of high numbers of layers to increase cargo loading per surface area. Next, assembled iPEMs were incubated in buffer solutions and, at indicated time points, substrates and release solutions were analyzed by spectrophotometry. These studies revealed decreasing cargo loading on substrates (**Figure 7.6D**) and corresponding increases in GpG released into the buffer solution (**Figure 7.6E**) as a function of time. Together, the results in **Figure 7.6** suggest that iPEMs can be assembled from Poly1 and GpG and break down over time

as expected. Future studies could inform the mechanism of degradation, analyzing the molecular weight and migration capacity of release solutions to explore whether GpG is released in free form or complexed with intact or degraded Poly1 fragments.

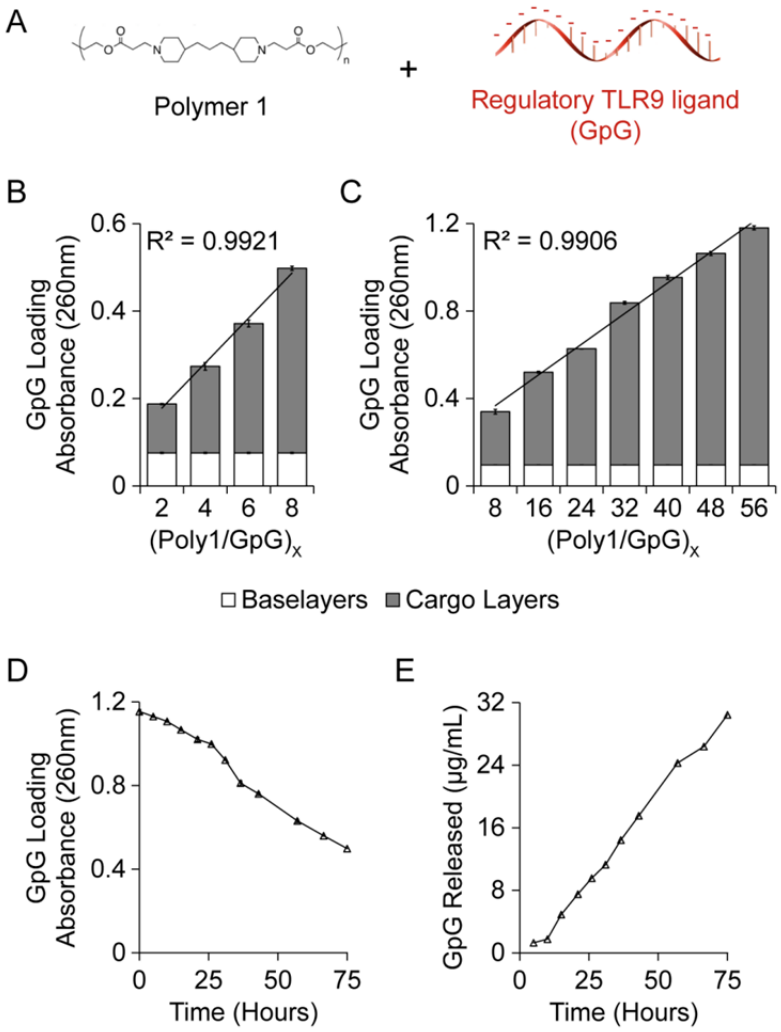

Figure 7.6 Synthesis and stability of Poly1/GpG iPEM assemblies.
A) Cargos incorporated in dissolvable iPEMs, Polymer 1 and the TLR9 antagonistic ligand, GpG. Planar quartz substrates were prepared and coated in baselayers of strong polyelectrolytes. Poly1/GpG cargo layers were then deposited on baselayer-coated substrates and layer-dependent GpG loading was monitored by UV/Vis spectrophotometry (B) every two bilayers through eight total bilayers, or (C) every eight bilayers through fifty-six total bilayers. A linear trendline was fit to the growth of GpG loading. Cargo-coated substrates were then incubated in PBS and monitored for kinetic release through 75 hours. D) Decreased GpG loading on substrates and (E) a corresponding increase in GpG loading in the release solution were observed by spectrophotometry. Data in panels (B-E) are results on a single substrate representative of at least three similiar experiments. In panels B-D, for each measurement, loading was recorded at three independent locations and averaged and data represents mean ± s.e.m..

An important question, however, was whether the released GpG maintains biologic function. Thus, release studies were repeated as above, and solutions collected at different time points were incubated with different primary cell populations *in vitro*. First, release solutions from days 1, 3, 5, and 7 of incubation were collected from iPEMs synthesized from Poly1 and either GpG or irrelevant oligonucleotide (CTRL) to isolate the effects of GpG. Release solutions were analyzed by spectrophotometry to demonstrate increased nucleic acid loading with increased release time and were then incubated with DCs isolated from naïve C57BL/6J mice and activated with soluble CpG at indicated doses (**Table 7.2**). Soluble GpG and CTRL at matched doses were also incorporated as control samples. We observed minimal effects on DC viability (**Figure 7.7A**) with all treatments, but a dramatic restraint of DC activation, as measured by the expression of CD40 (**Figure 7.7B**), CD80 (**Figure 7.7C**), and CD86 (**Figure 7.7D**), when cells were incubated with Poly1/GpG release solutions or soluble GpG, but not Poly1/CTRL release solutions or soluble CTRL.

Table 7.2 Quantification of GpG or CTRL oligonucleotides released from iPEM incubations.
Release solutions from Poly1/GpG or Poly1/CTRL iPEMs were incubated for indicated time points in preparation for *in vitro* studies. Loading of the oligonucleotides (ODNs) was quantified by UV/Vis spectrophotometry and the dose administered to cells is reported.

Day	ODN dose (μg/well)
1	1.30
3	4.13
5	8.20
7	11.30

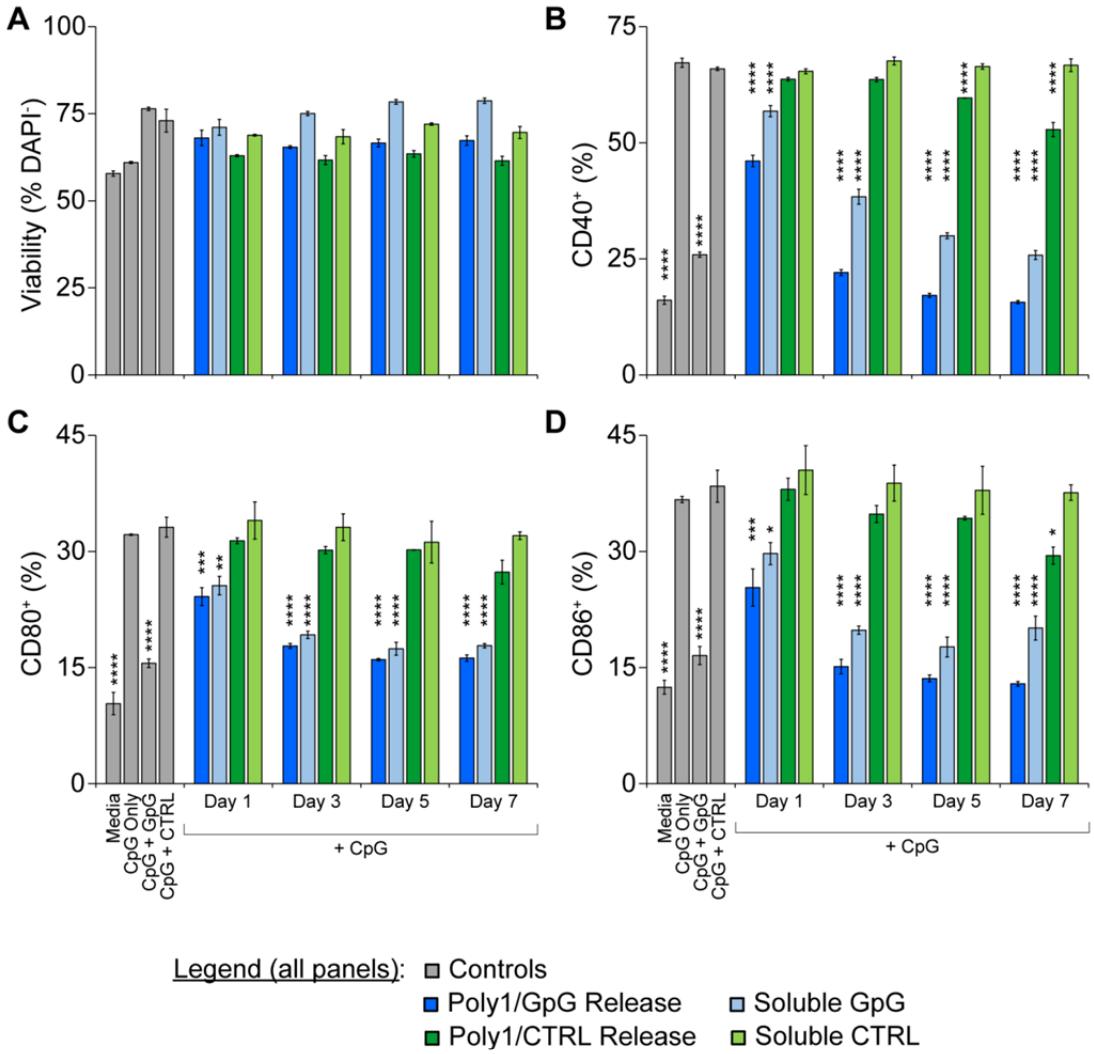

Figure 7.7 Poly1/GpG, but not Poly1/CTRL iPEM release solutions restrain activation of DCs without toxicity.
$CD11c^+$ DCs were isolated from naïve C57BL/6J mice, plated and, with the exception of media only controls, activated with soluble CpG (1 μg/well). To CpG-activated wells, soluble GpG (10 μg), soluble CTRL (10 μg), release solutions from Poly1/GpG or Poly1/CTRL iPEMs after incubation for indicated timepoints, or soluble GpG or CTRL at matched doses to each timepoint was added. Cultures were incubated for 16h and then analyzed by flow cytometry for (A) viability (i.e., $DAPI^-$), and the expression of (B) CD40, (C) CD80, and (D) CDD86. Representative results from one of three similar experiments are shown. Data represents mean ± s.e.m. for wells prepared in triplicate. Statistical comparisons in panels B-D indicate the results of one-way ANOVA comparing each treatment to the control of CpG Only. For clarity, only statistically significant differences are indicated (* = $P \leq 0.05$; ** = $P \leq 0.01$; *** = $P \leq 0.001$; **** = $P \leq 0.0001$).

To test the potential of Poly1/GpG iPEMs to polarize antigen-specific T cell function, the next step in the immune cascade, co-cultures of DCs isolated from naïve C57BL/6J mice and $CD4^+$ T cells isolated from 2D2 mice were screened, as in **Chapter 6**. In these studies, DCs were activated with soluble CpG and soluble MOG

peptide and then treated with iPEM release solutions or matched doses of soluble GpG or CTRL as in DC studies (**Table 7.2**). The degree of myelin-triggered T cell proliferation, indicated by a decreased median fluorescence intensity of the proliferation dye, CFSE, was similar across all samples treated with MOG and CpG, irrespective of the addition of release solution or soluble nucleic acid (**Figure 7.8A**). However, when the supernatants of these co-cultures were analyzed for the secretion of pro-inflammatory IL-6, a dramatic decrease in cytokine levels was observed in wells treated with soluble GpG or Poly1/GpG release solutions compared with soluble CTRL or Poly1/CTRL release solutions. Together, the results from **Figure 7.8** suggest that, similar to MOG-R_3/GpG iPEMs, release solutions from Poly1/GpG assemblies shift the function of proliferated T cells away from pro-inflammatory activity.

Overall, our current results reveal the potential for released GpG cargo to attenuate inflammation in primary cells, but we are actively studying several open questions. First, co-culture studies will be repeated to expand the cytokine profile examined and, in addition, to assess the phenotype of T cells to study whether iPEMs enhance the frequency of T_{REGS}. In addition, to verify that the molecular specificity of GpG is retained following incorporation into – and subsequent release from – iPEMs, studies will be repeated in TLR9 reporter cells, and could also be conducted in primary cells with direct analysis of TLR9 signaling levels and other downstream aspects of the pro-inflammatory cascade. Future experiments should also explore coating colloidal substrates to facilitate cell and animal studies, rather than the current release solution

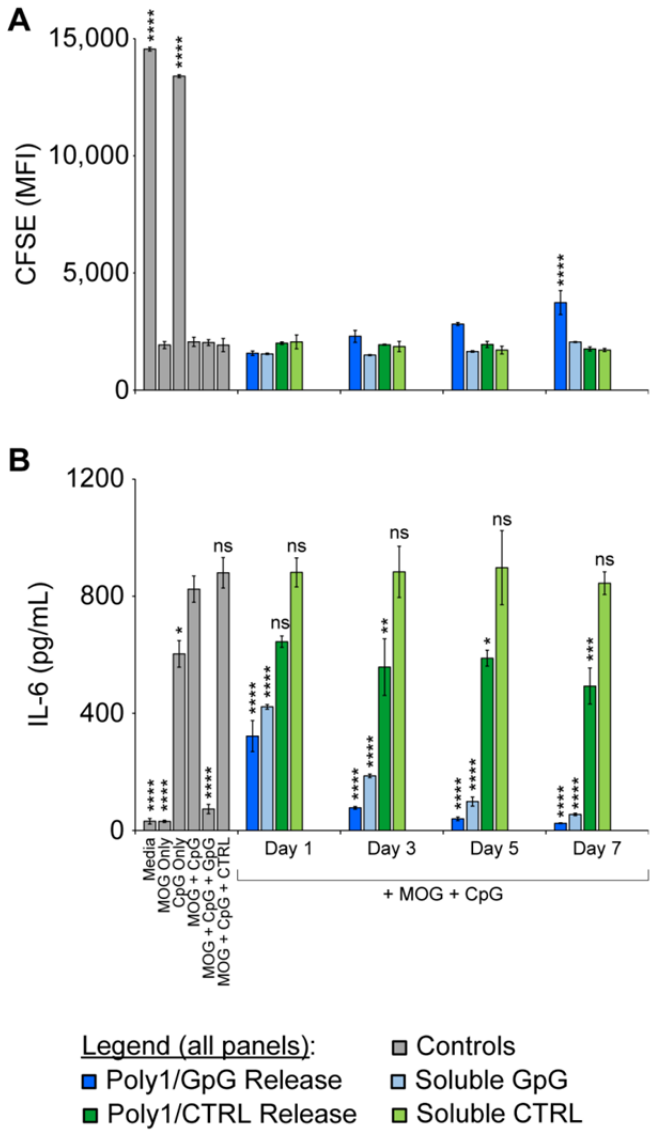

Figure 7.8 (Poly1/GpG) iPEM release solutions polarize proliferating antigen specific T cell away from inflammatory function.
A) CD11c^{+} DCs were isolated from naïve C57BL/6J mice, plated and, as above with the exception of media controls, activated with soluble MOG (0.2 μg/well) and CpG (1 μg/well). To activated wells, soluble GpG (10 μg), soluble CTRL (10 μg), release solutions from Poly1/GpG or Poly1/CTRL iPEMs after incubation for indicated timepoints, or soluble GpG or CTRL at matched doses to each timepoint was added. Additional controls of MOG only and CpG only were prepared at matched-doses to dual-activated wells. Cultures were incubated for 16 h and then CD4^{+} T cells isolated from 2D2 mice and labeled with a fluorescent proliferation dye (CFSE) were added to wells. Co-cultures were incubated for three days and then analyzed by flow cytometry for viability (i.e., DAPI^{-}), the expression of CD4, and proliferation by dilution of dye intensity corresponding to cell division (i.e., CFSE MFI). B) Supernatants from co-cultures in (A) were analyzed for the expression of IL-6 by ELISA. Data in all panels represents mean ± s.e.m. for wells prepared in triplicate. In panels (A-B), one-way ANOVA was used to compare each treatment to a control of MOG + CpG. In panel A, only significant comparisons are indicated for clarity. * = $P \leq 0.05$; ** = $P \leq 0.01$; *** = $P \leq 0.001$; **** = $P \leq 0.0001$; ns = no significant difference.

approach. A potential limitation of this approach is that there is less flexibility in the

number of bilayers we can deposit on colloidal substrates compared with the planar materials discussed above. This limitation is primarily due to observed aggregation with increased numbers of bilayers, though future troubleshooting could assist with this challenge. As proof of concept, we have demonstrated that Poly1/GpG iPEMs exhibit layer-dependent incorporation of fluorescently-tagged GpG on microparticle templates, indicated qualitatively through fixed exposure time fluorescence microscopy images (**Figure 7.9A**) and confirmed quantitatively through pixel intensity analyses (**Figure 7.9B**). Finally, future iterations could incorporate myelin peptide back into the iPEM structure, either through alternating cationic layers between Poly1 or MOG-R_3 or blending Poly1 and myelin peptide together in a single cationic cargo coating solution. This modification could confer antigen-specificity to observed restraint of inflammation for applications targeting tolerance in models of MS.

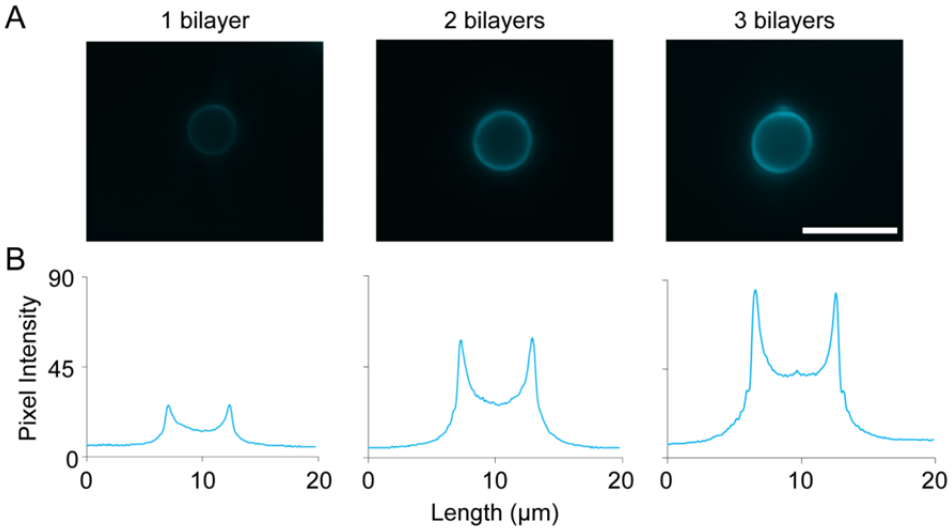

Figure 7.9 Layer-dependent incorporation of fluorescently-labeled GpG into Poly1/GpG iPEMs
Three bilayers of Poly1 and Cy5-labeled GpG were deposited on $CaCO_3$ microparticles. A) Fixed exposure fluorescence microscopy images and (B) pixel intensity analysis revealed a layer-dependent increase in GpG loading qualitatively and quantitatively, respectively. Scale bar, 10 μm.

7.4. Microneedle-mediated delivery of a clinical MS drug

In parallel to the ongoing work described above, I am also developing a strategy to deliver a clinically-approved MS drug, glatiramer acetate (brand name, Copaxone) *via* microneedles. Current treatment regimens require patients to self-administer either daily subcutaneous injections or, more recently-approved, an injection of twice the dosage three times per week. Both regimens require refrigeration of the medication and generate biological sharps from injection syringes. Further, as disease progresses, patients lose motor coordination and, eventually, function. This symptom makes it challenging or impossible for patients to self-administer *via* injection, requiring the assistance of a caretaker or medical professional to receive medication. Thus, approaches that could enhance the stability of the drug, as well as offer simple, injection-free administration routes, without sacrificing therapeutic efficacy could significantly benefit patients. These challenges could be targeted using a microneedle patch, composed of an array of micron-scale needles long enough to penetrate skin and deliver therapeutic cargos. Excitingly, these projections are not long enough to reach pain receptors, resulting in minimal pain associated with application, and can also be either coated onto polymer array templates, or designed to dissolve on application, offering the potential to eliminate biological sharps waste. This strategy, however, remains relatively unexplored in the context of autoimmunity, and efficacy in restraint of disease models has not yet been demonstrated, offering potential for a novel delivery platform to promote tolerance.

In our lab, we have previously explored microneedles coated with combinations of antigens and TLR agonists to combat cancer. My project has focused on using a delivery system with the same geometry and dimensions, but to instead deliver the clinically-approved human MS drug. Excitingly, in pilot studies in the EAE model, we have observed that application of dissolvable MNs composed of Copaxone attenuated disease severity to a similar level as that of a matched dose of the drug administered in soluble form through a typical injection route (intraperitoneal, IP) (**Figure 7.10**), while vehicle control arrays composed of mannitol exhibited no therapeutic efficacy. Ongoing studies aim to enhance drug loading in MN arrays as well as to test alternative designs (e.g., more needles per array) and, subsequently, optimize therapeutic efficacy by varying dose and treatment regimen.

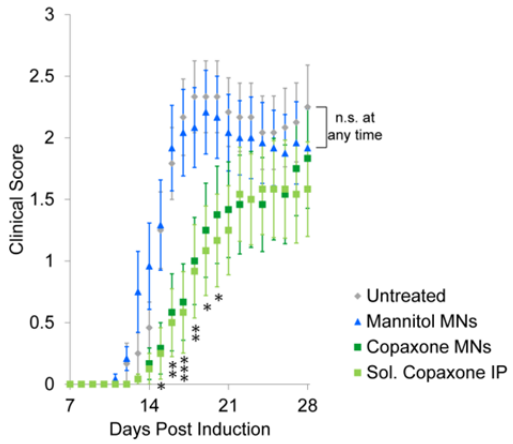

Figure 7.10 Dissolvable MNs composed of Copaxone attenuate EAE severity.
Mice were induced with EAE, randomized into groups and either left untreated, or on days 5, 10, and 15 administered a Copaxone MN array for 10 minutes to the ear, a vehicle control array (i.e., mannitol MNs) to the ear for 10 minutes, or administered a matched dose of Copaxone *via* intraperitoneal (IP) injection. Mice were then monitored for disease severity through clinical score. (For all groups, N=12). Statistical comparisons are the results of a two-way ANOVA comparing each treatment to the control of induced, untreated mice. Significant differences indicate results of untreated vs. both Copaxone groups. Mannitol MNs exhibited no significant difference throughout the study (n.s.) (* = $P \leq 0.05$; ** = $P \leq 0.01$; *** = $P \leq 0.001$).

In parallel, I have initiated studies that will allow for more fundamental or mechanistic analyses of the effects of MN-mediated delivery. Because Copaxone is a peptide-based therapy – composed of a random co-polymer of four amino acids present in myelin basic protein – I began by running control studies using the peptide epitope relevant to the mouse model, EAE (i.e., MOG). For example, I have applied MNs to mouse ears and conducted staining with Trypan blue to verify successful penetration of the skin in the expected pattern of the array (**Figure 7.11A**). In addition, I have synthesized dissolvable MNs composed of fluorescently-tagged MOG peptide (**Figure 7.11B**) using the same approach employed to generate the Copaxone MNs in **Figure 7.10**. Following application to the mouse ear for ten minutes, as in the treatment regimen used in **Figure 7.10**, fluorescent signal from the labeled MOG peptide in the pattern of the MN array could be observed by microscopy (**Figure 7.11C** left). Yet, when identically-treated ears were images one day later at the same exposure time, the fluorescent signal was no longer discretely distributed in the pattern of the MNs (**Figure 7.11C,** right). This finding motivates future studies to repeat these experiments using fluorescently tagged Copaxone, and to expand readouts to explore biodistribution of the drug. These studies could reveal whether the drug is draining through the lymphatics or interacting with different APC or other cell populations after transdermal administration. These types of studies might lead to improved understanding of the mechanism of therapeutic efficacy following MN-mediated delivery of Copaxone. Coupled with parallel experiments aimed to maximize therapeutic efficacy, our goal is for these studies to reveal an injection-free approach to effectively deliver an existing clinically-approved drug.

Our aim, supported by the use of an existing drug, is to initiate clinical trials to apply this approach to human disease on a relatively short time scale compared with that of an entirely new therapeutic approach.

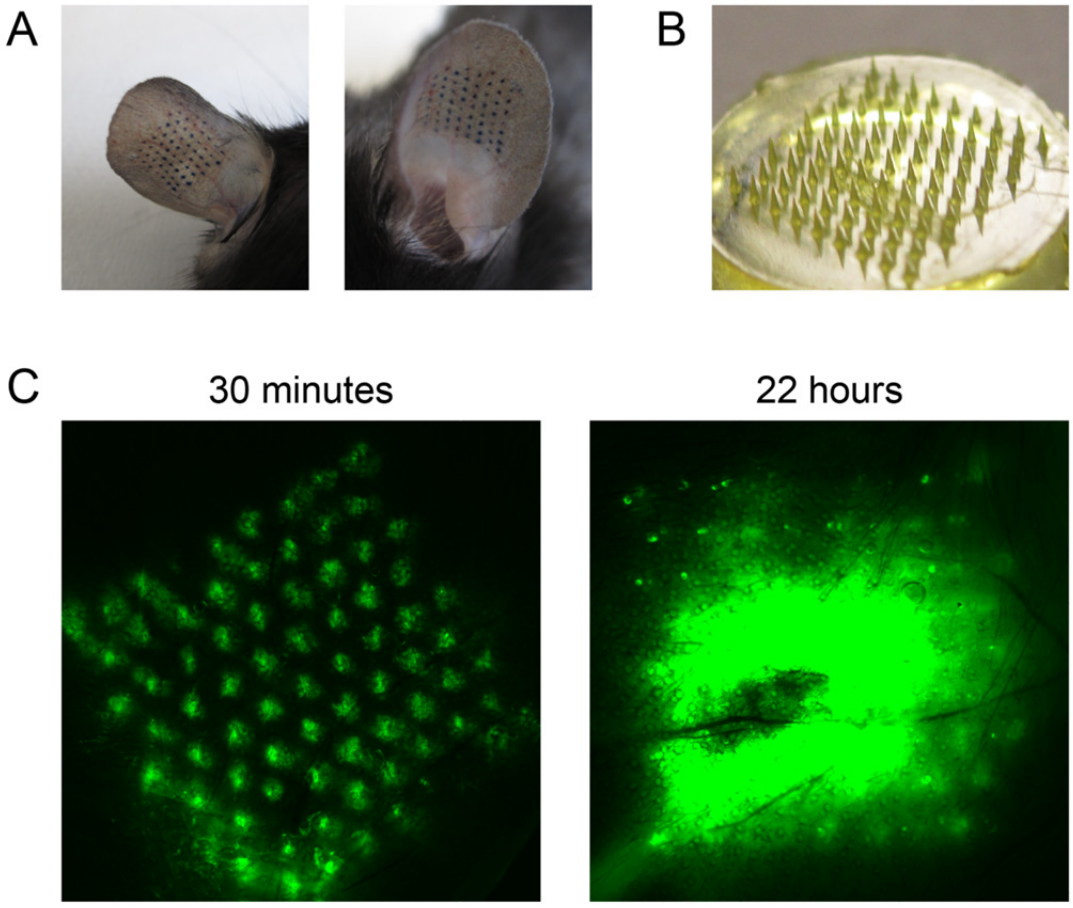

Figure 7.11 Microneedle-mediated delivery of fluorescent peptide to the skin.
A) To confirm successful penetration of skin, MNs were applied to mouse ears for 10 minutes. Mice were then euthanized and Trypan blue staining was used to confirm a compromised skin barrier in the pattern of the MN array. To confirm cargo delivery with application, dissolvable MN arrays composed of fluorescently-tagged MOG peptide were synthesized (B) and applied to ears for10 minutes as in (A). C) At indicated time points after MN application, mice were euthanized, ears were removed, briefly rinsed in PBS, and imaged by fluorescence microscopy was used to assess the delivery of cargo. Photographs in (A) and (B) and fluorescence images in (C) are representative of at least two independent experiments (i.e., two mice or two arrays).

Chapter 8. Contributions

My research has resulted in fifteen published manuscripts, including five as first-author and ten as a supporting author. Two of my first-author papers were review articles, with one focused on harnessing biomaterials to target antigen presenting cells to promote tolerance, and one centered on strategies that employ self-assembly for immunological applications. Two additional first-author papers focused on intra-lymph node delivery of biomaterials, one detailing the methods of the approach, and one describing the application of this strategy to study and promote tolerance in a mouse model of MS. My final published first-author publication involved employing self-assembly to co-deliver immune signals in carrier-free capsules, demonstrating the potential to restrain inflammation and promote tolerance in three systems: primary mouse cells, a mouse model of MS, and human MS patient samples. I also have four first-author manuscripts in preparation, centered on i) the degradable iPEMs detailed in **Section 7.3.3**, ii) a follow-up paper on the iPEM capsules described in **Chapter 6** to understand the mechanism and specificity of induced tolerance, iii) microneedle-mediated delivery of a clinical MS drug described in **Section 7.4**, and iv) an education paper describing outcomes from a mentoring and outreach program I have been involved with, described below. For the ten papers on which I am a contributing author, my roles included technical assistance in cell and animal studies as well as assistance in study design, particularly in the EAE model, and statistical analyses of data.

In addition to collaborative efforts within the lab, I have had the opportunity to work with two external labs on my projects. First, our lab partnered with the Bromberg lab at the University of Maryland School of Medicine for the work described in Aim 1. Dr. Bromberg and his team are experts in lymph nodes, particularly how these tissues remodel during immunity or tolerance, providing valuable advice, discussion, and technical skills. In particular, a postdoctoral researcher, Dr. Thomas Simon, helped us to analyze samples from mice that I had prepared, exploring treated vs. non-treated LNs, as well as a key site of disease, the spinal cord, through immunofluorescent staining and quantification of the frequency and localization of the expression of CD11c, Foxp3, and CD3e, markers of DCs, T_{REGS}, and infiltrating T cells in the CNS, respectively (**Figures 4.4, 4.6, 4.11**). In our ongoing and future work, we will continue to collaborate on studies in both mouse models of MS and models of transplantation, which I have been working with Dr. Yanbao Xiong, as described in **Section 7.2.4**. The Bromberg Lab, along with the Pierson Lab, also at the University of Maryland School of Medicine, is also an integral part of the research team working to initiate non-human primate studies this summer.

For the work described in Aim 2, our lab partnered with Dr. Walter Royal, at the University of Maryland School of Medicine and the Baltimore Department of Veterans Affairs. Through his work and role as the Associate Director for Research at the National MS Center for Excellence, Dr. Royal has gained expertise in the challenges associated with treating and designing new therapies for human MS, particularly through his involvement in several clinical trials. We partnered with a

researcher in the Royal lab, Dr. Ming Guo, who has extensive experience working with human peripheral blood mononuclear cells, to characterize how iPEMs I synthesized interact with samples from their human MS patient cohort. Pilot studies investigated metabolic activity and cytokine secretion (**Figure 6.15**) in samples from three patients. Future studies will expand to statistically-relevant groups of patients, explore other indicators of immune function (e.g., proliferation, T cell phenotype), and aim to couple findings with accompanying de-identified patient data to gain insight into the role of TLR signaling in human disease, as described in **Section 7.3.2**.

I am listed as an inventor on five intellectual property filings, one of which was a finalist for the 2014 University of Maryland Invention of the Year competition. I have presented my research at seven national and international conferences, where my submissions were recognized with awards including the Biomedical Engineering Society (BMES) Research & Design Award, the Society for Biomaterials (SFB) Student Travel Award Recognition (STAR), and the World Biomaterials Congress Trainee Award. I also received university-sponsored travel awards for conferences, including the Jacob K. Goldhaber Travel Award and the International Conference Student Support Award.

My doctoral work has been supported through the National Science Foundation, from which I was awarded three years of funding through the Graduate Research Fellowship Program (GRFP). I was recently awarded a 2017 Lemelson-MIT Graduate Student Prize, awarded to five graduate students nationally for inventions

spanning healthcare, agriculture, transportation, and consumer devices. I was also a recipient of the department's First Year Graduate Student Merit Award and received the 2015 Fischell Fellowship for my research proposal to test our biomaterials in human MS patient samples.

In terms of scientific mentoring, I have participated in programs aimed to enhance STEM exposure, including co-designing and leading workshops for over 500 local high school students. I have also directly mentored four students from Wheaton High School in year-long bioengineering projects through the Program to Enhance Participation in Research (PEPR). PEPR is an NSF-funded initiative aimed to provide exposure to research and develop skills in reading and interpreting scientific literature and presentation through a poster session at the end of the year. Outcomes from the PEPR program are the focus of one of my first-author manuscripts in preparation. Within the university, I served as a teaching assistant for two semesters and have mentored three undergraduate- and two graduate-level researchers in our lab. In particular, I have worked with one undergraduate student, Boyan Xia, for nearly four years. Boyan was awarded a Howard Hughes Medical Institute Undergraduate Fellowship ($7,000 award) for her research proposal and was selected to present her results in an oral presentation at the 2016 annual meeting of the Biomedical Engineering Society. With input from Dr. Jewell, we have a plan to publish a paper in the coming year, based on the data in **Section 7.3.3**, in which Boyan will assume an integral role.

In terms of contribution to the field, my research applying intra-lymph node delivery of biomaterials to a mouse model of MS represents the first application of this technique to combat autoimmune disease. While this strategy could enable new therapeutic strategies, the approach also offers potential as a platform technology or tool to enable the study of systemic, antigen-specific immune tolerance as a function of the local signaling environment in discrete lymph nodes. Our research team's current progress has catalyzed mechanistic studies, collaborative efforts to test this idea in models of transplant – including non-human primate trials beginning this summer – expansion to investigate this strategy in type 1 diabetes and other models of MS, and motivates more fundamental studies that could inform understanding of the development of tolerance. My work adapting the iPEM platform to deliver myelin self-antigen and a regulatory TLR9 ligand, GpG, is the first application of polyelectrolyte multilayers aimed to promote immunological tolerance. Further, targeting TLRs in autoimmunity, particularly incorporating biomaterials with TLR targeting, remains relatively unexplored. Thus, this approach could support new therapeutic strategies to combat self-reactivity, while eliminating synthetic carrier components that complicate design and may exacerbate disease, as well as offer potential to study the role of TLR signaling in human disease through continued, expanded study of samples from human MS patients.

Appendix A: List of Publications

PUBLISHED FIRST AUTHOR (* indicates equal contributions)

1. **L. H. Tostanoski**, and C. M. Jewell, "Engineering self-assembled materials to study and direct immune function." *Advanced Drug Delivery Reviews* **2017** (*In press*).
   ***Featured as part of Immuno-Engineering special issue

2. **L. H. Tostanoski**, Y. C. Chiu, J. I. Andorko, M. Guo, X. Zeng, P. Zhang, W. Royal III, and C. M. Jewell, "Design of polyelectrolyte multilayers to promote immunological tolerance." *ACS Nano* **2016**, 10, 9334-9345.
   ***Featured in American Chemical Society's C&E News online (Link) and in print
   ***Featured in Controlled Release Society newsletter

3. **L. H. Tostanoski**, Y. C. Chiu, J. M. Gammon, T. Simon, J. I. Andorko, J. S. Bromberg, and C. M. Jewell, "Reprogramming the local lymph node microenvironment promotes systemic antigen-specific tolerance." *Cell Reports* **2016**, 16, 2940-2952.
   ***Featured on *Cell* Press Blog (Link)
   ***Featured in American Chemical Society Press Conference (Link)

4. **L. H. Tostanoski**, E. A. Gosselin, and C. M. Jewell, "Engineering tolerance using biomaterials to target and control antigen presenting cells." *Discovery Medicine* **2016**, 21, 403-410.

5. J. I. Andorko*, **L. H. Tostanoski***, E. Solano, M. Mukhamedova, and C. M. Jewell, "Intra-lymph node injection of biodegradable polymer particles." *Journal of Visual Experiments* **2014**, 83, e50984.

PUBLISHED CO-AUTHOR (* indicates equal contributions)

6. J. M. Gammon, E. A. Gosselin, **L. H. Tostanoski**, Y. C. Chiu, X. Zeng, Q. Zeng, and C. M. Jewell, "Low-dose controlled release of mTOR inhibitors maintains T cell plasticity and enhances T cell expansion." *Journal of Controlled Release* **2017** (*In press*).
   ***Featured as part of NanoDDS 2016 special issue

7. E. A. Gosselin, **L. H. Tostanoski**, and C. M. Jewell, "Controlled release of second generation mTOR inhibitors to restrain inflammation in primary immune cells." *The American Association of Pharmaceutical Scientists (AAPS) Journal* **2017**, 19, 1175-1185.

8. K. L. Hess, E. Oh, **L. H. Tostanoski**, J. I. Andorko, K. Susumu, J. R. Deschamps, I. L. Medintz, and C. M. Jewell, "Engineering immunological tolerance using

quantum dots to tune the density of self-antigen display." *Advanced Functional Materials* **2017**, 27, 1700290. (*front cover article*)

9. Q. Zeng, J. M. Gammon, **L. H. Tostanoski**, Y. C. Chiu, and C. M. Jewell, "*In vivo* expansion of melanoma-specific T cells using microneedle arrays coated with immune-polyelectrolyte multilayers." *ACS Biomaterials Science & Engineering* **2017**, 3, 195-205.
   ***Featured on cover and highlighted in editorial (Link)

10. K. L. Hess, J. I. Andorko, **L. H. Tostanoski**, and C. M. Jewell, "Polyplexes assembled from self-peptides and regulatory nucleic acids blunt toll-like receptor signaling to combat autoimmunity." *Biomaterials* **2017**, 118, 51-62.

11. J. I. Andorko*, J. M. Gammon*, **L. H. Tostanoski**, Q. Zeng, and C. M. Jewell, "Targeted programming of the lymph node environment causes evolution of local and systemic immunity." *Cellular and Molecular Bioengineering* **2016**, 9, 418-432.
   ***Featured as part of Young Innovators special issue

12. Y. C. Chiu, J. M. Gammon, J. I. Andorko, **L. H. Tostanoski**, and C. M. Jewell, "Assembly and immunological processing of polyelectrolyte multilayers composed of antigens and adjuvants." *ACS Applied Materials and Interfaces* **2016**, 8, 18722-18731.

13. Y. C. Chiu, J. M. Gammon, J. I. Andorko, **L. H. Tostanoski**, and C. M. Jewell, "Modular vaccine design using carrier-free multilayer capsules assembled from polyionic immune signals." *ACS Biomaterials Science & Engineering* **2015**, 1, 1200-1205. (*cover article*)

14. J. M. Gammon, **L. H. Tostanoski**, A. R. Adapa, Y. C. Chiu, and C. M. Jewell, "Controlled delivery of a metabolic modulator promotes regulatory T cells and restrains autoimmunity." *Journal of Controlled Release* **2015**, 210, 169-178.

15. P. Zhang, Y. C. Chiu, **L. H. Tostanoski**, and C. M. Jewell, "Polyelectrolyte multilayers assembled entirely from immune signals on gold nanoparticle templates promote antigen-specific T cell response." *ACS Nano* **2015**, 9, 6465-6477.

IN PROGRESS

16. P. Zhang, Q. Zeng, X. Zeng, **L. H. Tostanoski**, and C. M. Jewell, "Advanced manufacturing of microdisk vaccines for uniform control of material properties and immune cell function." **2017** (*In revision*).

Appendix B: List of Intellectual Property Filings

1. "Local engineering of the lymph node environment to promote immune tolerance." C. M. Jewell, J. I. Andorko, **L. H. Tostanoski**. U.S. Patent No. 9,610,349; Issued April 4, **2017**.

2. "Direct intra-lymph node delivery of biomaterials to promote transplant tolerance." C. M. Jewell, **L. H. Tostanoski**, J. S. Bromberg. U.S. Patent Application No. 62/480,870; Filed April 3, **2017**.

3. "Microneedle-mediated delivery of tolerogenic immunotherapeutics." C. M. Jewell, **L. H. Tostanoski**, E. A. Gosselin. U.S. Patent Application No. 62/471,807; Filed March 15, **2017**.

4. "Reprogramming the local lymph node microenviroment promotes tolerance that is systemic and antigen specific." C. M. Jewell, **L. H. Tostanoski**. U.S. Patent Application No. 62/385,750; Filed September 9, **2016**.

5. "Polyelectrolyte multilayers assembled from immune signal compounds." C. M. Jewell, **L. H. Tostanoski**, Y. Chiu. Patent Application No. PCT/US16/18002; Filed February 16, **2016**.

References

[1] S.N. Mueller, R.N. Germain, Stromal cell contributions to the homeostasis and functionality of the immune system, Nat Rev Immunol, 9 (2009) 618-629.

[2] B.D. Pereira, C. Fraefel, Novel Immunotherapeutic Approaches in Targeting Dendritic Cells with Virus Vectors, Discov Med, 20 (2015) 111-119.

[3] A.E. Morelli, A.W. Thomson, Tolerogenic dendritic cells and the quest for transplant tolerance, Nat Rev Immunol, 7 (2007) 610-621.

[4] J.I. Andorko, K.L. Hess, C.M. Jewell, Harnessing biomaterials to engineer the lymph node microenvironment for immunity or tolerance, AAPS J, 17 (2015) 323-338.

[5] R.A. Maldonado, U.H. von Andrian, How Tolerogenic Dendritic Cells Induce Regulatory T Cells, Adv Immunol, 108 (2010) 111-165.

[6] S. Manicassamy, B. Pulendran, Dendritic cell control of tolerogenic responses, Immunol Rev, 241 (2011) 206-227.

[7] P. Soroosh, T.A. Doherty, W. Duan, A.K. Mehta, H. Choi, Y.F. Adams, Z. Mikulski, N. Khorram, P. Rosenthal, D.H. Broide, M. Croft, Lung-resident tissue macrophages generate Foxp3+ regulatory T cells and promote airway tolerance, J Exp Med, 210 (2013) 775-788.

[8] F. Osorio, C. Fuentes, M.N. Lopez, F. Salazar-Onfray, F.E. Gonzalez, Role of Dendritic Cells in the Induction of Lymphocyte Tolerance, Front Immunol, 6 (2015) 535.

[9] R.J. Salmond, R. Zamoyska, The influence of mTOR on T helper cell differentiation and dendritic cell function, Eur J Immunol, 41 (2011) 2137-2141.

[10] T. Taner, H. Hackstein, Z. Wang, A.E. Morelli, A.W. Thomson, Rapamycin-treated, alloantigen-pulsed host dendritic cells induce ag-specific T cell regulation and prolong graft survival, Am J Transplant, 5 (2005) 228-236.

[11] A.W. Thomson, H.R. Turnquist, G. Raimondi, Immunoregulatory functions of mTOR inhibition, Nat Rev Immunol, 9 (2009) 324-337.

[12] S.A. Chalmers, V. Chitu, M. Ramanujam, C. Putterman, Therapeutic targeting of macrophages in lupus nephritis, Discov Med, 20 (2015) 43-49.

[13] A. Louveau, I. Smirnov, T.J. Keyes, J.D. Eccles, S.J. Rouhani, J.D. Peske, N.C. Derecki, D. Castle, J.W. Mandell, K.S. Lee, T.H. Harris, J. Kipnis, Structural and functional features of central nervous system lymphatic vessels, Nature, 523 (2015) 337-341.

[14] A. Aspelund, S. Antila, S.T. Proulx, T.V. Karlsen, S. Karaman, M. Detmar, H. Wiig, K. Alitalo, A dural lymphatic vascular system that drains brain interstitial fluid and macromolecules, J Exp Med, 212 (2015) 991-999.

[15] K. Mankia, P. Emery, Is Localized Autoimmunity the Trigger for Rheumatoid Arthritis? Unravelling New Targets for Prevention, Discov Med, 109 (2015) 129-135.

[16] A. Singh, N.A. Peppas, Hydrogels and scaffolds for immunomodulation, Adv Mater, 26 (2014) 6530-6541.

[17] K. Shao, S. Singha, X. Clemente-Casares, S. Tsai, Y. Yang, P. Santamaria, Nanoparticle-based immunotherapy for cancer, ACS Nano, 9 (2015) 16-30.

[18] C.H. Jones, A. Hill, M. Chen, B.A. Pfeifer, Contemporary approaches for nonviral gene therapy, Discov Med, 19 (2015) 447-454.

[19] D.J. Irvine, M.A. Swartz, G.L. Szeto, Engineering synthetic vaccines using cues from natural immunity, Nat Mater, 12 (2013) 978-990.

[20] S.T. Reddy, A.J. van der Vlies, E. Simeoni, V. Angeli, G.J. Randolph, C.P. O'Neil, L.K. Lee, M.A. Swartz, J.A. Hubbell, Exploiting lymphatic transport and complement activation in nanoparticle vaccines, Nat Biotechnol, 25 (2007) 1159-1164.

[21] J.C. Sunshine, K. Perica, J.P. Schneck, J.J. Green, Particle shape dependence of CD8+ T cell activation by artificial antigen presenting cells, Biomaterials, 35 (2014) 269-277.

[22] C. Foged, B. Brodin, S. Frokjaer, A. Sundblad, Particle size and surface charge affect particle uptake by human dendritic cells in an in vitro model, Int J Pharm, 298 (2005) 315-322.

[23] J.C. Sunshine, J.J. Green, Nanoengineering approaches to the design of artificial antigen-presenting cells, Nanomedicine (Lond), 8 (2013) 1173-1189.

[24] C.L. van Broekhoven, C.R. Parish, C. Demangel, W.J. Britton, J.G. Altin, Targeting dendritic cells with antigen-containing liposomes: a highly effective

procedure for induction of antitumor immunity and for tumor immunotherapy, Cancer Res, 64 (2004) 4357-4365.

[25] Y.J. Kwon, E. James, N. Shastri, J.M. Frechet, In vivo targeting of dendritic cells for activation of cellular immunity using vaccine carriers based on pH-responsive microparticles, Proc Natl Acad Sci U S A, 102 (2005) 18264-18268.

[26] H. Liu, K.D. Moynihan, Y. Zheng, G.L. Szeto, A.V. Li, B. Huang, D.S. Van Egeren, C. Park, D.J. Irvine, Structure-based programming of lymph-node targeting in molecular vaccines, Nature, 507 (2014) 519-522.

[27] C.M. Jewell, S.C. Lopez, D.J. Irvine, In situ engineering of the lymph node microenvironment via intranodal injection of adjuvant-releasing polymer particles, Proc Natl Acad Sci U S A, 108 (2011) 15745-15750.

[28] F.A. Sharp, D. Ruane, B. Claass, E. Creagh, J. Harris, P. Malyala, M. Singh, D.T. O'Hagan, V. Petrilli, J. Tschopp, L.A. O'Neill, E.C. Lavelle, Uptake of particulate vaccine adjuvants by dendritic cells activates the NALP3 inflammasome, Proc Natl Acad Sci U S A, 106 (2009) 870-875.

[29] J.I. Andorko, K.L. Hess, K.G. Pineault, C.M. Jewell, Intrinsic immunogenicity of rapidly-degradable polymers evolves during degradation, Acta Biomater, 32 (2016) 24-34.

[30] J.S. Lewis, T.D. Zaveri, C.P. Crooks, 2nd, B.G. Keselowsky, Microparticle surface modifications targeting dendritic cells for non-activating applications, Biomaterials, 33 (2012) 7221-7232.

[31] G.A. Hudalla, T. Sun, J.Z. Gasiorowski, H. Han, Y.F. Tian, A.S. Chong, J.H. Collier, Gradated assembly of multiple proteins into supramolecular nanomaterials, Nat Mater, 13 (2014) 829-836.

[32] P. Zhang, Y.C. Chiu, L.H. Tostanoski, C.M. Jewell, Polyelectrolyte Multilayers Assembled Entirely from Immune Signals on Gold Nanoparticle Templates Promote Antigen-Specific T Cell Response, ACS Nano, 9 (2015) 6465-6477.

[33] Y.C. Chiu, J.M. Gammon, J.I. Andorko, L.H. Tostanoski, C.M. Jewell, Modular Vaccine Design Using Carrier-Free Capsules Assembled from Polyionic Immune Signals, ACS Biomater Sci Eng, 1 (2015) 1200-1205.

[34] L. Northrup, M.A. Christopher, B.P. Sullivan, C. Berkland, Combining antigen and immunomodulators: Emerging trends in antigen-specific immunotherapy for autoimmunity, Adv Drug Deliv Rev, 98 (2016) 86-98.

[35] K.A. Hlavaty, X. Luo, L.D. Shea, S.D. Miller, Cellular and molecular targeting for nanotherapeutics in transplantation tolerance, Clin Immunol, 160 (2015) 14-23.

[36] S. Tsai, A. Shameli, J. Yamanouchi, X. Clemente-Casares, J. Wang, P. Serra, Y. Yang, Z. Medarova, A. Moore, P. Santamaria, Reversal of autoimmunity by boosting memory-like autoregulatory T cells, Immunity, 32 (2010) 568-580.

[37] A. Lutterotti, R. Martin, Antigen-specific tolerization approaches in multiple sclerosis, Expert Opin Inv Drugs, 23 (2014) 9-20.

[38] J.A. Bluestone, H. Bour-Jordan, M. Cheng, M. Anderson, T cells in the control of organ-specific autoimmunity, J Clin Invest, 125 (2015) 2250-2260.

[39] D.R. Getts, A.J. Martin, D.P. McCarthy, R.L. Terry, Z.N. Hunter, W.T. Yap, M.T. Getts, M. Pleiss, X. Luo, N.J. King, L.D. Shea, S.D. Miller, Microparticles bearing encephalitogenic peptides induce T-cell tolerance and ameliorate experimental autoimmune encephalomyelitis, Nat Biotechnol, 30 (2012) 1217-1224.

[40] Z. Hunter, D.P. McCarthy, W.T. Yap, C.T. Harp, D.R. Getts, L.D. Shea, S.D. Miller, A biodegradable nanoparticle platform for the induction of antigen-specific immune tolerance for treatment of autoimmune disease, ACS Nano, 8 (2014) 2148-2160.

[41] J. Bryant, K.A. Hlavaty, X. Zhang, W.T. Yap, L. Zhang, L.D. Shea, X. Luo, Nanoparticle delivery of donor antigens for transplant tolerance in allogeneic islet transplantation, Biomaterials, 35 (2014) 8887-8894.

[42] T.S. Griffith, T.A. Ferguson, Cell death in the maintenance and abrogation of tolerance: the five Ws of dying cells, Immunity, 35 (2011) 456-466.

[43] S. Kontos, I.C. Kourtis, K.Y. Dane, J.A. Hubbell, Engineering antigens for in situ erythrocyte binding induces T-cell deletion, Proc Natl Acad Sci U S A, 110 (2013) E60-68.

[44] A.J. Grimm, S. Kontos, G. Diaceri, X. Quaglia-Thermes, J.A. Hubbell, Memory of tolerance and induction of regulatory T cells by erythrocyte-targeted antigens, Sci Rep, 5 (2015) 15907.

[45] D.R. Getts, R.L. Terry, M.T. Getts, C. Deffrasnes, M. Muller, C. van Vreden, T.M. Ashhurst, B. Chami, D. McCarthy, H. Wu, J. Ma, A. Martin, L.D. Shae, P. Witting, G.S. Kansas, J. Kuhn, W. Hafezi, I.L. Campbell, D. Reilly, J. Say, L. Brown, M.Y. White, S.J. Cordwell, S.J. Chadban, E.B. Thorp, S. Bao, S.D. Miller, N.J. King, Therapeutic inflammatory monocyte modulation using immune-modifying microparticles, Sci Transl Med, 6 (2014) 219ra217.

[46] L. Northrup, J.O. Sestak, B.P. Sullivan, S. Thati, B.L. Hartwell, T.J. Siahaan, C.M. Vines, C. Berkland, Co-delivery of autoantigen and b7 pathway modulators suppresses experimental autoimmune encephalomyelitis, AAPS J, 16 (2014) 1204-1213.

[47] R.A. Maldonado, R.A. LaMothe, J.D. Ferrari, A.H. Zhang, R.J. Rossi, P.N. Kolte, A.P. Griset, C. O'Neil, D.H. Altreuter, E. Browning, L. Johnston, O.C. Farokhzad, R. Langer, D.W. Scott, U.H. von Andrian, T.K. Kishimoto, Polymeric synthetic nanoparticles for the induction of antigen-specific immunological tolerance, Proc Natl Acad Sci U S A, 112 (2015) E156-165.

[48] S. Jhunjhunwala, G. Raimondi, A.W. Thomson, S.R. Little, Delivery of rapamycin to dendritic cells using degradable microparticles, J Control Release, 133 (2009) 191-197.

[49] K.Y. Dane, C. Nembrini, A.A. Tomei, J.K. Eby, C.P. O'Neil, D. Velluto, M.A. Swartz, L. Inverardi, J.A. Hubbell, Nano-sized drug-loaded micelles deliver payload to lymph node immune cells and prolong allograft survival, J Control Release, 156 (2011) 154-160.

[50] K.J. Peine, M. Guerau-de-Arellano, P. Lee, N. Kanthamneni, M. Severin, G.D. Probst, H. Peng, Y. Yang, Z. Vangundy, T.L. Papenfuss, A.E. Lovett-Racke, E.M. Bachelder, K.M. Ainslie, Treatment of experimental autoimmune encephalomyelitis by codelivery of disease associated Peptide and dexamethasone in acetalated dextran microparticles, Mol Pharm, 11 (2014) 828-835.

[51] A.C. Shirali, M. Look, W. Du, E. Kassis, H.W. Stout-Delgado, T.M. Fahmy, D.R. Goldstein, Nanoparticle delivery of mycophenolic acid upregulates PD-L1 on dendritic cells to prolong murine allograft survival, Am J Transplant, 11 (2011) 2582-2592.

[52] M. Look, E. Stern, Q.A. Wang, L.D. DiPlacido, M. Kashgarian, J. Craft, T.M. Fahmy, Nanogel-based delivery of mycophenolic acid ameliorates systemic lupus erythematosus in mice, J Clin Invest, 123 (2013) 1741-1749.

[53] J.S. Lewis, N.V. Dolgova, Y. Zhang, C.Q. Xia, C.H. Wasserfall, M.A. Atkinson, M.J. Clare-Salzler, B.G. Keselowsky, A combination dual-sized microparticle system modulates dendritic cells and prevents type 1 diabetes in prediabetic NOD mice, Clin Immunol, 160 (2015) 90-102.

[54] J.M. Gammon, L.H. Tostanoski, A.R. Adapa, Y.C. Chiu, C.M. Jewell, Controlled delivery of a metabolic modulator promotes regulatory T cells and restrains autoimmunity, J Control Release, 210 (2015) 169-178.

[55] C. Wang, N. Yosef, J. Gaublomme, C. Wu, Y. Lee, C.B. Clish, J. Kaminski, S. Xiao, G. Meyer Zu Horste, M. Pawlak, Y. Kishi, N. Joller, K. Karwacz, C. Zhu, M. Ordovas-Montanes, A. Madi, I. Wortman, T. Miyazaki, R.A. Sobel, H. Park, A. Regev, V.K. Kuchroo, CD5L/AIM Regulates Lipid Biosynthesis and Restrains Th17 Cell Pathogenicity, Cell, 163 (2015) 1413-1427.

[56] M.D. Buck, D. O'Sullivan, E.L. Pearce, T cell metabolism drives immunity, J Exp Med, 212 (2015) 1345-1360.

[57] M.A. Swartz, S. Hirosue, J.A. Hubbell, Engineering approaches to immunotherapy, Sci Transl Med, 4 (2012) 148rv149.

[58] M. Adamina, R. Rosenthal, W.P. Weber, D.M. Frey, C.T. Viehl, M. Bolli, R.W. Huegli, A.L. Jacob, M. Heberer, D. Oertli, W. Marti, G.C. Spagnoli, P. Zajac, Intranodal immunization with a vaccinia virus encoding multiple antigenic epitopes and costimulatory molecules in metastatic melanoma, Mol Ther, 18 (2010) 651-659.

[59] A. Ribas, J.S. Weber, B. Chmielowski, B. Comin-Anduix, D. Lu, M. Douek, N. Ragavendra, S. Raman, E. Seja, D. Rosario, S. Miles, D.C. Diamond, Z. Qiu, M. Obrocea, A. Bot, Intra-lymph node prime-boost vaccination against Melan A and tyrosinase for the treatment of metastatic melanoma: results of a phase 1 clinical trial, Clin Cancer Res, 17 (2011) 2987-2996.

[60] G. Senti, B.M. Prinz Vavricka, I. Erdmann, M.I. Diaz, R. Markus, S.J. McCormack, J.J. Simard, B. Wuthrich, R. Crameri, N. Graf, P. Johansen, T.M. Kundig, Intralymphatic allergen administration renders specific immunotherapy faster and safer: a randomized controlled trial, Proc Natl Acad Sci U S A, 105 (2008) 17908-17912.

[61] P. Johansen, T. Storni, L. Rettig, Z. Qiu, A. Der-Sarkissian, K.A. Smith, V. Manolova, K.S. Lang, G. Senti, B. Mullhaupt, T. Gerlach, R.F. Speck, A. Bot,

T.M. Kundig, Antigen kinetics determines immune reactivity, Proc Natl Acad Sci U S A, 105 (2008) 5189-5194.

[62] G.J. Randolph, V. Angeli, M.A. Swartz, Dendritic-cell trafficking to lymph nodes through lymphatic vessels, Nat Rev Immunol, 5 (2005) 617-628.

[63] D.J. Irvine, C.M. Jewell, Vaccine and Immunotherapy Delivery, in: P. Ducheyne, K. Healy, D.E. Hutmacher, D.W. Garinger, C.J. Kirkpatrick (Eds.) Comprehensive Biomaterials 2011.

[64] J.J. Moon, B. Huang, D.J. Irvine, Engineering nano- and microparticles to tune immunity, Adv Mater, 24 (2012) 3724-3746.

[65] S.T. Reddy, A.J. van der Vlies, E. Simeoni, C.P. O'neil, M.A. Swartz, J.A. Hubbell, Exploiting lymphatic transport and complement activation in nanoparticle vaccines, Tissue Eng Pt A, 14 (2008) 734-735.

[66] A. Bershteyn, J. Chaparro, R. Yau, M. Kim, E. Reinherz, L. Ferreira-Moita, D.J. Irvine, Polymer-supported lipid shells, onions, and flowers, Soft matter, 4 (2008) 1787-1791.

[67] P. Johansen, A.C. Haffner, F. Koch, K. Zepter, I. Erdmann, K. Maloy, J.J. Simard, T. Storni, G. Senti, A. Bot, B. Wuthrich, T.M. Kundig, Direct intralymphatic injection of peptide vaccines enhances immunogenicity, Eur J Immunol, 35 (2005) 568-574.

[68] D. Mohanan, B. Slutter, M. Henriksen-Lacey, W. Jiskoot, J.A. Bouwstra, Y. Perrie, T.M. Kundig, B. Gander, P. Johansen, Administration routes affect the quality of immune responses: A cross-sectional evaluation of particulate antigen-delivery systems, J Control Release, 147 (2010) 342-349.

[69] M.I. Harrell, B.M. Iritani, A. Ruddell, Lymph node mapping in the mouse, J Immunol Methods, 332 (2008) 170-174.

[70] H. He, A.N. Courtney, E. Wieder, K.J. Sastry, Multicolor flow cytometry analyses of cellular immune response in rhesus macaques, J Vis Exp, (2010) e1743.

[71] M.P. Matheu, I. Parker, M.D. Cahalan, Dissection and 2-photon imaging of peripheral lymph nodes in mice, J Vis Exp, (2007) 265.

[72] H. Salmon, A. Rivas-Caicedo, F. Asperti-Boursin, C. Lebugle, P. Bourdoncle, E. Donnadieu, Ex vivo imaging of T cells in murine lymph node slices with widefield and confocal microscopes, J Vis Exp, (2011) e3054.

[73] J.G. Donaldson, Immunofluorescence Staining, Current Protocols in Immunology: Immunofluorescence Staining, John Wiley & Sons, Inc. 2001.

[74] F. Hofman, Immunohistochemistry, Current Protocols in Immunology: Immunohistochemistry, John Wiley & Sons, Inc. 2001.

[75] K. Holmes, L.M. Lantz, B.J. Fowlkes, I. Schmid, J.V. Giorgi, Preparation of Cells and Reagents for Flow Cytometry, Current Protocols in Immunology: Preparation of Cells and Reagents for Flow Cytometry, John Wiley & Sons, Inc. 2001.

[76] S.O. Sharrow, Overview of Flow Cytometry, Current Protocols in Immunology: Overview of Flow Cytometry, John Wiley & Sons, Inc. 2001.

[77] S.O. Sharrow, Analysis of Flow Cytometry Data, Current Protocols in Immunology: Analysis of Flow Cytometry Data, John Wiley & Sons, Inc. 2001.

[78] J.M. Anderson, M.S. Shive, Biodegradation and biocompatibility of PLA and PLGA microspheres, Adv Drug Deliv Rev, 28 (1997) 5-24.

[79] F. Danhier, E. Ansorena, J.M. Silva, R. Coco, A. Le Breton, V. Preat, PLGA-based nanoparticles: an overview of biomedical applications, J Control Release, 161 (2012) 505-522.

[80] M. Comabella, S.J. Khoury, Immunopathogenesis of multiple sclerosis, Clin Immunol, 142 (2012) 2-8.

[81] C.A. Dendrou, L. Fugger, M.A. Friese, Immunopathology of multiple sclerosis, Nat Rev Immunol, 15 (2015) 545-558.

[82] F. Piehl, A changing treatment landscape for multiple sclerosis: challenges and opportunities, J Intern Med, 275 (2014) 364-381.

[83] L. Steinman, J.T. Merrill, I.B. McInnes, M. Peakman, Optimization of current and future therapy for autoimmune diseases, Nat Med, 18 (2012) 59-65.

[84] M. Esposito, F. Ruffini, M. Bellone, N. Gagliani, M. Battaglia, G. Martino, R. Furlan, Rapamycin inhibits relapsing experimental autoimmune

encephalomyelitis by both effector and regulatory T cells modulation, J Neuroimmunol, 220 (2010) 52-63.

[85] P.P. Ho, P. Fontoura, M. Platten, R.A. Sobel, J.J. DeVoss, L.Y. Lee, B.A. Kidd, B.H. Tomooka, J. Capers, A. Agrawal, R. Gupta, J. Zernik, M.K. Yee, B.J. Lee, H. Garren, W.H. Robinson, L. Steinman, A suppressive oligodeoxynucleotide enhances the efficacy of myelin cocktail/IL-4-tolerizing DNA vaccination and treats autoimmune disease, J Immunol, 175 (2005) 6226-6234.

[86] A. Yeste, M. Nadeau, E.J. Burns, H.L. Weiner, F.J. Quintana, Nanoparticle-mediated codelivery of myelin antigen and a tolerogenic small molecule suppresses experimental autoimmune encephalomyelitis, Proc Natl Acad Sci U S A, 109 (2012) 11270-11275.

[87] X. Clemente-Casares, J. Blanco, P. Ambalavanan, J. Yamanouchi, S. Singha, C. Fandos, S. Tsai, J. Wang, N. Garabatos, C. Izquierdo, S. Agrawal, M.B. Keough, V.W. Yong, E. James, A. Moore, Y. Yang, T. Stratmann, P. Serra, P. Santamaria, Expanding antigen-specific regulatory networks to treat autoimmunity, Nature, 530 (2016) 434-440.

[88] A.H. Cross, R.T. Naismith, Established and novel disease-modifying treatments in multiple sclerosis, J Intern Med, 275 (2014) 350-363.

[89] J.I. Andorko, L.H. Tostanoski, E. Solano, M. Mukhamedova, C.M. Jewell, Intra-lymph node injection of biodegradable polymer particles, J Vis Exp, (2014) e50984.

[90] H. Sah, A new strategy to determine the actual protein content of poly(lactide-co-glycolide) microspheres, J Pharm Sci, 86 (1997) 1315-1318.

[91] K.J. Warren, D. Iwami, D.G. Harris, J.S. Bromberg, B.E. Burrell, Laminins affect T cell trafficking and allograft fate, J Clin Invest, 124 (2014) 2204-2218.

[92] T. Korn, J. Reddy, W. Gao, E. Bettelli, A. Awasthi, T.R. Petersen, B.T. Backstrom, R.A. Sobel, K.W. Wucherpfennig, T.B. Strom, M. Oukka, V.K. Kuchroo, Myelin-specific regulatory T cells accumulate in the CNS but fail to control autoimmune inflammation, Nat Med, 13 (2007) 423-431.

[93] M. van Zwam, R. Huizinga, M.J. Melief, A.F. Wierenga-Wolf, M. van Meurs, J.S. Voerman, K.P. Biber, H.W. Boddeke, U.E. Hopken, C. Meisel, A. Meisel, I. Bechmann, R.Q. Hintzen, B.A. t Hart, S. Amor, J.D. Laman, L.A. Boven,

Brain antigens in functionally distinct antigen-presenting cell populations in cervical lymph nodes in MS and EAE, J Mol Med, 87 (2009) 273-286.

[94] M.G. Mohammad, V.W. Tsai, M.J. Ruitenberg, M. Hassanpour, H. Li, P.H. Hart, S.N. Breit, P.E. Sawchenko, D.A. Brown, Immune cell trafficking from the brain maintains CNS immune tolerance, J Clin Invest, 124 (2014) 1228-1241.

[95] M. van Zwam, R. Huizinga, N. Heijmans, M. van Meurs, A.F. Wierenga-Wolf, M.J. Melief, R.Q. Hintzen, B.A. t Hart, S. Amor, L.A. Boven, J.D. Laman, Surgical excision of CNS-draining lymph nodes reduces relapse severity in chronic-relapsing experimental autoimmune encephalomyelitis, J Pathol, 217 (2009) 543-551.

[96] G. Senti, T.M. Kundig, Intralymphatic immunotherapy, World Allergy Organ J, 8 (2015) 9.

[97] A.L. Croxford, M. Lanzinger, F.J. Hartmann, B. Schreiner, F. Mair, P. Pelczar, B.E. Clausen, S. Jung, M. Greter, B. Becher, The Cytokine GM-CSF Drives the Inflammatory Signature of CCR2+ Monocytes and Licenses Autoimmunity, Immunity, 43 (2015) 502-514.

[98] R.W. Nelson, D. Beisang, N.J. Tubo, T. Dileepan, D.L. Wiesner, K. Nielsen, M. Wuthrich, B.S. Klein, D.I. Kotov, J.A. Spanier, B.T. Fife, J.J. Moon, M.K. Jenkins, T cell receptor cross-reactivity between similar foreign and self peptides influences naive cell population size and autoimmunity, Immunity, 42 (2015) 95-107.

[99] M. White, G. Webster, D. O'Sullivan, S. Stone, A.C. La Flamme, Targeting innate receptors with MIS416 reshapes Th responses and suppresses CNS disease in a mouse model of multiple sclerosis, PLoS One, 9 (2014) e87712.

[100] E. De Gregorio, The path forward, Vaccine, 33 Suppl 2 (2015) B60-63.

[101] T.J. Moyer, A.C. Zmolek, D.J. Irvine, Beyond antigens and adjuvants: formulating future vaccines, J Clin Invest, 126 (2016) 799-808.

[102] S. Plotkin, History of vaccination, Proc Natl Acad Sci U S A, 111 (2014) 12283-12287.

[103] I. Melero, G. Gaudernack, W. Gerritsen, C. Huber, G. Parmiani, S. Scholl, N. Thatcher, J. Wagstaff, C. Zielinski, I. Faulkner, H. Mellstedt, Therapeutic vaccines for cancer: an overview of clinical trials, Nat Rev Clin Oncol, 11 (2014) 509-524.

[104] J.H. Doroshow, S. Kummar, Translational research in oncology--10 years of progress and future prospects, Nat Rev Clin Oncol, 11 (2014) 649-662.

[105] L. Steinman, Inverse vaccination, the opposite of Jenner's concept, for therapy of autoimmunity, J Intern Med, 267 (2010) 441-451.

[106] A.J. McMichael, P. Borrow, G.D. Tomaras, N. Goonetilleke, B.F. Haynes, The immune response during acute HIV-1 infection: clues for vaccine development, Nat Rev Immunol, 10 (2010) 11-23.

[107] G.T. Motz, G. Coukos, Deciphering and reversing tumor immune suppression, Immunity, 39 (2013) 61-73.

[108] J.A. Bluestone, K. Herold, G. Eisenbarth, Genetics, pathogenesis and clinical interventions in type 1 diabetes, Nature, 464 (2010) 1293-1300.

[109] K.T. Gause, A.K. Wheatley, J. Cui, Y. Yan, S.J. Kent, F. Caruso, Immunological Principles Guiding the Rational Design of Particles for Vaccine Delivery, ACS Nano, 11 (2017) 54-68.

[110] J. Leleux, K. Roy, Micro and nanoparticle-based delivery systems for vaccine immunotherapy: an immunological and materials perspective, Adv Healthc Mater, 2 (2013) 72-94.

[111] J.M. Curtsinger, M.F. Mescher, Inflammatory cytokines as a third signal for T cell activation, Curr Opin Immunol, 22 (2010) 333-340.

[112] D.T. O'Hagan, C.B. Fox, New generation adjuvants--from empiricism to rational design, Vaccine, 33 Suppl 2 (2015) B14-20.

[113] C.B. Fox, J. Haensler, An update on safety and immunogenicity of vaccines containing emulsion-based adjuvants, Expert Rev Vaccines, 12 (2013) 747-758.

[114] S.G. Reed, M.T. Orr, C.B. Fox, Key roles of adjuvants in modern vaccines, Nat Med, 19 (2013) 1597-1608.

[115] H. Kanzler, F.J. Barrat, E.M. Hessel, R.L. Coffman, Therapeutic targeting of innate immunity with Toll-like receptor agonists and antagonists, Nat Med, 13 (2007) 552-559.

[116] B. Pulendran, R. Ahmed, Immunological mechanisms of vaccination, Nat Immunol, 12 (2011) 509-517.

[117] L. Gu, D.J. Mooney, Biomaterials and emerging anticancer therapeutics: engineering the microenvironment, Nat Rev Cancer, 16 (2016) 56-66.

[118] J.M. Gammon, N.M. Dold, C.M. Jewell, Improving the clinical impact of biomaterials in cancer immunotherapy, Oncotarget, 7 (2016) 15421-15443.

[119] B.L. Hartwell, L. Antunez, B.P. Sullivan, S. Thati, J.O. Sestak, C. Berkland, Multivalent nanomaterials: learning from vaccines and progressing to antigen-specific immunotherapies, J Pharm Sci, 104 (2015) 346-361.

[120] L.H. Tostanoski, E.A. Gosselin, C.M. Jewell, Engineering tolerance using biomaterials to target and control antigen presenting cells, Discov Med, 21 (2016) 403-410.

[121] I.A. Bettencourt, J.D. Powell, Targeting Metabolism as a Novel Therapeutic Approach to Autoimmunity, Inflammation, and Transplantation, J Immunol, 198 (2017) 999-1005.

[122] E.L. Pearce, Metabolism in T cell activation and differentiation, Curr Opin Immunol, 22 (2010) 314-320.

[123] A.O. Kamphorst, K. Araki, R. Ahmed, Beyond adjuvants: immunomodulation strategies to enhance T cell immunity, Vaccine, 33 Suppl 2 (2015) B21-28.

[124] K.N. Pollizzi, J.D. Powell, Integrating canonical and metabolic signalling programmes in the regulation of T cell responses, Nat Rev Immunol, 14 (2014) 435-446.

[125] M.O. Li, A.Y. Rudensky, T cell receptor signalling in the control of regulatory T cell differentiation and function, Nat Rev Immunol, 16 (2016) 220-233.

[126] N.A. Hotaling, L. Tang, D.J. Irvine, J.E. Babensee, Biomaterial Strategies for Immunomodulation, in: M.L. Yarmush (Ed.) Annual Review of Biomedical Engineering, Vol 17, Annual Reviews, Palo Alto, 2015, pp. 317-349.

[127] D.J. Irvine, M.C. Hanson, K. Rakhra, T. Tokatlian, Synthetic Nanoparticles for Vaccines and Immunotherapy, Chem Rev, 115 (2015) 11109-11146.

[128] E. van Riet, A. Ainai, T. Suzuki, G. Kersten, H. Hasegawa, Combatting infectious diseases; nanotechnology as a platform for rational vaccine design, Adv Drug Deliv Rev, 74 (2014) 28-34.

[129] S. Eskandari, T. Guerin, I. Toth, R.J. Stephenson, Recent advances in self-assembled peptides: Implications for targeted drug delivery and vaccine engineering, Adv Drug Deliv Rev, 110-111 (2017) 169-187.

[130] H. Acar, S. Srivastava, E.J. Chung, M.R. Schnorenberg, J.C. Barrett, J.L. LaBelle, M. Tirrell, Self-assembling peptide-based building blocks in medical applications, Adv Drug Deliv Rev, 110-111 (2017) 65-79.

[131] E.J. Lee, N.K. Lee, I.S. Kim, Bioengineered protein-based nanocage for drug delivery, Adv Drug Deliv Rev, 106 (2016) 157-171.

[132] Y. Tahara, K. Akiyoshi, Current advances in self-assembled nanogel delivery systems for immunotherapy, Adv Drug Deliv Rev, 95 (2015) 65-76.

[133] N.K. Jain, N. Sahni, O.S. Kumru, S.B. Joshi, D.B. Volkin, C. Russell Middaugh, Formulation and stabilization of recombinant protein based virus-like particle vaccines, Adv Drug Deliv Rev, 93 (2015) 42-55.

[134] D.M. Smith, J.K. Simon, J.R. Baker, Jr., Applications of nanotechnology for immunology, Nat Rev Immunol, 13 (2013) 592-605.

[135] J.A. Rosenthal, L. Chen, J.L. Baker, D. Putnam, M.P. DeLisa, Pathogen-like particles: biomimetic vaccine carriers engineered at the nanoscale, Curr Opin Biotechnol, 28 (2014) 51-58.

[136] Q. Zhao, S. Li, H. Yu, N. Xia, Y. Modis, Virus-like particle-based human vaccines: quality assessment based on structural and functional properties, Trends Biotechnol, 31 (2013) 654-663.

[137] J.T. Schiller, X. Castellsague, S.M. Garland, A review of clinical trials of human papillomavirus prophylactic vaccines, Vaccine, 30 Suppl 5 (2012) F123-138.

[138] S.M. Garland, M. Hernandez-Avila, C.M. Wheeler, G. Perez, D.M. Harper, S. Leodolter, G.W. Tang, D.G. Ferris, M. Steben, J. Bryan, F.J. Taddeo, R. Railkar, M.T. Esser, H.L. Sings, M. Nelson, J. Boslego, C. Sattler, E. Barr, L.A. Koutsky, I.I. Females United to Unilaterally Reduce Endo/Ectocervical Disease, Quadrivalent vaccine against human papillomavirus to prevent anogenital diseases, N Engl J Med, 356 (2007) 1928-1943.

[139] F.I.S. Group, Quadrivalent vaccine against human papillomavirus to prevent high-grade cervical lesions, N Engl J Med, 356 (2007) 1915-1927.

[140] R. Herrero, A. Hildesheim, A.C. Rodriguez, S. Wacholder, C. Bratti, D. Solomon, P. Gonzalez, C. Porras, S. Jimenez, D. Guillen, J. Morales, M. Alfaro, J. Cyr, K. Morrisey, Y. Estrada, B. Cortes, L.A. Morera, E. Freer, J. Schussler, J. Schiller, D. Lowy, M. Schiffman, G. Costa Rica Vaccine Trial, Rationale and design of a community-based double-blind randomized clinical trial of an HPV 16 and 18 vaccine in Guanacaste, Costa Rica, Vaccine, 26 (2008) 4795-4808.

[141] J. Paavonen, D. Jenkins, F.X. Bosch, P. Naud, J. Salmeron, C.M. Wheeler, S.N. Chow, D.L. Apter, H.C. Kitchener, X. Castellsague, N.S. de Carvalho, S.R. Skinner, D.M. Harper, J.A. Hedrick, U. Jaisamrarn, G.A. Limson, M. Dionne, W. Quint, B. Spiessens, P. Peeters, F. Struyf, S.L. Wieting, M.O. Lehtinen, G. Dubin, H.P.s. group, Efficacy of a prophylactic adjuvanted bivalent L1 virus-like-particle vaccine against infection with human papillomavirus types 16 and 18 in young women: an interim analysis of a phase III double-blind, randomised controlled trial, Lancet, 369 (2007) 2161-2170.

[142] W.J. McAleer, E.B. Buynak, R.Z. Maigetter, D.E. Wampler, W.J. Miller, M.R. Hilleman, Human hepatitis B vaccine from recombinant yeast, Nature, 307 (1984) 178-180.

[143] J.S. Rudra, T. Sun, K.C. Bird, M.D. Daniels, J.Z. Gasiorowski, A.S. Chong, J.H. Collier, Modulating adaptive immune responses to peptide self-assemblies, ACS Nano, 6 (2012) 1557-1564.

[144] L. He, N. de Val, C.D. Morris, N. Vora, T.C. Thinnes, L. Kong, P. Azadnia, D. Sok, B. Zhou, D.R. Burton, I.A. Wilson, D. Nemazee, A.B. Ward, J. Zhu, Presenting native-like trimeric HIV-1 antigens with self-assembling nanoparticles, Nat Commun, 7 (2016) 12041.

[145] P.J. Carrillo, M. Medrano, A. Valbuena, A. Rodriguez-Huete, M. Castellanos, R. Perez, M.G. Mateu, Amino Acid Side Chains Buried along Intersubunit Interfaces in a Viral Capsid Preserve Low Mechanical Stiffness Associated with Virus Infectivity, ACS Nano, 11 (2017) 2194-2208.

[146] C. Hivroz, M. Saitakis, Biophysical Aspects of T Lymphocyte Activation at the Immune Synapse, Front Immunol, 7 (2016) 46.

[147] R.S. O'Connor, X. Hao, K. Shen, K. Bashour, T. Akimova, W.W. Hancock, L.C. Kam, M.C. Milone, Substrate rigidity regulates human T cell activation and proliferation, J Immunol, 189 (2012) 1330-1339.

[148] H. Deng, J. Li, Y. Zhang, H. Pan, G. Xu, A new strategy for label-free electrochemical immunoassay based on "gate-effect" of beta-cyclodextrin modified electrode, Anal Chim Acta, 926 (2016) 48-54.

[149] A.P. Le Brun, A. Soliakov, D.S. Shah, S.A. Holt, A. McGill, J.H. Lakey, Engineered self-assembling monolayers for label free detection of influenza nucleoprotein, Biomed Microdevices, 17 (2015) 9951.

[150] E. Zacco, C. Anish, C.E. Martin, V.B. H, E. Brandenburg, P.H. Seeberger, B. Koksch, A Self-Assembling Peptide Scaffold for the Multivalent Presentation of Antigens, Biomacromolecules, 16 (2015) 2188-2197.

[151] Z. Li, B. Zhao, D. Wang, Y. Wen, G. Liu, H. Dong, S. Song, C. Fan, DNA nanostructure-based universal microarray platform for high-efficiency multiplex bioanalysis in biofluids, ACS Appl Mater Interfaces, 6 (2014) 17944-17953.

[152] M.F. Bachmann, G.T. Jennings, Vaccine delivery: a matter of size, geometry, kinetics and molecular patterns, Nat Rev Immunol, 10 (2010) 787-796.

[153] R. Mammadov, G. Cinar, N. Gunduz, M. Goktas, H. Kayhan, S. Tohumeken, A.E. Topal, I. Orujalipoor, T. Delibasi, A. Dana, S. Ide, A.B. Tekinay, M.O. Guler, Virus-like nanostructures for tuning immune response, Sci Rep, 5 (2015) 16728.

[154] S. Yi, S.D. Allen, Y.G. Liu, B.Z. Ouyang, X. Li, P. Augsornworawat, E.B. Thorp, E.A. Scott, Tailoring Nanostructure Morphology for Enhanced Targeting of Dendritic Cells in Atherosclerosis, ACS Nano, 10 (2016) 11290-11303.

[155] Y. Wen, A. Waltman, H. Han, J.H. Collier, Switching the Immunogenicity of Peptide Assemblies Using Surface Properties, ACS Nano, 10 (2016) 9274-9286.

[156] L.A. Brito, D.T. O'Hagan, Designing and building the next generation of improved vaccine adjuvants, J Control Release, 190 (2014) 563-579.

[157] H. Shirota, D.M. Klinman, Recent progress concerning CpG DNA and its use as a vaccine adjuvant, Expert Rev Vaccines, 13 (2014) 299-312.

[158] R.L. Coffman, A. Sher, R.A. Seder, Vaccine adjuvants: putting innate immunity to work, Immunity, 33 (2010) 492-503.

[159] M.L. Mbow, E. De Gregorio, N.M. Valiante, R. Rappuoli, New adjuvants for human vaccines, Curr Opin Immunol, 22 (2010) 411-416.

[160] N. Chen, M. Wei, Y. Sun, F. Li, H. Pei, X. Li, S. Su, Y. He, L. Wang, J. Shi, C. Fan, Q. Huang, Self-assembly of poly-adenine-tailed CpG oligonucleotide-gold nanoparticle nanoconjugates with immunostimulatory activity, Small, 10 (2014) 368-375.

[161] J.O. Jin, H. Park, W. Zhang, J.W. de Vries, A. Gruszka, M.W. Lee, D.R. Ahn, A. Herrmann, M. Kwak, Modular delivery of CpG-incorporated lipid-DNA nanoparticles for spleen DC activation, Biomaterials, 115 (2017) 81-89.

[162] G.M. Lynn, R. Laga, P.A. Darrah, A.S. Ishizuka, A.J. Balaci, A.E. Dulcey, M. Pechar, R. Pola, M.Y. Gerner, A. Yamamoto, C.R. Buechler, K.M. Quinn, M.G. Smelkinson, O. Vanek, R. Cawood, T. Hills, O. Vasalatiy, K. Kastenmuller, J.R. Francica, L. Stutts, J.K. Tom, K.A. Ryu, A.P. Esser-Kahn, T. Etrych, K.D. Fisher, L.W. Seymour, R.A. Seder, In vivo characterization of the physicochemical properties of polymer-linked TLR agonists that enhance vaccine immunogenicity, Nat Biotechnol, 33 (2015) 1201-1210.

[163] K. Mohri, E. Kusuki, S. Ohtsuki, N. Takahashi, M. Endo, K. Hidaka, H. Sugiyama, Y. Takahashi, Y. Takakura, M. Nishikawa, Self-assembling DNA dendrimer for effective delivery of immunostimulatory CpG DNA to immune cells, Biomacromolecules, 16 (2015) 1095-1101.

[164] E.F. Khisamutdinov, H. Li, D.L. Jasinski, J. Chen, J. Fu, P. Guo, Enhancing immunomodulation on innate immunity by shape transition among RNA triangle, square and pentagon nanovehicles, Nucleic Acids Res, 42 (2014) 9996-10004.

[165] S.N. Thomas, E. Vokali, A.W. Lund, J.A. Hubbell, M.A. Swartz, Targeting the tumor-draining lymph node with adjuvanted nanoparticles reshapes the anti-tumor immune response, Biomaterials, 35 (2014) 814-824.

[166] J.S. Rudra, Y.F. Tian, J.P. Jung, J.H. Collier, A self-assembling peptide acting as an immune adjuvant, Proc Natl Acad Sci U S A, 107 (2010) 622-627.

[167] J.S. Rudra, S. Mishra, A.S. Chong, R.A. Mitchell, E.H. Nardin, V. Nussenzweig, J.H. Collier, Self-assembled peptide nanofibers raising durable antibody responses against a malaria epitope, Biomaterials, 33 (2012) 6476-6484.

[168] J. Chen, R.R. Pompano, F.W. Santiago, L. Maillat, R. Sciammas, T. Sun, H. Han, D.J. Topham, A.S. Chong, J.H. Collier, The use of self-adjuvanting nanofiber vaccines to elicit high-affinity B cell responses to peptide antigens without inflammation, Biomaterials, 34 (2013) 8776-8785.

[169] R.R. Pompano, J. Chen, E.A. Verbus, H. Han, A. Fridman, T. McNeely, J.H. Collier, A.S. Chong, Titrating T-cell epitopes within self-assembled vaccines optimizes CD4+ helper T cell and antibody outputs, Adv Healthc Mater, 3 (2014) 1898-1908.

[170] T. Sun, H. Han, G.A. Hudalla, Y. Wen, R.R. Pompano, J.H. Collier, Thermal stability of self-assembled peptide vaccine materials, Acta Biomater, 30 (2016) 62-71.

[171] P. Li, G. Shi, X. Zhang, H. Song, C. Zhang, W. Wang, C. Li, B. Song, C. Wang, D. Kong, Guanidinylated cationic nanoparticles as robust protein antigen delivery systems and adjuvants for promoting antigen-specific immune responses in vivo, J Mater Chem B, 4 (2016) 5608-5620.

[172] Y.F. Liu, Z.Y. Sun, P.G. Chen, Z.H. Huang, Y. Gao, L. Shi, Y.F. Zhao, Y.X. Chen, Y.M. Li, Glycopeptide Nanoconjugates Based on Multilayer Self-Assembly as an Antitumor Vaccine, Bioconjug Chem, 26 (2015) 1439-1442.

[173] A. Purwada, Y.F. Tian, W. Huang, K.M. Rohrbach, S. Deol, A. August, A. Singh, Self-Assembly Protein Nanogels for Safer Cancer Immunotherapy, Adv Healthc Mater, 5 (2016) 1413-1419.

[174] M. Tamborrini, N. Geib, A. Marrero-Nodarse, M. Jud, J. Hauser, C. Aho, A. Lamelas, A. Zuniga, G. Pluschke, A. Ghasparian, J.A. Robinson, A Synthetic Virus-Like Particle Streptococcal Vaccine Candidate Using B-Cell Epitopes from the Proline-Rich Region of Pneumococcal Surface Protein A, Vaccines, 3 (2015) 850-874.

[175] X. Zhang, K. Wang, Q. Lin, M. Zheng, Q. Li, T. Li, Q. Hong, Q. Zheng, H. Yu, Y. Gu, S. Li, N. Xia, A shared N-terminal hydrophobic tail for the formation of nanoparticulates, Nanomedicine (Lond), 11 (2016) 2289-2303.

[176] Z. Luo, P. Li, J. Deng, N. Gao, Y. Zhang, H. Pan, L. Liu, C. Wang, L. Cai, Y. Ma, Cationic polypeptide micelle-based antigen delivery system: a simple and robust adjuvant to improve vaccine efficacy, J Control Release, 170 (2013) 259-267.

[177] Q. Guo, D. Dasgupta, T.A. Doll, P. Burkhard, D.E. Lanar, Expression, purification and refolding of a self-assembling protein nanoparticle (SAPN) malaria vaccine, Methods, 60 (2013) 242-247.

[178] Y. Yang, P. Ringler, S.A. Muller, P. Burkhard, Optimizing the refolding conditions of self-assembling polypeptide nanoparticles that serve as repetitive antigen display systems, J Struct Biol, 177 (2012) 168-176.

[179] M. Black, A. Trent, Y. Kostenko, J.S. Lee, C. Olive, M. Tirrell, Self-assembled peptide amphiphile micelles containing a cytotoxic T-cell epitope promote a protective immune response in vivo, Adv Mater, 24 (2012) 3845-3849.

[180] C.B. Chesson, E.J. Huelsmann, A.T. Lacek, F.J. Kohlhapp, M.F. Webb, A. Nabatiyan, A. Zloza, J.S. Rudra, Antigenic peptide nanofibers elicit adjuvant-free CD8(+) T cell responses, Vaccine, 32 (2014) 1174-1180.

[181] Z.H. Huang, L. Shi, J.W. Ma, Z.Y. Sun, H. Cai, Y.X. Chen, Y.F. Zhao, Y.M. Li, A totally synthetic, self-assembling, adjuvant-free MUC1 glycopeptide vaccine for cancer therapy, J Am Chem Soc, 134 (2012) 8730-8733.

[182] A. Trent, B.D. Ulery, M.J. Black, J.C. Barrett, S. Liang, Y. Kostenko, N.A. David, M.V. Tirrell, Peptide amphiphile micelles self-adjuvant group A streptococcal vaccination, AAPS J, 17 (2015) 380-388.

[183] Z.T. Shen, A.B. Sigalov, SARS Coronavirus Fusion Peptide-Derived Sequence Suppresses Collagen-Induced Arthritis in DBA/1J Mice, Sci Rep, 6 (2016) 28672.

[184] C.B. Fox, S.J. Sivananthan, M.S. Duthie, J. Vergara, J.A. Guderian, E. Moon, D. Coblentz, S.G. Reed, D. Carter, A nanoliposome delivery system to synergistically trigger TLR4 AND TLR7, J Nanobiotechnology, 12 (2014) 17.

[185] S.M. Goldinger, R. Dummer, P. Baumgaertner, D. Mihic-Probst, K. Schwarz, A. Hammann-Haenni, J. Willers, C. Geldhof, J.O. Prior, T.M. Kundig, O. Michielin, M.F. Bachmann, D.E. Speiser, Nano-particle vaccination combined with TLR-7 and -9 ligands triggers memory and effector CD8(+) T-cell responses in melanoma patients, Eur J Immunol, 42 (2012) 3049-3061.

[186] C.E. Brubaker, V. Panagiotou, D. Demurtas, D.K. Bonner, M.A. Swartz, J.A. Hubbell, A Cationic Micelle Complex Improves CD8+T Cell Responses in Vaccination Against Unmodified Protein Antigen, ACS Biomater Sci Eng, 2 (2016) 231-240.

[187] S. Sevimli, F.C. Knight, P. Gilchuk, S. Joyce, J.T. Wilson, Fatty Acid-Mimetic Micelles for Dual Delivery of Antigens and Imidazoquinoline Adjuvants, ACS Biomater Sci Eng, 3 (2016) 179-194.

[188] P.O. Ilyinskii, C.J. Roy, C.P. O'Neil, E.A. Browning, L.A. Pittet, D.H. Altreuter, F. Alexis, E. Tonti, J. Shi, P.A. Basto, M. Iannacone, A.F. Radovic-Moreno, R.S. Langer, O.C. Farokhzad, U.H. von Andrian, L.P. Johnston, T.K. Kishimoto, Adjuvant-carrying synthetic vaccine particles augment the immune response to encapsulated antigen and exhibit strong local immune activation without inducing systemic cytokine release, Vaccine, 32 (2014) 2882-2895.

[189] C.B. Chesson, S. Ekpo-Otu, J.J. Endsley, J.S. Rudra, Biomaterials-Based Vaccination Strategies for the Induction of CD8+T Cell Responses, ACS Biomater Sci Eng, 3 (2016) 126-143.

[190] E.A. Scott, A. Stano, M. Gillard, A.C. Maio-Liu, M.A. Swartz, J.A. Hubbell, Dendritic cell activation and T cell priming with adjuvant- and antigen-loaded oxidation-sensitive polymersomes, Biomaterials, 33 (2012) 6211-6219.

[191] S. Keller, J.T. Wilson, G.I. Patilea, H.B. Kern, A.J. Convertine, P.S. Stayton, Neutral polymer micelle carriers with pH-responsive, endosome-releasing activity modulate antigen trafficking to enhance CD8(+) T cell responses, J Control Release, 191 (2014) 24-33.

[192] J.T. Wilson, S. Keller, M.J. Manganiello, C. Cheng, C.C. Lee, C. Opara, A. Convertine, P.S. Stayton, pH-Responsive nanoparticle vaccines for dual-delivery of antigens and immunostimulatory oligonucleotides, ACS Nano, 7 (2013) 3912-3925.

[193] J.T. Wilson, A. Postma, S. Keller, A.J. Convertine, G. Moad, E. Rizzardo, L. Meagher, J. Chiefari, P.S. Stayton, Enhancement of MHC-I antigen presentation via architectural control of pH-responsive, endosomolytic polymer nanoparticles, AAPS J, 17 (2015) 358-369.

[194] S. De Koker, L.J. De Cock, P. Rivera-Gil, W.J. Parak, R. Auzely Velty, C. Vervaet, J.P. Remon, J. Grooten, B.G. De Geest, Polymeric multilayer capsules delivering biotherapeutics, Adv Drug Deliv Rev, 63 (2011) 748-761.

[195] Y. Yan, M. Bjonmalm, F. Caruso, Assembly of Layer-by-Layer Particles and Their Interactions with Biological Systems, Chem Mater, 26 (2014) 452-460.

[196] S.F. Chong, A. Sexton, R. De Rose, S.J. Kent, A.N. Zelikin, F. Caruso, A paradigm for peptide vaccine delivery using viral epitopes encapsulated in degradable polymer hydrogel capsules, Biomaterials, 30 (2009) 5178-5186.

[197] B.G. De Geest, M.A. Willart, B.N. Lambrecht, C. Pollard, C. Vervaet, J.P. Remon, J. Grooten, S. De Koker, Surface-engineered polyelectrolyte multilayer capsules: synthetic vaccines mimicking microbial structure and function, Angew Chem Int Ed Engl, 51 (2012) 3862-3866.

[198] Y.C. Chiu, J.M. Gammon, J.I. Andorko, L.H. Tostanoski, C.M. Jewell, Assembly and Immunological Processing of Polyelectrolyte Multilayers Composed of Antigens and Adjuvants, ACS Appl Mater Interfaces, 8 (2016) 18722-18731.

[199] Q. Zeng, J.M. Gammon, L.H. Tostanoski, Y.C. Chiu, C.M. Jewell, In Vivo Expansion of Melanoma-Specific T Cells Using Microneedle Arrays Coated with Immune-Polyelectrolyte Multilayers, ACS Biomater Sci Eng, 3 (2017) 195-205.

[200] P. Zhang, J.I. Andorko, C.M. Jewell, Impact of dose, route, and composition on the immunogenicity of immune polyelectrolyte multilayers delivered on gold templates, Biotechnol Bioeng, 114 (2017) 423-431.

[201] L.H. Tostanoski, Y.C. Chiu, J.I. Andorko, M. Guo, X. Zeng, P. Zhang, W. Royal, 3rd, C.M. Jewell, Design of Polyelectrolyte Multilayers to Promote Immunological Tolerance, ACS Nano, (2016).

[202] ACIP votes down use of LAIV for 2016-2017 flu season, (2016).

[203] F.S. Quan, Y.T. Lee, K.H. Kim, M.C. Kim, S.M. Kang, Progress in developing virus-like particle influenza vaccines, Expert Rev Vaccines, 15 (2016) 1281-1293.

[204] N. Wibowo, Y.P. Chuan, L.H.L. Lua, A.P.J. Middelberg, Modular engineering of a microbially-produced viral capsomere vaccine for influenza, Chem Eng Sci, 103 (2013) 12-20.

[205] U. Kartoglu, J. Milstien, Tools and approaches to ensure quality of vaccines throughout the cold chain, Expert Rev Vaccines, 13 (2014) 843-854.

[206] D. Kristensen, D. Chen, Strategies to advance vaccine technologies for resource-poor settings, Vaccine, 31 Suppl 2 (2013) B157-162.

[207] D.P. Patterson, A. Rynda-Apple, A.L. Harmsen, A.G. Harmsen, T. Douglas, Biomimetic antigenic nanoparticles elicit controlled protective immune response to influenza, ACS Nano, 7 (2013) 3036-3044.

[208] D. Zheng, S. Chen, D. Qu, J. Chen, F. Wang, R. Zhang, Z. Chen, Influenza H7N9 LAH-HBc virus-like particle vaccine with adjuvant protects mice against homologous and heterologous influenza viruses, Vaccine, 34 (2016) 6464-6471.

[209] M.W. Wolf, U. Reichl, Downstream processing of cell culture-derived virus particles, Expert Rev Vaccines, 10 (2011) 1451-1475.

[210] Y. Chen, Y. Liu, G. Zhang, A. Wang, Z. Dong, Y. Qi, J. Wang, B. Zhao, N. Li, M. Jiang, Human papillomavirus L1 protein expressed in Escherichia coli self-assembles into virus-like particles that are highly immunogenic, Virus Res, 220 (2016) 97-103.

[211] B.M. Friedrich, D.W. Beasley, J.S. Rudra, Supramolecular peptide hydrogel adjuvanted subunit vaccine elicits protective antibody responses against West Nile virus, Vaccine, 34 (2016) 5479-5482.

[212] R.F. Grenfell, L.M. Shollenberger, E.F. Samli, D.A. Harn, Vaccine self-assembling immune matrix is a new delivery platform that enhances immune responses to recombinant HBsAg in mice, Clin Vaccine Immunol, 22 (2015) 336-343.

[213] S.T. Koshy, D.J. Mooney, Biomaterials for enhancing anti-cancer immunity, Curr Opin Biotechnol, 40 (2016) 1-8.

[214] A.Y. Lin, J.P. Almeida, A. Bear, N. Liu, L. Luo, A.E. Foster, R.A. Drezek, Gold nanoparticle delivery of modified CpG stimulates macrophages and inhibits tumor growth for enhanced immunotherapy, PLoS One, 8 (2013) e63550.

[215] G. Zhu, Y. Liu, X. Yang, Y.H. Kim, H. Zhang, R. Jia, H.S. Liao, A. Jin, J. Lin, M. Aronova, R. Leapman, Z. Nie, G. Niu, X. Chen, DNA-inorganic hybrid nanovaccine for cancer immunotherapy, Nanoscale, 8 (2016) 6684-6692.

[216] Z.Y. Sun, P.G. Chen, Y.F. Liu, B.D. Zhang, J.J. Wu, Y.X. Chen, Y.F. Zhao, Y.M. Li, Multi-component self-assembled anti-tumor nano-vaccines based on MUC1 glycopeptides, Chem Commun (Camb), 52 (2016) 7572-7575.

[217] B.G. De Geest, M.A. Willart, H. Hammad, B.N. Lambrecht, C. Pollard, P. Bogaert, M. De Filette, X. Saelens, C. Vervaet, J.P. Remon, J. Grooten, S. De Koker, Polymeric multilayer capsule-mediated vaccination induces protective immunity against cancer and viral infection, ACS Nano, 6 (2012) 2136-2149.

[218] P.C. DeMuth, Y. Min, B. Huang, J.A. Kramer, A.D. Miller, D.H. Barouch, P.T. Hammond, D.J. Irvine, Polymer multilayer tattooing for enhanced DNA vaccination, Nat Mater, 12 (2013) 367-376.

[219] L. Huang, H.P. Lemos, L. Li, M. Li, P.R. Chandler, B. Baban, T.L. McGaha, B. Ravishankar, J.R. Lee, D.H. Munn, A.L. Mellor, Engineering DNA nanoparticles as immunomodulatory reagents that activate regulatory T cells, J Immunol, 188 (2012) 4913-4920.

[220] L. Huang, L. Li, H. Lemos, P.R. Chandler, G. Pacholczyk, B. Baban, G.N. Barber, Y. Hayakawa, T.L. McGaha, B. Ravishankar, D.H. Munn, A.L. Mellor, Cutting edge: DNA sensing via the STING adaptor in myeloid dendritic cells induces potent tolerogenic responses, J Immunol, 191 (2013) 3509-3513.

[221] H. Lemos, L. Huang, P.R. Chandler, E. Mohamed, G.R. Souza, L. Li, G. Pacholczyk, G.N. Barber, Y. Hayakawa, D.H. Munn, A.L. Mellor, Activation of the STING adaptor attenuates experimental autoimmune encephalitis, J Immunol, 192 (2014) 5571-5578.

[222] F.J. Quintana, G. Murugaiyan, M.F. Farez, M. Mitsdoerffer, A.M. Tukpah, E.J. Burns, H.L. Weiner, An endogenous aryl hydrocarbon receptor ligand acts on dendritic cells and T cells to suppress experimental autoimmune encephalomyelitis, Proc Natl Acad Sci U S A, 107 (2010) 20768-20773.

[223] L.H. Tostanoski, Y.C. Chiu, J.M. Gammon, T. Simon, J.I. Andorko, J.S. Bromberg, C.M. Jewell, Reprogramming the Local Lymph Node Microenvironment Promotes Tolerance that Is Systemic and Antigen Specific, Cell Rep, 16 (2016) 2940-2952.

[224] K.L. Hess, J.I. Andorko, L.H. Tostanoski, C.M. Jewell, Polyplexes assembled from self-peptides and regulatory nucleic acids blunt toll-like receptor signaling to combat autoimmunity, Biomaterials, 118 (2017) 51-62.

[225] K.E. Balashov, L.L. Aung, A. Vaknin-Dembinsky, S. Dhib-Jalbut, H.L. Weiner, Interferon-beta inhibits toll-like receptor 9 processing in multiple sclerosis, Ann Neurol, 68 (2010) 899-906.

[226] T. Celhar, R. Magalhaes, A.M. Fairhurst, TLR7 and TLR9 in SLE: when sensing self goes wrong, Immunol Res, 53 (2012) 58-77.

[227] K. Derkow, J.M. Bauer, M. Hecker, B.K. Paap, M. Thamilarasan, D. Koczan, E. Schott, K. Deuschle, J. Bellmann-Strobl, F. Paul, U.K. Zettl, K. Ruprecht, S. Lehnardt, Multiple sclerosis: modulation of toll-like receptor (TLR) expression by interferon-beta includes upregulation of TLR7 in plasmacytoid dendritic cells, PLoS One, 8 (2013) e70626.

[228] P.N. Kelly, D.L. Romero, Y. Yang, A.L. Shaffer, 3rd, D. Chaudhary, S. Robinson, W. Miao, L. Rui, W.F. Westlin, R. Kapeller, L.M. Staudt, Selective interleukin-1 receptor-associated kinase 4 inhibitors for the treatment of autoimmune disorders and lymphoid malignancy, J Exp Med, 212 (2015) 2189-2201.

[229] M. Prinz, F. Garbe, H. Schmidt, A. Mildner, I. Gutcher, K. Wolter, M. Piesche, R. Schroers, E. Weiss, C.J. Kirschning, C.D. Rochford, W. Bruck, B. Becher, Innate immunity mediated by TLR9 modulates pathogenicity in an animal model of multiple sclerosis, J Clin Invest, 116 (2006) 456-464.

[230] J.M. Reynolds, G.J. Martinez, Y. Chung, C. Dong, Toll-like receptor 4 signaling in T cells promotes autoimmune inflammation, Proc Natl Acad Sci U S A, 109 (2012) 13064-13069.

[231] M. Santoni, K. Andrikou, V. Sotte, A. Bittoni, A. Lanese, C. Pellei, F. Piva, A. Conti, M. Nabissi, G. Santoni, S. Cascinu, Toll like receptors and pancreatic diseases: From a pathogenetic mechanism to a therapeutic target, Cancer Treat Rev, 41 (2015) 569-576.

[232] P.P. Ho, P. Fontoura, P.J. Ruiz, L. Steinman, H. Garren, An immunomodulatory GpG oligonucleotide for the treatment of autoimmunity via the innate and adaptive immune systems, J Immunol, 171 (2003) 4920-4926.

[233] H. Yim, W. Park, D. Kim, T.M. Fahmy, K. Na, A self-assembled polymeric micellar immunomodulator for cancer treatment based on cationic amphiphilic polymers, Biomaterials, 35 (2014) 9912-9919.

[234] M.J. Webber, J.B. Matson, V.K. Tamboli, S.I. Stupp, Controlled release of dexamethasone from peptide nanofiber gels to modulate inflammatory response, Biomaterials, 33 (2012) 6823-6832.

[235] T. Gajanayake, R. Olariu, F.M. Leclere, A. Dhayani, Z. Yang, A.K. Bongoni, Y. Banz, M.A. Constantinescu, J.M. Karp, P.K. Vemula, R. Rieben, E. Vogelin, A single localized dose of enzyme-responsive hydrogel improves long-term survival of a vascularized composite allograft, Sci Transl Med, 6 (2014) 249ra110.

[236] L.L. Aung, P. Fitzgerald-Bocarsly, S. Dhib-Jalbut, K. Balashov, Plasmacytoid dendritic cells in multiple sclerosis: chemokine and chemokine receptor modulation by interferon-beta, J Neuroimmunol, 226 (2010) 158-164.

[237] D.F. Moyano, M. Goldsmith, D.J. Solfiell, D. Landesman-Milo, O.R. Miranda, D. Peer, V.M. Rotello, Nanoparticle hydrophobicity dictates immune response, J Am Chem Soc, 134 (2012) 3965-3967.

[238] G. Decher, J.D. Hong, Buildup of Ultrathin Multilayer Films by a Self-Assembly Process .1. Consecutive Adsorption of Anionic and Cationic Bipolar Amphiphiles on Charged Surfaces, Makromol Chem-M Symp, 46 (1991) 321-327.

[239] E. Donath, G.B. Sukhorukov, F. Caruso, S.A. Davis, H. Mohwald, Novel hollow polymer shells by colloid-templated assembly of polyelectrolytes, Angewandte Chemie-International Edition, 37 (1998) 2202-2205.

[240] S. De Koker, B.G. De Geest, S.K. Singh, R. De Rycke, T. Naessens, Y. Van Kooyk, J. Demeester, S.C. De Smedt, J. Grooten, Polyelectrolyte microcapsules as antigen delivery vehicles to dendritic cells: uptake, processing, and cross-presentation of encapsulated antigens, Angew Chem Int Ed Engl, 48 (2009) 8485-8489.

[241] S. De Koker, R. Hoogenboom, B.G. De Geest, Polymeric multilayer capsules for drug delivery, Chem Soc Rev, 41 (2012) 2867-2884.

[242] J. Cui, R. De Rose, J.P. Best, A.P. Johnston, S. Alcantara, K. Liang, G.K. Such, S.J. Kent, F. Caruso, Mechanically tunable, self-adjuvanting nanoengineered polypeptide particles, Adv Mater, 25 (2013) 3468-3472.

[243] S. De Koker, K. Fierens, M. Dierendonck, R. De Rycke, B.N. Lambrecht, J. Grooten, J.P. Remon, B.G. De Geest, Nanoporous polyelectrolyte vaccine microcarriers. A formulation platform for enhancing humoral and cellular immune responses, J Control Release, 195 (2014) 99-109.

[244] A. Lutterotti, S. Yousef, A. Sputtek, K.H. Sturner, J.P. Stellmann, P. Breiden, S. Reinhardt, C. Schulze, M. Bester, C. Heesen, S. Schippling, S.D. Miller, M.

Sospedra, R. Martin, Antigen-specific tolerance by autologous myelin peptide-coupled cells: a phase 1 trial in multiple sclerosis, Sci Transl Med, 5 (2013) 188ra175.

[245] D.V. Volodkin, N.I. Larionova, G.B. Sukhorukov, Protein encapsulation via porous CaCO3 microparticles templating, Biomacromolecules, 5 (2004) 1962-1972.

[246] D.V. Volodkin, A.I. Petrov, M. Prevot, G.B. Sukhorukov, Matrix polyelectrolyte microcapsules: new system for macromolecule encapsulation, Langmuir, 20 (2004) 3398-3406.

[247] E. Bettelli, Y. Carrier, W. Gao, T. Korn, T.B. Strom, M. Oukka, H.L. Weiner, V.K. Kuchroo, Reciprocal developmental pathways for the generation of pathogenic effector TH17 and regulatory T cells, Nature, 441 (2006) 235-238.

[248] G. Rydzek, Q.M. Ji, M. Li, P. Schaaf, J.P. Hill, F. Boulmedais, K. Ariga, Electrochemical nanoarchitectonics and layer-by-layer assembly: From basics to future, Nano Today, 10 (2015) 138-167.

[249] P. Schaaf, J.C. Voegel, L. Jierry, F. Boulmedais, Spray-assisted polyelectrolyte multilayer buildup: from step-by-step to single-step polyelectrolyte film constructions, Adv Mater, 24 (2012) 1001-1016.

[250] T.Y. Wu, M. Singh, A.T. Miller, E. De Gregorio, F. Doro, U. D'Oro, D.A. Skibinski, M.L. Mbow, S. Bufali, A.E. Herman, A. Cortez, Y. Li, B.P. Nayak, E. Tritto, C.M. Filippi, G.R. Otten, L.A. Brito, E. Monaci, C. Li, S. Aprea, S. Valentini, S. Calabromicron, D. Laera, B. Brunelli, E. Caproni, P. Malyala, R.G. Panchal, T.K. Warren, S. Bavari, D.T. O'Hagan, M.P. Cooke, N.M. Valiante, Rational design of small molecules as vaccine adjuvants, Sci Transl Med, 6 (2014) 263ra160.

[251] S.L. Bailey, B. Schreiner, E.J. McMahon, S.D. Miller, CNS myeloid DCs presenting endogenous myelin peptides 'preferentially' polarize CD4+ T(H)-17 cells in relapsing EAE, Nat Immunol, 8 (2007) 172-180.